

UNIVERSITY OF LIÈGE  
Faculty of Sciences  
Geographical sciences

# Modelling the hydrological response of an urban watershed

Diachronic analysis of the effects of land use changes  
on storm runoff generation in the Upper Bukit Timah  
basin, Singapore

*Master thesis submitted by:*

***Emilie CÉSAR***

*in partial fulfilment of the requirements for the degree of:*

*Master of geographical sciences*

*Academic year:*

*2010-2011*





# ACKNOWLEDGMENTS

I would like convey my gratitude to Prof. Aurélia Hubert-Ferrari, my supervisor, for agreeing to support me in this project. Her advice, either for this research or for the university, was essential.

I wish to express my sincere thanks to Jean Van Campenhout, for his indispensable assistance and invaluable guidance in the fulfilment of this work. The two computer programs he built, used for recording RADAR and discharge data, contributed to overcoming the lack of data. Moreover, his numerous explications allowed me to learn indispensable things for the future, such as the use of several computer programs (ArcGis, Hec-GeoHMS, SWMM, Statistica, etc.).

I would like to thank Prof. François Petit and Serge Schmitz, my two lecturers, for reading this work and evaluating it.

This master thesis would not have been possible without the help and support of Prof. Avijit Gupta. I wish to express my sincere gratitude to him, for interesting me in the urban hydrology with his lectures at the University of Leeds. The trip to Singapore, the walks around the city, the numerous conversations, and the welcoming at the National University of Singapore are all examples for which I could never thank him enough. I am honoured to have worked with him.

Due merit also goes to the National University of Singapore for access to the university campus and the Central Library. Special thanks go to the Department of Geography, especially to Prof. Matthias Roth for access to the meteorological data of the weather station, Prof. Mak Choong Weng for the digital elevation model of Singapore and Ms Wong Lai Wa for the welcome in the department, the access to a student local and her availability. Thanks again to Prof. Avijit Gupta, without whom all these people would not have met.

The trip to Singapore would not have been possible without the hospitality and support of the Jamar family. Their wonderful welcome truly helped me feel comfortable in this unknown country. I would also thank Alex and Sophie for their great hospitality during the three last weeks of the trip and for helping me to discover another Singapore. Recognition also goes to Justin, my Singaporean friend, for his kindness in solving administrative problems, getting essential articles and welcoming me at the university.

These acknowledgments would not be complete without expressing my appreciation to all moral supporters and to those who have assisted in one way or another. Among them, I would like to particularly thank my family and my parents for their constant encouragements during these past five years, Pierrick for his daily support, Corine for the printing of this work, Meg and Rob for their patience in reviewing my drafts and also Nath, Tom and Vi for their support during my years at the university.



## Table of contents

<b>1. Introduction.....</b>	<b>7</b>
<b>2. Study Area and Hypotheses .....</b>	<b>9</b>
2.1. General context.....	9
2.2. Upper Bukit Timah Catchment.....	13
2.3. Hypotheses.....	18
<b>3. Literature Review .....</b>	<b>19</b>
3.1. Concepts .....	19
3.2. Urbanisation versus physical environment.....	22
3.3. Floods propensity .....	24
3.4. Urban hydrology of the Upper Bukit Timah basin.....	25
3.5. Urban watershed models .....	26
3.6. Literature review conclusion .....	29
<b>4. Pre-Treatments for Data Acquisition.....</b>	<b>31</b>
4.1. Georeferencing .....	31
4.2. Digital Elevation Model (DEM).....	32
4.3. Land use.....	38
4.4. Pre-treatments conclusion.....	40
<b>5. Modelling .....</b>	<b>41</b>
5.1. SWMM model .....	41
5.2. SWMM computational methods.....	42
5.3. SWMM subcatchments parameters .....	49
5.4. SWMM conduits and junctions parameters.....	56
5.5. Discharge and rainfall data .....	59
5.6. Evapotranspiration.....	66
5.7. SWMM pre-parameterisation .....	67
5.8. Final SWMM adjustment .....	70
5.9. SWMM verification.....	76
5.10. HEC-HMS model.....	85
5.11. Conclusion .....	89
<b>6. Diachronic analysis .....</b>	<b>91</b>
6.1. Rational method.....	91
6.2. Past and future urbanisation .....	92

6.3. Synthetic design hyetographs .....	97
6.4. Impact of land use changes on flow .....	99
6.5. Identification of critical areas .....	103
6.6. Diachronic analysis conclusion .....	105
<b>7. Final conclusion .....</b>	<b>107</b>
<b>Bibliography .....</b>	<b>111</b>
<b>Tutorial .....</b>	<b>119</b>
<b>Appendices List .....</b>	<b>155</b>

# 1. INTRODUCTION

Urbanisation produces numerous changes in the natural environment it replaces. The impacts include hydrological, morphological and sedimentological changes. The amount of storm water runoff is generally increased due to the removal of vegetation and the rise in impervious areas, resulting in a rise in the frequency and magnitude of floods. Moreover, the increased stream powers alter the shape of channels and sediment supplies are disturbed. The reduction of perviousness also results in a reduction in groundwater. Finally, the quality of water is lowered due to urban sources of pollution. The major factors controlling the effects of urbanisation are the impervious proportion of the drainage basin, the size of the catchment and the nature of rainstorms. Today, in addition to the necessity to increase social awareness about the protection and management of the water resources, there is a need for planners to obtain information regarding the drainage system response to the changing environment.

Singapore is naturally flood prone due to its particular physiography – small drainage basin, relatively steep hillslopes – and its equatorial climate characterised by intense rainfall of limited duration. Since the 1960s, the country has undergone widespread land development. As Singapore expanded, slopes were covered by impervious surfaces and floodplains were converted into arterial roads next to a stream transformed into a straight concrete canal. The natural propensity of flood has therefore increased. In this context of urban growth, management of the quantity and quality of water has become an important issue.

The effects of urbanisation on the hydrological environment can be quantified and predicted through detailed characterisation and modelling of the concerned urban area. Watershed models have become essential for water resources planning, development and management and their role will be increased in the future. Models are used to understand interactions between climate and hydrology; they are able to perform simulation of the effects of watershed processes and anthropogenic activities on water quality and quantity. They allow a great variety of applications, from the simulation of transport and treatment of storm water pollutants to the computation of discharge in each point of the catchment and the detection of the sensitive areas. These models require a high number of parameters in order to accurately describe the relationships between rainfall, runoff and watershed characteristics. These parameters are sometimes hard to quantify and data are not always readily available.

The Upper Bukit Timah basin, a watershed of 6.8 km<sup>2</sup> situated in the central part of Singapore constitutes a worthwhile case study of Singapore's increased flood probability with urban development. This area has been quiet widely researched upon during the past, but most of the studies concerned the old pattern of the catchment. Moreover, only few of them established a link between urbanisation and hydrological changes.

The aim of this work consists in modelling the Upper Bukit Timah catchment in order to perform a diachronic analysis of the effect of changes in imperviousness and roughness on hydrology. This objective will be achieved through the development of the SWMM model. In this case, only few data are available. The first step therefore consists in developing a methodological approach to build a correct watershed model of the Upper Bukit Timah catchment, using a variety of data sources. The second phase relies on the application of the watershed model previously constructed to underline the hydrological changes due to urbanisation.

One of the primary motivations behind this research is to help the future user to understand the hydrological processes of an urban watershed model and to show how indirect data can be exploited. Moreover, the model developed will provide a framework that can easily be reused to incorporate other available hydrologic/hydraulic processes data. The methodology used here could also be applied to another urban area. It is why all manipulations are described in details at the end of the work (see tutorial).

The work is organised as follows. Chapter 2 brings a short overview of the physical environment of Singapore and the Upper Bukit Timah basin (location topography, climate and physiography). It also details the hypotheses which are tested here. Chapter 3 summarises a review of the literature relevant to this research and revises the key concepts constituting the roots of the work. Chapter 4 explains the pre-treatments required to obtain basic data, namely topographic and land use data. Chapter 5 describes the methodology applied to achieve our goals. It first gives a brief presentation of the model and its computational methods and describes how parameters necessary for the model to run are determined. Then, it presents the results of the parameterisation of the model and its final adjustment. Chapter 6 focuses on the second research objective by performing the diachronic analysis and presenting the results. Chapter 7 draws some final conclusions before discussing the limitations of the work and briefly describing the research to be conducted in the future.

## 2. STUDY AREA AND HYPOTHESES

This chapter is a brief summary of the physical geography of Singapore and the Upper Bukit Timah basin. The catchment is detailed in terms of location, climate, topography, drainage, geology, soil and land use. The hypotheses are detailed at the end of the chapter.

### 2.1. General context

#### 2.1.1. Location, demography and economy

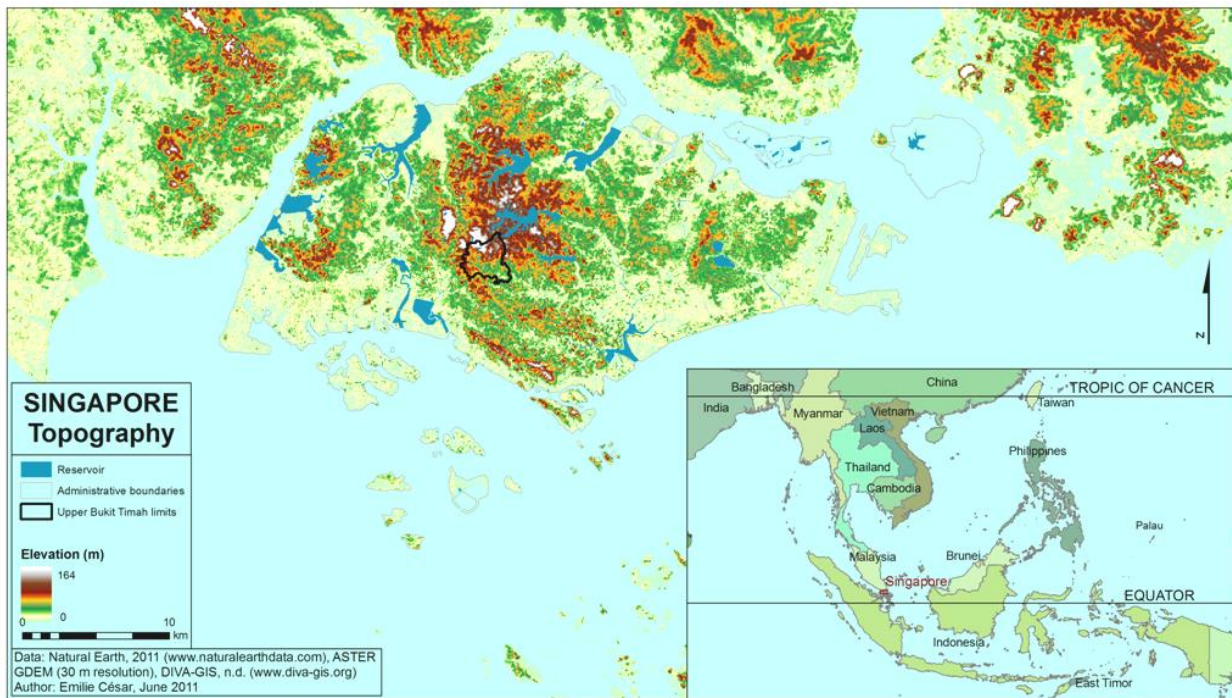
Singapore, officially the Republic of Singapore, is a tropical city-state of Southeast Asia situated at the coordinates of 1°22' N - 103°48' E, on the southern tip of the Malay Peninsula (figure 1). The Straits of Johor separates it from Malaysia to its north and the Singapore Strait from Indonesia to its south. It is made up of 63 islands and its total land area is 712.4 km<sup>2</sup> (Singapore Department of Statistics, 2010). The main island of Singapore is about 42 km from west to east and 23 km from north to south (Check, 1997).

The population recorded in 2009 was 5.076 million (Singapore Department of Statistics, 2010). Since its independence from Britain in 1965, it has seen a massive increase in wealth due to the strict controls imposed by the one-party government to build a wealthy, modern city (Campbell, 2008). The economy of the country depends heavily on the industry sector and the service sector, sharing 26.3% and 69.1% of GDP respectively (Yee *et al.*, 2010). This important growth has triggered the encroachment into the rainforest-covered areas during British colonization followed by radical alterations during the planned post-1960 urbanisation when hills were removed, forests cleared, and mangrove swamps reclaimed to build residential, commercial, and industrial areas (Chatterjea, 1993). This resulted in a series of changes in the geomorphic environment, both in time and space (*ibid.*). Today, the country is highly urbanised, apart for the Bukit Timah Nature Reserve, the only significant remaining tropical rainforest.

#### 2.1.2. Topography

Singapore has a moderately low relief (figure 1). The highest point, the Bukit Timah Peak, is 163 m, but 64 % of the main island lies within 15 m of mean sea level, 10 % over 30 m and only 1 % over 60 m (Pitts, 1994). The slopes are relatively low with 76 % of them being lower than 6°. In spite of the limited catchment relief, the hillsides can be steep. According to Gupta (1982), there are more than forty watersheds in Singapore, with a surface of less than 13 km<sup>2</sup>. This constitutes a flood prone topography (Gupta, 1994). The natural state of the island was constituted of small streams carrying a large amount of sediments and running down the

hillslopes to join larger rivers occupying the flat valley floors. This type of physiography led to flooding of the valley flats and, once the vegetative cover had been removed, accelerated the erosion and sediment transport (*ibid.*). Much of the present Singapore landscape is the result of anthropogenic changes brought on by urbanisation.

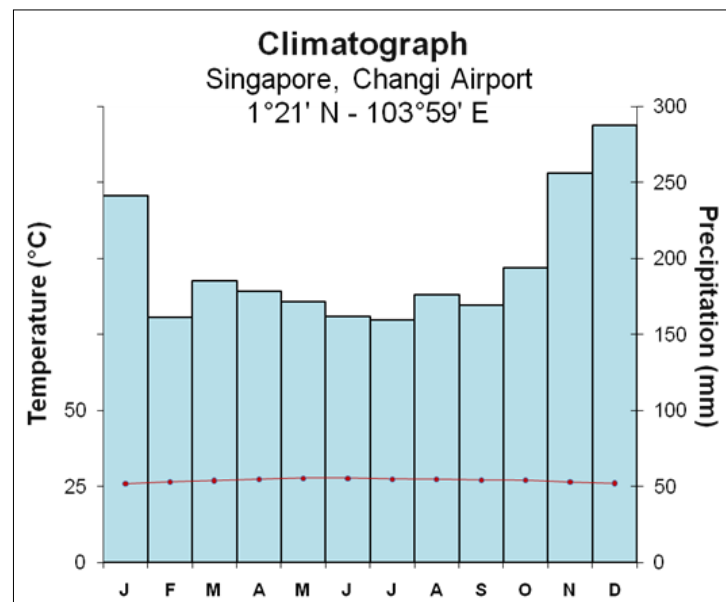


**Figure 1. Location and topography of Singapore**

### 2.1.3. Climate

Singapore can be classified as having an equatorial climate characterised by evenly high temperatures, humidity and rainfall throughout the year (Sien and Fook, 1991). Figure 2 illustrates it with the climatograph of the Changi Airport climate station. The yearly rainfall lies between 1650 and 2550 mm, depending on gauge location (Gupta, 1994). Rainstorms are brief, localised and intense and fall 179 days of the year (*ibid.*). The rainfall intensity-duration-frequency curve for the island shows that the 30-minute two-year rainstorm is estimated to bring 90 mm of rainfall and the 30-minute ten-year rainstorm is supposed to bring 120 mm (appendix 1). Temperatures usually range from 23 to 32°C (National Environment Agency, 2009). The mean 24-hour maximum relative humidity is close to 100 % throughout the year while the mean 24-hour minimum varies between 60 and 70 % (Sien and Fook, 1991). This climate is influenced by the monsoons which introduce variations of wind speed and direction. This produces wet and dry seasons over the year: the Northeast monsoon season which lasts from late November to March and the Southwest monsoon season from late May to September (Check, 1997). The Northeast monsoon winds are generally cooler and bring wet weather which may persist for several days while the Southwest monsoon season brings winds occasionally strong, often accompanied by heavy rain and thunder (*ibid.*). The nature of Singapore's rainfall is thus conducive to frequent short-term flooding.



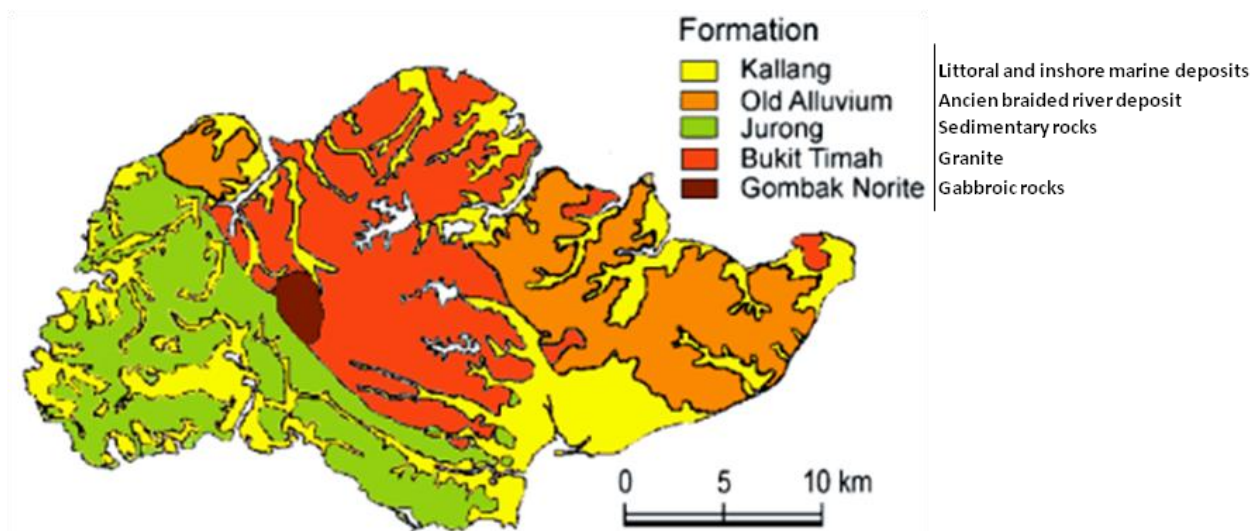


**Figure 2. Climatograph of the Changi climate station, Singapore** (constructed from data of the National Environment Agency (2011). Rainfall period of record: 1869-2010, temperatures period of record: 1929-1941, 1948-2010)

#### 2.1.4. Geology and soils

Singapore comprises mainly sedimentary rocks of the Jurong Formation containing six sedimentary facies (Triassic to Early Jurassic), granite and granodiorite rocks of the Bukit Timah Granite Formation (lower-mid Triassic age), coarse sand-gravels interpreted by Gupta *et al.* (1987) as being the proximal facies of an ancient braided river deposit and referred to as the Old Alluvium (Pleistocene) as well as Holocene alluvial, littoral and inshore marine deposits forming the Tekong and the Kallang formations (Public Works Department Singapore, 1976). The igneous rocks consisting of the Bukit Timah granite occupy the north and central-north region of Singapore, the sedimentary rocks of the Jurong formation occupy the west and southwest region, the Quaternary deposit of the Old Alluvium lies in the eastern region and the recent deposits of the Tekong and Kallang formations are distributed throughout the island (figure 3).

Due to the particular climatic and topographic conditions, the rocks are deeply weathered and the drainage has reached the point where the rivers are of low gradient with a mature profile (Public Works Department Singapore, 1976). The average thickness of weathering profiles over igneous rocks is 10 to 20 m (Pitts, 1994). The upper portion consists of clayey silt soils while the lower section consists of completely weathered granitic rocks (Rahardjo *et al.*, 2004). The sedimentary Jurong formation has a degree of weathering which is variable, and which normally depends on the parent rock types such as mudstone, siltstone and limestone (*ibid.*). Weathering profiles over the Old Alluvium rarely exceed 6-7 m and consist mainly of clayey silty sand (Pitts, 1994). Gupta (1982) indicated that sediment produced over most of Singapore is generally in the medium to coarse sand class along with a small portion of silt and clay.



**Figure 3. Simplified geological map of Singapore** (modified from Rahardjo *et al.* (2004), p.158)

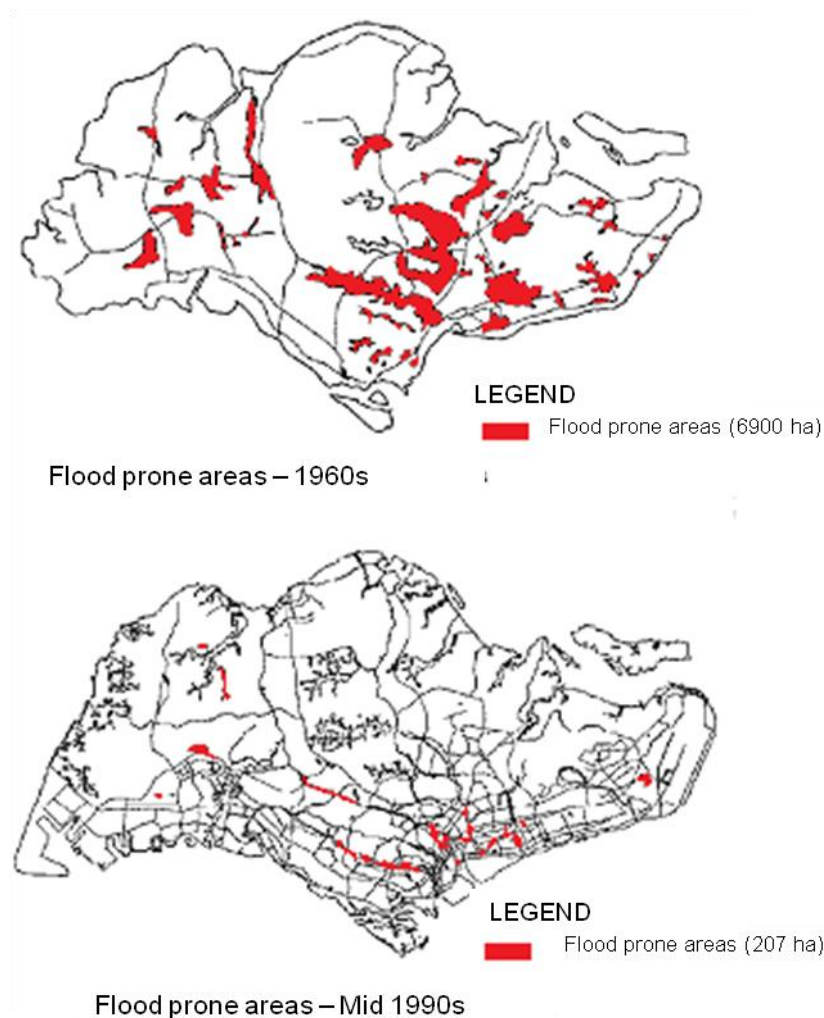
### 2.1.5. Flood propensity

Singapore has a long history of flooding. The natural physiography and climate of the country result in frequent flooding due to the high volume and intensity of rainfall, the undulating topography with breaks in slope between the hillside and the valley floor, and the low altitude of the country (Gupta, 1982). Although the flood potential of the island has always been high, urbanisation has triggered a considerable growth of its flood propensity since the 1960s-1970s. According to Check (1997), the old drainage systems have always been inadequate to drain away storm water runoff but it is the new land developments of the 1970s that aggravated the flooding problem in Singapore. From this time, urbanisation reduced ground infiltration, natural storage and shortened the time of flow concentration resulting in changes in the hydrological characteristics (*ibid.*).

However, the urbanisation of the island involved drastic transformations of the drainage system from a pattern of natural streams and rivers into a network of concrete-lined drains and canals. Logically, the increase in urbanisation required that the drainage system keep up with the increasing runoff generated (Ching, 1997). In the 1960s, about 13 % of the island was susceptible to severe flooding, associated with inadequate drainage systems and the low-lying nature of the built-up areas (Check, 1997). During this period, drainage matters came under the centralised control of authorities. The problem of flooding has been more or less eliminated with the prompt improvements of the drainage system (Ching, 1997) (figure 4). Today, at every stage of any new development proposal, the Drainage Department is consulted to implement control strategies. The implementation of drainage development schemes is consequently more efficient than before. Flooding is alleviated in several ways: elevation of areas below flood levels prior to construction, sufficient systems of drains, rooftop detention, and porous pavements, for example. Drainage channels in Singapore are planned on the basis of a 5-year recurrence interval (PUB, 2010).

Nevertheless, flooding remains a recurring problem for several parts of Singapore, especially the Bukit Timah catchment. In fact, in the context of rapid environmental modification, recurrence

intervals change rapidly. Therefore, a good drainage condition may become inadequate in time, thus requiring re-designing of drainage channels (Gupta, 1982).



**Figure 4. Flood prone areas in the 1960s (6900 ha) and mid 1990s (207 ha)** (Modified from: Check, 1997, p.185)

## 2.2. Upper Bukit Timah Catchment

### 2.2.1. Location

The Upper Bukit Timah subbasin<sup>1</sup> is located in the central part of Singapore (figure 5). This subcatchment occupies an area of approximately 6.8 km<sup>2</sup> and is roughly circular in shape. It constitutes a worthwhile case study since five rain gauge stations and three gauging stations are present within the basin. Unfortunately, all these data were not available for this study because of the non-cooperation of the authorities in charge of these stations. The general pattern of Singapore's climate described above persists but the annual rainfall of the Upper Bukit

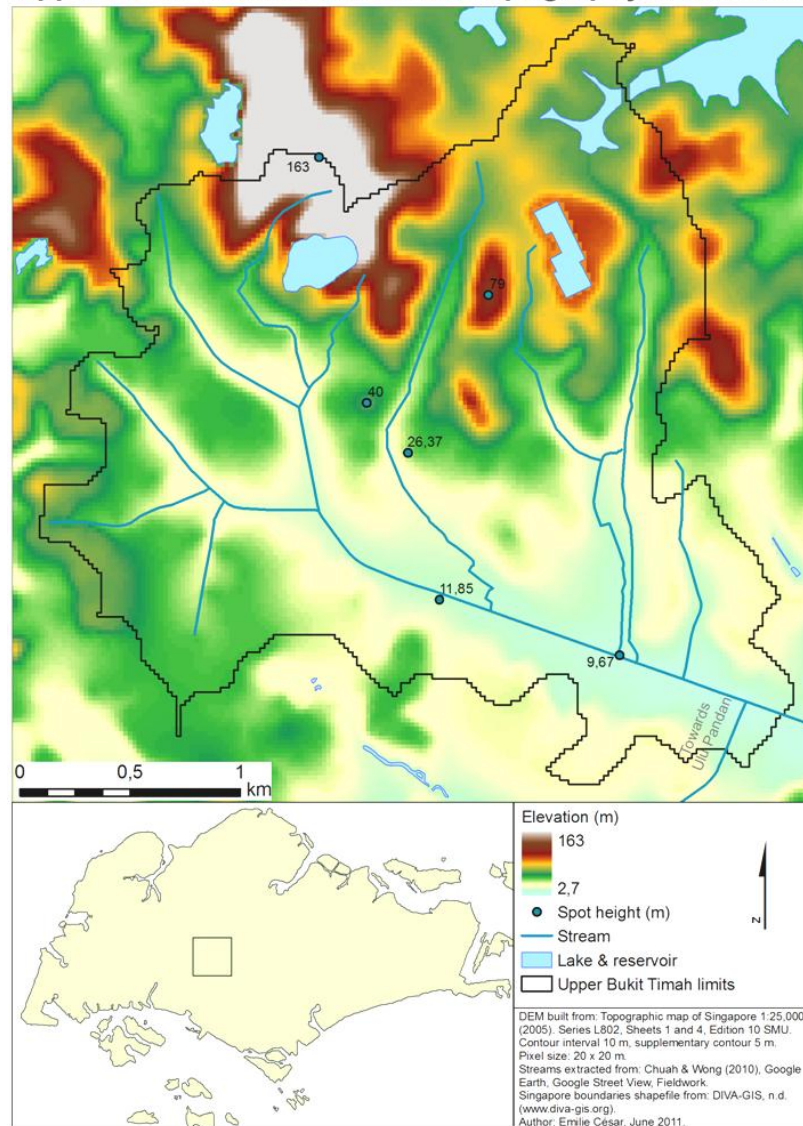
<sup>1</sup> Although the Upper Bukit Timah basin is only a part of the Bukit Timah catchment, it is suitable to use only the upstream part of the whole watershed because part of the water is diverted to the neighboring Ulu Pandan Valley at the outlet (appendix 2). Consequently, the term « catchment », « watershed » or « basin » will be used instead of « subcatchment », « subwatershed » or « subbasin » in the following pages.

Timah basin is around 2400 mm (Gupta, 1994). This amount, however, is not evenly distributed and there are considerable spatial and temporal variations within the catchment (Kaur, 1981). The appendix 2 contains a general map of the Upper Bukit Timah basin, showing the major roads and streams.

### 2.2.2. Topography

The relief of this catchment is not uniform (figure 5). The northeastern part of the catchment, comprising the Bukit Timah Nature Reserve, is considerably higher than the rest of the area and the slopes are steeper. The relief of the other parts of the basin is undulating with isolated low hills. The highest point of Singapore is within the basin and reaches an altitude of 163 m. The remaining of the catchment is very flat and the mean height is about 30 m above sea level. We have calculated that 70 % of the area is between 15 m and 50 m and only 2 % is above 100 m. The median slope is about 9 %.

**Upper Bukit Timah Catchment, Topography & Location**



**Figure 5. Topography and location of the Upper Bukit Timah basin**



### 2.2.3. Drainage

The Upper Bukit Timah is a part of the Bukit Timah basin. The drainage pattern is entirely man-made and constituted of drain channels of varying dimensions. The streams flow from north to south in the upper half of the catchment while the main channel flows from northwest to southeast in the lower half of the basin (figure 5).

In the early 1960s, the Bukit Timah basin was prone to severe flooding (Check, 1997). A scheme was implemented in two phases to alleviate the flooding. The first phase was implemented in 1966 when a diversion canal was constructed to divert flow toward the southwest from the Upper Bukit Timah basin to Ulu Pandan (figure 6). This constitutes the outlet of the Upper Bukit Timah catchment. This scheme was completed in 1971 (Ching, 1997). Phase 2A of the scheme, downstream from the Upper Bukit Timah basin, was implemented because of the growing flood problem of the 1980s. It consisted of building a second diversion canal to the Kallang River toward the east (*ibid.*). This phase was completed in 1990. The Upper Bukit Timah basin is currently drained at the outlet by a trapezoidal concrete lined channel with a low flow section (figure 7). This channel is being modified, its widening and deepening just upstream of the diversion is in progress (Wei, 2011). It begun in late November 2011 and is targeted to be completed by the end of 2012. This concerns a 600 m section and is the first stage of an overall drainage scheme to improve the Bukit Timah First Diversion Canal (bukittimah.net, 2011). Thus, the two major methods of flood control in Singapore, namely the increase of drainage capacity and the diversion of flow from a channel to a separated outlet (Gupta, 1982), are illustrated in the Upper Bukit Timah basin.



**Figure 6 (left). Diversion of the Bukit Timah Canal towards Ulu Pandan (17/09/10)**  
**Figure 7 (right). Bukit Timah Canal at the intersection of Bukit Timah road and 6<sup>th</sup> Avenue (02/10/10)**

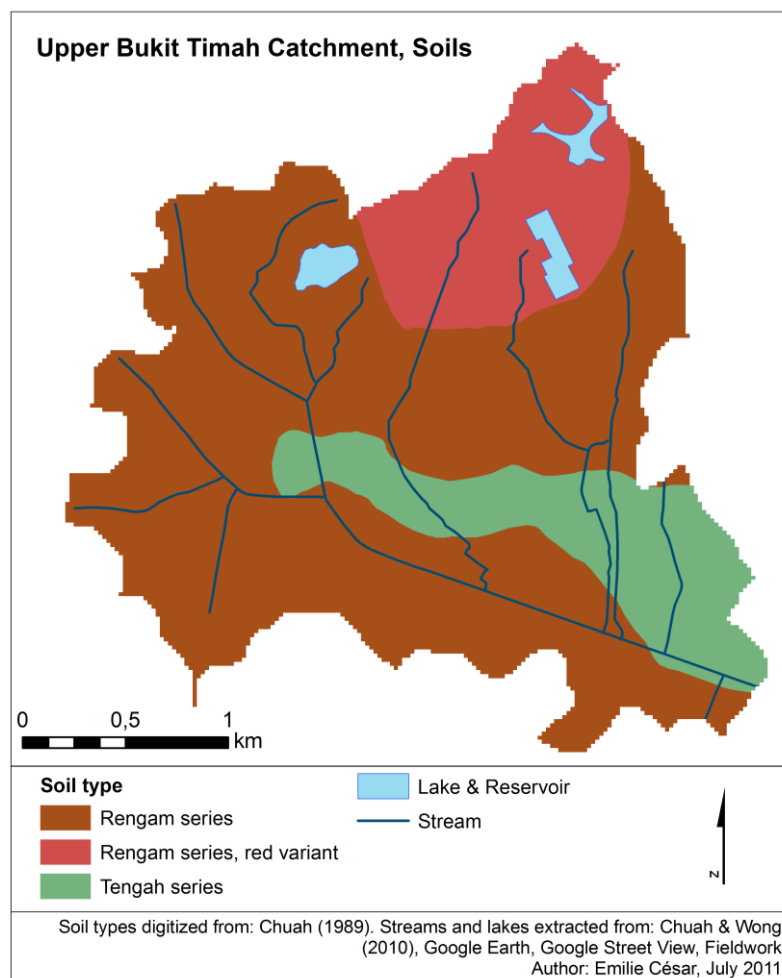
### 2.2.4. Geology

Essentially, the catchment can be divided into two geological units: the granite and recent alluvial deposits. In general, apart from the valley-floor, the Upper Bukit Timah consists of

granitic hills. The term “granite” includes granite and associated igneous rocks such as granodiorite (Chuah, 1987). The Bukit Timah granite belongs to the mid-Triassic. It is undoubted that the geology of this basin influences the relief and the land use associated with it.

### 2.2.5. Soils

Two soil units are developed over both dominant geological units: the Rengam and Tengah series (Chuah, 1987). Chemical weathering in the Upper Bukit Timah catchment is intense and rapid and has given rise to thick regolith (*ibid.*). The Rengam series is dominant and it has a red variant in the northern part of the basin. Soils of the Rengam series are well drained and the topsoils have textures consisting in sandy loam while the deeper subsoils consist in fine to coarse sandy clay. The red variant, however, has coarse textures even near the surface (Chia, 1979). The topsoils have a depth of about 10 to 20 cm (Chuah, 1987). Soils in the Tengah series are extremely variable in texture and appearance. But, generally, they consist in a dark, loamy horizon over a heavy, grey clay or silty loam (*ibid.*). Their drainage is relatively poor compared to the Rengam series (*ibid.*). Figure 8 represents the different soil types covering the basin.



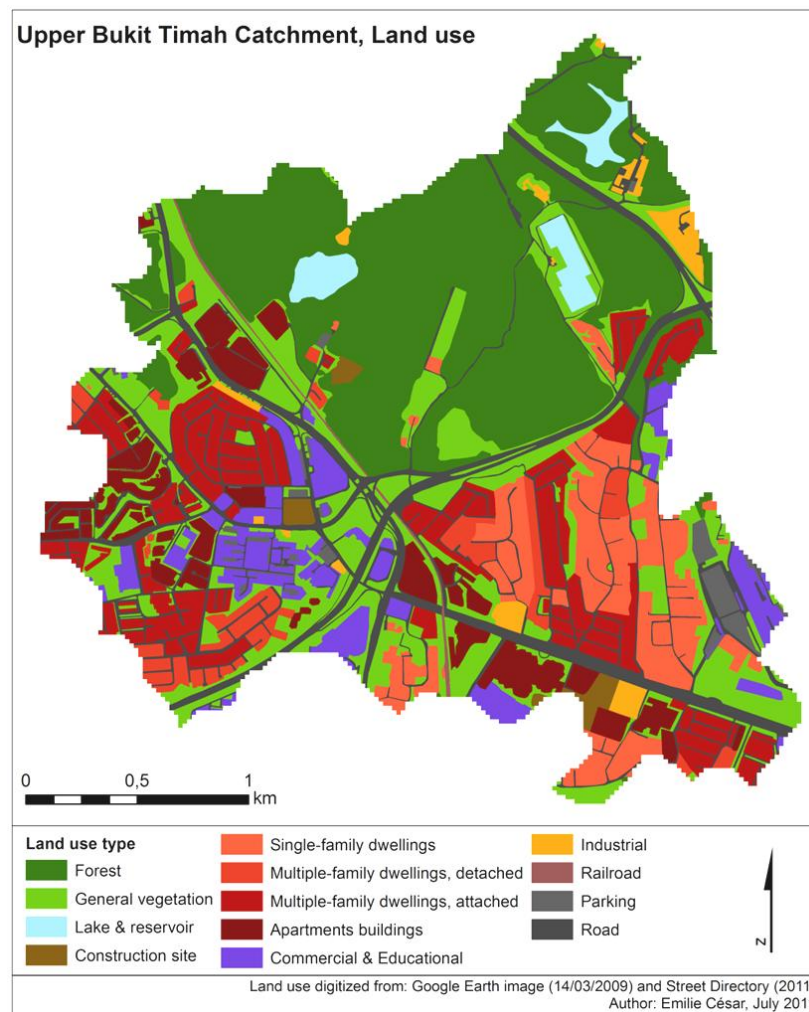
**Figure 8. Simplified soil map of the Upper Bukit Timah catchment**

### 2.2.6. Land use

Originally confined to the main valley floor or the lower slopes, the urban development has moved up the tributary valleys (Gupta, 1994). This has led to accelerated localised slope failure, excessive sediment production and increased flooding of the Bukit Timah valley floor (*ibid.*).

Although the higher northern parts of the basin are still covered by rainforest, the rest of the basin is urbanised. It has been calculated that 30 % of the basin is forested, but the Bukit Timah Nature Reserve only covers an area of 75 ha. General vegetation consists in parks, grass, green spaces and open spaces. It is dispersed throughout the catchment. It constitutes 18 % of the Upper Bukit Timah basin. The valley floor is crossed from northwest to southeast by one of the major roads of Singapore: the Bukit Timah/Dunearn road. The north-eastern part is also crossed by some important roads: the Upper Bukit Timah road and the Jalang Jurong Kechil (see appendix 2). This is a commercially developed area. Personal calculations have shown that the highest impervious surfaces, namely roads and car parks, cover 13 % of the catchment. Single-family dwellings, consisting of houses surrounded by a small, open space, are mainly found on the north of the Bukit Timah/Dunearn road, as in the past. Other types of dwellings are situated throughout the basin. The residential function occupies 28 % of the catchment.

Figure 9 shows a map representing the present land use of the Upper Bukit Timah catchment.



**Figure 9. Land use of the Upper Bukit Timah basin**

## **2.3. Hypotheses**

This study attempts to model the rainfall-runoff relationships in the Upper Bukit Timah catchment in Singapore in order to highlight and quantify the effect urbanisation has on runoff. The SWMM model is used mostly used. The purpose of this study is to verify the two following hypotheses:

- It is possible to model an urbanised catchment with little data. Working with “free” data is not an easy task. It will be shown how to use them and integrate them into the SWMM model. Then, the watershed model will be verified using as more as possible available data. The strategy and methodology to build a correct model from data of a variety of sources will be presented and details about all manipulations will be found in the tutorial in order to help future user to repeat the same steps.
- There is a link between runoff and urbanisation for the Upper Bukit Timah basin and it is possible to quantify this relationship as well as identify runoff producing areas with the model previously built. The basin has undergone rapid urbanisation during the last few decades. A diachronic analysis will be presented in order to show the evolution of the basin in terms of imperviousness and linked runoff and discharge. The runoff-producing zones will be underlined using the model potentialities.



### 3. LITERATURE REVIEW

This chapter first gives a short overview of different key-concepts that need to be understood before getting started with the modelling of an urban catchment. It then presents the general changes in the physical environment in relation to urbanisation before detailing the works about impacts of land use changes on geomorphology in Singapore. Next, the flood prone nature of Singapore and Bukit Timah basin is highlighted through the presentation of several works. The studies undergone about physical geography of the Upper Bukit Timah catchment are presented in the following section. Finally, watershed models are overviewed and the different works about the modelling of the Upper Bukit Timah basin are briefly explained.

#### 3.1. Concepts

The term « hydrology » names the « *science that encompasses the occurrence, distribution, movement and properties of the waters of the earth and their relationship with the environment within each phase of the hydrologic cycle* » (USGS, 2011). Penman (1961 cited in Singh and Woolhiser, 2002, p. 270) simplified the definition of « hydrology » as the science that attempts to answer the question, « what happens to the rain »? This seems to be a simple question, but the hydrological response of a basin may be difficult to determine due to the heterogeneity of the land surface, soils, vegetation, land use, etc. as well as the variability in inputs over the scales of time and space (Cantone, 2010).

The term « watershed hydrology » was defined by Singh and Woolhiser (2002) as the « *branch of hydrology that deals with the integration of hydrological processes at the watershed scale to determine the watershed response* ». Cantone (2010) defined « urban hydrology » as the « *branch of hydrology that deals with the integration of hydrological and hydraulic processes at the urban scale to determine watershed response* ». Hydrologic processes and their spatial non-uniformity are defined by climate, topography, geology, soils, vegetation, and land use and are related to the basin size (Singh and Woolhiser, 2002). Hydraulic processes define the mechanisms that take place in the river channel, pipes, pumps etc. and that can be quantified by the mechanical properties of liquids. « Urban hydrology » is therefore a branch of « urban geomorphology ». This term has been defined by Gupta and Ahmad (1999) as the part of the geomorphology that « *combines the ambient geology, landforms, and geomorphological processes with the evaluation of impacts brought to these by urbanisation* ». According to Chengtai (1996), the urban geomorphological environment can be divided into three parts: physical landforms (not or hardly built by human activities), artificial landforms (man-made architectures) and physic-artificial landforms (formed in varying degrees by human beings). Studies in urban geomorphology encompass different topics in a wider range than urban

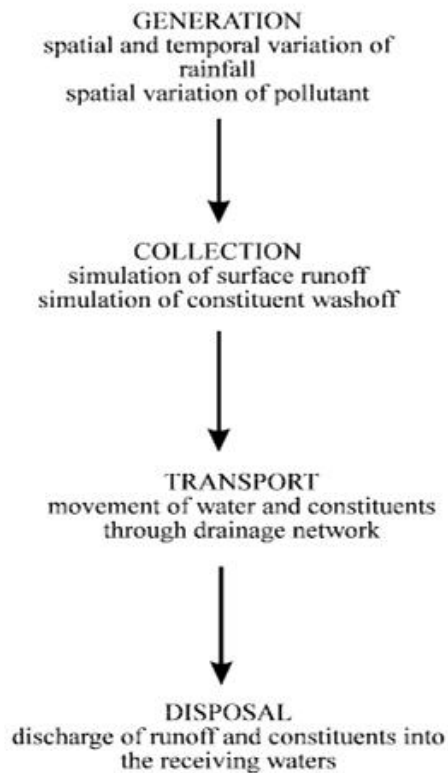
hydrology such as slope instability, seismic hazards, increased flood problems and land subsidence.

There are essential differences between natural and urban watersheds. Land surface characteristics represent the key physical distinction between the two: urban catchments tend to be highly impermeable (predominant land use is residential, commercial and industrial); natural watersheds tend to be highly pervious (land use is dominated by pastures, crop land, etc.) (Cantone, 2010). Moreover, urban catchments typically encompass a smaller range of space scales (of the order of hectares or square kilometres) (*ibid.*). Due to these characteristics, natural watersheds can have time scales ranging from minutes to years while urban catchments typically have time scales lying between minutes and hours (*ibid.*).

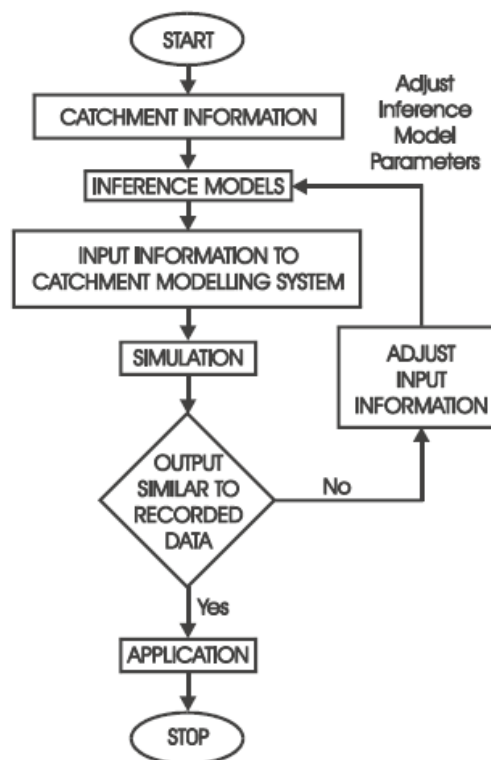
In 2008, the U.S. Environmental Protection Agency (EPA) defined the term « model » as a physical representation of natural systems, with or without a series of mathematical equations (mathematical models). The processes included in a watershed model can be complex and may require knowledge of several ongoing systems. Including all processes which influence the response of the system to the various climatic conditions is not possible since generation and transmission of surface runoff require complex mathematical description and data available to define the parameters are limited in both space and time (Choi and Ball, 2002). As a result of these limitations, simplifying assumptions are made and the real situation is idealised (*ibid.*). A typical watershed model can be divided into four conceptual modules, which are represented in figure 10: first, the spatial and temporal variation of the water is represented (*generation*); then, the model predicts the temporal variation of the quantity and quality of storm water at the entry points of the transport module (*collection, hydrologic component*); next, the quantity and quality of storm water is routed through the links in the drainage system (*transport, hydraulic component*); finally, the storm water is discharged into the receiving water (*disposal*). According to Cantone (2010), there is a principal difference when considering a natural watershed or an urban catchment. For the former, all of the hydrological processes may be accounted for in the hydrologic model while for the latter only subsets of these hydrological processes are generally considered (precipitation, infiltration excess, overland flow and channel flow).

The steps to follow in hydrological modelling were reviewed by Blöschl and Sivapalan (1995). These ones constituted a basis for this study. They are illustrated in figure 11 and consist in:

- collecting and analysing data;
- describing the important hydrological characteristics of the catchment (drainage network, topography, soils, imperviousness, etc.) and determining various parameters from these characteristics;
- translating these data into a mathematical model;
- calibrating the model to fit real data by adjusting various inferred parameters, which are parameters determined from the application of the model, contrarily to the measured parameters;
- applying the model.



**Figure 10. The four conceptual components of a watershed model** (Source: Choi and Ball, 2002)



**Figure 11. Procedure to follow in hydrological modelling** (Source: Choi and Ball, 2002)

### 3.2. Urbanisation versus physical environment

This section presents a theoretical statement of the impacts of urbanisation on hydrologic and geomorphic processes and details the works concerning the effects of urbanisation in Singapore.

The urbanisation of a watershed triggers significant changes in geomorphic processes (Gupta, 1994). There are three different stages, constituting the Wolman's time-sequence:

- Pre-urbanisation: natural vegetation or agriculture, channels adjusted to existing conditions;
- Construction: very high increase in erosion during a brief period of time, channels in disequilibrium due to the high amount of sediments reaching drains;
- New urban landscape: impervious surface, concrete storm drains and sewers, increase of floods frequency, diminution of sediment supply, channels still in disequilibrium that may or may not adjust to the changed environment.

The resulting changes in the nature of the hydrologic environment due to urbanisation can be regrouped into three categories (Gupta, 1994).

- hydrological changes:  
Development of an urban area involves covering the surface with imperviousness, which increases the amount of surface runoff due to a lower infiltration and removal of vegetative cover (Leopold, 1986). It thus results in an increase the total volume of water in the channel while the amount of water available for ground water storage is diminished (*ibid.*). The rate at which water is transmitted to stream channels is higher, as surface runoff travels quicker over impervious surfaces and through drains that it does in natural conditions. The consequence is a rise in the frequency of floods. Finally, the rapid runoff of storm water causes pollutants to be washed off the surface.
- morphological changes:  
The changes of the flow characteristics listed above cause adjustments in the stream channels to accommodate the flows (*ibid.*). The larger volume, velocity and duration of flow cause higher erosion, resulting in an enlargement of channels and instability of their banks.
- sedimentological changes:  
The exposure of the soil during construction triggers more effective erosion which results in the deposition of sediments in the channels (Gupta, 1994). This stage is followed by a diminution of sediment yield when the urban landscape is set up.

Chatterjea (1989) quantified the changes occurring during the three stages of the Wolman's sequence over several areas in Singapore. He presented an overview of the sequential changes in the nature and rates of fluvial and slope processes that take place in Singapore, leading to environmental changes of both temporal and spatial types. Data were obtained from field studies on three different sites: forested hillslopes, bare sites under construction and urban concrete or grass covered slopes. This was done in order to observe the impact rainwater has on soil moisture conditions, surface microtopography, runoff generation, sediment movement, and

ground lowering. He found that the primary natural conditions are altered when areas are cleared for construction leading to the development of gullies, augmentation of erosion, high runoff generation and high sediments release. With increasing urban development, this highly erosive phase changes and accelerated erosion is replaced by frequent floods from the impermeable surfaces.

One of the first observations on the effects of urbanisation on runoff in Singapore has been done by Gupta (1982). According to him, the proportion of catchment urbanised, the size of the drainage basin and the nature of rainstorms are the three principal factors controlling the effects of urbanisation on stream generation and channel characteristic. The impacts are most pronounced on a small channel draining a small catchment (*ibid.*). They are also heightened by the occurrence of intense rainfall of limited duration the presence of some relief and of storm sewers (*ibid.*). Therefore, urbanisation in Singapore has led to a rise in flood frequency and channel degradation. The factors cited below are found in the Upper Bukit Timah catchment. The area is therefore manifestly suitable for studying the effect of urbanisation on runoff since the extension of impervious surfaces, establishment of storm sewers and lining of drainage channels are happening at a great speed.

Gupta (1982 cited in Gupta, 1982, p. 143) examined the intensity of land use changes in a part of the Bukit Timah basin by mapping repeatedly the area according to several categories (open space, construction areas and different classes of built-up areas). A one year time-sequence of land use changes in this area has been created for the period from August 1981 to December 1982. He concluded that the open space is representative of the pre-urban environment, where only large storms would involve serious flooding and sediment loss. The construction areas provide a high quantity of sediment and after a certain time would create flooding downslope as a result of the blockage of certain channels caused by sediment build-up and the sealing of pores in the exposed soil surface by rainsplash. Some built-up areas allow 90 % of the rainwater to reach a drainage channel via surface runoff. Single-family dwellings, constituted of houses surrounded by a green space, probably have a hydrologic environment approaching that of the open space. Gupta showed that there were noticeable local variations in runoff and sediment production in a given area at a certain time and that these changed over time. Unfortunately, he did not specify the changes in the quantity of runoff and sediment over the period studied. He asserted a progressive increase in runoff from this part of the Bukit Timah basin in the future. In order to estimate the effect of denudation through time over this area, long term measurements of runoff and change in land use are necessary. However, it is usually not available for most areas (Gupta, 1982).

The physical adjustments in response to the urbanisation of Singapore have been underlined in a book edited by Gupta and Pitts in 1994. This book covered a wide variety of themes, from the landscape change to the evolution of the country during the Quaternary through the changing vegetation and the newly reclaimed land or the stability of slopes. Gupta (1994) has devoted a chapter to floods and sediment production in Singapore. According to him, the flood propensity has been increased considerably by the urban growth associated with the expansion of impervious areas and the establishment of storm drains. The main channel, connected to such drains, is therefore incapable of carrying all the contributed water arriving rapidly. In order to

overcome the problem, the solution of temporarily detaining the water at various points throughout the catchment is implemented (*ibid.*). Certain areas of Singapore, like the Bukit Timah Valley for example, have been more flood prone than others, mainly due to physiographic reasons (*ibid.*). The location of arterial roads in the valley bottom, the Bukit Timah Road for example, highlights the flood prone nature of the environment. The Bukit Timah catchment is therefore an interesting area to focus on.

### **3.3. Floods propensity**

Flooding has always been an issue in Singapore. Several specific works on floods in Singapore have highlighted the flood prone nature of Singapore and the Bukit Timah catchment particularly. They are cited below.

A general appraisal of floods in Singapore was undertaken by Foo in 1986 in order to provide a comprehensive overview of the flood problem in the country. It analysed the man-flood hazard relationship by describing and analysing the effects, causes and characteristics of floods as well as the responses to the flood hazard (structural and non-structural adjustments) and the future scenario of the flood problem in Singapore. A special reference to the Upper Bukit Timah catchment has been made. He estimated that the frequency of flooding in the catchment has been increasing. This bachelor dissertation did not provide any statistical analysis; it was more concentrated on a review of the literature.

In this context, Ching (1997) studied the drainage canals in Singapore and evaluated the developments of a drainage system through time for flood control as well as other uses. This exercise sought to overview the history of the drainage canal network, to evaluate the design and efficiency in disposing excessive runoff of such drains and to discuss the aesthetic treatment of the drainage canals and their utilisation beyond flood control. This work did not bring a quantitative assessment of the effects of the drains on the urban environment. It constituted a descriptive appreciation of the history of drainage canals and the perception people have of them.

Simultaneously, Check (1997) presented a paper dealing with the strategies adopted by Singapore's government to keep the flood situation under control despite the new developments that are continuously taking place. It discusses the drainage development programmes that were implemented for flood mitigation. It gives a good general overview of the flood situation and also explains the Bukit Timah Flood Alleviation Scheme, a plan describing the strategies setting up to prevent flooding in the Bukit Timah Basin.

Nevertheless, it is important to keep in mind that, according to Gupta and Ahmad (1999), the geomorphological problems (floods and landslides particularly) in Singapore are small-scale, almost entirely anthropogenic, and successfully managed. Effectively, the city enjoys efficient technical and managerial capacities. Financial resources are available to face geomorphology hazards. According to these authors, although urbanisation brought in impervious cover on the slopes and conversion of the floodplain wetlands into arterial roads next to a channel, flood alleviation in Singapore managed to keep up with the urbanisation of the valleys and flooding

has a low destructive component. On the other hand, the frequency of such disruption to normal activities is high (Gupta, 1994).

Gupta (1994) reported three major floods with great consequences in past flood records. The first happened the 9<sup>th</sup> and 10<sup>th</sup> of December, 1954, when about 25 km<sup>2</sup> or 3.6 % of the island was under water. The next major flood happened the 9<sup>th</sup> and 10<sup>th</sup> of December, 1969, when 27.5 km<sup>2</sup> were inundated after 467 mm of precipitation in one day. The flood of the 2<sup>nd</sup> and 3<sup>rd</sup> of December, 1978, was triggered by 512 mm of rainfall in 24 hours and affected 32 km<sup>2</sup>. This is the highest rainfall recorded in Singapore over a period of 24 hours (Straits Times, 2010). Since the publication cited above, some 366 mm within one day fell on December 19<sup>th</sup>, 2006, which resulted in massive flooding (*ibid.*). The flood of November 19<sup>th</sup>, 2009, was also reported as one of the worst floods and was triggered by 92 mm of precipitation within 30 minutes (PUB, 2009 cited in Channelnewasia, 2009). More recently, the flood of the June 25<sup>th</sup>, 2011, triggered by 65 mm of precipitation within 30 minutes, caused damage in several areas of the island (Channelnewasia, 2011). PUB, Singapore's national water Agency, said it was the worst flood since 25 years (*ibid.*).

### **3.4. Urban hydrology of the Upper Bukit Timah basin**

The Upper Bukit Timah basin is one of the few areas in Singapore that has been widely researched upon, especially with respect to the physical geography of the area. According to Gupta (1994), it is a worthwhile case study of flooding in Singapore's watersheds. Since the land use of the watershed has changed strikingly since the 1950s, the basin provides good examples of flood increases following urbanisation. In fact, the percentage of forest cover has decreased from 10.91 % in 1950 to 8.36 % in 1986 and grass and open space fell from 68.05 % in 1950 to 29.24 % in 1986 (*ibid.*). On the other hand, the percentage of built-up areas has increased from 12.94 % in 1950 to 48.92 % in 1986 (Chuah, 1987). The percentage of built-up areas today is even higher still and will be illustrated in this work. The main canal has undergone many transformations since the 1960s to overcome the increase of urbanisation (Gupta and Ahmad, 1999).

In 1981, Kaur realised an exercise regrouping five methods to estimate the runoff from rainfall data in the Upper Bukit Timah Basin. These methods were direct correlation, Rational formula, unit hydrographs, water budgeting and computer simulation. The increase in the runoff-rainfall ratio between the periods of 1969-1973 and 1978-1980, associated with the increase of the built-up area and the decrease of vegetation, has been calculated. This ratio grew from 54.52 % to 59.44 % for the two periods respectively. This trend of increase in runoff has also been reflected in the 45 minutes duration unit hydrograph where an increase in discharge from 13 m<sup>3</sup>/s to 15 m<sup>3</sup>/s has been observed for the periods 1969-1974 and 1976-1981 respectively. He found that in most cases, the methods used provided a fairly good estimate of the runoff volumes. An identification of critical parameters in each technique has underlined the careful consideration in the selection of these parameters when estimating runoff.

Research on the hydrological impact land use changes has on runoff in the Upper Bukit Timah basin was done by Chuah in 1987. The first part of her exercise was an attempt to analyse the changing land use in the Upper Bukit Timah basin, in terms of increase in impervious area for the period 1950-1986. She used the topographic maps and aerial photographs of the region. Then the relation between the changing land use and the change in runoff in terms of peak discharge and time of concentration was established, using the Rational formula. This method estimates the peak runoff  $Q$  from only three parameters: the watershed area  $A$ , the runoff coefficient  $C$  and the storm intensity  $I$ . Her analysis showed that the average coefficient of runoff  $C$ , depending on the land use, gradually increased from 0.55 in 1950 to 0.65 in 1980 and the time of concentration decreased from about 100 minutes to 60 minutes during the same period of time. Consequently, she discovered an increasing trend of the 5-year peak discharge since 1950: 73 m<sup>3</sup>/s in 1950, 78 m<sup>3</sup>/s in 1959, 79 m<sup>3</sup>/s in 1973, 82 m<sup>3</sup>/s in 1980 and 91 m<sup>3</sup>/s in 1986. It is important to note that the Rational formula is the simplest way to determine the peak runoff and is not the best in the field. However, according to Gupta (1994), given that the data available are not rigorous and the drainage basin is small, it is perhaps the most appropriate technique to obtain suitable peak discharge estimations.

In 1990, Rahman underlined the hydrological processes under changing land use in humid-equatorial conditions with a special focus on the Upper Bukit Timah. His article presented the results of different studies (Chia (1979), Kaur (1981), Foo (1986), Chuah (1987), cited here).

### **3.5. Urban watershed models**

According to Singh and Woolhiser (2002), watershed models are employed to understand dynamic interactions between climate and land-surface hydrology. They are used to plan, design, and operate projects, to conserve water and soil resources and to protect their chemical and biological qualities. They are fundamental to assess, develop, and manage water resources (*ibid.*). According to Jacobson (2011, in press), urban watershed models provide powerful tools to inform management decisions about how changes in urban basins will impact flows and to assess the likely impacts of climate change and changing rainfall patterns on urban runoff. Research is needed to improve our understanding of the changes linked to urbanisation in urban catchments, and to develop planning strategies in order to minimise the impact of future urban growth (*ibid.*). This section discusses the choice of taking SWMM and HEC-HMS to model the Upper Bukit Timah. Then, it reviews the different models implemented on this basin over the past decades.

In their article, Singh and Woolhiser (2002) discussed new developments and challenges in watershed models. According to them, the SWMM model, a dynamic rainfall-runoff simulation model that computes runoff quantity and quality from primarily urban areas, was one of the earliest models developed and is currently a widely used model throughout the world. HEC-HMS, a model designed to simulate the precipitation-runoff processes of watershed systems in a wide range of geographic areas, is one of the most commonly used watershed models in United States (*ibid.*). Among the watershed models identified by Singh and Woolhiser (2002), SWMM and HEC-HMS are most commonly used for urban catchment hydrologic modelling. Gironás *et*



*al.* (2009) published a manual regrouping some examples illustrating how the SWMM model can be used to model some of the more common types of storm water management. The manual highlighted the main applications of the watershed model: it could compute runoff for both pre- and post development conditions as well as analyse the hydraulics of simple collection systems, simulate the build-up, washoff, transport and treatment of stormwater pollutants and so on. Likewise, the U.S. Army Corps of Engineers published an applications guide in 2008 illustrating the wide range of applications of the computer program HEC-HMS. There are a variety of studies undertaken by this model: urban flooding, flood-frequency, flood-loss reduction, flood-warning system planning studies, reservoir design studies and so on. SWMM and, to a lesser extent, HEC-HMS models have been chosen in this study as they are adapted to the urbanised environment. They are physically based models, which means that they require a lot of subcatchments characteristics parameters to simulate runoff. Their computational methods will be discussed in chapter 5. The steps for their application cited above (figure 11) can be applied to these models.

Several models were attempted on the Upper Bukit Timah in the past. In 1975, Wong modelled the Upper Bukit Timah watershed hydrology by using a Tank model, a very simple model considered to correspond to the zonal structure of underground water. This model was composed of four reservoirs: the first one containing precipitation minus evaporation (“gain”); all of them possessing outputs, representing surface discharge, intermediate discharge, sub-base discharge and base discharge (“loss”).

In 1979, a computer simulation on rainfall-runoff relationship was carried out by Chia. The basin hydrological cycle was conceptualised as a deterministic box cascading system. Processes included in the model were, among others, interception, infiltration, overland flow in pervious and impervious areas and evapotranspiration. These processes were coded in FORTRAN/3000. The model developed the hydrological response of the basin that generates synthetic streamflow data. This model was considered as a first approximation, as it could have been greatly improved.

In 1987, Selvalingam *et al.* published a paper on the use of RORB and SWMM models in the Upper Bukit Timah basin for the purpose of storm water drainage design and management. They presented the data preparation needed for the testing of each of the models, and discussed the limitation and constraints of the parameter estimation. They concluded that the use of the SWMM model is a good replacement for the Rational method, method currently in use by the Public Utility Board to estimate the peak runoff (PUB, 2010). According to them, SWMM is a sophisticated model capable of taking into account a large variety of parameters. This reinforced our decision to use this model in this study. Since then, the SWMM model has obviously undergone several modifications. This paper was useful since it gave us an idea of what parameters would be required for the application of the SWMM model. One hydrograph was also used in this work.

Liong *et al.* (1993) and Liong *et al.* (1991) applied the Knowledge-Based Storm Water Management Model (KBSWMM) on the Upper Bukit Timah catchment. This model regroups the calibration parameters into ‘traditional’ and ‘non-traditional’ parameters. The distinction

between the two was based on how the parameters are estimated: the former is obtained through calibration; the latter is estimated based on field measurements. The KBSWMM contains the features of the SWMM but a new calibration component (“Knowledge-Based”) is added to it. Current SWMM model does not have this special calibration component. Liong *et al.* (1993) and Liong *et al.* (1991) evaluated the model in the perspective of interactivity and presentation of data and results and the KBSWMM was considered as user-friendly. They also presented the important features of the model and highlighted their particular calibration methodology composed of eight calibration parameters and six storm events (three used for calibration, three for verification). The application on the Upper Bukit Timah catchment showed good agreement between the simulated and the measured peak flows ( $r^2 \approx 1$ ). The hydrographs and hyetographs presented in that paper were used for the verification of our model.

SWMM model does not allow automatic calibration of the parameters. SWMM users are able to compare simulation results with actual measurements but the calibration parameters have to be modified manually in order to adjust the model to reality. In 1998, Javaheri submitted a thesis on automatic calibration of the SWMM. They were based on two different optimisation algorithms (Downhill Simplex method and Shuffled Complex Evolution method). The consistency of the Shuffled Complex Evolution method in estimating the SWMM model parameters was assessed under two different scenarios: using ‘error-free’ data and using observed data. The observed data have been collected for the Upper Bukit Timah watershed by Liong *et al.* (1993). The optimisation algorithm follows several particular steps. Initially, the model calibration is done with eight parameters, using the synthetic data. Then, based on the sensitivity of these parameters, the number of calibration parameters is reduced, while still maintaining the same level of accuracy. The author found that the percentage of impervious areas and the catchment width are the two most effective parameters to use in the calibration of SWMM. The application of this method for the Upper Bukit Timah catchment showed that the Shuffled Complex Evolution method-based calibration scheme was able to provide accurate parameters.

More recently, Liong *et al.* (2002) published a paper on Genetic Programming, an evolutionary algorithm-based methodology utilised as a flow forecasting tool. Genetic Programming is a member of the evolutionary algorithm family, based upon Darwin’s natural selection theory of evolution where a computer program is progressively improved by selectively discarding the not-so-fit one. Each computer program contains different watershed parameters, varying from one program to another. The advantage of this model is that, in contrast to physically based models like SWMM which require a lot of catchments characteristics parameters, Genetic Programming only requires rainfall and runoff data. The model was tested on the Upper Bukit Timah catchment for six old events of different intensities and durations that took place between 1978 and 1987. The runoff prediction accuracy was measured in terms of root mean square error. Although the results showed a higher value of computed runoff compared to the observed data, the authors concluded that it can be a viable alternative to traditional rainfall-runoff models.

In 2003, Khu and Werner explored the possibility to reduce simulation runs for uncertainty estimation in hydrological modelling (regardless the model). They developed a hybrid genetic algorithm, just as Liong *et al.* (2002), and an artificial neural network, a computational model consisting of an interconnected group of parameters, both forming the GAANN model. This

‘pre’ model discards the parameter sets that give non-behavioural model runs before running the hydrological model. This method is applied to different cases among which we find the Upper Bukit Timah. For this basin, the procedure was tested on the SWMM model for the storm of March 2<sup>nd</sup>, 1984. According to the authors their technique reduces significantly the computational effort involved in investigating model parameter uncertainty.

Chua and Wong (2010) provided a detailed study on an event-based rainfall-runoff process simulation. Three types of artificial neural network models were used (as Khu and Werner, 2003). These are based on the association between rainfall and runoff patterns measured for past storm events to make predictions. A kinematic wave model was also developed. This model uses the kinematic wave method for routing flows through the drainage system and is based on physical properties of the catchment, as well as the determination of rainfall and losses. The point of the study was to combine the two different models in order to simulate better hydrographs. Three sets of rainfall-runoff data were used, among them one obtained from the Upper Bukit Timah catchment. The storm data used to calibrate the model dated from 1988 and 1989. It was concluded that the kinematic wave model was not able to accurately produce hydrographs. Indeed, the modelled discharges presented in the paper showed very high values compared to the measured ones. On the other hand, one of the artificial neural network models was able to produce hydrographs that were much closer to the measured hydrographs. This article provided essential information about the basin (notably drain characteristics and hydrographs).

### **3.6. Literature review conclusion**

The Upper Bukit Timah basin is a suitable area for this study for several reasons. First of all, it is a small catchment where the occurrence of floods is higher than in most of the other regions of Singapore today despite the large channel and the two downstream diversions. In fact, although the floods are generally limited in extent, numerous major floods with great impact have been recorded on this particular basin. Secondly, the area has undergone many developments in a short period of time. It is therefore interesting to quantify the effect of urbanisation on runoff in this region. Finally, the Upper Bukit Timah is a worthwhile case study which has been quite well studied over the past. Therefore, the different studies about the basin have provided essential information when the authorities did not cooperate in providing the data.

This chapter has shown that the past Upper Bukit Timah catchment studies, even the ones carried on in the past few years, concern old storms which happened in the 1970s and 1980s. It is therefore important to bring a new approach taking into account the current pattern of the area as well as some current storm events. It was also essential to use current powerful tools like watershed models to achieve the objectives. Moreover, the major part of the studies was satisfied with the development of models without any application studies. Only the works using the Rational formula tempted to quantify the link between urbanisation and peak discharge.

Models are powerful tools that provide useful information about the changes in urban catchment needed for planning strategies. The SWMM and HEC-HMS models are suitable for urban

environments. The SWMM is currently used worldwide and has been applied in the past on the Upper Bukit Timah catchment. This explains our decision to develop this model, and in a lesser extent, the HEC-HMS model. These one-dimensional models allow a huge variety of applications which cannot be understood with the Rational formula: detection of the areas which produce runoff, quantification of the discharge in each drainage canal of the catchment, modification of a variety of parameters function of the changing environment and so on.

## 4. PRE-TREATMENTS FOR DATA ACQUISITION

A large number of data is required for the application of any watershed model in order to accurately describe the complex relationships between rainfall, runoff and catchment characteristics. In this study, it was particularly difficult to obtain valuable data from the authorities or from the National University of Singapore (NUS). This chapter describes how the basic data used to determine the necessary parameters of the SWMM and HEC-HMS models (described in the next section) have been obtained. The first step consisted in the geo-referencing of the maps available. Then, a Digital Elevation Model (DEM) was created from the topographic map and the land use data was extracted from the Google Earth image. All these pre-treatments were realised in ArcMap. All technical details concerning the manipulation can be found in the tutorial.

### 4.1. Georeferencing

#### 4.1.1. Topographic sheets

The topographic map is the basis of any catchment characterisation. Unfortunately, only photos of the topographic map of Singapore were available from the National University of Singapore (NUS). There was no digital raster map available. Therefore, the first step consisted of georeferencing the available maps. All details concerning the steps to georeference images, topographic sheets and projections characteristics can be found in the tutorial. The topographic map was principally used to realise the DEM.

##### 4.1.1.1. *Rectified Skew Orthomorphic projection*

The 1:25,000 topographic map published by the Mapping Unit of the Ministry of Defence in 2005 was used. This map was chosen mainly because its scale is smaller than the other maps available, and the contour interval is 10 m, with a supplementary contour of 5 m. The projection, the Rectified Skew Orthomorphic (RSO) projection, is based on the Everest 1830 Modified spheroid. The latitude and longitude of the projection centre are respectively 4°00'N and 102°15'E. The RSO projection method is defined as oblique cylindrical (ESRI, 2009). The local shapes and angles are true and the distances are true along the centre line (*ibid.*). Distortion increases rapidly away from the central line. The use of this projection is therefore limited to areas of Borneo and Malaysia, for which the projection was developed (*ibid.*). The Everest 1830 Modified Spheroid has its origin in Central India, in Kalyanpur (Gopi, 2005). It is a local

ellipsoid, designed to match the geoid in that area. In order to georeference the photos on the basis of this projection, a ground control point (GCP) was added for each junction of the projection lines figuring on the map. A total of about 25 GCP were selected for each photo (tutorial, section 1). Once the residual errors were acceptable, the image was rectified. It was then set as the “Kertau RSO Malaya Meters” projection of Arcmap, whose characteristics correspond to the ones figuring on the map (*Define Projection* function).

#### *4.1.1.2. Universal Transverse Mercator projection*

The Malaysian coordinate system was converted into a universal coordinate system, the Universal Transverse Mercator (UTM), in order to set all the geographic data on a same universal basis (*Project* function). This was done in two steps: first, the local coordinate system RSO was transformed into the geographic coordinate system longitude-latitude (WGS 84); then, the geographic coordinate system was converted in UTM. After that, the four photos were assembled using ERDAS Imagine software. The UTM projection is a cylindrical conformal transverse projection (Donnay, 2010). The longitude of origin is the central meridian of each zone while the latitude of origin is the Equator. Singapore is situated in the UTM 48N zone, the central meridian being at 105° E.

#### **4.1.2. Google Earth image**

The last accurate Google image of the Upper Bukit Timah dates from the 14<sup>th</sup> of March, 2009. It has been projected in UTM 48 N by using 35 GCP. These GCP were taken from the Google Earth interface. This image was used to characterise the land use of the area and, to a lesser extent, to complete our database concerning the drainage network.

### **4.2. Digital Elevation Model (DEM)**

#### **4.2.1. ASTER Global Digital Elevation Model**

The ASTER Global Digital Elevation Model (GDEM) is available to users at no charge. It supplies DEM images of about 60 km by 60 km ground area which cover land surfaces between 83° N and 83° S (ASTER GDEM Validation Team, 2009). Accuracies for this DEM are 20 m at 95 % confidence for vertical data and the resolution is 30 m at 95 % confidence (*ibid.*). ASTER GDEM does contain anomalies and artefacts that degrade its overall accuracy. It is particularly the case for areas where residual cloud-related anomalies exist. The large elevation errors noticed on the area of study, in addition to the too weak resolution, were highly problematic. All tests realised in order to characterise the Upper Bukit Timah (water system extraction, watershed delimitation, slope determination etc.) using this DEM have shown incorrect results. Thus, we built an independent DEM from the topographic map.

#### 4.2.2. DEM based on topographic map

Contour lines and quoted points of the 1:25,000 topographic map of 2005 were used to realise a more accurate interpolated DEM. Waterways and lakes figuring on the map were also useful. The contour interval of the topographic map is 10 m, but supplementary contour lines of 5 m intervals are present. Still, several difficulties were encountered and are detailed below. All manipulations are explained in the tutorial.

##### 4.2.2.1. Digitisation and first surface interpolation test

Each contour line of the area containing the Upper Bukit Timah basin and a buffer zone of several hundred meters was digitised. Its value was simultaneously specified in the attribute table. Likewise, quoted points and lakes were also digitised.

The *Topo to Raster* function of Arcmap was tested on the digitised dataset. The function uses an interpolation method specifically designed for the creation of a hydrologically correct DEM from points (quoted points), lines (contour lines), and polygon data (lakes) (ERSI, 2009). At the beginning of the interpolation process, a generalised model is built on a very coarse grid resolution using information inherent to the contour lines (*ibid.*). The problem is then solved at succeeding finer resolutions, until the final user-specified resolution is obtained (Hutchinson, 1996). Starting values for each succeeding grid resolution are obtained by bilinear interpolation from the preceding coarser grid (*ibid.*). At each resolution the elevation data are simply allocated to the centre of the nearest grid cell (*ibid.*). This interpolation method is optimised to have the computational efficiency of local interpolation methods without losing the surface continuity of global interpolation methods (ESRI, 2009). *Topo to Raster* also imposes constraints on the interpolation process in order to obtain accurate drainage structure and correct representation of ridges and streams (*ibid.*).

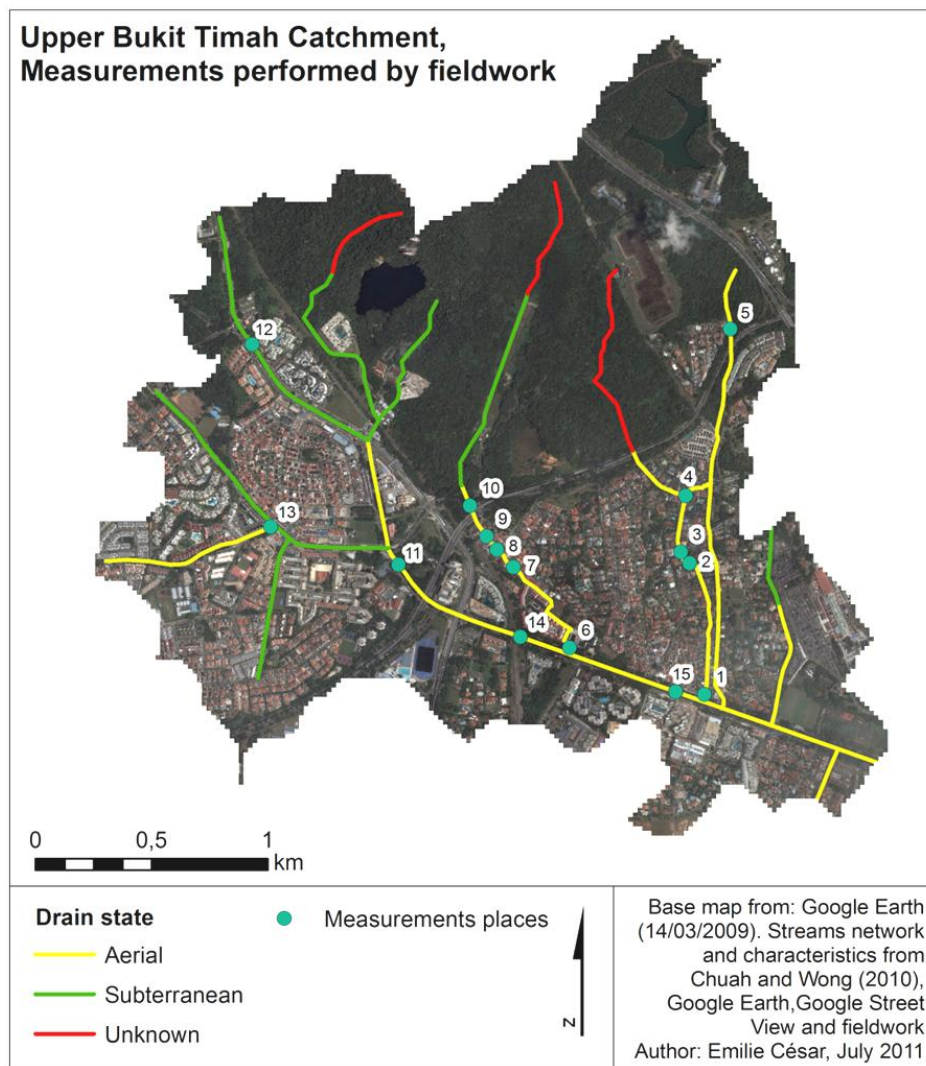
Unfortunately, the function did not provide a correct DEM. In fact, the *Flow Accumulation* function, which gives the general pattern of the stream network, showed that the waterways constructed from the DEM did not match real data. Other manipulations were necessary to obtain a correct DEM. They are described below.

##### 4.2.2.2. Streams characterisation and transformation into points

In order to constrain the DEM to accurately represent the drainage structure, the streams paths were integrated in the DEM generation process. The digitisation and characterisation of the stream network was based on the Chuah and Wong (2010)'s sketch previously georeferenced and on Google Earth imagery. The streams were characterised by their type (concrete or earth channel), state (aerial or subterranean), Manning's coefficient, length, slope, channel shape (trapezoidal, rectangular or triangular), width, depth and side slope. These data were provided by Chuah and Wong's article (2010), Google Earth, Google Street View and personal fieldwork. Figure 12 illustrates the places where field measurements have been performed, and an

illustration for some of the drains measured<sup>2</sup>. Figure 13 shows an example of the determination of the drain depth from Google Street View when more accurate data were not available.

The polylines of stream network were then transformed into points using *ET GeoWizard* in order to provide new quoted points for interpolation. One point every 50 m was created for each digitised drain of the water system. The elevation of all points was specified in the attributes table. The elevation of a first point was determined using a quoted point of the topographic map; for the remaining points, known drain depth and slopes and distance between points were used to compute each stream profile. Other points representing the drain sides were also created in order to form a 3D water system. Their altitudes were encoded thanks to the known drain depth.



**Figure 12a. Measurements performed by fieldwork**

<sup>2</sup> Measuring drains in an urban environment without high resolution field mapping devices is a difficult task. For example, the major channel in the middle of the Bukit Timah/Dunearn Road is not accessible. Only pedestrian bridges allowed a view on the channel. Moreover, several drains are subterranean, impeding field data collection. Measurements from fieldwork are therefore insufficient and the data from Chuah and Wong (2010) were used to verify ours or when field data were not available.





**Figure 12b. Photos corresponding to some of the points figuring on the map**

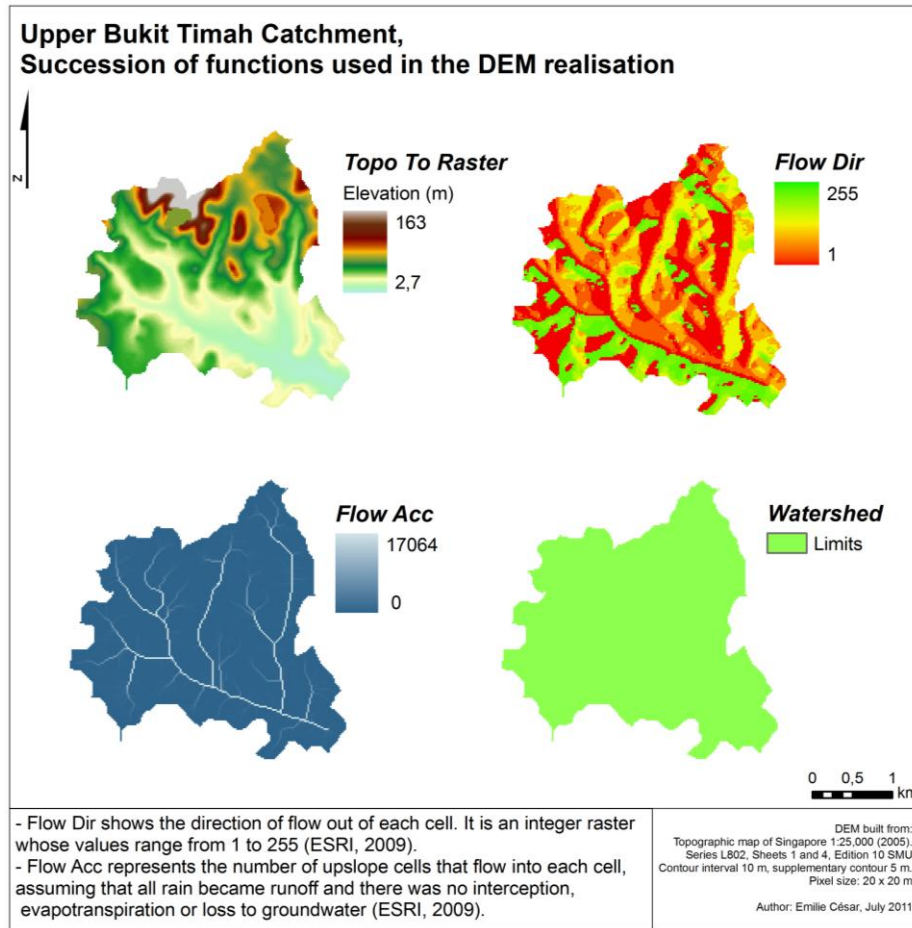


**Figure 13. Determination of the depth from steps (~ 20 cm) in Google Street View**

#### 4.2.2.3. *Final DEM*

Using the digitised contour lines, quoted points and points forming the water system in 3D, several tests were first performed using the TIN interpolation. TIN is made up of triangular facets built following the Delaunay's criteria (Donnay, 2010). Each apex of a triangle is made of quoted points. Therefore, this interpolation method gives exact results for each quoted point. It was decided not to use it since it only gave accurate results for the areas surrounding the drains.

About forty tests were realised with the *Topo to Raster* function. Each test was a succession of different functions, as illustrated in figure 14. At the end of each test, the hydrological consistency of the model was checked. Between each test, the resolution was changed and contour lines were redigitised or deleted. Also, a new sample of points forming the water system was created; the distance between them being set at 5 m instead of 50 m. The altitude of the points forming the drains was extracted from the TIN since it gave good results along the drains. Finally, the *Flow Acc* and *Watershed* functions showed a realistic look after the test of the *Topo to Raster* function with some contour lines modified, with quoted points and newly created points used as inputs. A hydrologically-correct DEM was constructed, with a resolution of 20 m.



**Figure 14. Succession of functions used in each test for the DEM realisation. These are the results of the final interpolation.**

#### 4.2.2.4. Evaluation of the DEM

The most common evaluation of the quality of the output DEM is to create contours from the new surface and compare them to the input contour data (ESRI, 2009). Although the contour lines of the new DEM were not strictly identical to the actual ones, they were closed from each other and were therefore considered realistic. An example of comparison of the contour lines is shown in the tutorial, section 2.

According to ESRI (2009), another common method for evaluating the quality of an interpolated surface is to subtract the height of the known quoted points after generating the surface. It is therefore possible to examine how closely the new surface represents the true surface. These differences can be used to calculate the RMS error, a common measure of the differences between modelled values and actual values. It is expressed as:

$$RMS\ error = \sqrt{\frac{\sum_{i=1}^N (p_i^{interpolated} - p_i^{real})^2}{N}} \quad (1)$$

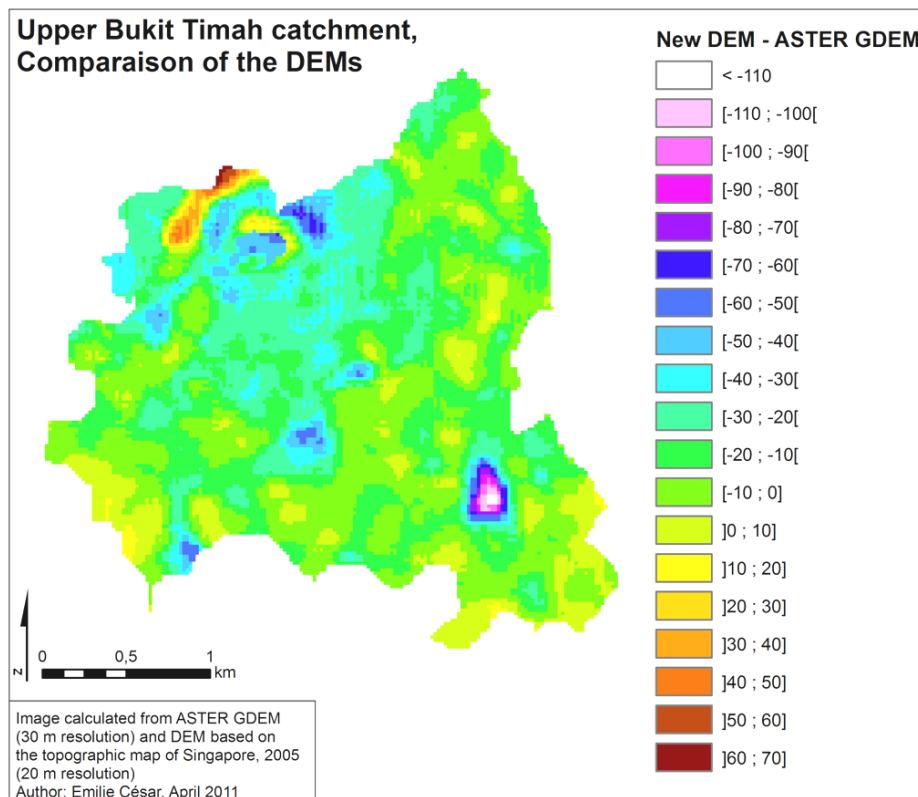
where,  $p_i^{interpolated}$  refers to the  $i^{th}$  interpolated point value,  $p_i^{real}$  refers to the  $i^{th}$  known quoted point value and  $N$  is the number of sample points. The RMS error was calculated from the fifteen quoted points situated inside the limits of the basin. A value of 1.1 m was obtained.

It is important to note that, in this case, the primordial objective was to obtain a hydrologically correct DEM, for which the *Flow Acc* function gives continuous streams. Also, after a visual comparison of the drainage cover with the known streams, the new DEM was considered acceptable as the two water systems almost coincided. This third method also constitutes a mean to evaluate the consistency of a DEM (ESRI, 2009).

#### 4.2.3. ASTER GDEM and new DEM comparison

The first difference between the two DEMs is that the ASTER GDEM has a resolution of 30 m while the new DEM resolution is of 20 m. In order to compare them in terms of elevation, the ASTER GDEM was subtracted from the new DEM (with resampling). The result is shown in figure 15. The maximum difference between the two DEMs is -114 m, in the southeastern part of the basin. Moreover, the ASTER GDEM gives a value of 91 m for the Upper Bukit Timah summit instead of 164 m, resulting in a divergence of 73 m between the two DEMs. The mean difference is -13 m and the standard deviation is 15 m.

The RMS error was also calculated for the ASTER GDEM, with the fifteen quoted points used previously. A value of 10.1 m was obtained, showing that the new DEM is definitely better than the ASTER GDEM. In an ideal case, LIDAR DEM would be the most suitable high resolution elevation data to use in hydrologic modelling but this kind of dataset was not available in Singapore.



**Figure 15. Comparison between the DEMs.**

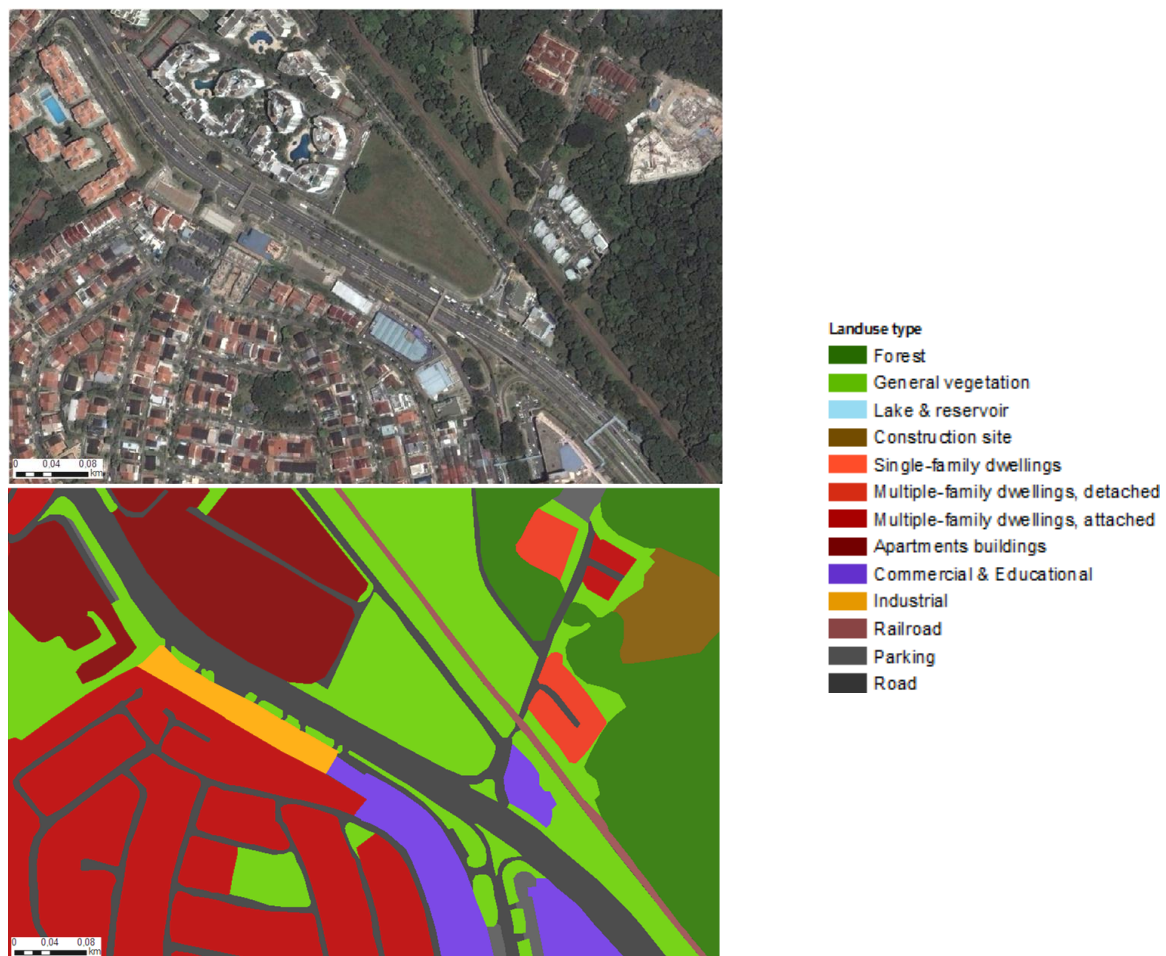
### 4.3. Land use

Holding a precise land use map of the Upper Bukit Timah basin was indispensable to characterise the surface imperviousness. No accurate map was available for the area. Thus, we digitised the Google Earth image as precisely as possible. The tutorial (section 3) gives an overview of the land use digitisation steps.

#### 4.3.1. Land use classes and digitisation

Above all, it was imperative to define the classes characterising the surface. The imperviousness is an important parameter used in watershed models. Values for the coefficient of imperviousness have been found in various writings (see next chapter), and the classes used in these different works determined our choices. Then each class was precisely defined before the digitising step in order to avoid any subjective identification. The appendix 3 regroups the criteria of differentiation between the classes. The final step consisted of the digitisation of each land use class by following the criteria set up previously. The land use classes generated are noted below. Figure 9 in chapter 2 presents a land use map of the catchment.

Figure 16 below illustrates an example of digitisation, with a part of the Google Earth image and its corresponding digitisation.



**Figure 16.** Example of digitisation. Above: Google Earth image of the Upper Bukit Timah road; below, the corresponding image reclassified.



#### 4.3.2. Quality of the digitisation

In this case, it is difficult to evaluate the quality of digitisation for several reasons. Firstly, although the land use classes were well defined, errors inherent to the subjectivity in the class choices have triggered uncertainties in the determination of certain areas (figure 17). Secondly, errors due to the impossibility to draw exact limits of a polygon being digitising are inevitable (figure 18). Thirdly, the quality of a manual digitisation can also be lowered because of the georeferencing of the image on which the digitisation is based. The Google Earth image has been georeferenced from the Google Earth interface with a great number of GCP (35) in order to obtain a small RMS error. However, it is unavoidable that the areas delimited by the digitisation are linked to an uncertainty related to the georeferencing. To a lesser extent, an alteration due to a too small screen resolution can also affect the quality of the digitisation (Donnay, 2010).



**Figure 17. Subjectivity in the class choice: (left) multiple family dwelling attached or detached? (right) polygon defined as attached.**



**Figure 18. Difficulty in drawing the exact limits: (left) limit of the road hidden by the trees, (right) digitisation of the road following the visible limit.**

#### **4.4. Pre-treatments conclusion**

This chapter presented an overview of the pre-treatments performed to acquire a basic dataset. First, a hydrologically correct DEM was constructed in order to characterise the surface of the Upper Bukit Timah catchment based on topographic contours, quoted points, lakes and stream networks. Although there are certain errors inherent to such a manipulation, it was shown that building a new DEM was the best solution. Effectively, the ASTER GDEM presented too many artefacts and the comparison with the new DEM showed that the latter was decidedly better, with a RMS error of 1.1 against 10.1 m. Secondly, a land use classification using a georeferenced Google image was built. It will be used in the models to determine the imperviousness of the catchment. Land use was defined as precisely as possible. The quality of the manual digitisation is uncertain but the models will show the effects of its accuracy on the results. The next chapter will present both the watershed models, SWMM and HEC-HMS, and the methodology used to constrain the parameters and variables necessary for their application.

## 5. MODELLING

This chapter brings a short introduction about the SWMM model and its computational methods intended to model surface runoff and channelled flow. Then, it reviews the methodology used to determine the necessary parameters which must be encoded into the SWMM model. These parameters characterise the Upper Bukit Timah catchment in terms of imperviousness, slope, roughness, infiltration, water network and so on. Once the necessary variables are defined, a pre-parameterisation of the model is realised. A final adjustment is then effected in order to adjust the simulated data to the observed ones. At last, the SWMM model is verified, using different data. A brief overview of the HEC-HMS model and its application on the Upper Bukit Timah basin is given at the end of the chapter.

### 5.1. SWMM model

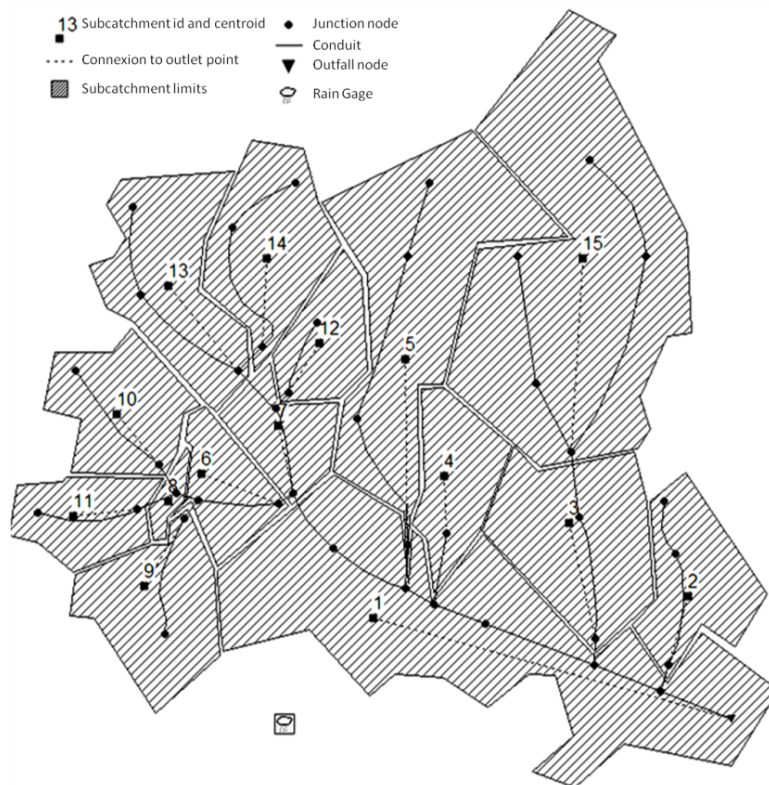
#### 5.1.1. What is SWMM?

The Storm Water Management Model (SWMM) is a one dimensional, physically based model produced by the Water Supply and Water Resources Division of the U.S. EPA's National Risk Management Research Laboratory. It is “*a dynamic rainfall-runoff simulation model used for single event or long-term (continuous) simulation of runoff quantity and quality from primarily urban areas*” (Rossman, 2010 (SWMM user's manual)). SWMM was first developed in 1971 and has undergone major improvements since then (*ibid.*). The current model, SWMM 5, is user-friendly as it provides an integrated environment for editing study area, input data, running simulations and viewing the results in a variety of forms (time series graphs and tables, profile plots, scatter plots and colour-coded maps). The data required for modelling include hydrometeorologic (mainly rainfall), geomorphologic (topography), hydraulic (drain dimensions), pedologic (soil type, infiltration), agricultural (land use) and hydrologic (discharge) properties. SWMM is a widely accepted model and is currently used throughout the world for planning, analysis and design related to water systems in urban areas (*ibid.*).

#### 5.1.2. Subcatchments, conduits and junctions

Spatial variability of various hydrologic processes that produce runoff, like topography, drainage pathways, land use and soil characteristics, imposes the division of the basin into several homogeneous subcatchments. A subcatchment is a hydrologic unit of land containing a mix of pervious and impervious surfaces whose drainage system elements run off to a common outlet point (Rossman, 2010). Each of these subbasins represents idealised runoff areas with uniform slope (Javaheri, 1998).

The user is responsible for dividing a study area into an appropriate number of subcatchments. This step was done in ArcMap by identifying an outlet point for each subcatchment and delimiting them automatically using the *Watershed* function. The runoff block of SWMM models the generation of runoff (and pollution) from the collection of subcatchments that receive precipitation. The routing block of SWMM transports this runoff through the system of conduits and allows the quantification of runoff and flow generated within each conduit or subcatchment of the study area. Conduits are pipes or channels that move water from one node to another in the water system (Rossman, 2010). A junction node is a point where conduits join together, representing the confluence of channels or pipes. A junction node is also needed where conduit characteristics are modified. Outfalls are terminal nodes of the drainage system used to define final downstream boundaries (*ibid.*). The drain network of the basin was created using the *Flow Acc* output, for which a threshold value was applied to select cells with a high accumulated flow, representing the water network. Once each component of the study area was defined, the SWMM sketch could be drawn. It is shown in figure 19. The spatial representation does not need to be exact since only the property of each subcatchment, conduit and junction are taken into account. These ones are presented in the following sections.



**Figure 19. Sketch representing the study area in SWMM.**

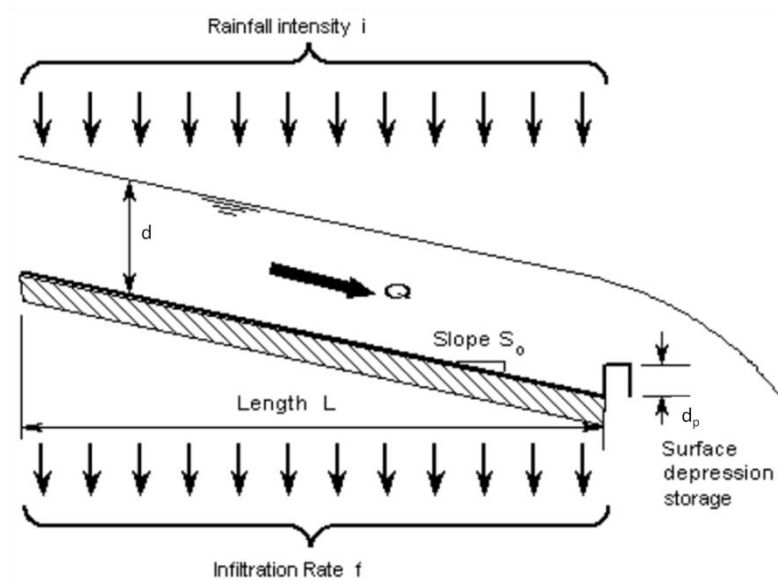
## 5.2. SWMM computational methods

SWMM is a physically based, discrete-time simulation model. It employs principles of conservation of mass, energy, and momentum wherever appropriate (Rossman, 2010). This section describes the methods SWMM uses to model surface runoff and flow within conduits.



### 5.2.1. Surface runoff

The conceptual view of surface runoff used by SWMM is summarised in figure 20 below. This method employs the surface water budget (Smith, 2010). Each subcatchment surface is considered as a nonlinear reservoir with inflows, assembling precipitation and any upstream subcatchment flow, and outflows, including infiltration, evaporation and surface runoff (Rossman, 2010). The capacity of the reservoir is the maximum depression storage  $d_p$ . Surface runoff  $Q$  occurs only when the depth of water in the subcatchment  $d$  is higher than the maximum depression storage  $d_p$  (*ibid.*). The water in storage is also depleted by evaporation and infiltration<sup>3</sup>, modelled by the Horton's equation or Curve Number method (see section 5.2.3).



**Figure 20. SWMM runoff conceptual view** (Source: Smith, 2010)

The concept is applied to each subcatchment. The model of surface runoff is based on two equations (Pitt *et al.*, 1999). The first governing equation is the continuity of mass equation, which calculates the depth of water over the subcatchment and updates it with time:

$$\frac{dV}{dt} = \frac{d(A \cdot d)}{dt} = A \cdot i_e - Q \quad (2)$$

where  $\frac{dV}{dt} = \frac{d(A \cdot d)}{dt}$  is the change in volume stored on the subwatershed per time unit and  $A \cdot i_e$  is the rainfall excess of the subwatershed; with  $V = A \cdot d$  being the volume of water on the subwatershed ( $\text{m}^3$ ),  $A$  the area of the subwatershed ( $\text{m}^2$ ),  $d$  is the water depth on the subwatershed (m),  $t$  the time (s),  $i_e$  the rainfall excess (m/s) (rainfall intensity minus evaporation/infiltration rate), and  $Q$  is the runoff flow rate from the subwatershed ( $\text{m}^3/\text{s}$ ) (*ibid.*).

The second equation is based on Manning's equation and is used to model the overland flow rate (or surface runoff):

<sup>3</sup> Infiltrated water is routed through upper and lower subsurface zones and may contribute to total runoff through groundwater flow. In this case, no information concerning groundwater flow has been encoded in the model. Therefore, infiltrated water is considered as lost.

$$Q = \frac{A_c R_h^{2/3} S_0^{1/2}}{n} \quad (3)$$

where  $A_c$  is the cross-sectional area of flow over the subcatchment ( $\text{m}^2$ ), equal to the width of overland flow  $W$  multiplied by the flow depth  $(d - d_p)$ ,  $n$  is the Manning's coefficient,  $S_0$  is the slope of the subcatchment and  $R_h$  is the hydraulic radius of flow over the subcatchment (m) (*ibid.*). The hydraulic radius is defined as the ratio of cross section area  $A_c$  to the wet perimeter. It is evident that the flow width is significantly larger than the flow depth and therefore the hydraulic radius converges towards the flow depth  $(d - d_p)$ . Considering that, the previous equation becomes:

$$Q = \frac{W(d - d_p)^{5/3} S_0^{1/2}}{n} \quad (4)$$

Substituting this equation into equation (1) and dividing by  $A$  gives the second governing equation used in SWMM:

$$\frac{dd}{dt} = i_e - \frac{W(d - d_p)^{5/3} S_0^{1/2}}{A \cdot n} \quad (5)$$

The two governing equations are solved numerically as follows. The continuity of mass equation [equation (1)] is approximated by:

$$\frac{d_{n+1} - d_n}{dt} = i_e - \frac{Q}{A} = i_e - \frac{W(d - d_p)^{5/3} S_0^{1/2}}{A \cdot n} \quad (6)$$

where  $t_{n+1} - t_n = \Delta t$  is the time step (s),  $i_e$  is the average precipitation intensity during time step  $n + 1$  (m/s),  $Q$  is the average runoff flow rate during time step  $n + 1$  ( $\text{m}^3/\text{s}$ ), and  $d$  is the average depth of flow during time step  $n + 1$  (m), equal to  $\frac{d_n - d_{n+1}}{2}$  (*ibid.*). The differential term  $\frac{dd}{dt}$  is therefore firstly approximated by a finite difference of value of depth at two points in time  $n$  and  $n + 1$  and then approximated by the average of the terms on the right-hand side evaluated at the beginning and end of the time step.

This nonlinear equation (6), having one unknown term at any time,  $(d_{n+1})$  is solved numerically using the Newton-Raphson technique, a widely used technique for solving equations numerically (Smith, 2010). The calculated  $d_{n+1}$  is then used in equation (4) to compute the value of  $Q$  at the end of the time step (Pitt *et al.*, 1999). According to Smith (2010), this method assumes that the depth of flow over the surface is quasi-uniform, which over-estimates the volume on the surface. This would result in a surestimation of the peak runoff.

### 5.2.2. Flow routing

Flow routing is a procedure to determine the time and magnitude of flow at a point in the system based on known or assumed hydrographs at one or more points upstream (Cantone, 2010). Flow routing within a conduit in SWMM is governed by the conservation of mass and momentum equations for gradually varied, unsteady open channel flow (Rossman, 2010). These equations are the Saint-Venant equations. The SWMM allows the user to choose the level of sophistication used to solve the equations. The Kinematic Wave and the Dynamic Wave routing methods are described below. They are distributed models, which means that the routing of the flow is

calculated as a function of space and time (Cantone, 2010). Therefore, they are able to describe the passage of water through channels, accounting for flow rate, velocity and depth (*ibid.*).

#### 5.2.2.1. Saint-Venant equations

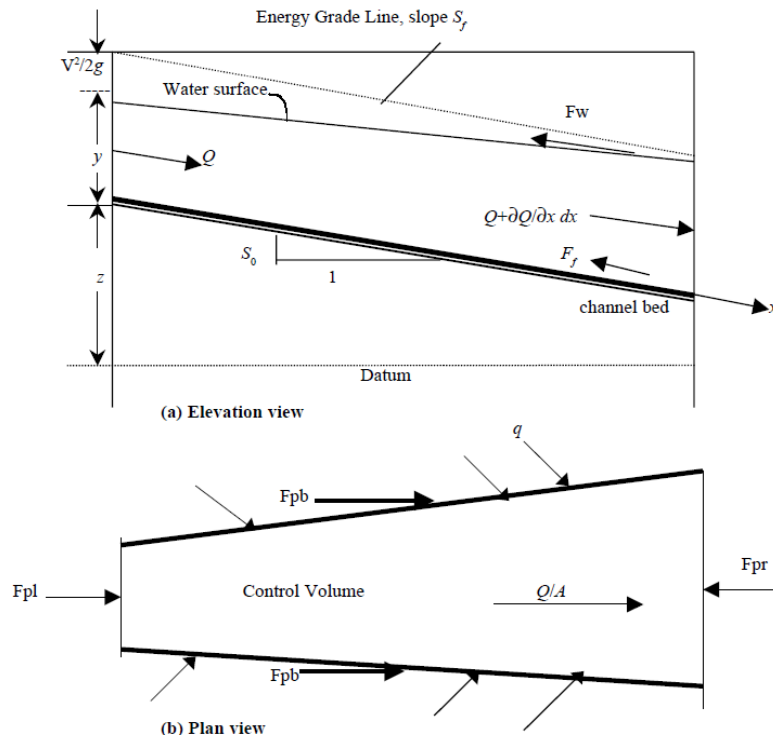
Flow can be represented by the two Saint-Venant partial differential equations. The momentum equation is defined by:

$$\frac{1}{A} \frac{\partial Q}{\partial t} + \frac{1}{A} \frac{\partial}{\partial x} \left( \frac{Q^2}{A} \right) + g \frac{\partial y}{\partial x} - g(S_0 - S_f) = 0 \quad (7)$$

The continuity equation is:

$$\frac{\partial Q}{\partial x} + \frac{\partial A}{\partial t} = 0 \quad (8)$$

Where  $y$  is the flow depth (m),  $x$  is the distance along the conduit (m),  $t$  is the time (s),  $g$  is the acceleration due to gravity (9.8m/s<sup>2</sup>),  $S_f$  is the friction slope (m/m),  $S_0$  is the bed slope (m/m),  $Q$  is the flow rate (m<sup>3</sup>/s) and  $A$  is the cross-sectional area of flow (m<sup>2</sup>) (Pitt *et al.*, 1999). In SWMM, the flow rate is related to the flow depth, bed slope and friction slope by employing the Manning's equation (Rossman, 2010). Each of these variables is represented in figure 21.



**Figure 21. An elementary channel reach for derivation of the Saint-Venant Equations (from top to bottom: elevation view, plan view) (Source: Mujumdar, 2001)**

The terms in the momentum equation describe the physical processes that govern the flow momentum. These terms are:

- $\frac{1}{A} \frac{\partial Q}{\partial t}$  : local acceleration term, describing change in momentum due to the change in velocity over time;

- $\frac{1}{A} \frac{\partial}{\partial x} \left( \frac{Q^2}{A} \right)$  : convective acceleration term, describing the change in momentum due to the change in velocity along the channel;
- $g \frac{\partial y}{\partial x}$  : pressure force term, denoting the change in the water depth along the channel;
- $g(S_0 - S_f)$  : gravity force term, proportional to the bed slope and friction force term, proportional to the friction slope (Mujumdar, 2001).

The terms in the continuity equations represent:

- $\frac{\partial Q}{\partial x}$  : inflows and outflows to and from a control volume or the rate of change of channel flow width distance;
- $\frac{\partial A}{\partial t}$  : change in amount of water in control volume or the rate of change of area with time (*ibid.*).

It is not possible to solve Saint-Venant equations analytically (Mujumdar, 2001). Numerical solutions are possible and depending on the desired accuracy, routing flow equations are either generated by using the complete momentum equation or by eliminating some of its terms (*ibid.*). In all cases, finite difference approximations, as used for the runoff surface routing, are used to numerically solve the two partial differential equations (Pitt *et al.*, 1999).

#### 5.2.2.2. Kinematic Wave routing

The Kinematic Wave method neglects the local acceleration, convective acceleration, and pressure terms in the momentum equation (Cantone, 2010). According to Mujumdar (2001), it is thus represented by:

$$g(S_0 - S_f) = 0 \text{ or } S_f = S_0 \quad (9)$$

The Kinematic Wave model cannot account for backwater effects, entrance/exit losses, flow reversal or flow acceleration (Mujumdar, 2001). According to Rossman (2010) it can usually maintain numerical stability with moderately large time steps (5 to 15 minutes). It is the simplest approximation of the Saint-Venant momentum equation.

#### 5.2.2.3. Dynamic Wave Routing

Dynamic Wave routing solves the complete Saint-Venant flow equations and therefore produces the most theoretically accurate results (Rossman, 2010). Dynamic wave routing can account for channel storage, backwater effects, entrance/exit losses, flow reversal, and pressurized flow (*ibid.*). However, the computation time is longer than with the other method.

### 5.2.3. Infiltration model

Infiltration represents the loss due to rainfall penetrating the ground surface into the unsaturated soil zone of pervious areas of a subcatchment (Rossman, 2010). It is influenced by several

factors including the condition of the soil surface and its vegetative cover, the properties of the soils (porosity, hydraulic conductivity), and the current moisture content of the soil. SWMM offers three choices for modelling infiltration, among which Horton's equation method and Curve Number method, the two methods tested in this work. According to Gironàs *et al.* (2009), there is no general agreement on which method is the more appropriate. The Horton model has a long history of use in dynamic simulations while the Curve Number method is derived from the SCS Curve Number method used in simplified runoff models.

#### 5.2.3.1. Horton's equation

The Horton method is based on empirical observations showing that, if the soil has infiltration capacities ( $\text{mm.h}^{-1}$ ), infiltration decreases exponentially from an initial maximum rate to a minimum rate during a long rainfall event for which the rain intensity is greater than the infiltration capacity (Rossman, 2010). The decrease in infiltration capacity is the result of the operation of the following processes: packing of the soil-surface by rain, dilation of the soil openings and filling of the soil-surface openings by fine materials (Beven, 2004). Therefore, in the case of rainfall excess, surface runoff will occur. If the rain falls at rates less than the infiltration capacity, all water will infiltrate (*ibid.*), without any runoff. The appendix contains a figure which illustrates the Horton method.

This model includes the following parameters. The first one is the maximum infiltration rate ( $\text{mm/h}$ ), which is the initial infiltration rate at the start of a storm. It depends on soil type, initial moisture content and surface vegetation (Javaheri, 1999). The second parameter is the minimum infiltration rate ( $\text{mm/h}$ ), which is the limiting infiltration rate that the soil attains when fully saturated and is equal to the soil's saturated hydraulic conductivity (Gironàs *et al.*, 2009). The third one is the decay coefficient ( $\text{h}^{-1}$ ), that describes how quickly the rate decreases over time, and the time it takes a fully saturated soil to completely dry (*ibid.*). The infiltration rate  $f_t$  at time  $t$  is therefore equal to:

$$f_t = f_c + (f_0 - f_c)e^{kt} \quad (10)$$

where  $f_c$  is the minimum infiltration rate,  $f_0$  is the initial infiltration rate or maximum infiltration rate (at time  $t = 0$ ), and  $k$  is the decay coefficient (Beven, 2004).

#### 5.2.3.2. Curve Number method

The Curve Number method, developed by the U.S. Department of Agriculture (USDA) also called the Soil Conservation Service (SCS), assumes that the total infiltration capacity of a soil can be found from the soil's Curve Number (CN) (Rossman, 2010), a parameter characterising the runoff properties for a particular soil and ground cover. In other words, the CN method can be used to estimate the depth of direct runoff from the rainfall importance, given an index describing runoff response characteristics (Boonstra, 1994). The CN method is based on the facts that when a long-duration, high-intensity rain falls over a small drainage basin, the runoff only starts after a certain quantity of rainfall has accumulated, and the curve is asymptotic (*ibid.*). To describe this curve, USDA assumes that the ratio of actual retention  $F$  to potential maximum retention  $S$  is equal to the ratio of actual runoff  $Q$  to potential maximum runoff, being rainfall  $P$

minus initial abstraction  $I_a$  (*ibid.*).  $I_a$  represents all losses before runoff begins, including water retained in surface depression, intercepted by vegetation, evaporation and infiltration (USDA, 1986) while  $F$  is the loss of additional rainfall in the form of infiltration after runoff has begun and  $S$  is the potential maximum retention, reached with increasing rainfall (Boonstra, 1994). The equation is therefore:

$$\frac{F}{S} = \frac{Q}{P - I_a} \quad (11)$$

where all parameters are expressed in millimetres.

After runoff has started, all additional rainfall becomes either runoff or actual retention so the actual retention  $F$  is the difference between rainfall  $P$  minus initial abstraction  $I_a$  and runoff  $Q$ :

$$F = P - I_a - Q \quad (12)$$

The SCS runoff equation is therefore obtained by combining the two previous equations:

$$Q = \frac{(P - I_a)^2}{(P - I_a) + S} \quad (13)$$

$I_a$  was found to be correlated with  $S$  as:

$$I_a = 0.2S \quad (14)$$

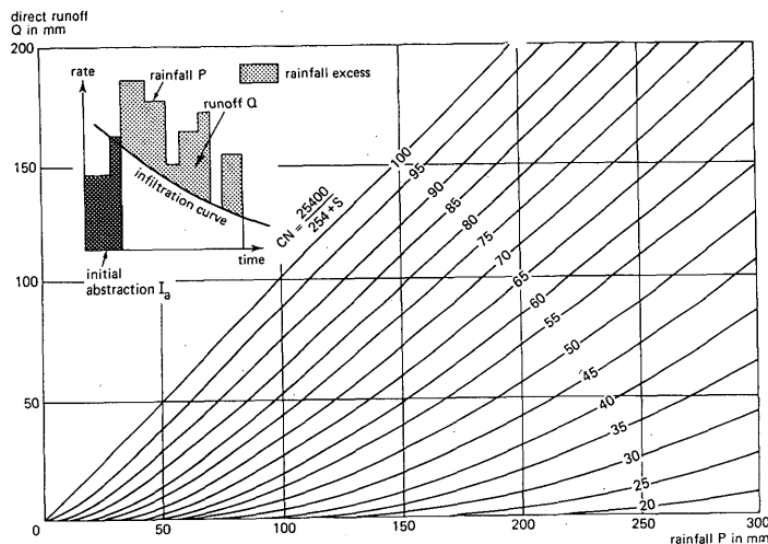
Therefore, by combining equation (13) and equation (14):

$$Q = \frac{(P - 0.2S)^2}{(P + 0.8S)} \text{ for } P > 0.2S \quad (15)$$

where the potential maximum retention  $S$  is related to the soil and cover conditions through the CN by:

$$CN = \frac{25400}{254 + S} \quad (16)$$

where the CN, depending on the cover type, hydrologic condition and hydrologic soil group, is determined thanks to the SCS CN table. Figure 22 shows the graphical solution of the SCS equation [equation (15)]. It shows that a high CN, being 100 for roads where potential maximum retention is 0 for example, causes all rainfall to appear as runoff while lower CN, for permeable areas, produces less runoff.



**Figure 22. Runoff depth  $Q$  as a function of rainfall depth  $P$  and CN (Source: Boonstra, 1994)**

### 5.3. SWMM subcatchments parameters

In order to solve the equations presented in the previous chapter, several variables need to be encoded into the model. For each subcatchment, the following parameters must be provided for the model to run: area, width, slope, percent of imperviousness, infiltration coefficients, and the Manning's coefficient and depression storage for both pervious and impervious areas. Different values for each parameter were calculated when it was possible, in order to assess its influence on the modelling for the adjustment. All details about technical manipulations are given in the tutorial (section 4). All subcatchments parameters are summarised at the end of this section, in

#### 5.3.1. Area

The area is determined from the resolution of the *Watershed* output (20 m) and the number of pixels contained in each subcatchment. It is then transformed into hectares. Subcatchments 1 and 15 are the largest ones, with surfaces of 141 and 143 ha respectively.

#### 5.3.2. Width of overland flow

According to Cantone (2010), the width has no real physical meaning. In theory, it represents the width over which surface runoff occurs (Pitts *et al.*, 1999). If overland flow runs downslope off an idealised rectangular catchment which has a channel on its middle, the width of the subcatchment is the physical width of the overland flow (Javaheri, 1998). This parameter reflects the time of concentration – the traveltime for the first drop of effective precipitation at the most hydraulically distant point in the watershed to reach the watershed outlet (Straub *et al.*, 2000) – for a given subcatchment: a small value of the subcatchment width increases the storage of the catchment; a large value decreases the storage and causes the peak flow to occur sooner. Since real watersheds are irregularly shaped, it may be difficult to determine the width of the subcatchment. Moreover, there are several ways to determine it. This parameter is therefore considered a calibration parameter whose value can be adjusted to produce a good match between observed and modelled hydrographs (Gironàs *et al.*, 2009). Rossman (2010) also considers that adjustments should be made to this parameter to produce good matches to measured hydrographs. Three methods used in the determination of this parameter are presented below.

Rossman (2010) and Gironàs *et al.* (2009) estimate the width of the subcatchment as its area divided by the average maximum overland flow length. In applying this approach, the channelled flow is not included as part of the flow path. The longest overland flow path was determined using the HEC-GeoHMS extension of ArcMap. It was edited manually to exclude the channelled flow. The length of each subbasin overland flow path was calculated and the subcatchment area was divided by it to determine the width.

Javaheri (1998) computes the width in a different way. First, a skew factor is calculated. It is defined as:

$$\gamma = \frac{A_2 - A_1}{A} \quad (17)$$

Where  $\gamma$  is the skew factor (comprised between 0 and 1),  $A_1$  is the area to one side of the main channel,  $A_2$  is the area to the other side of the main channel and  $A$  is the total area of the subcatchment ( $A = A_1 + A_2$ ). The width is then defined as:

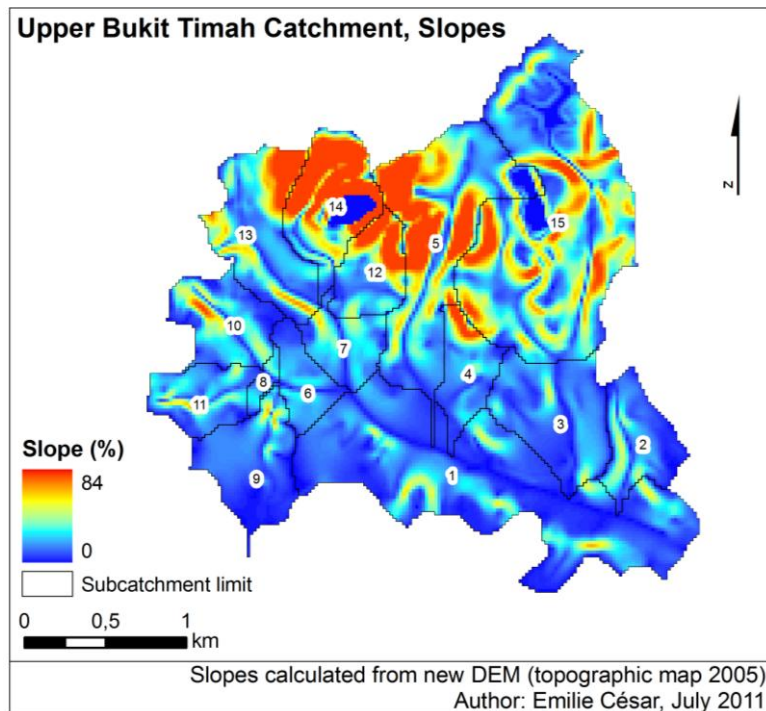
$$W = (2 - \gamma) \times L \quad (18)$$

Where  $L$  is the length of the main drainage channel. Manipulations to calculate the width using this method were done using the editing tools in ArcMap.

Finally, Cantone (2010) considers that subcatchment width should be approximately twice the length of the main drainage channel through the catchment. This method was also tested. The width calculated with this method showed particularly high values.

### 5.3.3. Slope

The slope associated to each subcatchment is the slope of the land surface over which runoff flows (Gironàs *et al.*, 2009). The slopes of the Upper Bukit Timah basin were calculated from the new generated DEM (*Slope* function). Figure 23 illustrates this. It can be seen that the area surrounding the Upper Bukit Timah summit is steeper than the rest of the basin. On the other hand, the main channel has a weak slope of less than one percent. A mean value for each subcatchment was calculated by multiplying each subcatchment mask by the slopes extracted from the DEM (using *Raster Calculator*). Subcatchments 5, 12, 14 have logically the highest mean slopes (14.0 %, 13.8 % and 23.1 % respectively).



**Figure 23. Slopes of the Upper Bukit Timah basin**



### 5.3.4. Percentage of impervious area

This parameter is expressed as the percentage of land area which is impervious, through which rainfall cannot infiltrate. According to Gironàs *et al.* (2009), it is one of the most sensitive parameter in the hydrologic characterisation. The mean percentage of imperviousness can be calculated from the coefficients of imperviousness associated to each land use class. A weighted percentage of impervious area can therefore be determined from the area of each land use class within the subcatchment, using the *Clip* function to extract the part of the land use that overlays the subcatchment.

There are many different imperviousness coefficients in the literature. As a first choice, the mean value from all literature sources was used. Other tests were realised using the coefficient of imperviousness provided by Guo (2003). Table 1 below gives the coefficients of imperviousness for each land use class. Figure 24 shows the percentage of imperviousness calculated for each subcatchment, using the values given by Guo (2003).

**Table 1. Coefficients of imperviousness for each land use class**

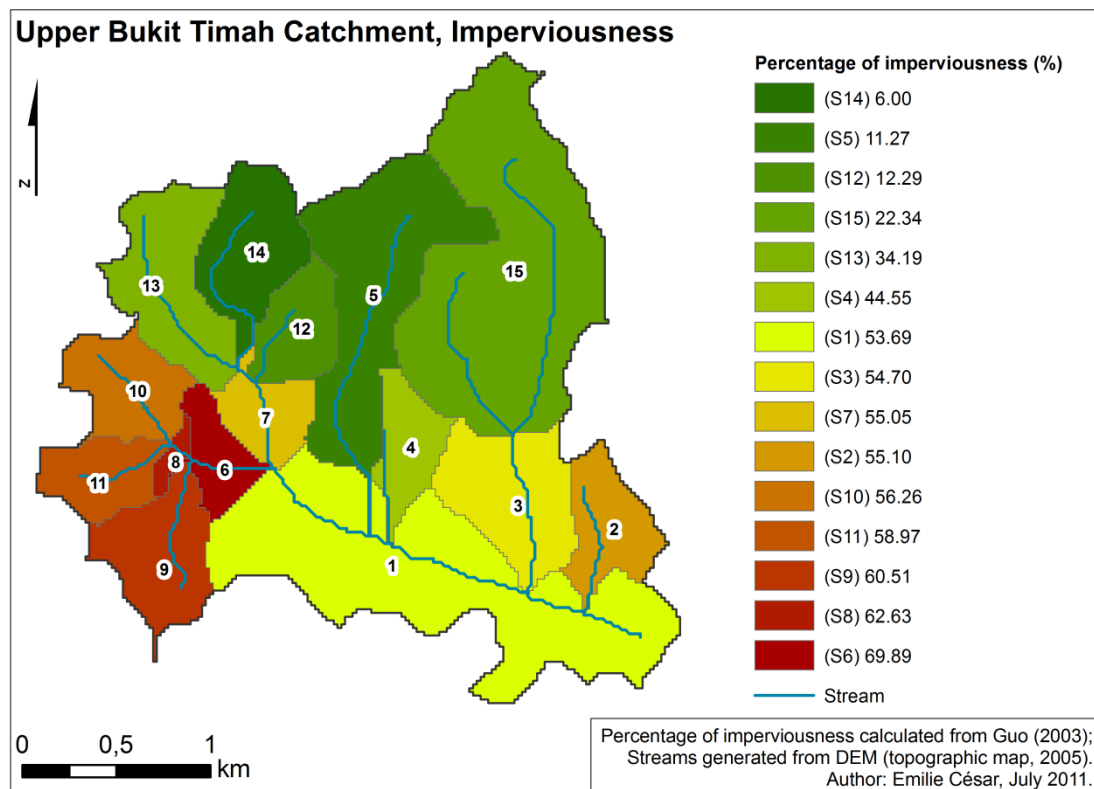
Land use classes	Coefficients of imperviousness	
	Mean values from several sources*	Values from Guo (2003)
Apartment	0.70	0.70
Multiple-family, attached	0.70	0.70
Multiple-family, detached	0.50	0.50
Single-family	0.50	0.50
Commercial & Educational	0.85	0.70
Industrial	0.82	0.80
General vegetation	0.10	0.07
Woodland	0.01	0.01
Car park	0.74	0.74
Road	0.96	1.00
Railroad	0.20	0.20
Lake	0.00	0.00
Construction site	0.60	0.60

\* County of San Diego Department of Planning and Land Use (2008), Guo (2003), Mason and Knight (2001), Pikes Peak Area Council of Governments (2005), Washburn *et al.* (2010), Wisconsin Department of Transportation (2007).

#### 5.3.4.1. Coefficients of imperviousness accuracy

There are several methods to determine the percentage of imperviousness of an area. Calculating the imperviousness by determining the land use category for each area and multiplying by the typical imperviousness coefficient of that category implies uncertainties. Firstly, the published coefficients vary for a land use category to another. Secondly, the imperviousness can be different within the same category of land use. With this method, it is difficult to outline specific impervious surfaces, like individual buildings and their surrounding open spaces, roads, etc. since. Moreover, the resolution is much lower than an aerial photograph. The most accurate methods for determining imperviousness are direct methods. Ground surveys result in very accurate outlines of features (Mason and Knight, 2001). Orthophotographies are also a solution to acquire land cover information, since distortion is removed from the original photograph and

since the resolution is higher than satellites images. Individual features can therefore be separated. However, these two direct methods are expensive and rarely feasible.



**Figure 24. Percentage of imperviousness associated to the subcatchments**

### 5.3.5. Infiltration parameters

Infiltration methods have been explained in section 5.2.3. These paragraphs present the values of the parameters used for the Horton and CN methods.

#### 5.3.5.1. Horton's parameters

Representative values of the maximum infiltration rate are given by Rossman (2010). For moist sandy loam soils<sup>4</sup>, which have drained but not dried out, the value has been calculated to be 33.8 mm/h. Javaheri (1999) gives a range of possible values of 6.75-160 mm/h. He chose, as well as Liong *et al.* (1993), values from 45 to 80 mm/h for the Upper Bukit Timah catchment. A value of 70 mm/h was adopted for this model, as proposed by Selvalingam *et al.* (1987) for the Upper Bukit Timah basin. The minimum infiltration rate is equal to the hydraulic conductivity, estimated at 10.9 mm/h by Rossman (2010) and between 7.6 and 11.4 mm/h by Akan (1993) for sandy loam soils. Butler and Davies (2004) give a value of 12 mm/h for medium textured soils, such as sandy loam soils. The initial estimates used in the research of Javaheri (1999) are the same than in the work of Liong *et al.* (1993) and, are 2.5-3.5 mm/h. Selvalingam *et al.* (1987) set this value between 2 and 5. Given the variability of the values from literature, a mean value of

<sup>4</sup> The Rengam series have sandy loam textures in the topsoil. These series are largely dominant on the Upper Bukit Timah basin; the representative values of the infiltration parameters have therefore been taken on the basis of this type of soil.

10 mm/h has been used for the model. The decay constant has been set to  $4 \text{ h}^{-1}$ , as Rossman specifies that it is comprised between 2 and  $7 \text{ h}^{-1}$  while Javaheri (1999) gives values ranging from 0.66 to  $4.07 \text{ h}^{-1}$  and specifies that a value of  $4.25 \text{ h}^{-1}$  could be used if no field data is available. Selvalingam *et al.* (1987) gives value in accordance with Javaheri (1999). Butler and Davies (2004), on the other hand, estimate that the decay coefficient is equal to  $2 \text{ h}^{-1}$  for every type of soils.

#### 5.3.5.2. *Horton's parameters uncertainty*

Ideally, the Horton's parameters should be estimated using results from field infiltrometer tests for several sites of the watershed and for different antecedent wetness conditions. Unfortunately, such measurements were not available in Singapore. It is certain that the parameters estimated above are only a first approximation based on different sources of the literature. Moreover, for all storms, the same value of all variables was used, the initial conditions assumed to be uniform for all events. However, the initial infiltration values can change due to initial wet conditions. A 60-70 % reduction in the initial infiltration rate is expected if initial conditions are wet (Javaheri, 1999). Also, each parameter was set to be the same for all subcatchments, the method does not take into account the variations in land use or soil type within the basin. But, the presence of vegetation, for example, can increase infiltration capacities. ASCE (1996) estimates that infiltration rates must be multiplied by a cover factor ranging from 3 to 7.5 for good permanent forest and grass.

#### 5.3.5.3. *Curve Number*

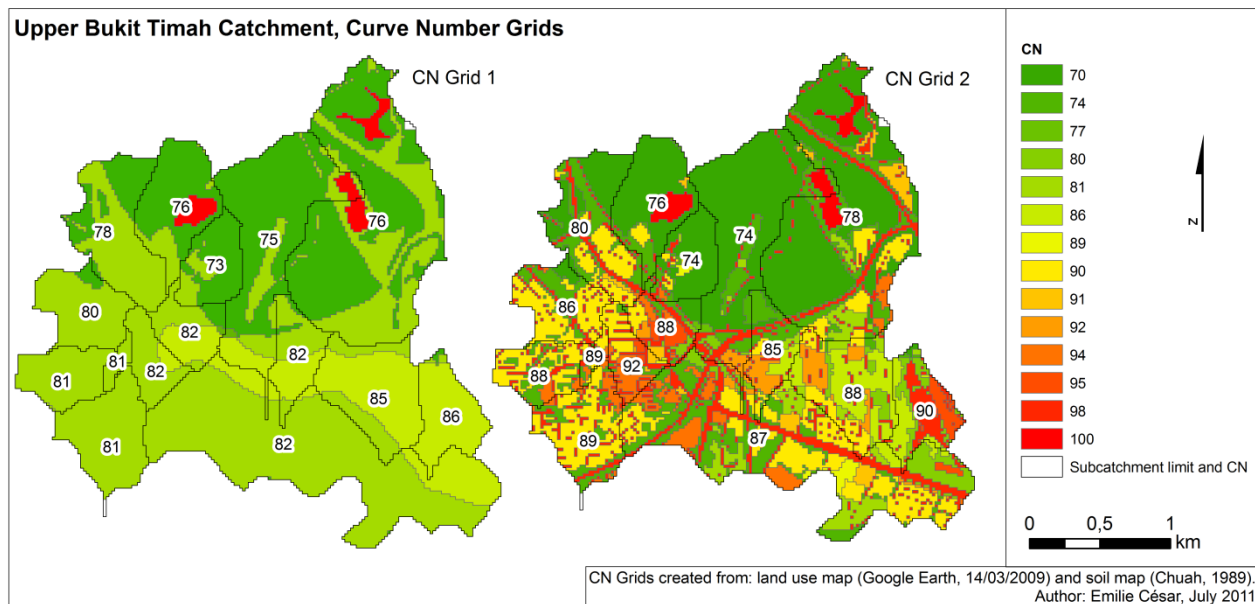
Two CN grids for the Upper Bukit Timah basin were computed using the method prepared by Merwade (2010). This method uses the *HEC-GeoHMS* extension of ArcMap to create a CN Grid from the land use and soil maps. To implement this method, a hydrologic soil group was associated to each type of soil, C for Rengam and red variant Rengam series, D for Tengah series, according to the SCS classification (tutorial, section 4). A CN was also associated to each type of land use and according to the soil group. All CN used here figure in table 2. The soil and land use data were then combined to create a curve number grid using *HEC-geoHMS*. A weighted CN was associated to each subcatchment by calculating the surfaces associated to one CN. Figure 25 shows a map of the CN grids created. The CN grid 2 presents CN sensibly higher than the CN grid 1.

**Table 2. CN table**

CN Grid 1*			CN Grid 2**		
Land use class	CN Soil C	CN Soil D	Land use class	CN Soil C	CN Soil D
Medium residential, (containing developed open space and developed areas from low to high intensity, according to Merwade (2010))	<b>81</b>	<b>86</b>	Apartment	<b>90</b>	<b>92</b>
			Multiple-family, attached	<b>90</b>	<b>92</b>
			Multiple-family, detached	<b>90</b>	<b>92</b>
			Single-family	<b>81</b>	<b>86</b>
			Commercial & Educational	<b>94</b>	<b>95</b>
			Industrial	<b>91</b>	<b>93</b>
			General vegetation	<b>74</b>	<b>80</b>
			Car park	<b>98</b>	<b>98</b>
			Road	<b>98</b>	<b>98</b>
			Construction site	<b>89</b>	<b>91</b>
Forest	<b>71</b>	<b>78</b>	Forest	<b>70</b>	<b>77</b>
Water	<b>100</b>	<b>100</b>	Lake	<b>100</b>	<b>100</b>

\*Land use classes and CN determined by Merwade (2010).

\*\*Land use classes determined by personal classification, CN determined from Dunne and Leopold (1978), Marek (2009) and USDA (1986).



**Figure 25. CN Grids created from the CN figuring in table 2 (annotations refer to each average subcatchment CN)**

#### 5.3.5.4. Curve number method quality

The advantage of this method is that a CN is associated to each subcatchment, in opposition to Horton's method for which the values were fixed for the entire basin. Moreover, the CN given in the literature did not show any variability, contrarily to the Horton parameters for which infiltration rates may in fact double from one source to another. Finally, this approach, which only requires soil and land use data, considers the temporal distribution of rainfall, all initial rainfall losses and an infiltration rate that decreases during the storm (Marek, 2009).

There are, however, some uncertainties concerning this method. Firstly, the effect of the basin initial wetness is not taken into account, whereas values of CN are expected to vary with site

moisture. By opposition, in the Horton method, initial moisture content can be considered (although, in this case, initial conditions remain constant for all storm events). Secondly, the soils of the area could have been identified from a soil survey report, and the associated precise soil map would have brought a better CN. In this case, the soil map was provided by Chuah (1987) which gave a simplified map, with uncertain limits between soil types. Thirdly, USDA (1986) notices that urbanisation involves the disturbance of the soil profile which can significantly change its infiltration characteristics. For example, mixture, removal of soil profiles, filling with material from other areas or compaction of the soil can severely affect the infiltration of the natural hydrologic soil group (Marek, 2009).

### **5.3.6. Manning's coefficient**

The Manning's roughness coefficient reflects the amount of resistance that overland flow meets as it runs off the subcatchment surface (Gironàs *et al.*, 2009). As described above, SWMM uses the widely used Manning's equation, originally developed to describe flow in channels, to compute the overland flow rate.

Separate values of Manning's roughness coefficient for overland flow are required for the impervious and pervious fractions of a subcatchment. This is because the pervious coefficient is generally an order of magnitude higher than the impervious one. Values of Manning's coefficient are not as well known for overland flow as they are for channel flow because of the considerable variability in ground cover, the very small depths of water on the surface and the complication in the estimation of its value due to the transitions between laminar and turbulent flow (Javaheri, 1999). It is therefore best to refer to the appropriate values applicable to the area of study. Selvalingam *et al.* (1987) gives the following values for the Upper Bukit Timah catchment. For impervious areas, the value was set to 0.028 while for pervious areas, it was set to 0.35 for every subcatchment. For the Upper Bukit Timah basin, Javaheri (1999) set the values at 0.012 and 0.3 while Liong *et al.* (1993) fixed the values at 0.02 and 0.3 for impervious and pervious areas respectively. Values chosen in this study differed from one land use class to another and from one catchment to another contrarily to these previous studies. They took into account the coefficients given by the two previous sources, but also the ones brought by Rossman (2010) and USDA (1986). Thus, the Manning's coefficient for impervious surfaces (industrial, parking and roads) was set at 0.011 while for general vegetation and forests, it was fixed at 0.24 and 0.6 respectively. Other pervious land use classes have a coefficient of 0.05. Thereby, a weighted coefficient was calculated for the impervious and pervious areas of each subcatchment.

### **5.3.7. Coefficient of storage and percentage of impervious area without depression storage**

Depression storage corresponds to a volume that must be filled prior to the occurrence of any runoff, such as surface ponding, interception by vegetation, etc. (Rossman, 2010). In this case, the DEM generation process has involved all sinks to be filled to ensure proper delineation of basins and streams. If closed depressions are not filled, the drainage network may be discontinuous. That is why a coefficient of storage value of 0 was chosen, by conception, for

both pervious and impervious fractions of each basin. Nonetheless, the model will show if this value needs to be modified.

The second parameter, the percentage of impervious area without depression storage, represents direct runoff that occurs at the start of rainfall before depression storage is satisfied (Gironàs *et al.*, 2009). Concretely, it represents pavement that has no surface ponding, rooftops that drain directly to street gutters, etc. (*ibid.*). In this particular case, there is no depression storage and therefore, the value of this parameter does not matter at first.

The assumption that there is no depression in the basin is in accordance with the DEM previously built. However, it is undeniable that the surface is not smooth and that a certain volume of rain is stored in depressions or intercepted by vegetation. As an example, the porous pavement in some areas allows precipitation to be stored in it instead of being able to run off the surface (figure 26).



**Figure 26. Porous pavement, car park at the Bukit Timah Nature Reserve (08/09/2010)**

## **5.4. SWMM conduits and junctions parameters**

For each conduit, the length, slope, Manning's coefficient, shape, width, and depth must be known. Forty-five conduits were represented in the model since a new conduit was needed in the model for each variation in its dimensions. For each junction, only the invert elevation is needed.

### **5.4.1. Conduits properties**

#### *5.4.1.1. Length and slope*

Upstream and downstream elevation of each conduit must be entered in the model in order to characterise the slope of each drain. Elevations were determined on the DEM, using the measuring tool of ArcMap. The length between the two elevations points was also measured.

#### *5.4.1.2. Manning's coefficient*

As the overland flow rate, the Manning's equation is used to express the flow rate  $Q$  in a channel of cross-sectional area  $A$ , hydraulic radius  $R_h$ , slope  $S$  and Manning's coefficient  $n$ :



$$Q = \frac{A R_h^{2/3} S^{1/2}}{n} \quad (19)$$

According to Rossman (2010), concrete lined channels have a Manning's roughness coefficient comprised between 0.011 and 0.02. Chuah and Wong (2010) estimate the concrete drains coefficient at 0.013 while Javaheri (1999) gives values of 0.012. Selvaligam *et al.* (1987) consider values between 0.028 and 0.056. This last source is considered as erroneous, maybe because the study is too old and drains have changed since then, thanks to drainage enhancements in Singapore. Some dirt channels are present in upstream areas of the basin. Their Manning's coefficient has been set to 0.03, as specified by Chuah and Wong (2010) and Rossman (2010). Several tests have been done with different values of Manning's coefficient for concrete channels.

#### 5.4.1.3. Cross-sectional geometry, width and depth

It has been explained in chapter 4 how the shape, width and depth of conduits were determined. The values for each drain were encoded in the SWMM manually. Three cross section shapes are represented in the Upper Bukit Timah basin: rectangular, trapezoidal or triangular channels (figure 27). The height and width must be encoded for all shapes. In addition, the side slopes are needed for trapezoidal channels. The depth varies from 0.5 m for channel situated upstream to 2.67 m for the large channel at the outlet. Likewise, the width varies from 0.66 m for small upstream triangular conduits to 5.8 m for the large Bukit Timah channel.



**Figure 27. Rectangular, trapezoidal and triangular drains at the Greenbank Park, the Bukit Timah road and the Toh Tuck road respectively (17/08/10)**

#### 5.4.2. Junctions invert elevation

Junctions invert elevations were encoded using the DEM; this corresponds to the upstream and downstream elevations of conduits.

Table 3. Subcatchment parameters

Subcat.	Area (ha)	Width (m)				Slope (%)	Percentage of imperv (%)	
		Method 1*	Method 2*	Method 3*	Method 4*		Mean	Guo (2003)
s1	140.72	505.89	3385.92	4104.95	4859.90	3.99	55.2663	53.6929
s2	26.48	258.44	943.01	1207.94	1525.69	4.64	57.6567	55.0958
s3	44.32	358.58	1137.27	1684.36	1835.98	4.21	54.6405	54.7012
s4	20.68	200.17	498.53	671.56	1216.57	7.49	44.8019	44.5463
s5	80.44	325.15	2384.23	4225.72	4287.35	14.05	11.3738	11.2740
s6	16.76	197.72	388.06	795.25	873.14	4.85	74.7014	69.8945
s7	19.44	262.91	1342.05	1197.22	1275.98	6.53	58.4356	55.0521
s8	3.92	98.49	121.96	261.35	306.27	6.02	65.7304	62.6340
s9	35.84	301.46	813.25	1276.42	1542.25	3.66	61.4759	60.5095
s10	28.92	308.38	983.06	1309.31	1321.67	6.83	57.1868	56.2578
s11	22.28	249.61	711.82	1153.28	1158.82	6.11	60.1724	58.9743
s12	22.92	273.70	613.76	741.17	925.69	13.8	12.5637	12.2898
s13	46.28	289.46	882.27	1947.49	2131.37	10.87	34.4178	34.1975
s14	37.80	272.33	1235.56	2031.22	2187.94	23.07	6.2633	6.0067
s15	142.92	601.30	4442.53	3458.03	3937.06	10.25	22.5886	22.3405

\* Method 1: Rossman (2010) and Gironas *et al.* (2009)'s method; Method 2: Rossman (2010) and Gironas *et al.* (2009)'s method (excluding chan. Flow); Method 3: Javaheri (1999)'s method (skew factor); Method 4: Cantone (2010)'s method

Subcat.	Infiltration model					Manning's coefficient			
	Horton method		Curve Number method		Weighted coefficient	Manning's coefficient		Manning's coefficient	
	Max. inflit. rate(mm/h)	Min. inflit. rate(mm/h)	Decay coeff. (h-1)			Perv. areas	Imperv. areas	Perv. areas	Imperv. areas
s1	70	10	4	81.79	86.74	0.120	0.011	0.3	0.02
s2	70	10	4	85.66	89.99	0.125	0.012	0.3	0.02
s3	70	10	4	84.56	87.55	0.073	0.011	0.3	0.02
s4	70	10	4	82.41	84.72	0.154	0.011	0.3	0.02
s5	70	10	4	74.71	74.30	0.521	0.011	0.3	0.02
s6	70	10	4	81.58	92.32	0.068	0.011	0.3	0.02
s7	70	10	4	82.11	88.36	0.194	0.011	0.3	0.02
s8	70	10	4	81.00	89.02	0.101	0.011	0.3	0.02
s9	70	10	4	81.00	88.81	0.094	0.011	0.3	0.02
s10	70	10	4	80.36	86.05	0.202	0.011	0.3	0.02
s11	70	10	4	81.00	87.62	0.107	0.011	0.3	0.02
s12	70	10	4	73.44	74.16	0.502	0.011	0.3	0.02
s13	70	10	4	77.58	80.39	0.329	0.011	0.3	0.02
s14	70	10	4	76.25	75.63	0.530	0.011	0.3	0.02
s15	70	10	4	76.06	77.66	0.468	0.011	0.3	0.02



## 5.5. Discharge and rainfall data

The most important hydrologic data requirement is the rainfall data (Rossman, 2010). In order to adjust a watershed model, discharge data at the outlet related to rainfall are also essential. Unfortunately, no discharge data were available from the authorities despite several attempts. Old hydrographs and hyetographs were extracted from literary articles. In order to make sure the model was correct for current data, rainfall and discharge data were also obtained with indirect methods. This section describes how these data were acquired. The details of all manipulation figure in the tutorial, sections 5 and 6.

### 5.5.1. Old hydrographs and hyetographs

Several authors studied the Upper Bukit Timah catchment and some of them published hydrographs related to hyetographs<sup>5</sup>. Although they date from the 1980s, they were extracted in order to be used for the model parameterisation. A total of sixteen hydrographs and hyetographs of different intensities, durations, seasons and recording intervals were used (table 1). These storm events cover a large spectrum of events, in order to illustrate the variability of rainfall within the watershed. For example, the storm event of the July 2<sup>nd</sup>, 1984, lasted for 16 hours and the rainfall intensity did not reach 10 mm/h, resulting in a discharge of 3.7 m<sup>3</sup>/s. In the other hand, the rainfall of the April 3<sup>rd</sup>, 1988, lasted for 6 hours, the rainfall intensity exceeded 92 mm/h and the discharge reached 27 m<sup>3</sup>/s. The data were extracted by georeferencing the graphs, digitising curves and histograms, extracting their values and reporting them in Excel. All details can be found in the tutorial, section 5.

**Table 4. Characteristics of storm events extracted from the literature**

Storm events	Duration (hh:mm)	Max. rainfall intensity (mm/h)	Max. discharge (m <sup>3</sup> /s)	Storm characteristics
12 Feb 78	03:30	84.3	29.1	Four major peaks, three minor
02 Dec 78	03:30	54.9	19.8	Three major peaks
01 June 79	07:00	64.2	18.1	One peak
03 Feb 84	03:30	34.1	19.3	Three major peaks, highly variable hydrograph
02 Mar 84	19:00	34.6	19.9	Six major peaks, highly variable hydrograph
02 Jul 84	14:30	9.3	3.7	Two major peaks
03 Jan 85	13:10	21.2	7.5	Two peaks, the 1 <sup>st</sup> smaller
01 Aug 86	19:00	27	14.5	Four major peaks, highly variable hydrograph
18 Jun 86	10:10	86.5	22.4	Two peaks, the 2 <sup>nd</sup> very small
07 Oct 86	10:10	71.9	20.3	Two peaks, the 2 <sup>nd</sup> very small
27 Nov 87	05:30	69.5	19	One peak
15 Feb 88	05:30	125.1	26.1	Two peaks, the 1 <sup>st</sup> one higher
03 Apr 88	06:00	92.5	27.7	One peak

<sup>5</sup> Liong *et al.* (1986), Selvalingam *et al.* (1987), Liong *et al.* (2002), Khu and Werner (2003), Chuah and Wong (2010).

[continued]

17 Apr 88	06:30	104.8	29.1	One peak, slow recession
11 Jul 88	05:45	66.5	21.4	One peak
18 Apr 89	03:30	154.9	23.7	One peak

#### 5.5.1.1. *Uncertainties concerning old data*

It is evident that there are several uncertainties concerning the quality of the data. These are linked to the method of extraction but also to the fact that the methods of data obtaining are not known. Indeed, there is no information about the techniques of measurement of discharge and rainfall and the estimation of these. This fact can represent a first approximation. Also, the old hyetographs and hydrographs show some imprecision inherent to their representation. For example, measured discharge curves sometimes merge with modelled curves; this fact has an impact on the digitisation. Then, the thick lines representing the axes and the discharge and rainfall data prevent an exact digitisation and georeferencing. Furthermore, the graduation is often too weak, which lowers the quality of georeferencing. Finally, the biggest error is certainly due to the fact that, since the articles are relatively recent in comparison to their discharge and rainfall data, their old hyetographs and hydrographs probably result from secondary sources and do not come from direct measurements. Thus, the data extracted by this mean is certainly tarnished with several errors

#### 5.5.2. **Recent discharge and rainfall data**

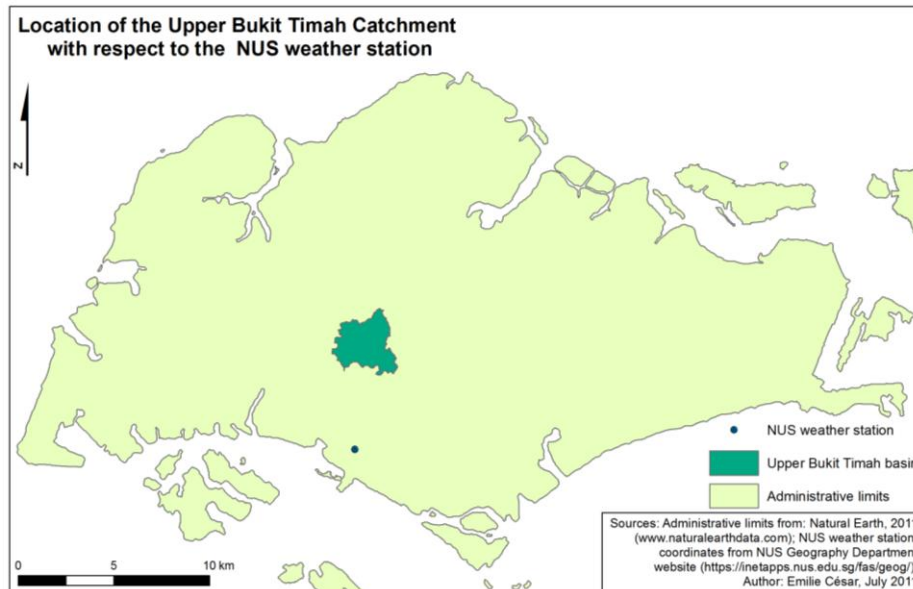
Finding recent data was not as simple. Several interesting storms events, for which the water depth at the outlet of the basin exceeded 1 m, were selected. Then, the rainfall and discharge data of these were obtained by different means, which are explained below.

##### 5.5.2.1. *Rainfall data*

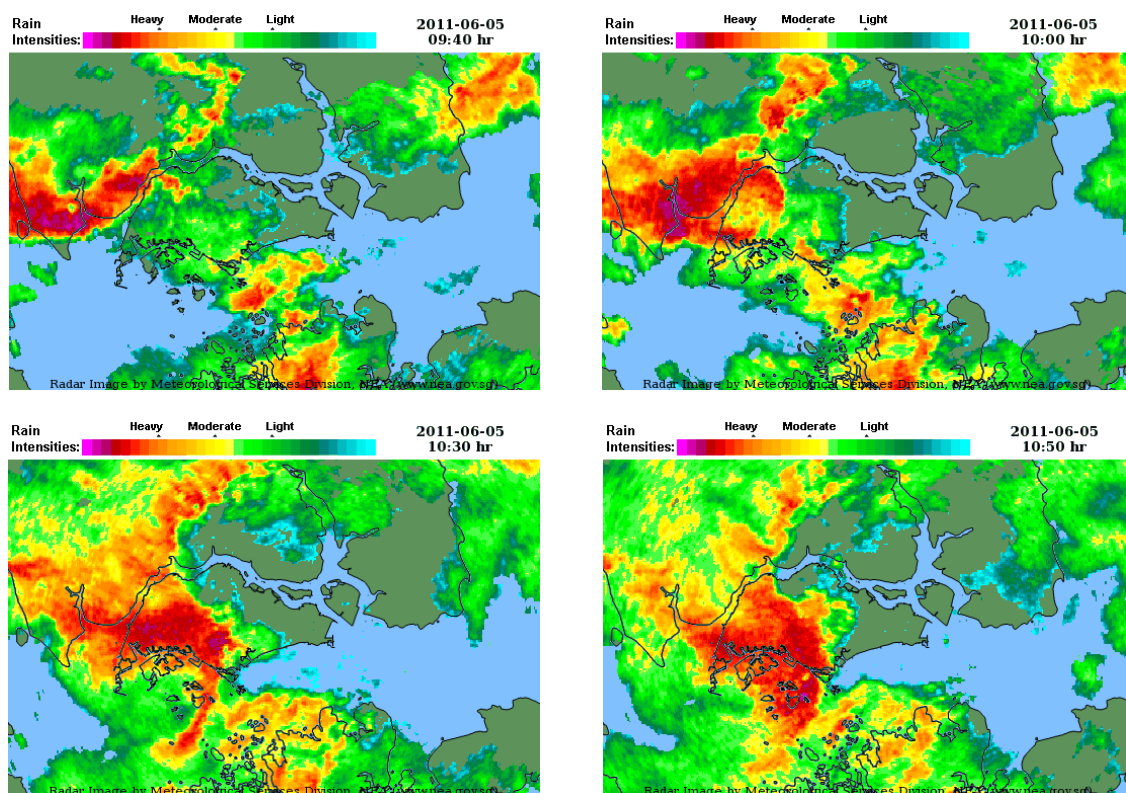
The National University of Singapore (NUS) provides, free of charge, rainfall data of the NUS weather station. The records cover the period of time from August, 2003 to the present. The weather station is situated on the university campus, in the southern part of the island. Our calculations show that the distance between the centre of the basin and the weather station is about 5.5 km (figure 28). Due to the too high spatio-temporal variability of rainfall in Singapore observed on the RADAR images and according to the literature, it was decided not to use the NUS rainfall data directly in the modelling.

RADAR images facilitate the inclusion of spatial and temporal variability of rainfall. Meteorological RADAR operates with the same principle as other RADAR but the wavelength of electromagnetic waves emitted varies from 3 to 10 cm (Alicime, 2008). The meteorological RADAR emits an electromagnetic signal and the energy received from the detected rain is directly related to the amount of precipitation (*ibid.*). This fact allows for the generation of circular maps for which the radius is within the range of 150 to 250 km (*ibid.*). This kind of map gives a qualitative value of the detected precipitation. In Singapore, the RADAR is located near the runways of the Singapore Changi International Airport in the eastern part of the island. Some 6000 RADAR images were downloaded from the Singapore's National Environment Agency's

website<sup>6</sup> during the period of May and June 2011 thanks to an automatic recording script (batch file). One image every 10 minutes is published on the website (figure 29). The resolution of these images is 220 m. In order to extract data from several storm events of May and June 2011, the aim was to transform the qualitative scale of the map into quantitative scale. To do so, rainfall data from the NUS station were used. The manipulations are explained below.



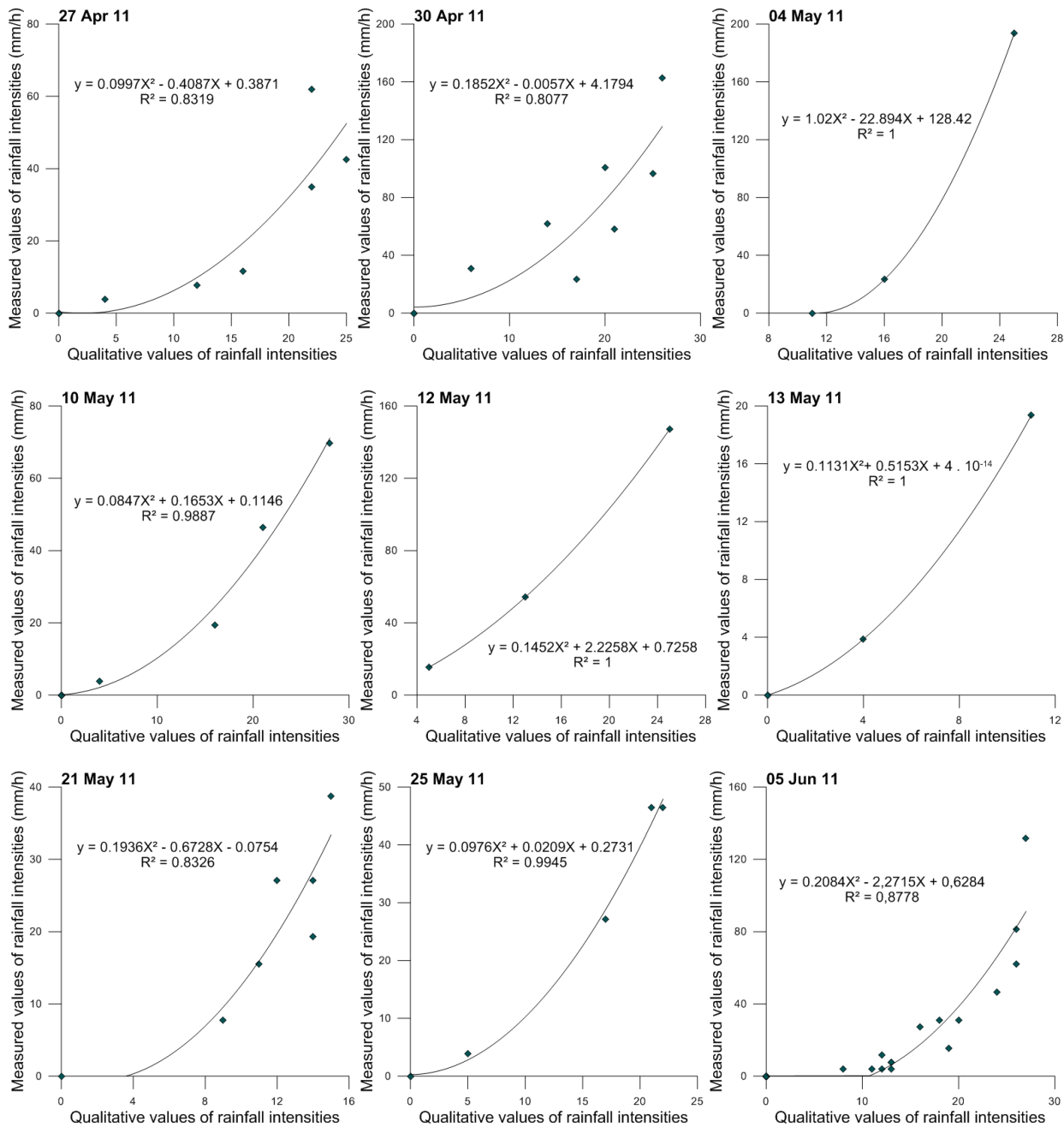
**Figure 28. Location of the NUS weather station**



**Figure 29. RADAR images of the 5<sup>th</sup> of June, 2011, storm. From left to right: 09:40, 10:00, 10:30 and 10:50 (Source: National Environment Agency, 2002)**

<sup>6</sup> National Environment Agency, 2002.

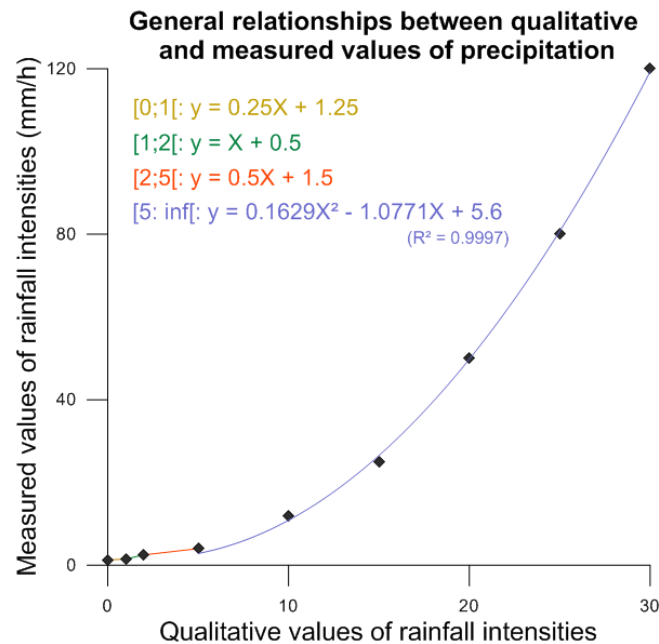
After several pre-treatments concerning the colours, each RADAR image was georeferenced in UTM 48N. Then, each image was reclassified to create thirty-one classes representing each colour of the qualitative scale, the remaining (background, title...) being set at 0. The qualitative value at the NUS weather station point previously created was then extracted (using the *Zonal Statistics as Table* function). For each event, one event being composed of six to forty-three images, the relationship between the qualitative values and the measured values at the NUS weather station was established for each point in time. The polynomial equation was calculated and some aberrant points<sup>7</sup> were deleted in order to obtain a coefficient of determination  $R^2$  superior to 0.8 (figure 30). A total of 143 images consisting of nine events have been used.



**Figure 30. Relationships between qualitative and quantitative values at NUS weather station for nine storm events**

<sup>7</sup> For example, a value of 0 in the qualitative scale sometimes gave a value superior to 0 in the quantitative scale. This fact is probably due to a possible time lag between the quantitative and qualitative values. These kinds of points have been deleted in order to obtain a realistic relationship.

From all polynomial equations, the “mean” relationship between the variables has been calculated in order to obtain the values of precipitation for the different classes of the qualitative scale (figure 31). Linear interpolations were used for qualitative values between 0 and 5 while a polynomial interpolation was used for qualitative values superior to 5. In order to quantify the rainfall events within the Upper Bukit Timah basin, a mean qualitative value was extracted using the *Zonal Statistics as Table* function and then was transformed in rainfall intensities using the general relationships previously established. This step was repeated for each image of every event.



**Figure 31. General relationships used to transform qualitative values into rainfall intensities for the Upper Bukit Timah basin**

#### 5.5.2.2. Discharge data

The PUB is the Singapore’s national water agency. Its role is to manage the country’s water supply, water catchment and used water in an integrated way (PUB, 2010). Although the PUB do not agree to share any discharge data, their website contains an interactive map which shows the water level in real time from ninety-three water level sensors around the island (PUB, 2011). The data are updated at an interval of 10 min. For the sake of this work, the water level at the outlet of the Upper Bukit Timah catchment (Bukit Timah 1st Diversion canal, 6th Avenue), was saved every 10 minutes starting with April 29th, 2011, thanks to another batch file used to download automatically the main website’s page<sup>8</sup> which contains the water level of each PUB’s station. For all the period of record, it was noticed that the minimum water depth, at the 1st Diversion canal station, was 0.27 m instead of 0 m. Since PUB did not provide any rating curve despite several attempts to obtain one, it was not possible to know the corresponding discharge. The flood of June 5<sup>th</sup> brought the information. In fact, several flash floods occurred in the central and eastern parts of Singapore at this date and numerous photos and testimonies were published on the

<sup>8</sup> <http://www.pub.gov.sg/general/pages/waterlevel.aspx> contains in its html code the name of each station, its location, the last recorded water level, the flood alert level and the timestamp of each observation



Internet (figure 32). It was reported on Twitter as well as several forums and blogs<sup>9</sup> that at about 11:00 AM the bank full flow was reached. At this hour, a water depth of 3 m was recorded by the PUB. But, according to Chuah (1989), the depth of the canal at the outlet is not 3 m but 2.67 m. By subtracting 0.27 m to 3 m, the resulting depth of 2.73 m could correspond to the value 2.67 m, the error caused by the divergence of information on the Internet and the latency of publishing messages on social websites. Therefore, it was supposed that the value of 0.27 m corresponds to a real water depth of 0 m. It was confirmed by the fact that the water level sensors do not take into account the low water channel, as shown in figure 33. All the measurements were therefore reduced by 0.27 m.



**Figure 32. Flood at the intersection of Bukit Timah Road and Swiss road, the morning of June 5<sup>th</sup>**  
(Source: SPUG forum, 2011)



**Figure 33. Water level sensors on the edge of the canal, not taking into account the level of water in the central notch: A: Bukit Timah Canal (Backmore), B: Sg Kallang Sub Drain (Upper Thomsan Rd), C: Stamford Canal (Handy Rd), D: Stamford Canal (Killiney Rd).** Sources: testech, n.d. (A), Google Street View (B), personal photographs (C, D)

<sup>9</sup> [www.stomp.com.sg/](http://www.stomp.com.sg/), <http://www.spug.sg/forums/>, <http://heresthenews.blogspot.com>, <http://www.expatsingapore.com/forum/>, for example.

Since PUB did not provide a rating curve, the water level measurements were transformed into discharge using the Manning formula. The wetted perimeter  $P$  of a trapezoidal channel (m) can be defined as:

$$P = b + y \left( \sqrt{1 + z_1^2} + \sqrt{1 + z_2^2} \right) \quad (20)$$

where  $b$  is the bottom width (m),  $y$  is the water depth (m) and  $z_1$  and  $z_2$  are the side slope on bank 1 and 2 respectively (m/m). The bottom width  $b$  at the outlet of the catchment is 5.791 m and the side slope is 1 on both sides (Chuah, 1989).

The area  $A$  of the cross-section is:

$$A = \frac{y}{2} (b + T) \quad (21)$$

where the top width  $T$  (m) is equal to:

$$T = b + y(z_1 + z_2) \quad (22)$$

The hydraulic radius  $R_h$  (m) can therefore be calculated by combining equations (21) and (22). Finally, from the velocity  $V$  (m/s) calculated from the Manning's equation, the discharge  $Q$  (m<sup>3</sup>/s) can be determined:

$$Q = AV = \frac{AR_h^{2/3} S^{1/2}}{n} \quad (23)$$

where  $S$  is the channel slope (m/m) and  $n$  is the Manning roughness coefficient (LMNO Engineering, Research, and Software, 2000). In this case, the channel slope  $S$  is 0.00125 while the Manning's coefficient was set to 0.015. A bank full discharge of 74 m<sup>3</sup>/s was obtained for the Bukit Timah channel. It should be noted that the flow in the central notch was not calculated, since it is negligible during a high flow event.

#### 5.5.2.3. *Extracted data and limits*

The discharge and rainfall intensity of eight recent storm events were determined for the basin (table 5). According to Channelnewasia (2011), the flood of June 5th was triggered by 65 mm of precipitation within 30 minutes. The values extracted from the RADAR images were in agreement with that fact, since a value of 63.7 mm was obtained between 10:20 and 10:50 AM. Moreover, this technique proves to be fairly accurate spatially, since the storm events centralised on the Upper Bukit Timah trigger higher discharges than storm events localised on the NUS weather station.

Nevertheless, the estimation of the rainfall intensity from RADAR images is affected by significant errors. Firstly, it is important to remember that the RADAR image resolution is 220 m. Therefore, when the rainfall extracted at the NUS weather station, a pixel of 48400 m<sup>2</sup>, is compared to the measured rainfall, the resulting value is certainly affected by this too high resolution. Secondly, although as many images as possible were used, the technique employed to transform the qualitative scale into quantitative scale is approximate. Indeed, the general relationships result from a mean of approximations between quantitative and qualitative values. Finally, rainfall estimation by RADAR technology is an indirect measure. It uses pulse-Doppler sensors, capable of detecting the motion and the size of rain droplets and the intensity of the

rainfall thanks to the reflectivity of radio waves on the drops. However, the quality of the estimation depends on the proper calibration of this reflectivity. Masking effects, attenuation or signal amplification can affect locally the estimation of the intensity and the location of the precipitation. The best solution is to dispose of direct rainfall measurement from the three weather stations within the basin and depending on their location, attribute them to the subcatchments. Unfortunately, rain gage data was not available for this work.

Discharge data are also uncertain. Since PUB did not provide a rating curve, the transformation of water depth into discharge remains an approximation. It was supposed that a bank full discharge of 74 m<sup>3</sup>/s at the outlet of the Bukit Timah canal was an acceptable value, but it was not verified. However, the different parameters used in equation (23) should be correct as they were provided by a precise sketch done by Chuah (1989).

**Table 5. Duration, maximum discharge and rainfall intensity of the eight recent storm events**

Storm events	Duration (hh:mm)	Max. discharge (m <sup>3</sup> /s)	Max. rainfall intensity (mm/h)
27 Apr 11	02:10	44.7	66.5
30 Apr 11	02:30	20.0	43.7
04 May 11	02:40	37.3	96.6
10 May 11	02:10	6.7	45.2
13 May 11	00:50	39.0	67.2
21 May 11	01:40	64.3	44.8
25 May 11	02:00	103.6*	49.6
05 June 11	07:30	79.7	101.5

\*aberrant value (the water depth published by PUB reached 3.9 m)

## 5.6. Evapotranspiration

Evapotranspiration encompasses all phenomena that cause water to vaporise. It is the addition of the evaporation from the subcatchments surfaces (lake, streams...), groundwater or vegetation and the transpiration from vegetation (Dassargues, 2010). It can be included in SWMM as an average monthly value. The monthly mean potential evapotranspiration  $E$  (mm/month) can be estimated from Thornthwaite's formula:

$$ETP = 16 \left( \frac{10 \bar{T}(m)}{I} \right)^a f(m, \varphi) \quad (24)$$

where  $\bar{T}(m)$  is the average daily temperature of the month (°C),  $f(m, \varphi)$  is a corrective factor depending on the month  $m$  and latitude  $\varphi$ ,  $a$  is a coefficient equal to:

$$a = 6.75 \cdot 10^{-7} I^3 + 7.71 \cdot 10^{-5} I^2 + 1.792 \cdot 10^{-2} I + 0.49 \quad (25)$$

and  $I$  is a heat index depending on the 12 monthly mean temperatures and equal to;

$$I = \sum_{m=1}^{12} i(m) = \sum_{m=1}^{12} \left( \frac{\bar{T}(m)}{5} \right)^{1.514} \quad (26)$$

Table 6 presents the calculated potential evapotranspiration. With a mean monthly value of 142 mm, or 4.6 mm per day, the influence of evapotranspiration is very weak. For example, for a



rainfall event of 50 mm within one hour, evapotranspiration only reduces it by 0.17 mm. After several tests, it was decided not to include it in the model. Evapotranspiration might only be detected in the annual or monthly balance, but not for individual storm events.

**Table 6. Monthly mean potential evapotranspiration (mm)**

Jan	Feb	Mar	Apr	May	Jun	Jul	Aug	Sep	Oct	Nov	Dec
127	133	147	143	170	144	148	148	143	147	123	127

(Monthly mean temperature from The Weather Channel, 2011)

## 5.7. SWMM pre-parameterisation

A pre-parameterisation of the SWMM model was done using the old storm events. This was realised in order to decide what the best methods for the parameter determination are (eg. Horton versus CN for infiltration parameters, Kinematic versus Dynamic Wave for flow routing, etc.). In addition to graphical techniques, the Nash-Sutcliffe coefficient was used to evaluate each test. Using the results of the pre-parameterisation, a final adjustment was performed to ameliorate the pre-parameterised model in a finer way (see next section).

### 5.7.1. Graphical techniques

A visual comparison of simulated and measured hydrographs can bring a first overview of model performance. In fact, hydrographs were observed in order to identify model bias, differences in timing and magnitude of peak flows and the shape of recession curves. According to Moriasi *et al.* (2007), it is recommended to use both graphical techniques and quantitative statistics to appropriately evaluate a model. The Nash-Sutcliffe coefficient constitutes the second method for model evaluation.

### 5.7.2. Nash-Sutcliffe coefficient

Moriasi *et al.* (2007) recommended that the Nash-Sutcliffe coefficient is a good parameter to evaluate the efficiency of a watershed model. This coefficient is a normalised statistic parameter that determines the relative magnitude of the residual variance compared to the measured data variance (*ibid.*). According to Javaheri (1999), who used the Nash-Sutcliffe coefficient to evaluate his parameterisation of the Upper Bukit Timah catchment model, it is a popular function that has gained importance. Also, Sevat and Dezetter (1991), who compared different approaches used in model calibration, estimated that the best function to use for calibration was the Nash-Sutcliffe coefficient. This coefficient is defined as follow:

$$NASH = 1 - \left( \frac{\sum_{i=1}^n (Y_i^{obs} - Y_i^{sim})^2}{\sum_{i=1}^n (Y_i^{obs} - Y_i^{mean})^2} \right) \quad (27)$$

where  $Y_i^{obs}$  is the  $i^{th}$  observed discharge,  $Y_i^{sim}$  is the  $i^{th}$  simulated discharge,  $Y_i^{mean}$  is the mean of observed discharge and  $n$  is the total number of observations.

Nash-Sutcliffe coefficient ranges between  $-\infty$  and 1, 1 being the optimal value. Values between 0 and 1 are generally acceptable whereas values inferior to 0 show an unacceptable performance of the model (Moriassi *et al.*, 2007). It has been estimated that model simulation can be judged as satisfactory if the Nash-Sutcliffe coefficient is superior to 0.5 (*ibid.*).

### 5.7.3. Pre-tests

Twenty one tests were done on the sixteen old storms events (= 336 tests) in order to underline what were the best methods for parameters determination (table 7). Each test (or project) was performed by changing the parameters manually. Subcatchments area and slope stayed constant for all tests. It was also the case for conduits properties, apart for the Manning's coefficient and depth.

This pre-parameterisation was performed in two stages. The first stage was made of several pre-project, used to test different parameters. The second stage consisted in modifying first stage best projects (projects 15, 22, 23, 24), for which some errors were found concerning conduits length. These errors did not impede the model to run and did not greatly influence the outcomes but it was preferred to correct them for the remaining of the parameterisation. As first stage projects show accurate results and allow to understand which parameterisation is best to be used, they are still shown here.

Table 7 shows that the Horton infiltration method gives very bad results compared to the CN method. Also, the methods 3 and 4 for calculating the widths, which show higher value than the other methods, seem not to be appropriate. In the other hand, smaller widths give better Nash-Sutcliffe coefficient value. Projects 25\_corr and 26\_corr, for which the conduits depth was increased to 5 m in order to take into account the one-dimensional model limitations and avoid the truncation of hydrographs during flood events, have the worst Nash-Sutcliffe value. It can be seen on the graphs that, for these projects, there is no loss of water during the modelling and the discharge is greatly overestimated. Table 7 shows that all calculated mean Nash-Sutcliffe coefficients are negative, which means that the model still have to be improved. The appendix 4 regroups all graphs of all events tested with each project with their corresponding Nash-Sutcliffe coefficient.

**Table 7. Pre-parameterisation projects characteristics**

Characteristics figuring in green show a good influence on the model, contrarily to characteristics in red.  
Nash-Sutcliffe coefficients are in conditional formatting: red colour shows very bad results, green colour shows better results.  
Proj\_final, in green, is the project selected for the model adjustment.

Project	Subcatchments properties			Infiltration	Flow routing	Conduit properties		Mean Nash-Sutcliffe coefficient (16 storm events)
	Width*	% of imperv.	Manning			Manning	Depth	
Proj6	Method 2	Higher values of the literature	Weighted coeff.	Horton	Dynamic	0.013 & 0.03	real	-1.626
Proj12	Method 2	Mean	Weighted coeff.	CN Grid 1	Dynamic	0.013 & 0.03	real	-1.003
Proj13	Method 2	Mean	Weighted coeff.	Horton	Dynamic	0.013 & 0.03	real	-1.421
Proj14	Method 3	Mean	Weighted coeff.	Horton	Dynamic	0.013 & 0.03	real	-1.580
Proj15	Method 2 - 500 m	Mean	Weighted coeff.	CN Grid 1	Dynamic	0.013 & 0.03	real	-0.525
Proj16	Method 2	Mean	Liong et al. (1993)	CN Grid 1	Dynamic	0.013 & 0.03	real	-0.797
Proj17	Method 3	Mean	Weighted coeff.	CN Grid 1	Dynamic	0.013 & 0.03	real	-1.085
Proj18	Method 4	Mean	Weighted coeff.	CN Grid 1	Dynamic	0.013 & 0.03	real	-1.156
Proj19	Method 2 - 200 m for upstream subc. (5;10;11;12;13;14;15)	Mean	Weighted coeff.	CN Grid 1	Dynamic	0.013 & 0.03	real	-0.944
Proj20	Method 2 - 200 m for downstream subc. (1;2;3;4;7;6;9)	Mean	Weighted coeff.	CN Grid 1	Dynamic	0.013 & 0.03	real	-0.973
Proj21	Method 2 - 200 m	Mean	Weighted coeff.	CN Grid 1	Dynamic	0.013 & 0.03	real	-0.915
Proj22	Method 2 - 300 m	Mean	Weighted coeff.	CN Grid 1	Dynamic	0.013 & 0.03	real	-0.889
Proj23	Method 1	Mean	Weighted coeff.	CN Grid 1	Dynamic	0.013 & 0.03	real	-0.185
Proj24	Method 2 - 400 m	Mean	Weighted coeff.	CN Grid 1	Dynamic	0.013 & 0.03	real	-0.694
Proj15_corr	Method 2 - 500 m	Mean	Weighted coeff.	CN Grid 1	Kinematic	0.013 & 0.03	real	-0.694
Proj22_corr	Method 2 - 300 m	Mean	Weighted coeff.	CN Grid 1	Kinematic	0.013 & 0.03	real	-1.102
Proj23_corr	Method 1	Mean	Weighted coeff.	CN Grid 1	Kinematic	0.013 & 0.03	real	-0.309
Proj24_corr	Method 2 - 400 m	Mean	Weighted coeff.	CN Grid 1	Kinematic	0.013 & 0.03	real	-0.775
Proj25_corr	Method 2 - 500 m	Mean	Weighted coeff.	CN Grid 1	Kinematic	0.013 & 0.03	5 m for all cond.	-2.030
Proj26_corr	Method 2 - 500 m	Mean	Weighted coeff.	CN Grid 1	Kinematic	0.015 & 0.03	5 m for all cond.	-2.389
Proj27_corr	Method 1	Mean	Manning perv. areas - 0.02	CN Grid 1	Kinematic	0.013 & 0.03	real	-0.728
Proj_final	Method 1	According to Guo (2003)	Weighted coeff.	CN Grid 1	Dynamic	0.015 & 0.03	real	-0.045

\* Method 1: Rossmann (2010) and Gironas et al. (2009)'s method; Method 2: Rossmann (2010) and Gironas et al. (2009)'s method (excluding chan. Flow); Method 3: Javaheri (1999)'s method (skew factor); Method 4: Cantone (2010)'s method

Project\_final was selected for SWMM adjustment (next section), since Nash-Sutcliffe coefficients and graphical analysis (see appendix 4) showed the best results. This project corresponds to the following characteristics:

- the width is determined by method 1, namely the subcatchment area divided by the maximum overland flow length;
- the percentage of imperviousness was calculated using the coefficients of imperviousness given by Guo (2003);
- the Manning's coefficients for both pervious and impervious surfaces is weighted for each subcatchment;
- the CN method of infiltration is used;
- the Dynamic Wave method is the flow routing;
- the Manning's coefficient for conduits is set at 0.015 and 0.03 for concrete and earth channel respectively, and;
- the depth of conduits is determined in the previous chapter.

## **5.8. Final SWMM adjustment**

The previous section showed that the Nash-Sutcliffe coefficients values obtained for project\_final were negative. It was observed on the graphs that SWMM model always overestimated the discharge. To improve the SWMM model, a finer parameterisation was performed in order to lower the simulated flow. A summary table below details the characteristics of the different projects used for the model adjustment (table 8). All graphs figure in the appendix 5.

### **5.8.1. Adjustment tests**

Since some authors identify the width as a calibration parameter (see above), several modifications of its value were done (width determined by method 1 minus 10, 20, 25, 50, 100, 200 m). The influence of the width on the model was thus observed. Simultaneously, the Manning's coefficient was also modified, because its values were uncertain due to the variability of the land cover (Javaheri, 1999). The modification consisted in increasing the Manning's coefficients of impervious surface by 0.002, 0.005, 0.01 and 0.05. Then, on the basis of the project for which the width was decreased by 200, several tests were done by modifying the Manning's coefficient for impervious surfaces. Finally, on the basis of the best previous test (width minus 200, Manning's coefficient plus 0.002), which gave a mean Nash-Sutcliffe value of 0.358, the percentage of imperviousness was lowered by 1, 5 and 7 %. In fact, according to Javaheri (1999), the percentage of imperviousness was one of the best calibration parameter, as the width. A last test was performed using the CN Grid 2. Table 8 below gives all the details of the adjustment tests.

**Table 8. Adjustment projects characteristics**

Each modification performed figures in blue.

Nash-Sutcliffe coefficients are in conditional formatting: red colour shows very bad results, green colour shows better results.

Proj\_final, in green, is the project selected.

Project	Subcatchments properties					Infiltration	Flow routing	Conduit properties	Mean Nash-Sutcliffe coefficient (16 storm events)
	Width*	Manning		% of imperv.					
		Perv.	Imperv.						
Proj_final	Method 1 - 10	Weighted coeff.	Weighted coeff.	According to Guo (2003)	CN Grid 1	Dynamic	0.015 & 0.03	-0.027	
Proj_final	Method 1 - 20	Weighted coeff.	Weighted coeff.	According to Guo (2003)	CN Grid 1	Dynamic	0.015 & 0.03	-0.017	
Proj_final	Method 1 - 25	Weighted coeff.	Weighted coeff.	According to Guo (2003)	CN Grid 1	Dynamic	0.015 & 0.03	-0.009	
Proj_final	Method 1 - 50	Weighted coeff.	Weighted coeff.	According to Guo (2003)	CN Grid 1	Dynamic	0.015 & 0.03	0.021	
Proj_final	Method 1 - 100	Weighted coeff.	Weighted coeff.	According to Guo (2003)	CN Grid 1	Dynamic	0.015 & 0.03	0.088	
Proj_final	Method 1 - 200	Weighted coeff.	Weighted coeff.	According to Guo (2003)	CN Grid 1	Dynamic	0.015 & 0.03	0.354	
Proj_final	Method 1	Weighted coeff.	Weighted coeff. + 0.002	According to Guo (2003)	CN Grid 1	Dynamic	0.015 & 0.03	-0.008	
Proj_final	Method 1	Weighted coeff.	Weighted coeff. + 0.005	According to Guo (2003)	CN Grid 1	Dynamic	0.015 & 0.03	0.019	
Proj_final	Method 1	Weighted coeff.	Weighted coeff. + 0.01	According to Guo (2003)	CN Grid 1	Dynamic	0.015 & 0.03	0.049	
Proj_final	Method 1	Weighted coeff.	Weighted coeff. + 0.05	According to Guo (2003)	CN Grid 1	Dynamic	0.015 & 0.03	0.057	
Proj_final	Method 1 - 200	Weighted coeff.	Weighted coeff. + 0.002	According to Guo (2003)	CN Grid 1	Dynamic	0.015 & 0.03	0.358	
Proj_final	Method 1 - 200	Weighted coeff.	Weighted coeff. + 0.01	According to Guo (2003)	CN Grid 1	Dynamic	0.015 & 0.03	0.348	
Proj_final	Method 1 - 200	Weighted coeff.	Weighted coeff. + 0.05	According to Guo (2003)	CN Grid 1	Dynamic	0.015 & 0.03	0.195	
Proj_final	Method 1 - 200	Weighted coeff.	Weighted coeff. + 0.002	According to Guo (2003) - 1%	CN Grid 1	Dynamic	0.015 & 0.03	0.379	
Proj_final	Method 1 - 200	Weighted coeff.	Weighted coeff. + 0.002	According to Guo (2003) - 5%	CN Grid 1	Dynamic	0.015 & 0.03	0.456	
Proj_final	Method 1 - 200	Weighted coeff.	Weighted coeff. + 0.002	According to Guo (2003) - 7%	CN Grid 1	Dynamic	0.015 & 0.03	0.482	
Proj_final	Method 1 - 200	Weighted coeff.	Weighted coeff. - 0.002	According to Guo (2003) - 7%	CN Grid 2	Dynamic	0.015 & 0.03	0.422	

\* Method 1: Rossman (2010) and Gironas *et al.* (2009)'s method (excluding chan. Flow); Method 3: Javaheri (1999)'s method (skew factor); Method 4: Cantone (2010)'s method

\* Method 1: Rossman (2010) and Gironas *et al.* (2009)'s method (excluding chan. Flow); Method 2: Rossman (2010) and Gironas *et al.* (2009)'s method (excluding chan. Flow); Method 3: Javaheri (1999)'s method (skew factor); Method 4: Cantone (2010)'s method

## 5.8.2. SWMM final parameterisation

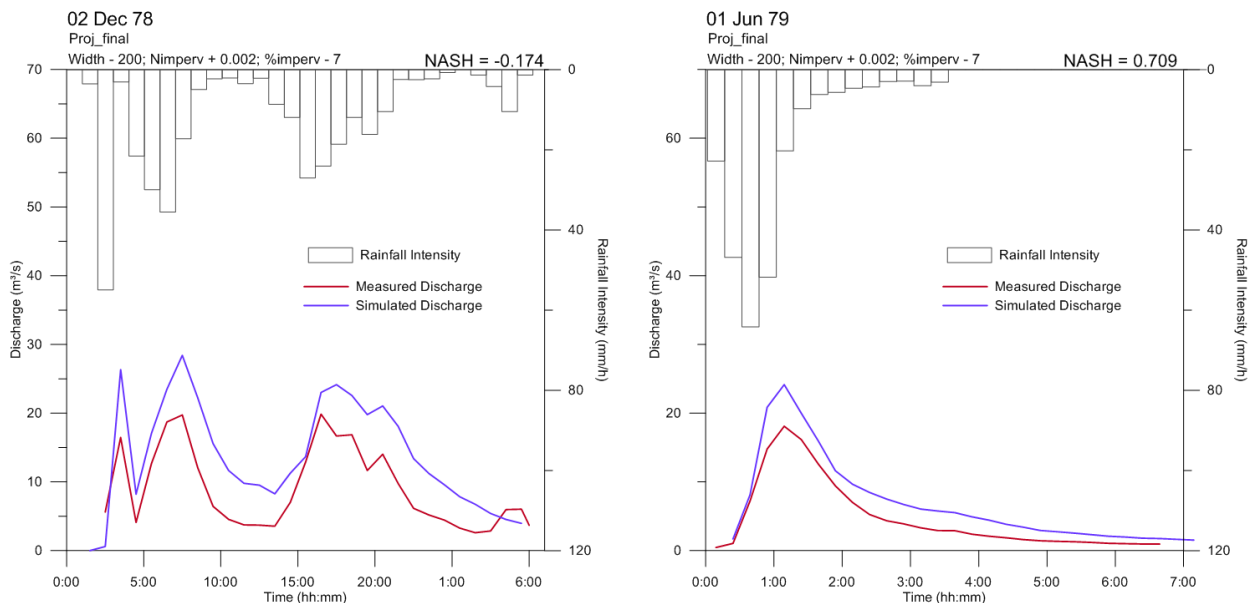
### 5.8.2.1. Characteristics

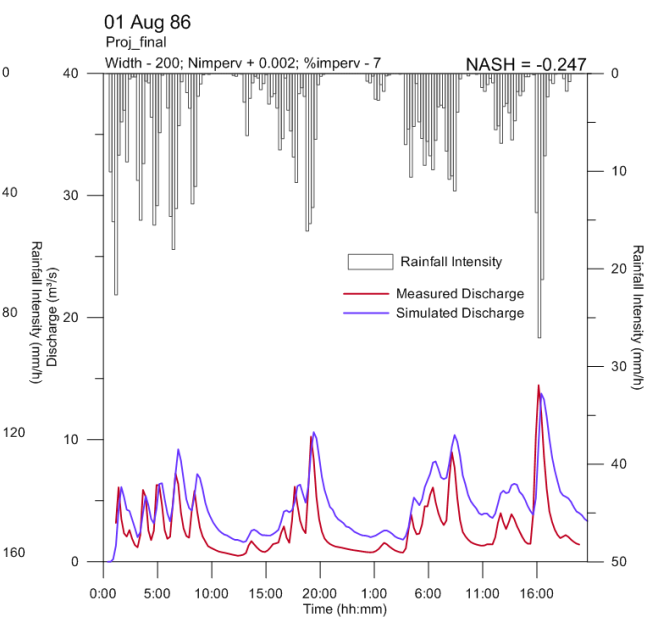
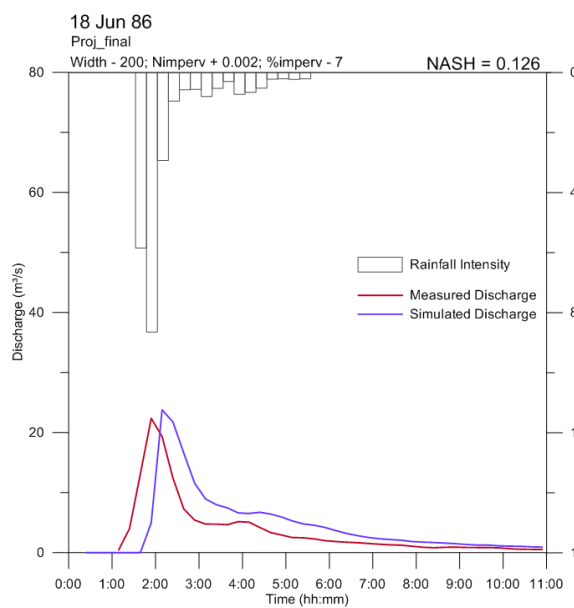
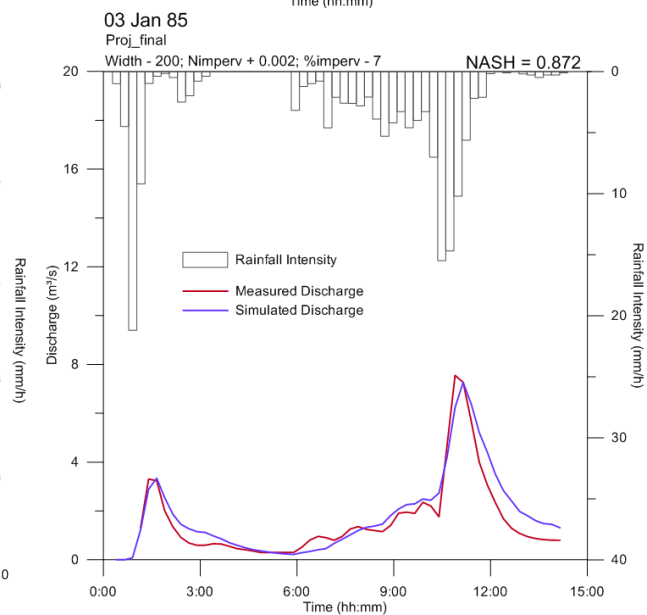
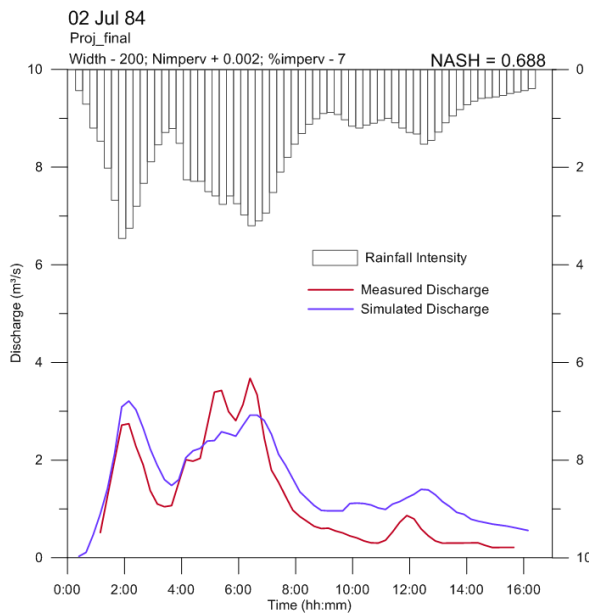
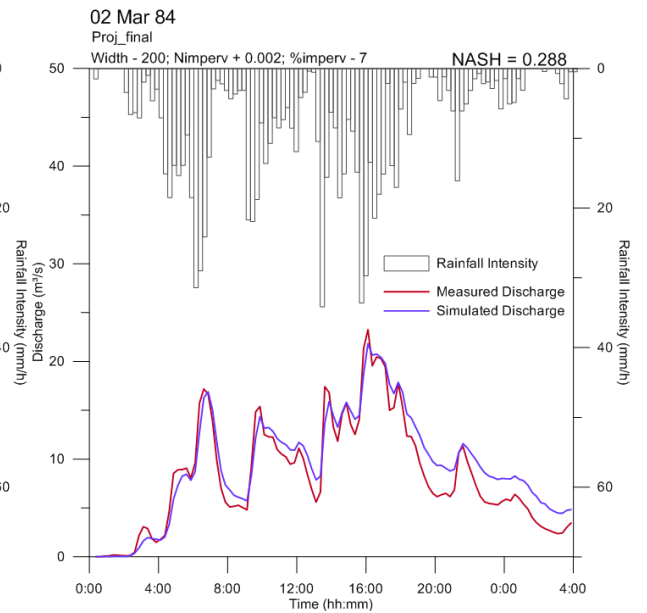
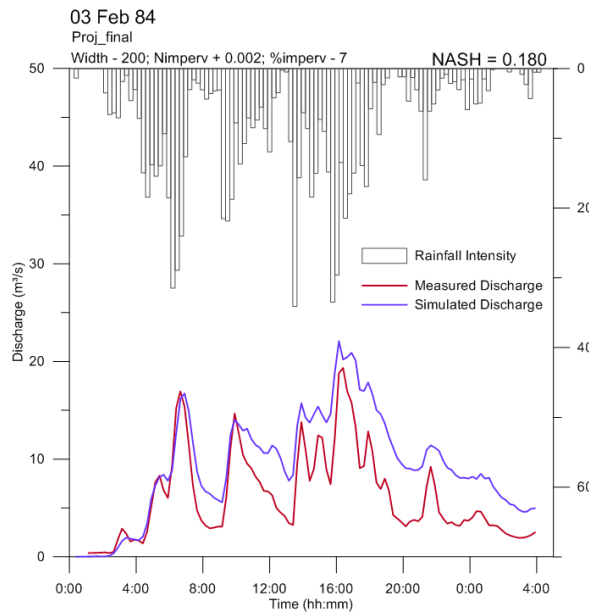
A final project was selected, the mean Nash-Sutcliffe coefficient being 0.482. The graphs corresponding to this project are grouped in figure 34. The selected project characteristics are defined as follows:

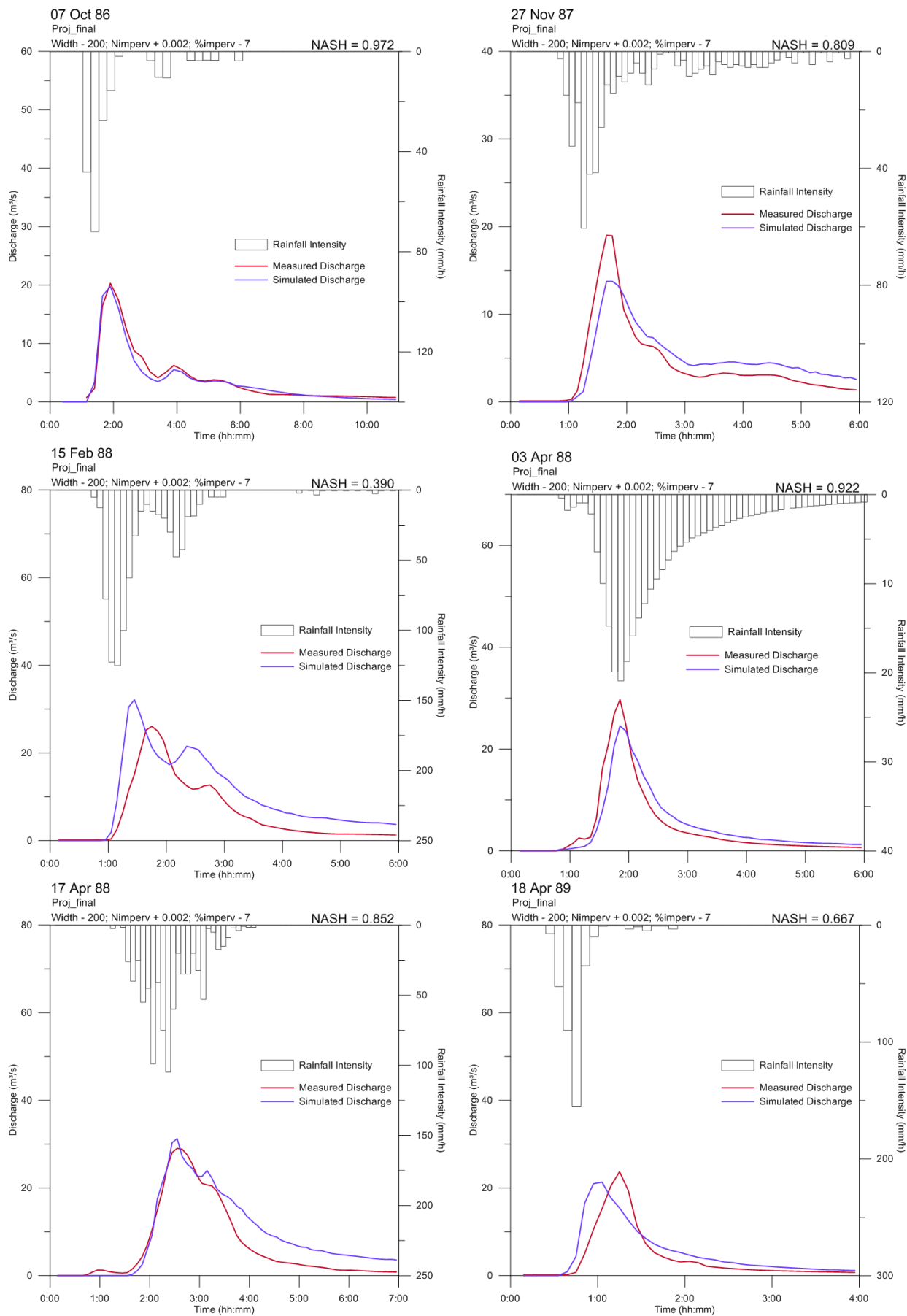
- the width is determined by method 1, its value is lowered by 200;
- the Manning's coefficient for pervious areas ( $N_{perv}$ ) is weighted for each subcatchment, for impervious surfaces ( $N_{imperv}$ ), it is increased by 0.002;
- the percentage of imperviousness ( $\%imperv$ ) corresponds to the land use imperviousness given by Guo (2003), its value is lowered by 7 %. This is certainly due to the fact that storm events tested here date from the 1980s while the imperviousness date from 2009;
- the CN method of infiltration is used, with CN grid 1;
- the Dynamic Wave method is the flow routing;
- the Manning's coefficient for conduit ( $N_{cond}$ ) is set at 0.015 and 0.03 for concrete and dirt channels respectively.

### 5.8.2.2. Final parameterisation evaluation

Although Moriasi *et al.* (2007) recommended a Nash-Sutcliffe coefficient superior to 0.5 for a watershed model adjustment, the mean value of 0.482 was considered as satisfactory. In fact, the graphs analysis showed that the simulated discharge matches the observed ones fairly well (figure 34). For some storm events (1 Aug 86), a negative Nash-Sutcliffe value was obtained because the simulated curve shifts, but the peak flow and curve shape were still acceptable. It is therefore important to perform a graphical analysis conjointly to a Nash-Sutcliffe coefficient determination.





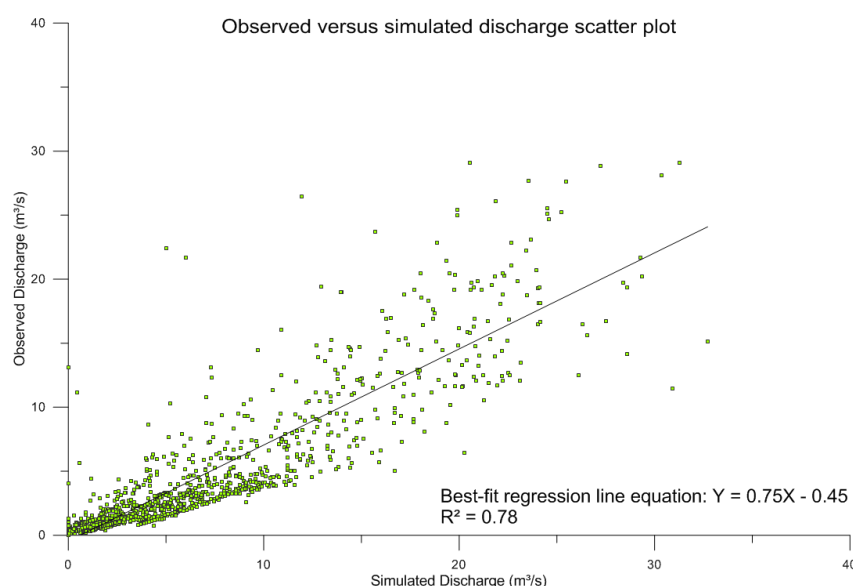


**Figure 34. Graphs corresponding to the final parameterisation project for all storm events.**



Other methods to evaluate a watershed model were tested for the final parameterisation project. The slope and y-intercept of the best-fit regression line can indicate how well simulated data matches measured data (*ibid.*). A slope of 1 indicates a perfect relationship between simulated and measured values while a y-intercept of 0 indicates that there is no lag between model prediction and measured data and that the data sets are perfectly aligned (*ibid.*). In this case, the value of the slope is 0.75, indicating that the model tends to overestimate the discharge. It can be observed on figure 34 that the model tends to overestimated discharge in the recession curve, but that the peak flow are relatively well estimated (eg 01 Aug 86, 02 Mar 84, 18 Apr 89). The y-intercept is -0.45, which means that there is a lag between observed and measured data. This can be observed on some graphs of figure 34 (eg. 15 Feb 88). According to Moriasi *et al.* (2007), care needs to be taken while using regression statistics because this method uses the assumption that all of the error variance is contained in simulated values and that measured data are error free. In reality, measured data are not error free since they have been extracted from graphs. Errors due to the georeferencing and digitisation of the graphs are inevitably present. Moreover, the method for estimating discharge and the technique of measurement of rainfall at the time the data were obtained are not known. This fact has been discussed in section 5.5.1.1.

The coefficient of determination  $R^2$  is also an indicator, and typically values greater than 0.5 are considered as acceptable (*ibid.*). A value of 0.78 was obtained.



**Figure 35. Relationship between observed and simulated discharge at the outlet for all 16 storm events**

Several error indices are commonly used in model evaluation, among which the widely used RMS and the RMS-observations standard deviation ratio (RSR), developed by Moriasi *et al.* (2007). RSR standardises RMS using the observation standard deviation  $SD$  so that the resulting statistic can apply to various constituents. In this case though, only the discharge was considered. RSR varies from the optimal value of 0 to a large positive value. It is calculated as follow:

$$RSR = \frac{RMSE}{SD} = \frac{\sqrt{\sum_{i=1}^n (Y_i^{obs} - Y_i^{sim})^2}}{\sqrt{\sum_{i=1}^n (Y_i^{obs} - Y^{mean})^2}} \quad (28)$$

where  $Y_i^{obs}$  is the  $i^{th}$  observed discharge,  $Y_i^{sim}$  is the  $i^{th}$  simulated discharge,  $Y^{mean}$  is the mean of observed discharge and  $n$  is the total number of observations. A RMS of 0.12 and a RSR of 0.68 were calculated. Model performance can be evaluated as satisfactory if RSR is inferior to 0.7 (*ibid.*).

The comparison between simulated and measured hydrographs, the Nash-Sutcliffe coefficients, the regression analysis, the coefficient of determination and the RMS and RSR parameters show that our SWMM model can be considered as satisfactory. The next section explains the application of this SWMM model on old and current storm events with their corresponding imperviousness.

## 5.9. SWMM verification

The pre-parameterisation and final adjustment of SWMM was done using the old storm events and the current imperviousness. The final model was tested for old storm events and their corresponding old land use as well as for current storm events and their corresponding imperviousness. This is a necessary step to show that the SWMM model can be used for both old and current patterns of the Upper Bukit Timah basin in order to realise a diachronic analysis of the effect of urbanisation on runoff.

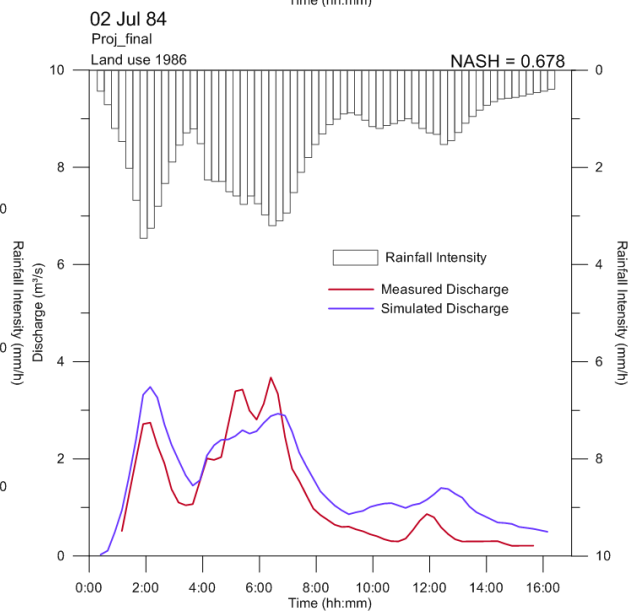
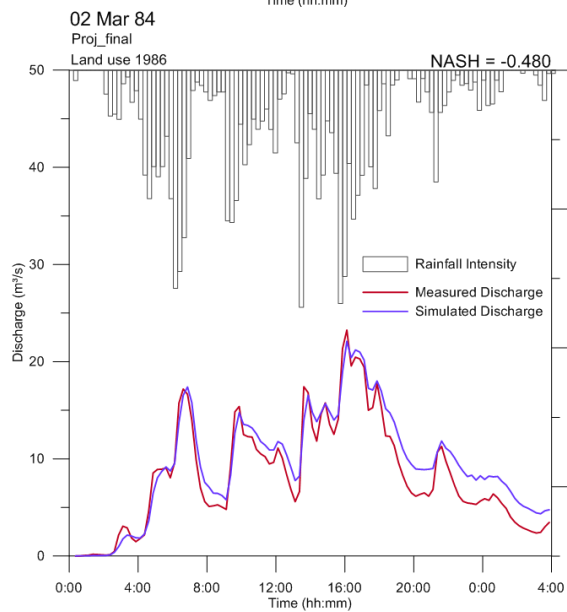
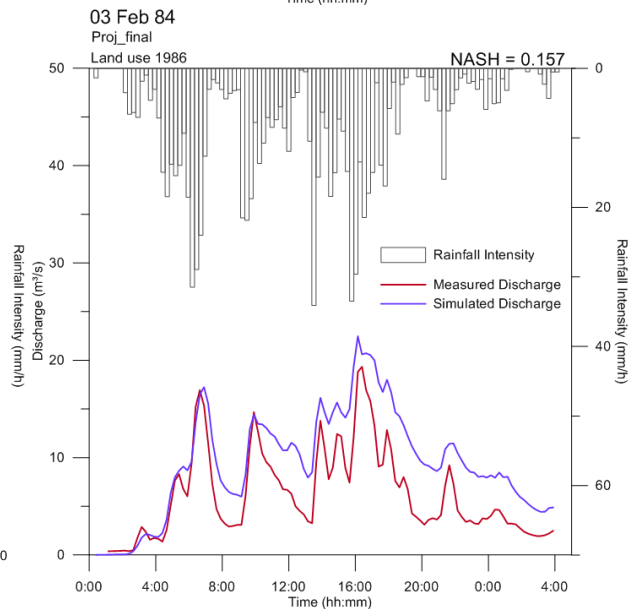
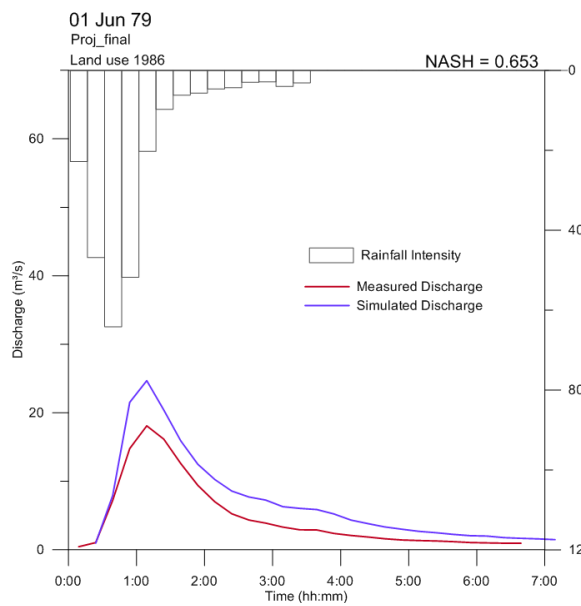
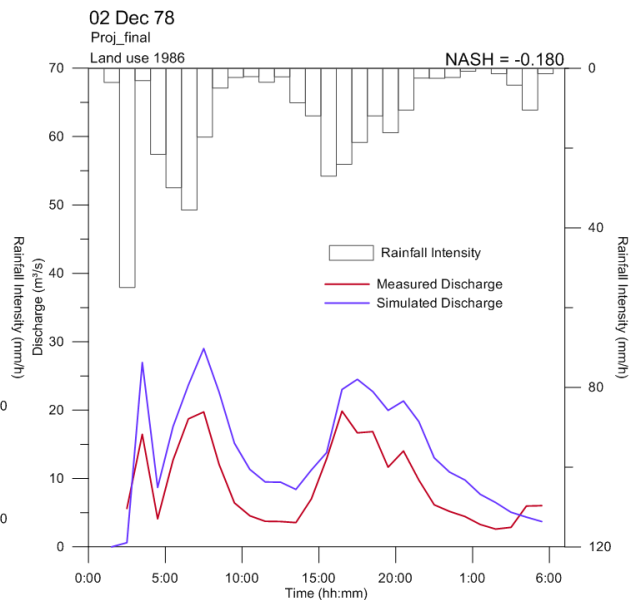
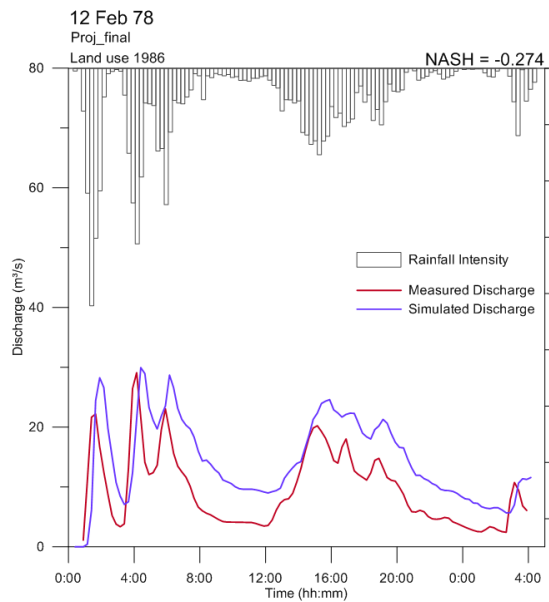
### 5.9.1. Old storm events

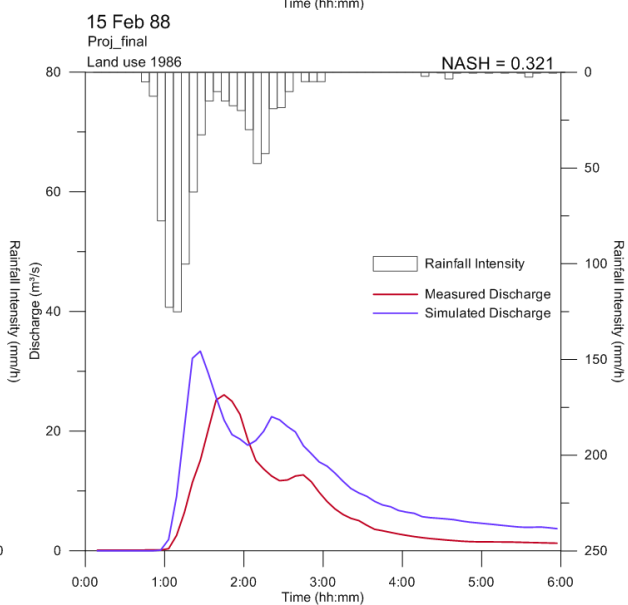
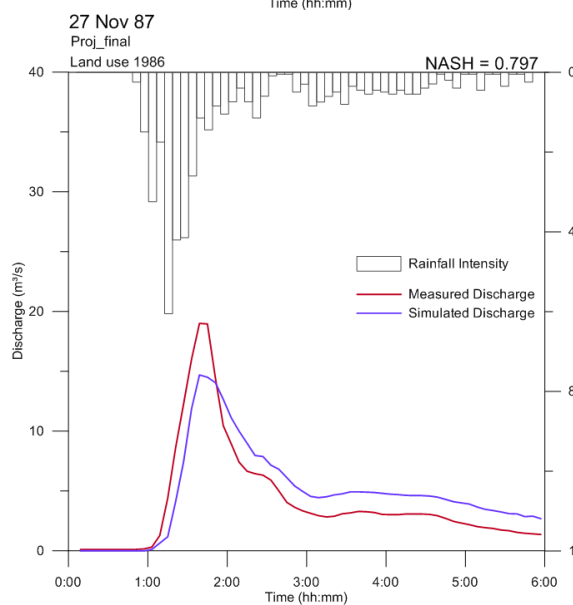
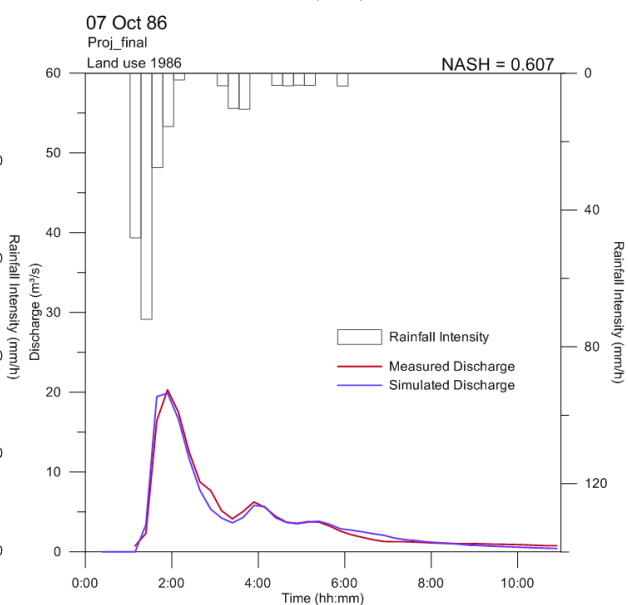
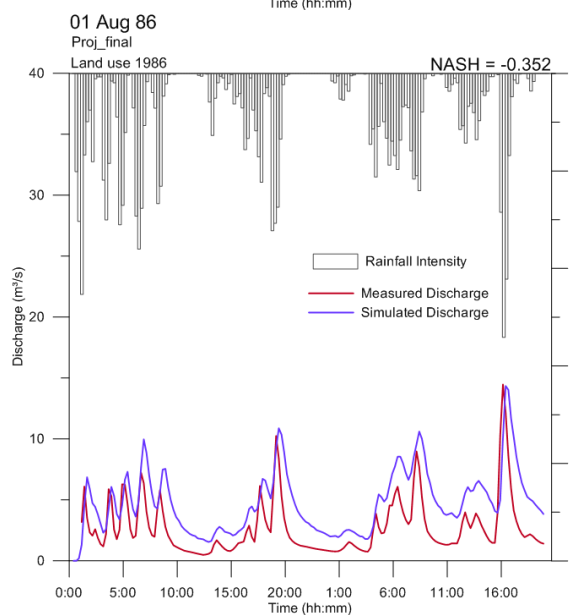
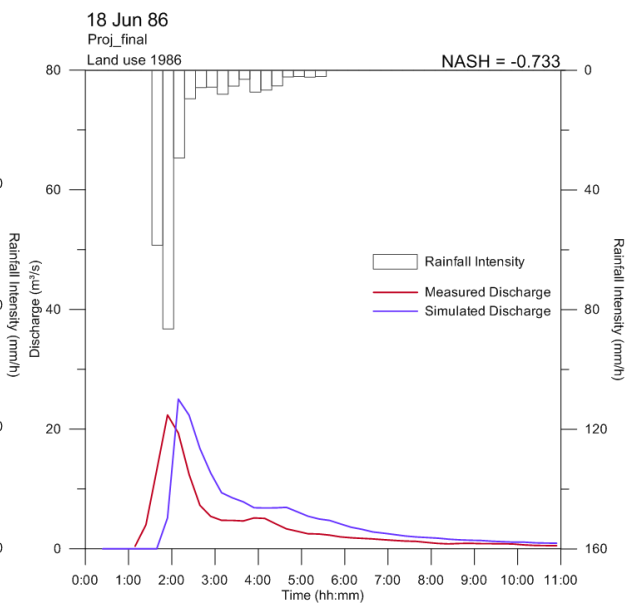
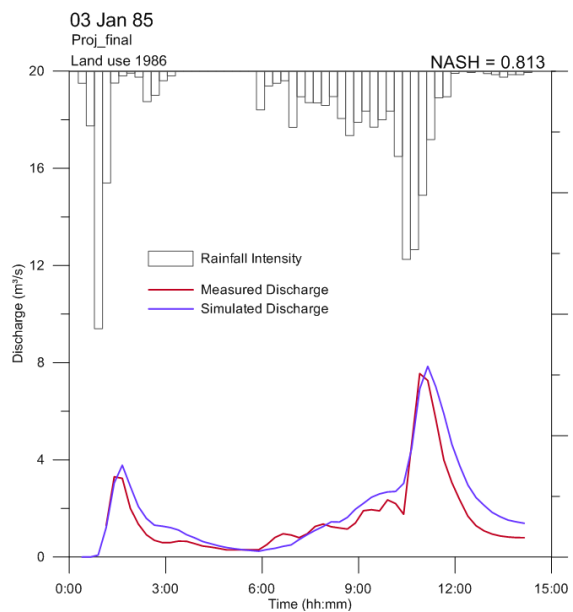
In order to characterise the imperviousness corresponding to the old storm events of the 1980s, the Chuah's land use map (1986) was georeferenced and digitised. Correspondences between the legend of the old map and current land use classification figure in the appendix 6. The percentage of imperviousness of the Upper Bukit Timah was calculated using the same technique as previously. On average, the difference between current and 1986 percentage of imperviousness is 3.8%, with a standard deviation of 6.7. Table 9 shows the percentage of imperviousness corresponding to the 1986 map.

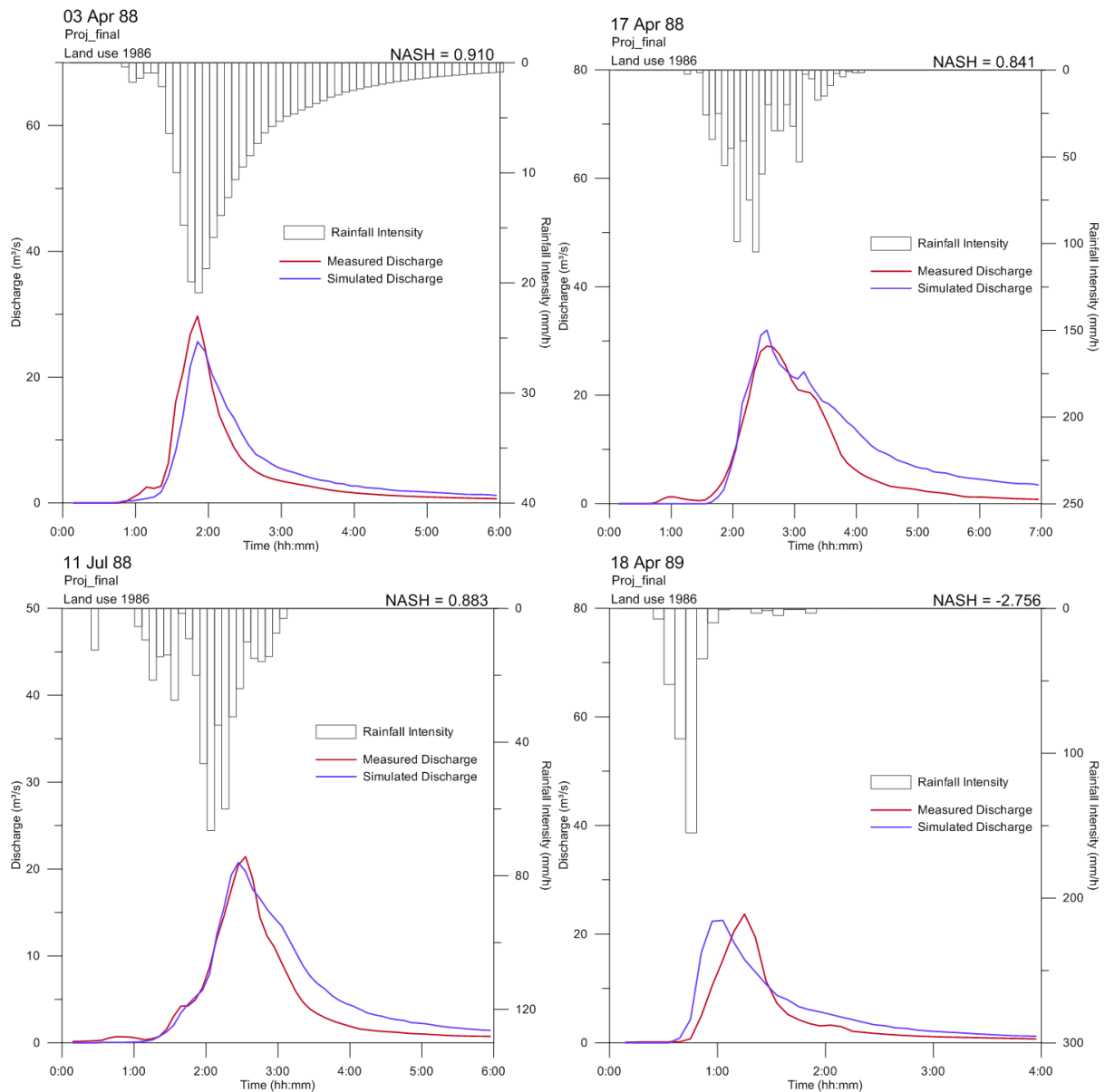
**Table 9. Percentage of imperviousness corresponding to the 1986 land use (%)**

S1	S2	S3	S4	S5	S6	S7	S8	S9	S10	S11	S12	S13	S14	S15
49.6	33.6	47.1	39.7	9.7	61.3	48.2	61.0	62.2	52.8	60.3	10.3	32.2	15.9	16.4

The final project presented in the previous section was tested using the percentages of imperviousness of table 9. A mean Nash-Sutcliffe coefficient of 0.44 was obtained for the sixteen old storm events tested here. This value, in addition to the graphs presented in figure 36, show that the model is adapted for the modelling of the Upper Bukit Timah associated with its past land use.







**Figure 36. Graphs corresponding to the project adapted to the 1986 land use map for all storm events.**

### 5.9.2. Recent storm events (2011)

The final parameterisation of the SWMM model<sup>10</sup> was tested on the eight storm events of May and June 2011. Unfortunately, this first test did not give as good results as for the sixteen old storm events. Several manipulations were done to try to improve the model.

#### 5.9.2.1. Influence of SWMM parameters on the hydrograph

To understand why the SWMM model did not work with current data and eventually find the parameters adapted to all current storm events, the influence of the variation of some parameters on modelled hydrograph was highlighted by several tests. Thirty-six tests were performed on the eight current storm events (table 10). The graphs of figure 37 (p.81) present an example of the

<sup>10</sup> Proj\_final, width – 200 ; Nimperv + 0.002 ; %imperv – 7 ; Ncond 0.015 ; Dynamic Wave ; CN Grid 1.

thirty-six tests executed on the May 13<sup>th</sup> event. All other resulting hydrographs figure in the appendix 7.

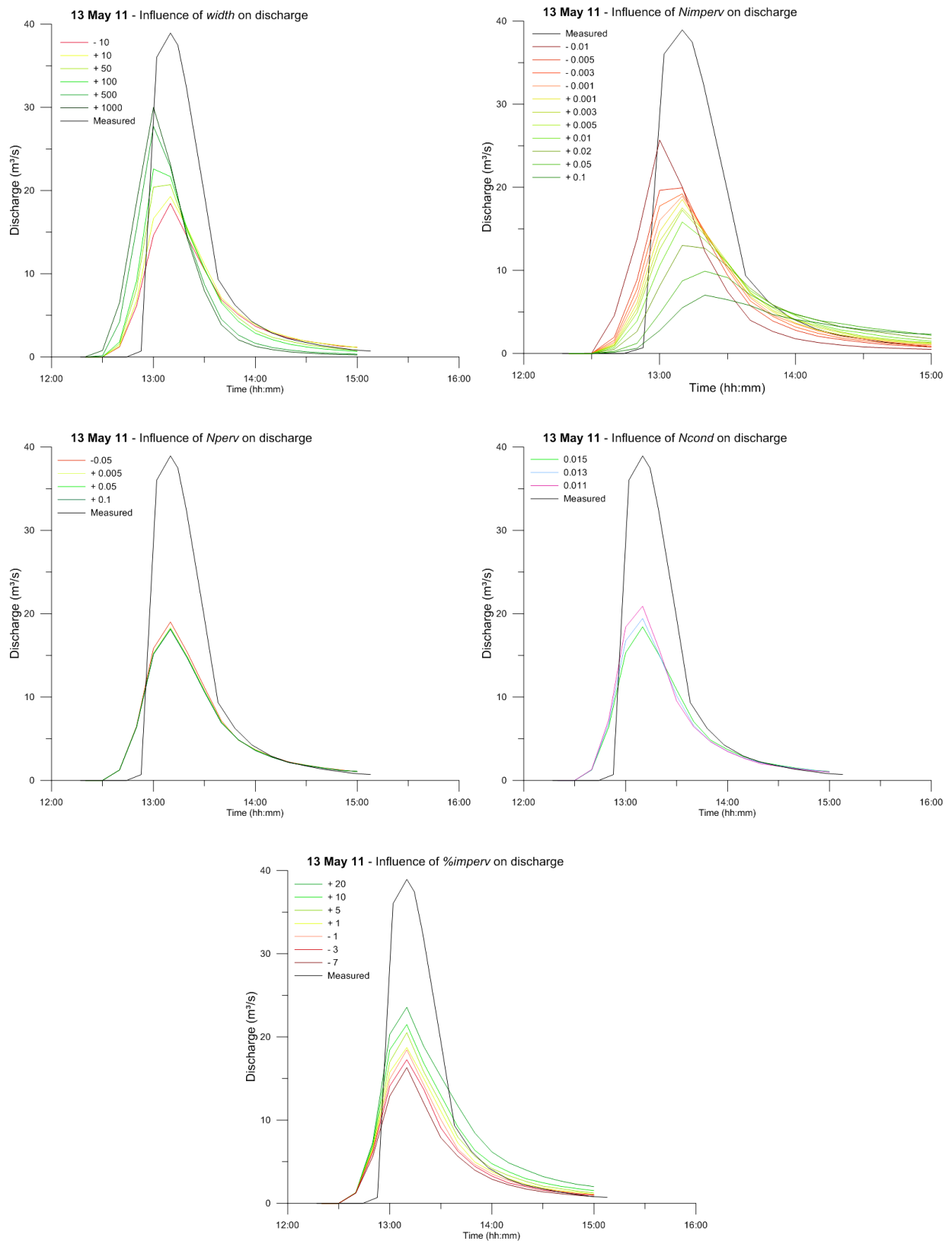
These graphs show that, for all events and all tests, the modelled discharge does not match the measured discharge at all. For some events, the shape of the modelled hydrograph is approximately correct while for others events, measured discharges seem aberrant (May the 4<sup>th</sup> and May the 25<sup>th</sup> for example). The hydrographs also show that the most influential parameters are the width and the Manning's coefficient of impervious area (*Nimperv*). On the other hand, the Manning's coefficient of pervious surfaces (*Nperv*) seems to be the less influential parameter.

**Table 10. Tests performed to establish the relationships between SWMM parameters and discharge for current storm events**

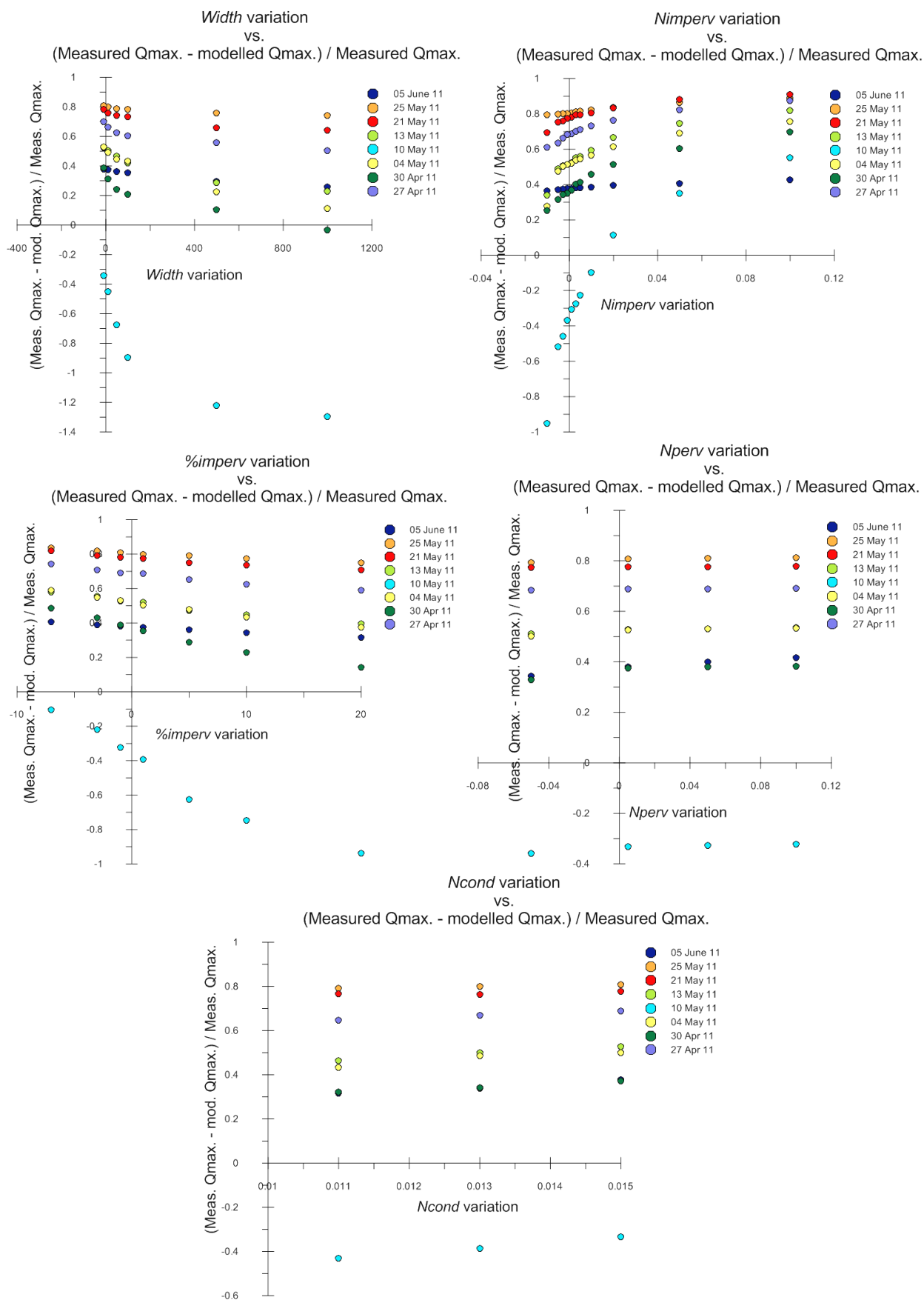
Parameter	Variations
Manning for concrete conduits ( <i>Ncond</i> )	Set at: 0.011 ; 0.013 ; 0.015.
Manning for imperv. areas ( <i>Nimperv</i> )	Increased by: 0.001 ; 0.003 ; 0.005 ; 0.01 ; 0.02 ; 0.05 ; 0.1 ; Lowered by: 0.001 ; 0.003 ; 0.005 ; 0.01.
Manning for perv. areas ( <i>Nperv</i> )	Increased by: 0.005 ; 0.05 ; 0.1 ; 0.05 ; Lowered by: 0.05
Percentage of imperv. (% <i>imperv</i> )	Increased by: 1 ; 5 ; 10 ; 20 ; Lowered by: 1 ; 3 ; 7 ; 10.
Width	Increased by: 10 ; 50 ; 100 ; 300 ; 500 ; 1000 ; Lowered by: 10 ; 30 ; 50 ; 100.

#### 5.9.2.2. Influence of SWMM parameters on maximum discharge

Failing the adjustment of the entire hydrograph curve, the peak flow of each test was extracted in order to eventually find a relationship between the maximum modelled discharge and each variation of the parameters and then to adjust the model to fit the maximum measured discharge. Graphs in figure 38 below show the relationships between the variation of parameters and the normalised difference between the measured maximum discharge and the modelled maximum discharge.



**Figure 37. Tests performed to show the influence of parameters variation on modelled discharge, Example of the May 13<sup>th</sup> event. From left to right, top to the bottom: influence of width,  $N_{imperv}$ ,  $N_{perv}$ ,  $N_{cond}$  and %imperv**



**Figure 38. Variation of parameters versus the normalised difference between maximum measured discharge and maximum modelled discharge**



This figure shows that the difference between measured and modelled maximum discharge depends on the storm event being modelled. The 25<sup>th</sup> of May, 21<sup>st</sup> of May and 27<sup>th</sup> of April events show the highest differences between measured and modelled maximum discharge. The 10<sup>th</sup> of May storm event is particular in the sense that modelled discharge is generally higher than observed discharge, contrarily to the other storm events. It is therefore highlighted that finding a general agreement to adjust the model for all storm event seems difficult. These graphs also confirm that the most influential parameters are the width and the Manning's coefficient for impervious areas (*Nimperv*).

Some storm events were found to be impossible to adjust because of problem in the discharge data. It can be seen on figure 38 that, for the May 25<sup>th</sup> event, a huge difference exists between the measured and modelled maximum discharge. In fact, the discharge showed an aberrant value higher than the bank full discharge of the channel (103.6 m<sup>3</sup>/s), which was reached in 7 minutes between 13:01 and 13:08. Also, a gap in the water depth data recorded by the PUB on the May 4<sup>th</sup> was found (figure 37). Between 14:58 and 16:21, no data were available, resulting in the impossibility to use the discharge data for this storm event. Concerning the storm event of the 30th of April, 2011, the water depth rose from 0.6 m to 1.25 m and then lowered to 0.7 m in 10 minutes. This shift was considered as incoherent. The 5th of June, 2011, flood event was examined with caution since the SWMM model does not take into account excess water at overcharged conduits and drains. It was noticed on figure 38 that the discharge associated to this particular event does not react to the variation of parameter in the same manner than the other storm events.

A last try was performed on the five remaining storm events to attempt a model adjustment by changing the two most influential parameters (width and *Nimperv*), it is explained below.

#### 5.9.2.3. *Iso-response curves*

The objective here consisted in finding a common variation of the width and *Nimperv* for which the SWMM project results would fit the measured maximum discharge. The previous sections have shown that the modelled discharge had to be increased by some 20 to 50 m<sup>3</sup>/s, except for the May 10th event for which the modelled maximum discharge almost fit the real one. Therefore, 180 tests<sup>11</sup> were performed on the five remaining storm events to establish, for each event, the iso-response curves showing the relationship between the width, Manning's coefficient for impervious surfaces and maximum discharge. These tests consisted in increasing the width and diminishing the Manning's coefficient of impervious areas, as it has been seen in previous section that these changes involve an increase in discharge. Figure 39 shows the iso-responses curves for the 27<sup>th</sup> of April, 10<sup>th</sup> of May, 13<sup>th</sup> of May and 21<sup>th</sup> of May storm events. Iso-responses curves for the 5<sup>th</sup> of June particular event figure in the appendix 8. These figures show that it was impossible to find a common adjustment of the model for all storm events. For example, the measured maximum discharge of the 27<sup>th</sup> of April event is 44.7 m<sup>3</sup>/s. Figure 39 shows that the modelled discharge, for a width increased by more than 10,000 and a Manning's

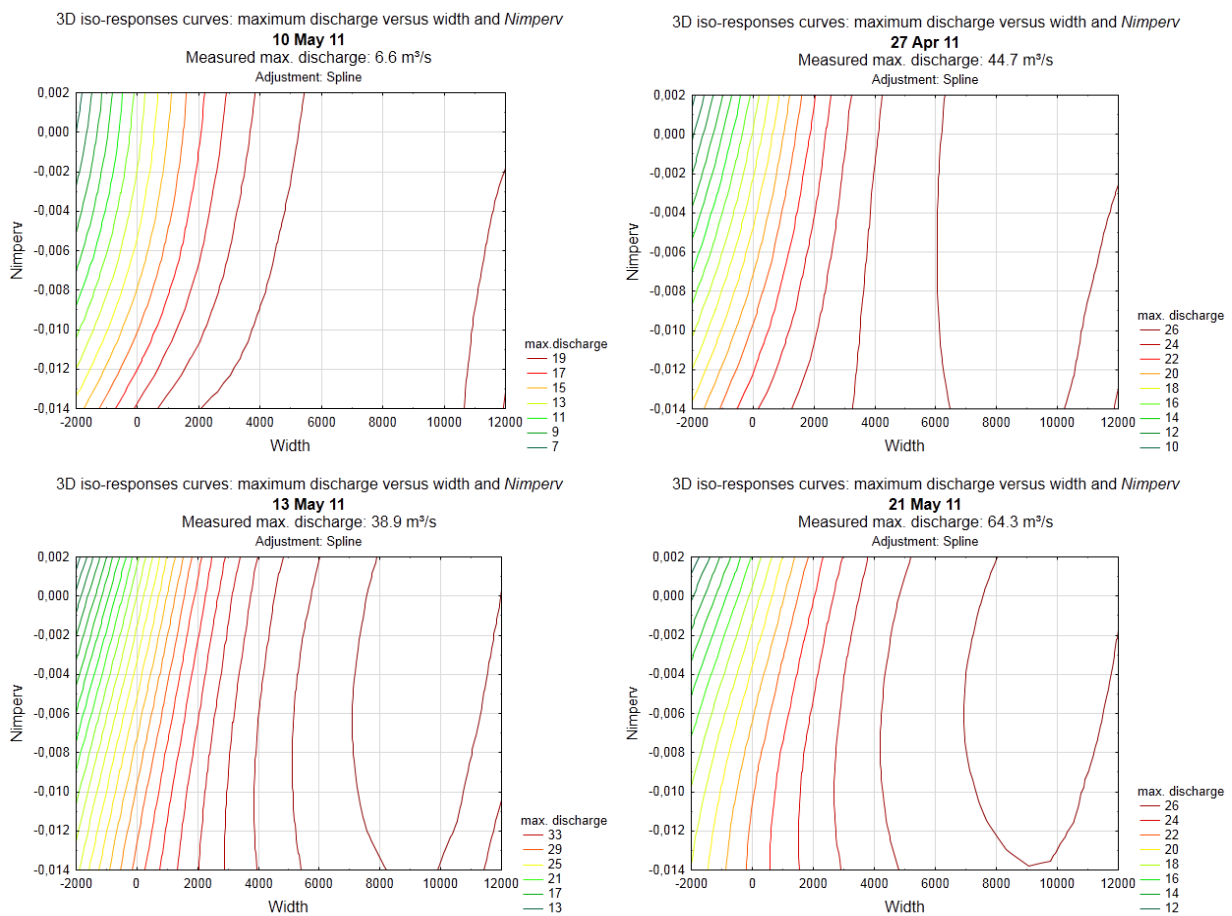
---

<sup>11</sup> The width was increased by 100, 200, 300, 400, 500, 1000, 1500, 2000, 2500, 3000, 3500, 4000, 6000, 8000, 10,000. Simultaneously, the *Nimperv* parameter was lowered by 0.001, 0.002, 0.003, 0.004, ..., 0.012. Fifteen tests multiplied by twelve tests equals 180 tests for each event.

coefficient lowered by 0.012, gives a maximum discharge of only 26 m<sup>3</sup>/s. The same case is observed for the 21<sup>th</sup> of May storm event for which the modelled discharge reach 26 m<sup>3</sup>/s while the measured one is 64.3 m<sup>3</sup>/s. On the other hand, the modelled discharge of the 10<sup>th</sup> of May event always exceeds the measured one which has a value of only 6.6 m<sup>3</sup>/s.

### 5.9.3. SWMM final model capabilities

SWMM final model gave good results for old storm events. On the other hand, it was impossible to find a common adjustment for recent storm events. From this analysis, it was concluded that the impossibility for the SWMM to model recent events is due to the low quality of the rainfall and discharge data as well as the partial knowledge of the water network and its characteristics. It has been discussed in section 5.5.2 that the indirect methods used to determine recent data contain lots of errors and uncertainties. The rainfall extracted from the RADAR images and the discharge calculated from the water depth without a rating curve probably contained too many errors to be used in the model. Therefore, the assumption that the SWMM final model gives acceptable results for old and recent data was taken for the rest of this work, although it was impossible to prove it for the latter.



**Figure 39. 3D iso-responses curves showing the relationships between maximum discharge, width and Manning's coefficient for impervious areas**

## 5.10. HEC-HMS model

HEC-HMS model was tested in order to compare its results and computational methods with the SWMM results. This section provides an overview of this model and its computational methods and parameters. The results of its application are then presented and shortly discussed.

### 5.10.1. Overview

HEC-HMS model is designed, as the SWMM model, to simulate the precipitation-runoff processes of watershed systems. The difference between these two is that HEC-HMS model is applicable in a wide range of geographic areas, contrarily to the SWMM model which can only be used in urban areas. The watershed is also separated into several subcatchments, reaches (or conduits) and junctions. The sketch representing the Upper Bukit Timah basin in SWMM model was reproduced in HEC-HMS, in order to dispose of two identical models. Figure 40 presents the HEC-HMS sketch of the basin.

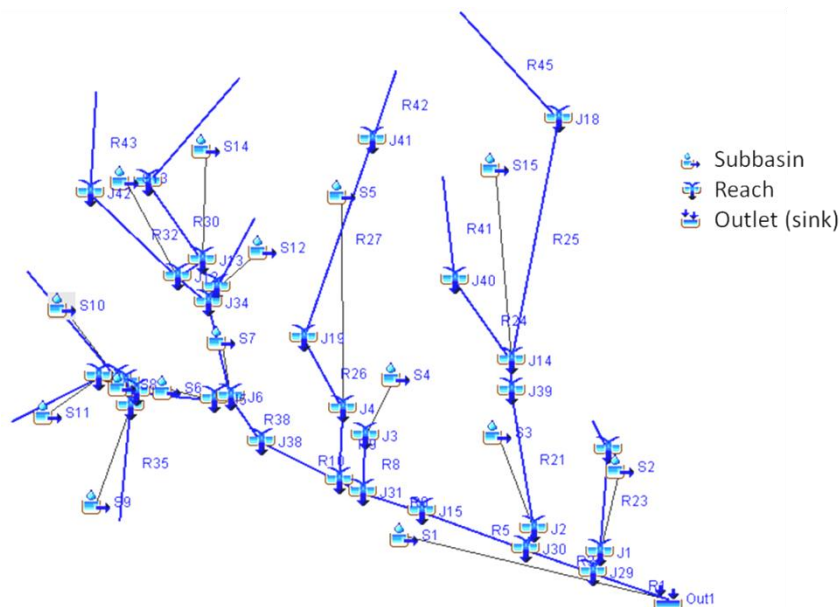


Figure 40. Basin Model in HEC-HMS

### 5.10.2. Computational methods and model parameters

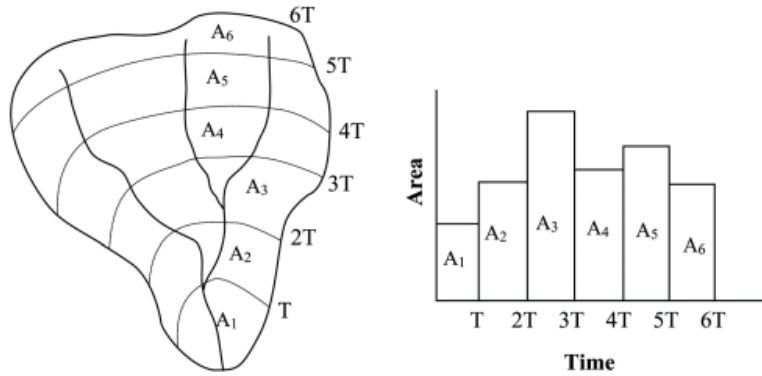
Several mathematical models used to calculate mass or energy flux of the hydrologic cycle are included in the HEC-HMS. In most cases, several model choices are available to represent the loss, surface runoff and flow in conduits. In this case, only few data were available. Therefore, the methods used here were the ones for which only a few parameters are needed for the model to run. The parameters needed in HEC-HMS did not differ from the parameters used in SWMM, with the exception of the time of concentration and the storage coefficient, both used for surface flow routing. The tutorial (section 7) details the manipulations needed for the determination of these remaining parameters.

### 5.10.2.1. Subbasin surface flow routing

The surface runoff calculation can be performed by different transformation methods in HEC-HMS. Here the Clark-Unit Hydrograph was used. It differs from the conceptual view of SWMM model since this method represents two processes in the transformation of excess precipitation to runoff: the processes of translation and attenuation (Straub *et al.*, 2000). Translation is the movement of flow downslope in response to gravity while attenuation is the reduction of the magnitude of the discharge from the frictional forces and channel-storage effects (*ibid.*). A time-area curve, expressing the fraction of watershed area contributing to runoff as a function of time (figure 41), is used to develop the translation hydrograph resulting from a burst of precipitation (US Army Corps of Engineers, 2010). In other words, the surface is subdivided into subareas separated by isochrones of equal time of concentration (Bhawan, 1998). This is represented in figure 41. The HEC-HMS model uses the following relationship to develop a time-area curve for a watershed:

$$\frac{A_{c,t}}{A_T} = \begin{cases} 1.414 \left(\frac{t}{t_c}\right)^{1.5} & \text{for } t \leq \frac{t_c}{2} \\ 1 - 1.414 \left(1 - \frac{t}{t_c}\right)^{1.5} & \text{for } t \geq \frac{t_c}{2} \end{cases} \quad (29)$$

where  $A_{c,t}$  is the cumulative watershed area contributing at time  $t$ ,  $A_T$  is the total watershed area and  $t_c$  is the time of concentration (hr) of the watershed (US Army Corps of Engineers, 2000).



**Figure 41. Time-area histogram for a watershed** (Source : Nicklow *et al.*, 2004)

The translated hydrograph (inflow  $I_t$ ) is obtained by multiplying the incremental areas  $A_i$  by one unit of depth of excess rainfall and then dividing by the computation time step  $\Delta t$  (US Army Corps of Engineers, 2000). To account for storage effects, the resulting hydrograph is then considered as an inflow to a conceptual linear reservoir with a certain storage (Nicklow *et al.*, 2004). The time rate of change of water in storage  $\frac{dS}{dt}$  at time  $t$  is calculated from the continuity equation:

$$\frac{dS}{dt} = I_t - Q_t \quad (30)$$

where  $I_t$  is average inflow, obtained from the time-area curve, to storage at time  $t$  and  $Q_t$  is outflow from storage at time  $t$  (*ibid.*). Storage at time  $t$  is related to outflow with the linear reservoir model:

$$S_t = RQ_t \quad (31)$$

where  $R$  is a constant linear reservoir parameter representing the storage effect of the watershed (hr) (*ibid.*). Combining and solving the equations using a simple finite difference approximation yields:

$$Q_t = C_1 I_t + C_2 Q_{t-1} \quad (32)$$

where  $C_1$  and  $C_2$  are coefficient calculated as:

$$C_1 = \frac{\Delta t}{R + 0.5\Delta t} \text{ and } C_2 = 1 - C_1 \quad (33)$$

The average outflow during period  $t$  is:

$$\bar{O}_t = \frac{O_{t-1} + O_t}{2} \quad (34)$$

Clark-Unit Hydrograph is therefore obtained by routing a unit depth of direct runoff in proportion to the time-area curve and routing the runoff entering the channel through a linear reservoir (*ibid.*).

This method thus uses only two parameters: the time of concentration  $t_c$  and the storage coefficient  $R$ . The storage coefficient  $R$  can be computed as the integrated surface under the hydrograph after the inflection point, divided by the value of the flow at the inflection point (US Army Corps of Engineers, 2000). As a first approximation, the mean value of  $R$  was calculated using four hydrographs. A value of 0.81 hr was obtained. There are several methods to determine the time of concentration. Six empirical methods were tested; they are presented in table 11.

**Table 11. Empirical equations used to estimate time of concentration (min)**

Method	Equation	Parameters
US. Federal Aviation Agency (FAA) (1965)*	$t_c = \frac{1.8(1.1 - C)L^{0.5}}{S_b^{0.33}}$	$C$ is the runoff coefficient; $L$ is the longest flow length (ft); $S$ is the slope (%); $L_c$ is the length channel (km); $D$ is the watershed equivalent diameter (km), equal to $\left(\frac{4A}{\pi}\right)^{0.25}$ ; $A$ is the area (km <sup>2</sup> ); $S_c$ is the channel slope (m/m); $W$ is the width (km); $S_b$ is the basin slope (m/m); $S_{nat}$ is the storage coefficient (in.) calculated from the subcatchment CN and equal to $\frac{1000}{CN} - 10$ .
Williams (1922)**	$t_c = \frac{16.32 L_c A^{0.4}}{D S_c^{0.2}}$	
Kirpich (1940)**	$t_c = 3.978 L_c A^{0.77} S_c^{-0.385}$	
Haktanir-Sezen (1990)**	$T_L = 26.85 L_c^{0.841}$ and $T_L = 0.6 t_c$	
Johnstone-Cross (1949)**	$t_c = 3.258 \left(\frac{L_c}{S_c}\right)^{0.5}$	
Simas-Hawkins (2002)**	$T_L = 53.14 W^{0.594} S_b^{-0.150} S_{nat}^{0.313}$ and $t_c = 1.417 T_L$	

Sources:\* LMNO Engineering, Research, and Software. 2003, \*\* Fang *et al.*, 2008

The value of the times of concentration calculated using the six empirical methods figure in the tutorial, section 7. FAA method gives the smaller value of time of concentration while Haktanir-Sezen and Williams's methods show sensibly higher values.

#### 5.10.2.2. Subbasin loss method

The SCS Curve Number method was used to model the infiltration loss from pervious surfaces. Section 5.3.5.3 overviews the method. The pervious portion is estimated from the percentage of impervious surface and the subbasin area, as previously.

#### 5.10.2.3. Flow routing in conduit

The process used to determine the time and magnitude of flow within a reach at a point in the system is the Kinematic Wave method. This method has already been explained in section 5.2.2.

### 5.10.3. Results

For each test, the Nash-Sutcliffe coefficient was calculated, and the modelled hydrograph was visually compared to the measured one. All graphs figure in the appendix 8. The mean Nash-Sutcliffe coefficient for all tests of all events was -0.06. The FAA methods gave the highest Nash-Sutcliffe coefficient, with a value of -0.05. Other methods gave values of -0.06, -0.24, -0.26, -0.33 and -0.52 for the Haktanir-Sezen, Simas-Hawkins, Kirpich, Johnstone-Cross and Williams methods respectively. Graphical analysis showed that for long storm events (eg. 12 Feb 78, 03 Feb 84, 02 Mar 84) the modelled discharge is generally surestimated, resulting in bad value of Nash-Sutcliffe coefficient. For these events, the Williams method results in a hydrograph which is smoothed in comparison with the measured hydrograph. For shorter event of low rainfall intensity, however, results are better and Nash-Sutcliffe coefficients are positive (eg. 02 Jul 84, 03 Jan 84). For short event of high rainfall intensities, modelled discharge is generally underestimated, resulting in bad Nash-Sutcliffe coefficients (27 Nov 87, 03 Apr 88, 11 Jul 88, 18 Apr 89).

The difficulty in estimating Clark-Unit Hydrograph parameters had an impact on the results of this model. Although the determination procedure for the coefficient of storage is simple, it requires an observed hydrograph with well defined point of inflection. In this case, the hydrographs extracted from the literature contain uncertainties that have been discussed in section 5.5.1.1. Furthermore, the identification of inflection point on the recession curve is a difficult task. Also, each hydrograph varies in shape and different  $R$  values were thus obtained. The average value of storage coefficient was therefore used. According to Ahmad *et al.* (2009), a unique value of  $R$  representing unique instantaneous unit hydrograph is difficult to achieve and the average value of storage coefficient obtained from different hydrograph do not result in the match between observed and measured hydrographs. The determination of the time of concentration was done using six empirical equations, originally developed for specific regions and for watersheds of different sizes. For example, Williams developed his equation in 1922 to study flood discharge in India, Kirpich proposed his equation in 1940 for small watersheds ( $< 0.45 \text{ km}^2$ ) in Tennessee and Johnstone and Cross presented their equation for watershed in Ohio (Fang *et al.*, 2008). Although six different equations were tested on each event, the model showed unacceptable results. It is thus evident that these equations are not well adapted to this case study. The HEC-HMS was not used for the rest of this study because the Clark-Unit

Hydrograph method did not show enough accurate results. Further analysis could have been done to adjust the model by using other methods for the surface flow routing, but no data were available to implement them.

### **5.11. Conclusion**

This chapter presented the SWMM and HEC-HMS models, as well as the parameters they require and the computational methods they use. SWMM model was parameterised, adjusted and verified using past and recent storm events. It was impossible to verify the model for current storm events, probably due to the numerous uncertainties in the determination of discharge and rainfall data. These uncertainties, as well as the ones linked to the determination of the parameters, have been discussed in details in the concerned sections. On the other hand, SWMM model showed accurate results for the old storm events. Less uncertainty was present for these ones. Although six methods were used to determine the time of concentration, HEC-HMS did not give good results. It was decided to use SWMM model for the rest of this work, with the assumption that the incorrect results of recent storm events were not due to the SWMM parameterisation. The two watershed models could have been improved if more data were available, but SWMM was judged satisfactory given the poor database available here. Next chapter presents a diachronic analysis of the effects of urbanisation on runoff, using the final SWMM model.





## 6. DIACHRONIC ANALYSIS

This chapter aims to present a diachronic analysis of the effects of urbanisation on runoff using the SWMM model. It first presents the results of an approximate method, the Rational formula, used to estimate the peak runoff resulting from a given rainfall intensity at different periods of time. Since the use of this method does not allow the user to compare hydrographs of different period of return, another approach was developed to compare the runoff at different dates. Next sections therefore present how the past and future imperviousness of the Upper Bukit Timah basin was characterised and how design hyetographs of a given period of return were constructed. It then analyses the results of the application of the SWMM model on these data. The final section attempts to identify the sensitive areas of the catchment in terms of runoff.

### 6.1. Rational method

Chuah (1987) used the Rational formula to characterise the effect of land use changes on peak flow. Following this work, the 2009 land use was also characterised using the Rational formula. This constitutes a first approach to appreciate the effect of urbanisation on peak runoff.

#### 6.1.1. Rational formula and evolution of the peak flow

The Rational method is based on a simple formula that relates the runoff-producing potential of the catchment, the intensity of rainfall and the watershed drainage area (Thompson, 2006). It assumes that a peak discharge occurs when a steady state is reached whereby the entire catchment is contributing to the runoff (Chuah, 1987). The peak discharge can be calculated using:

$$Q = 0.278 C I A \quad (35)$$

where  $Q$  is the peak runoff rate ( $\text{m}^3/\text{s}$ ),  $C$  is the runoff coefficient,  $I$  is the rainfall intensity ( $\text{mm/h}$ ) and  $A$  is the area of the watershed ( $\text{km}^2$ ) (Anctil *et al.*, 2005).

The dimensionless runoff coefficient  $C$  is the fraction of precipitation falling on the watershed that becomes runoff (Thompson, 2006). The runoff coefficient therefore depends on the land use class, just as the coefficient of imperviousness does (see appendix 10). A mean runoff coefficient for the whole 2009 Upper Bukit Timah catchment was calculated; its value is 0.47.  $I$  is the intensity of a constant intensity design storm (fictive event) with the specified design return (in this case, 5 years), and a storm duration equal to the time of concentration of the drainage area (Bengtson, 2010). The relation between these three components is represented by the intensity-duration-frequency (IDF) curves (appendix 1). Once the design return period and time of

concentration were calculated, the rainfall intensity was determined from the IDF curve. The time of concentration of the year 2009 was calculated using the FAA formula (see section 5.10.2). According to Chuah (1987), the peak flow grew from 73.68 in 1950 to 91.65 m<sup>3</sup>/s in 1986. For the year 2009, the calculated peak discharge is 102.6 m<sup>3</sup>/s, showing an increase of peak flow through time.

### **6.1.2. Evaluation of the method**

The Rational method is widely used to estimate the peak surface runoff rate in order to design a variety of drainage structures (Bengtson, 2010). The method is also used in Singapore (PUB, 2011). This method assumes four hypothesis: (1) the rainfall intensity is constant for the duration of the storm, (2) the coefficient of runoff does not change over the time, (3) the peak discharge is reached and maintained when the rainfall duration is longer than the time of concentration and (4) the drainage area does not change during the rainfall event (Anctil *et al.*, 2005). The first assumption is constraining since the rainfall intensity greatly varies in Singapore. The second assumption illustrates the limits of the method. As runoff is linked to the infiltration capacity which changes over the time, a constant runoff coefficient is an approximation. The quality of the Rational method also depends on the determination of the parameters. In this case, the time of concentration, for example, was determined using the FAA formula, for which the quality is uncertain. Also, the delimitation of land use, and therefore the determination of the runoff coefficient, was approximate. Finally, this method does not allow the definition of any hydrograph and just gives a rough approximation of the peak discharge for a given storm intensity. The use of this method is therefore not practical since hydrographs of different probability of occurrence can be obtained using the SWMM model. The following sections explain how this was done.

## **6.2. Past and future urbanisation**

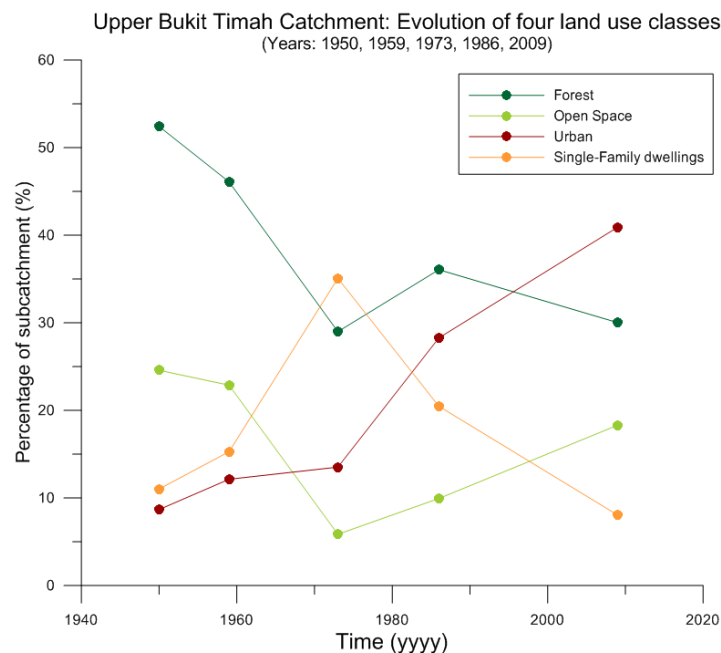
The first step necessary to apply the model on past and projected urbanisation consisted in the characterisation of the past and future imperviousness of the Upper Bukit Timah catchment. The techniques used for the determination of the percentage of imperviousness are explained below. In addition to the change in imperviousness, a modification of the CN of each subcatchment as well as the Manning's coefficient was indispensable since a change in infiltration and roughness due to urbanisation is expected. This is detailed in the last paragraphs of this section. In short, the calibrated model of the previous chapter was used to simulate a non-urbanised catchment for the years 1950, 1959, 1973, 1986, 2009 and 2020, using the corresponding percentage of impervious area, CN and Manning's coefficient, while keeping other model parameters constant.

## 6.2.1. Past land use and imperviousness

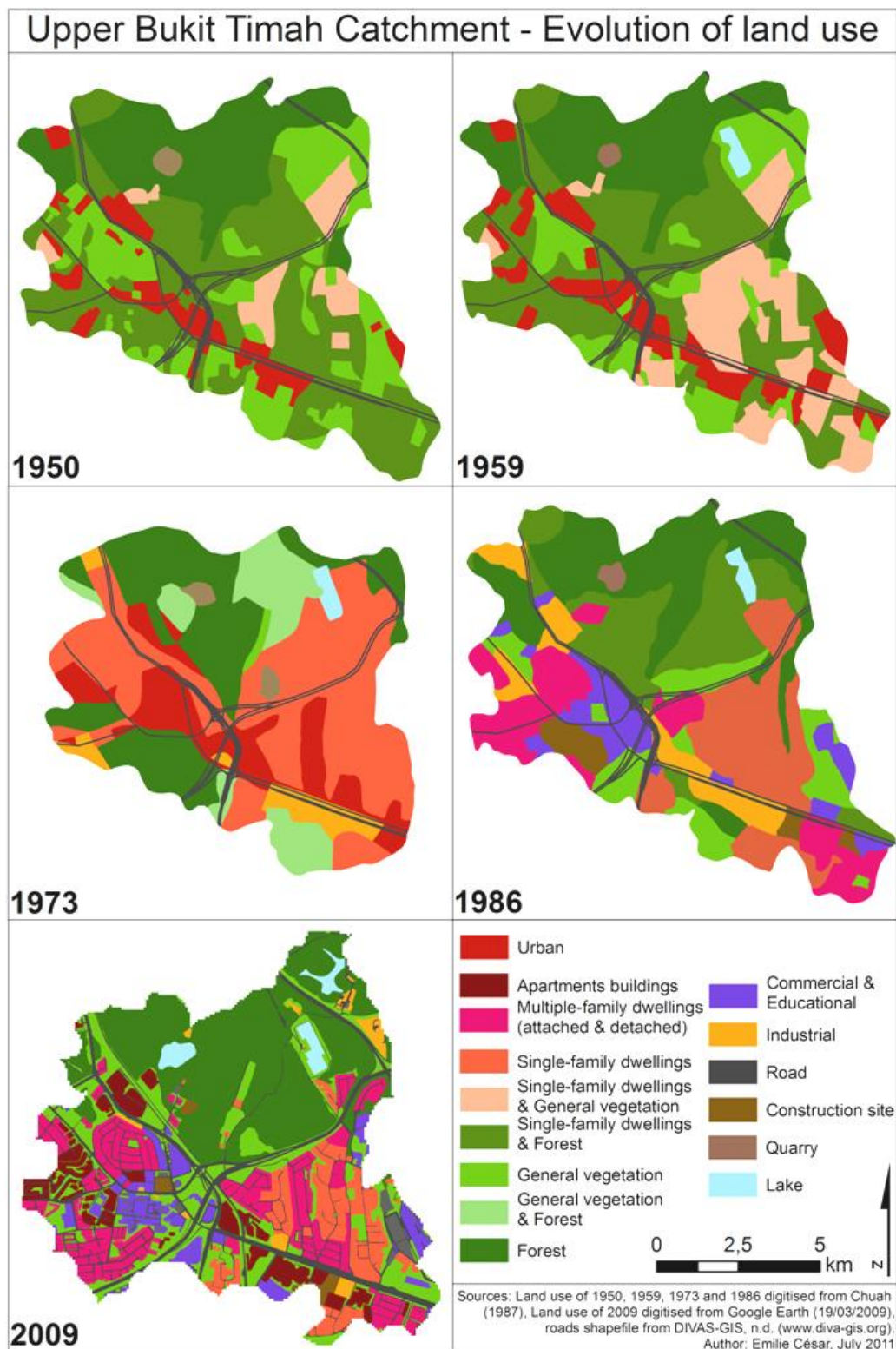
### 6.2.1.1. Chuah's maps (1987)

In 1987, Chuah analysed the changing land use of the Upper Bukit Timah basin, in terms of increase in impervious areas, for the period from 1950 to 1986. For the years 1950, 1959, 1973, 1986, she built land use maps on the basis of several sources, namely topographic maps, aerial photography, literature and fieldwork. These maps were georeferenced (using, on average, 13 GCP per map) and digitised in order to be used to estimate the imperviousness, CN and Manning's coefficient of each subcatchment. Figure 43 presents the maps extracted for each date. It can be seen on these ones, as well as in figure 42, that there is an increase in the built-up areas especially along and around the major roads. Also, the western part of the catchment become more and more urbanised along the years, mostly due to new commercial and residential features. The areas around the Nature Reserve, in the north part of the basin, remain more or less unaffected by developments. The single-family dwellings show a particular evolution, with an increase from 1950 to 1973 followed by a decline as they are being replaced by multiple-family dwellings since 1986.

The percentage of imperviousness was determined as previously: a weighted coefficient for each subcatchment was calculated on the basis of the coefficients of imperviousness and the surface of each land use class within each subcatchment. Our calculations showed that the mean percentage of imperviousness calculated for the whole Upper Bukit Timah catchment grew from 21.3 % in 1950 to 24.7 % in 1959 and then to 37.5 %, 40.0 % and 43.8 % for the years 1973, 1986 and 2009 respectively. The appendix 11 details the percentage of imperviousness for each subcatchment.



**Figure 42. Evolution of four land use classes: forest, open space, urban and single-family dwellings in the Upper Bukit Timah catchment, from 1950 to 2009.**



**Figure 43. Land use for the years 1950, 1959, 1973, 1986 and 2009** (NB: roads figuring on the 1950, 1959, 1973 and 1986 maps act as landmarks useful for comparison between maps)

#### 6.2.1.2. *Quality of the data*

It is evident that the quality of the data extracted from Chuah's map is uncertain for several reasons. Firstly, the compilation of the land use made by Chuah (1987) encountered some difficulties which are explained in her work. The 1950 land use is derived from the 1950 aerial photograph on a scale of 10 inches to a mile ( $\approx 1:6336$ ). Delimitation of land use on this black

and white photograph is not an easy task. For the 1959 map, the 1959 topographic data for the northern portion of the basin was not available and therefore, the land use for this section was derived from the years preceding and following 1959. The land use categories classified in the 1973 map, which derived from field surveys of past authors, differed from those of the other four years, and some difficulty was encountered for the comparison of land use changes over the years. The 1980 land use map derived from two past studies. The total area of the basin was slightly smaller than Chuah's other maps. The 1986 map derived from field survey. Chuah specified that, for all maps, the extent of the boundary of the different types of land use was approximately determined following roads. Where there were no road or reference points, the distance was determined approximately. All these maps are therefore tarnished by numerous errors. Secondly, Chuah delimited the boundary of the Upper Bukit Timah catchment manually on the 1980 topographic map, which is also a source of imprecision. As the catchment delimited by Chuah slightly differed from our basin, approximations were made when determining the percentage of imperviousness for the old maps. Indeed, the surface of the catchment was kept constant and the percentages of imperviousness of the old maps were adapted to our subcatchment delimitation. Thirdly, the land use maps presented by Chuah are simplified and can be considered as general land use maps. For example, minor land use types as green belts surrounding built-up areas are excluded, contrarily to our classification of the 2009 Google image. Fourthly, errors inherent to the georeferencing are also present, especially because almost no reference points (roads, streams, etc.) were present on the old land use maps. Some difficulties were therefore encountered to adjust these maps. Finally, Chuah's land use classes differed from our classification, resulting in a subjective appreciation of the old land use classes to adjust them to the classification. For example, the old 'forest and open space' class were considered as 50 % composed of forest and 50 % of open space, an uncertain assumption. Correspondences between old maps legends and the land use classification of this work are presented in the appendix 6.

These uncertainties are noticed in the figure 42 below, representing the evolution of four land use classes in the Upper Bukit Timah catchment. The decline of the forest in 1973 is certainly due to an overestimation in single-family dwellings, in the north part of the basin. In the same way, Chuah specified that small open spaces were not taken into account in her classification. This can be observed in figure 42, where an increase of open spaces in 2009 is observed, due to our more precise classification. However, this figure clearly shows the growth of the urbanisation (encompassing commercial, dense residential and industrial classes) over the years as well as the increase in single-family dwelling until 1973 followed by a decline due to their replacement by more dense residential features (apartment and multiple-family dwellings).

## **6.2.2. Predicted imperviousness**

### *6.2.2.1. Imperviousness versus population density*

Future imperviousness can be estimated using its relationship with population density. According to Exum *et al.* (2005), population density is a reasonable predictor of impervious cover arising from residential and commercial developments that support human settlement. Population growth can therefore be used to project an increase in impervious cover in a

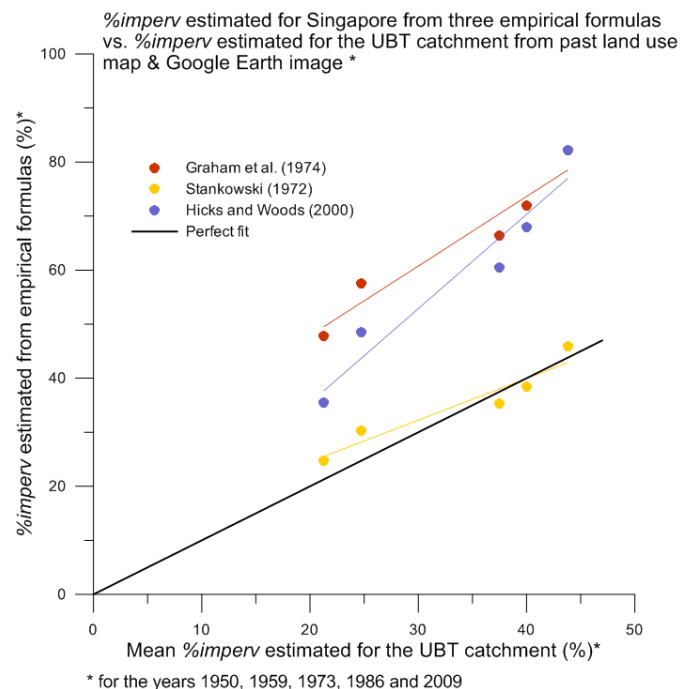
watershed. A number of relationships between population density and impervious cover have been developed. Three empirical relationships, with different functional forms to relate population density, were tested here (table 12).

**Table 12. Empirical relationships between population density and percentage of imperviousness**

Stankowski (1972)*	$\%imperv = 0.117 D^{0.792-0.039\log D}$	where D is the population density (persons/mi <sup>2</sup> ) and %imperv is the percentage of imperviousness (%)
Graham <i>et al.</i> (1974)**	$\%imperv = 91.32 - 69.34 (0.9309^{\frac{P}{640}})$	
Hicks and Woods (2000)**	$\%imperv = 95 - 94 \exp(-0.0001094P)$	

Sources: \*Hordon (1977) and Brabec *et al.* (2002), \*\* Exum *et al.* (2005)

The Singapore Department of Statistics estimated that the 2010 annual growth was 1.8 % (comprising Singapore citizens and permanent residents). If the annual growth stayed constant over the next ten years, the population in 2020 was calculated to be 6,068,191, resulting in a population density of 8517 persons/km<sup>2</sup> or 22190 person/mi<sup>2</sup>. Given this density, the value of percentage of imperviousness in 2020 estimated by Stankowski, Graham *et al.*, and Hicks and Woods was estimated at 48.9 %, 85.4 % and 86.6 % respectively. The three empirical estimations were evaluated by comparing their resulting percentages of imperviousness with the ones predicted for the Upper Bukit Timah basin (see section 6.2.1) for the years 1950, 1959, 1973, 1986 and 2009 (figure 44). The population densities corresponding to these dates were obtained from the Department of Statistics (2010). Figure 44 shows that the Stankowski (1972) relationship is the most appropriate, the two other methods overestimating the imperviousness. Stankowski's formula predicts a growth of 3.2 % from 2009 to 2020. The percentage of imperviousness of each subcatchment was therefore increased by this value and assumed to represent the imperviousness of the Upper Bukit Timah catchment in 2020.



**Figure 44. Percentages of imperviousness determined by empirical formulas and predicted for the Upper Bukit Timah catchment**

#### 6.2.2.2. Discussion about the method

The use of population density as a mean to estimate impervious cover provides a rapid technique to generate a quantitative estimation of projected imperviousness (Exum *et al.*, 2005). Moreover, the population density is generally a widely available population data (Brabec *et al.*, 2002). However, it is evident that this method is a rough approximation for different reasons. Firstly, imperviousness can considerably vary for a given density. Secondly, the use of a constant annual growth to estimate the future population density is uncertain since annual growth varies from year to year. Thirdly, the choice of the method relies on a comparison between imperviousness estimated from empirical formulas and imperviousness estimated for the Upper Bukit Timah catchment, itself containing uncertainties. Finally, the empirical methods were developed for particular regions: Stankowski for New Jersey, Graham *et al.* for Washington and Hick and Woods for Vancouver (Exum *et al.*, 2005) and could not be adapted to Singapore. Nevertheless, it was used as a first approach to illustrate the future possible urbanisation.

#### 6.2.3. Past and future infiltration and roughness

Infiltration, expressed via the CN is expected to change with urbanisation. The CN of each subcatchment for each old map was extracted as previously, using a combination of soil and land use maps in HEC-GeoHMS. The mean CN for the Upper Bukit Timah for the years 1950, 1959 and 1973 was lower than the mean CN of 1986, with a value surrounding 76 for the formers and a value of 79 for the latter. The mean CN of 2009 was even higher, with a value of 80. For the tests undergone on a non-urbanised catchment, the CN was set at 72, the mean value between forests and open space CN (Merwade, 2010)

Roughness, illustrated by the Manning's coefficient of overland flow for both pervious and impervious surfaces was calculated as previously, by taking a weighted coefficient for each subcatchment. Old land use maps constituted a basis to determine the mean Manning's coefficient associated to each land use classes. The Manning's coefficient for a non-urbanised basin was set at 0.4, the mean value of coefficients for forests and open spaces, as mentioned in Rossman (2010).

For 2020 projected urbanisation, CN and Manning's coefficients were identical to the 2009 parameters, as no information were available on any relationship between urbanisation, infiltration and roughness.

### 6.3. Synthetic design hyetographs

In the Rational method, the rainfall intensity is supposed to be constant over the storm period. However, the distribution of the rainfall over the time has a great influence on the generated discharge. Design hyetographs can account for variability of the intensity throughout a storm event. Thus, once these hyetographs are created, the SWMM can be used to model the discharge

of a given return period. This section explains how design hyetographs were created using the arithmetical mean method. The tutorial (section 8) gives all details concerning the steps for determining design hyetograph.

### 6.3.1. Definition and method

A design storm is a fictive rainfall event, supposed to statistically represent a real storm event for which a return period can be associated (Benabdesselam, 2009). This return period is expressed as the frequency that a certain storm event would be exceeded (Stanescu and Musy, 2006). A design rainfall is therefore used to assess the flood hydrograph of a certain return period since it is impossible to affect a return period to a measured hyetograph, which is aleatory. Characteristic elements of a design rainfall are: depth (mm), duration (hr), average intensity (mm/hr), maximum intensity and time distribution of the rain intensities (*ibid.*).

There are several ways to determine a design rainfall. It can be derived directly from the IDF curves, for which the temporal distribution is arbitrary, or from the observed rainfalls, from which the temporal distribution results (MDDEP and MAMROT, 2002). The method chosen here, the arithmetical mean derived from measured precipitation, belongs to the second category. The 5-minutes rainfall database of the NUS weather station from 2004 to the present was used. The procedure to follow consisted of: (1) selecting the observed storms having a daily rainfall volume reaching 50 mm or more. A total of 106 storm events were selected; (2) translating the maximum intensity of each event in time in order to match all maximum intensities of all events; (3) computing the mean of all selected events to obtain the structure of the design hyetograph for a given duration (in this case, 03:30); (4) expressing the depth of design hyetograph in each time step as a percentage of the total depth; (5) establishing the relationships between duration of the storm and intensity of rainfall for selected return period (2, 5, 10, 25, 50, 100 years); (6) determining the total volume of precipitation, given the duration and frequency of the storm; (7) multiplying the percentage of the total depth by the desired storm volume (Stanescu and Musy, 2006 and Picouet *et al.*, 2003).

In order to obtain several design storms of different durations, the procedure was repeated by selecting the storm events having a specific duration. Each of the 106 storm events was classified following its duration. Five classes were created: duration between 20 and 40 minutes (30-minutes design rainfall), 50 and 70 minutes (60-minutes design rainfall), 80 and 100 minutes (90-minutes design rainfall), 110 and 130 minutes (120-minutes design rainfall) and 160 and 200 minutes (180-minutes design rainfall). A design shape of hyetograph was therefore created for each duration. The design shape of hyetograph was multiplied by the rainfall volume determined by the IDF relationships. Thirty design hyetographs were therefore created, their total volume, depending on the return period and duration figure in table 13.



**Table 13. Total volume of precipitation (mm) of design hyetographs**

Return period (yrs)	Duration (min)				
	30	60	90	120	180
2	43	68	88	107	139
5	56	89	116	141	184
10	64	102	134	163	214
25	76	120	156	188	245
50	85	134	176	212	278
100	93	147	193	233	305

### 6.3.2. Comments about the arithmetical mean method

According to Stanescu and Musy (2006), the arithmetical average method is well adapted to a large range of catchment areas and time of concentration. Moreover, they allow for making a choice of the duration and return interval. This fact was interesting for this work, since the discharge associated to the synthetic hyetographs can also be characterised in terms of return period. Moreover, this method gives better results than other methods like Chicago-type storm, or triangular design rainfall for which the time distribution is arbitrary. Moreover, the parameters used to define the design hyetograph are easily derived from rainfall records.

There are, however, some limitations. Many storm events have to be considered in order to obtain an accurate design hyetograph (*ibid.*). In this case, 103 storm events were selected, which is considered as satisfactory. The main disadvantage of this method is the smoothing of temporal variation of the storm, resulting in a quite evenly distributed intensity or volume (*ibid.*). Although there were few extreme events in our selection (the mean maximum volume being 10 mm within 5 minutes, with nine storm events of rainfall volume superior to 15 mm), the hyetographs showed a great variability in intensities. All synthetic hyetographs are presented in the appendix 12.

## 6.4. Impact of land use changes on flow

Once the design hyetographs defined and the parameters modified, 210 computations were performed, representing each design hyetograph for each period of time (2, 5, 10, 25, 50, 100-year return period, 30, 60, 90, 120, 180-minute duration for a non-urbanised catchment and the years 1950, 1959, 1973, 1986, 2009, 2020). Three interrelated effects of land use changes on the hydrology of an area were analysed here: changes in hydrograph characteristics, changes in peak flow, and changes in the frequency of high flows.

### 6.4.1. Effects of urbanisation on hydrograph

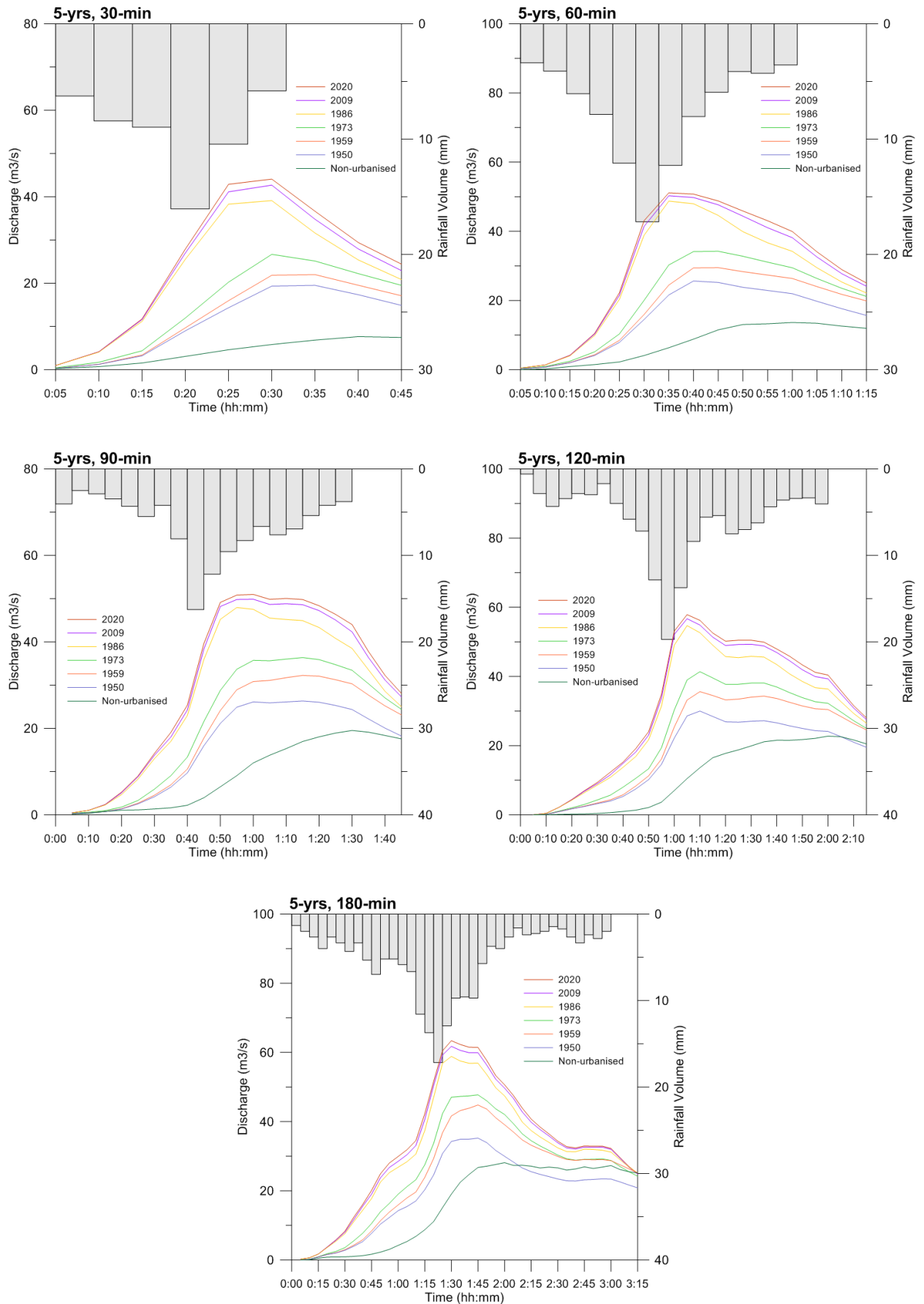
Urbanisation affects the roughness and imperviousness of the land surface, which increases the runoff volume. Figure 45 present the hydrographs obtained for 5-year return period rainfall events of different duration. Other hydrographs are presented in the appendix 13. These results show a significant discharge increase in Upper Bukit Timah watershed with the increase in urban

area, despite constant meteorological conditions. They also show that for the same return period, discharges are higher for long storm events than for short rainfall events, despite an almost constant maximum volume of rainfall (16-19 mm). This clearly shows the importance of initial moisture of the basin, since a maximum volume of rainfall occurring sooner (30-minute hyetograph) produces a smaller discharge than a maximum volume of rainfall occurring later (180-minute hyetograph).

As surface roughness is lowered and imperviousness increased, the stream exhibits a faster response time, in addition to a higher discharge. Lag time is thus altered by the effects of urbanisation. It is defined as the time interval between the centre of mass of the hyetograph and the centre of mass of the resultant hydrograph (Leopold, 1968). As water runs off faster from urban areas than from natural vegetated areas, the lag time is decreased with increasing urbanisation. Figure 45 clearly shows that the time to peak is shortened as urbanisation increases. Table 14 show the mean lag time values for the different storm events durations. The average value of lag time for all 210 computations was calculated as 41 minutes for a non-urbanised basin, 19 minutes for the year 1950, 21 minutes for 1959, 20 minutes for 1973 and 11 minutes for the years 1986, 2009 and 2020. The general tendency is thus a decrease in lag time with imperviousness, although the value of 1959 shows a smaller value than the value of 1973. It was noticed that the 90-minute storm event causes a higher value of 1973 time lag for all return periods, resulting in an average higher value. Overall, a decrease in lag time is observed with the increase in imperviousness.

**Table 14. Lag time calculated for storm events of different duration and for different period of time**

Years	Storm event duration (min)				
	30	60	90	120	180
Non-urbanised	00:23:20	00:35:00	00:50:50	01:05:00	00:34:10
1950	00:16:40	00:15:50	00:23:20	00:14:10	00:25:00
1959	00:16:40	00:16:40	00:35:00	00:15:00	00:25:00
1973	00:15:50	00:16:40	00:30:00	00:12:30	00:25:00
1986	00:11:40	00:10:50	00:15:50	00:10:00	00:10:00
2009	00:11:40	00:10:50	00:16:40	00:10:00	00:10:00
2020	00:11:40	00:10:50	00:16:40	00:10:00	00:10:00



**Figure 45. Design hydrographs of 5-year return period for storm events of different duration (30, 60, 90, 120, 180 minutes)**

### 6.4.2. Effect of urbanisation on peak flow

It is intuitive that an increased proportion of impervious areas brings shorter lag times and subsequently higher runoff peaks. Table 15 shows the peak flow at the outlet for several periods of return, and different dates with their corresponding percentage of imperviousness. For an average 5-year storm event, for example, the peak discharge reaches 18.33 m<sup>3</sup>/s for a non-urbanised catchment, 37.28 m<sup>3</sup>/s for a 30 % impervious catchment (1973) and 53.59 m<sup>3</sup>/s for a 47 % impervious basin (2020). The appendix 14 contains the detailed results. It shows that table 15 hides some disparities since, for the year 2009, a 5-year 30-minute storm event triggers a peak discharge of 44 m<sup>3</sup>/s while for a 180-minute rainfall event, the peak discharge reaches 62 m<sup>3</sup>/s. For the return periods of 10, 25, 50 and 100 years, the predicted 180-minute events of 2020 reach respectively 73 m<sup>3</sup>/s, 83 m<sup>3</sup>/s, 92 m<sup>3</sup>/s and 100 m<sup>3</sup>/s. Table 16 shows the mean percentage of increase in peak flow, from years to years. It can be seen that since 1950, peak flow has increased by almost 85 % and current peak flow is projected to increase by about 3 % to 2020.

**Table 15. Peak flow (m<sup>3</sup>/s) for different years and for return periods of 2, 5, 10, 25, 50, 100 years, average on all duration storm events**

Years	Mean % <i>imperv</i>	Peak discharge (m <sup>3</sup> /s) / increase in percent from the previous to the next year											
		T2		T5		T10		T25		T50		T100	
Non-urb.	4.0	12.4		18.3		22.2		26.7		30.7		34.0	
1950	21.3	21.1	70.4%	27.3	49.1%	31.8	43.5%	37.2	39.4%	41.6	35.6%	45.3	33.4%
1959	24.7	24.7	16.8%	32.8	20.1%	38.2	20.1%	44.6	19.8%	49.8	19.8%	53.9	18.9%
1973	29.7	28.3	14.8%	37.3	13.5%	42.6	11.5%	48.5	8.9%	53.3	7.0%	57.4	6.6%
1986	40.0	38.8	36.8%	49.9	33.8%	56.0	31.3%	63.5	31.0%	70.5	32.2%	76.7	33.5%
2009	43.8	41.7	7.6%	52.3	4.8%	58.6	4.7%	66.6	4.9%	74.3	5.3%	80.8	5.4%
2020	47.0	43.2	3.5%	53.5	2.4%	60.0	2.4%	68.5	2.8%	76.3	2.7%	83.2	2.9%

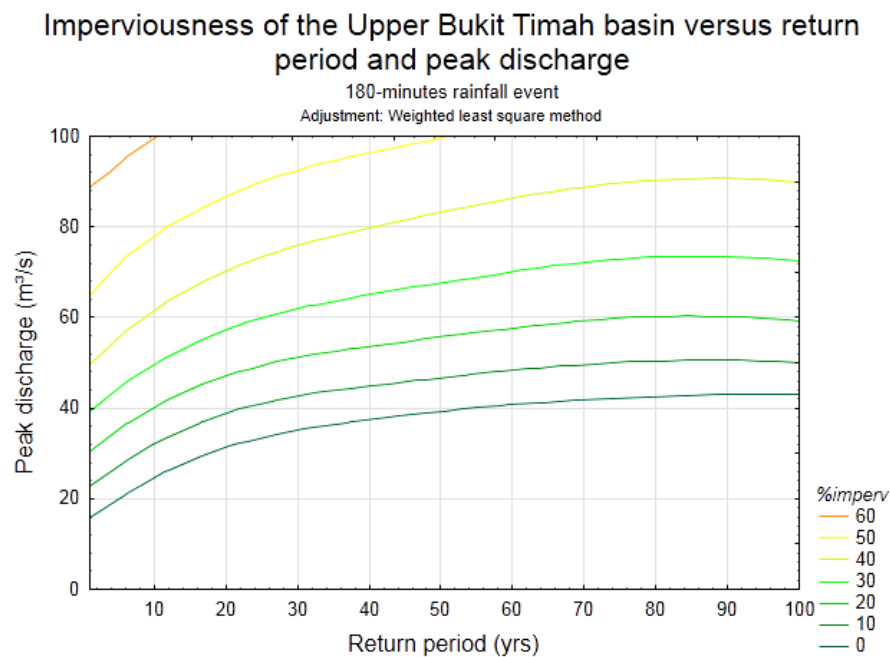
**Table 16. Increase in peak flow (%) between different periods of time**

	1950	1959	1973	1986	2009	2020
Non-urbanised	45.27%	73.13%	91.53%	155.18%	169.29%	176.83%
1950		19.25%	31.64%	75.22%	84.79%	89.92%
1959			10.41%	46.97%	55.01%	59.32%
1973				33.08%	40.35%	44.25%
1986					5.45%	8.37%
2009						2.77%

### 6.4.3. Effect of urbanisation on frequency of high flows

The effect of urbanisation on peak flows triggered by a 180-minute event is shown in figure 46. It is shown that the peak discharge-frequency curve under non-urbanised condition passes through a value of 24 m<sup>3</sup>/s to more than 76 m<sup>3</sup>/s for a 50 % impervious catchment for a 10-year return period storm event. With a 60 % impervious catchment, the peak flow can reach more than 90 m<sup>3</sup>/s for return period of less than 10 years. For a return period of 50 years, the peak flow is estimated at 40 m<sup>3</sup>/s for a non-urbanised basin and 100 m<sup>3</sup>/s for a 50 % impervious basin

(~2020 conditions). The appendix 15 groups the graphs concerning the other durations. Peak discharges are smaller for short duration events, but the effect of increase in impervious areas is still clearly shown. Obviously these curves remain extrapolations based on minimal data.



**Figure 46. Peak discharge for different degrees of urbanisation (measured by the percentage of impervious area) and for different return periods**

#### 6.4.4. Discussion about the results

It is important to note that these results are an approximation of past and future conditions. Our model gave smaller peak flows than Chuah's estimations, but these ones were not verifiable (section 6.1.1). In previous chapter, the bank full discharge was estimated at 74 m<sup>3</sup>/s and section 6.4.2 has shown that the bank full discharge was reached for a 10-year 180-minute storm event. This is probably underestimated. Effectively, the one-dimensional model probably underestimates the value of discharge for important events of great return periods, as the overbanking water is lost from the system. Moreover, SWMM was calibrated using events of weak amplitude, with a mean discharge of 30 m<sup>3</sup>/s. Also, as discussed earlier, the parameters used in the model contained some uncertainties inherent to their determination (section 6.2). It was also the case for the determination of design hyetograph (section 6.3).

### 6.5. Identification of critical areas

It is now evident that land use changes have the potential to increase average maximum flows. The identification of portions of the Upper Bukit Timah basin that have the highest contribution in runoff may also be interesting.

### 6.5.1. Evolution of runoff volume per subcatchment

This was done by computing the maximum runoff of each subcatchment for all 210 computations. To allow comparisons between subcatchments, the maximum runoff ( $\text{m}^3/\text{s}$ ) was transformed into specific runoff by dividing it by the surface of the concerned subcatchment and then into a volume (mm). For each date and each subcatchment, the mean maximum volume of runoff for all events of different duration and period of return was calculated. This allows the generation of critical areas maps (figure 47).

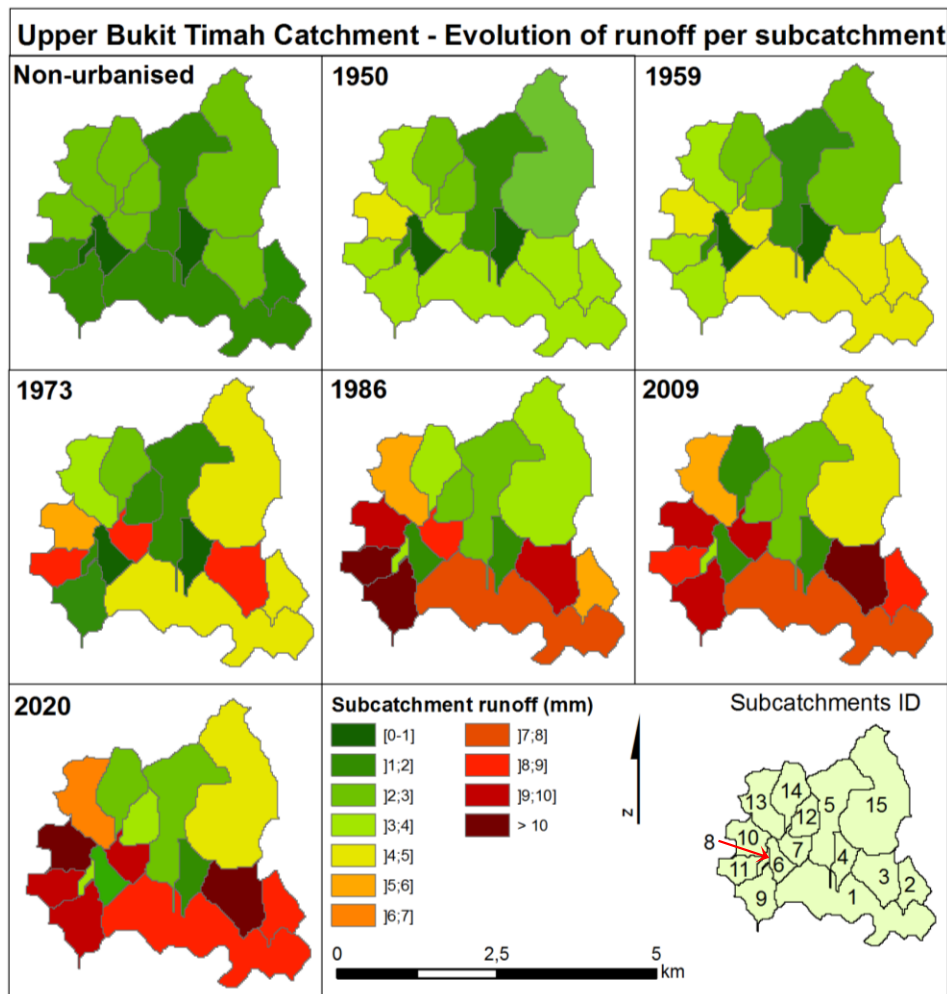
Table 17 presents the evolution of the mean volume of runoff for the Upper Bukit Timah catchment. The effect of urbanisation is noticeable. The runoff produced by the 2020 projected basin is more than the triple than the runoff from the non-urbanised catchment.

**Table 17. Average runoff (mm) produced by the Upper Bukit Timah catchment at different dates**

Non urba.	1950	1959	1973	1986	2009	2020
1.80	2.59	2.94	3.49	5.58	5.73	6.05

Figure 47 clearly shows the effect that urbanisation has on runoff volume. From the non-urbanised catchment to the 1950 basin, only north subcatchments (12, 14, 5, 15, 6 and 4) remain unaffected by the urbanisation. The highest mean runoff is found in subcatchment 10, and downstream subcatchments began to produce more runoff (3-4 mm). The 1959 pattern is similar to the situation of 1950 except that downstream subcatchments produce even more runoff, with a value between 4 and 5 mm. In 1973, subcatchments 3, 7 and 11 produce the highest quantity of runoff, with a value comprised between 8 and 9 mm. This corresponds to the new urban features set up along major roads (see figure 42). Even more runoff volume is produced in 1986, principally in subcatchments 9 and 11 where the value reached 10 mm, and in subcatchments 3, 7 and 10, where the mean depth of runoff is comprised between 8 and 10 mm. It is certainly due to the new commercial and residential features built along the Upper Bukit Timah road. In 2009, these subcatchments produce less runoff, probably due to the different land use classifications (more open spaces are taken into account in the 2009 classification, see section 6.2.1). Nevertheless, the total quantity of runoff produced in 2009 is still higher than in 1986. In 2020, it is predicted that all downstream subcatchments (1, 3, 2, 7, 9, 10, 11) will produce an average volume of runoff comprised between 7 to more than 10 mm. Finally, it is noticed that, for all dates, subcatchments 4 and 6 remain the less affected. Subcatchments in the north part of the basin (5, 12, 14), are also low runoff-producing zones. In this figure, it is even noticed that other characteristics than urbanisation influence the runoff. For example, for the non-urbanised catchment, subcatchments 10, 13 and 14 present a higher amount of runoff than other subcatchments, probably due to the higher slopes in this part of the basin.

In conclusion, it is shown that subcatchment 1, 2, 3, 7, 9, 10, 11 are the most critical areas, with a average production of runoff volume between 8 to more than 10 mm. Preserving the forests in the north part of the basin seems therefore essential to keep up with increasing runoff.



**Figure 47. Evolution of the average runoff for each subcatchment**

It is evident that the way these maps have been built hides some disparities. Indeed, the runoff volume produced by a short 2-year frequency storm is obviously smaller than for a long 100-year frequency storm. Nevertheless, the average of runoff for all kind of storm stays a good illustration of the effect of urban features on runoff since it allowed the identification of critical area associated to a quantity of runoff depth.

## **6.6. Diachronic analysis conclusion**

This chapter first characterised the evolution of the Upper Bukit Timah catchment in terms of imperviousness. Thanks to the construction of a large number of design hyetographs, the evolution of maximum discharge and runoff was performed. It was shown that, in average, urbanisation has increased the peak discharge by some 90 % and decreased the lag time by 8 minutes since 1950. Moreover, high flows are predicted to be more frequent if impervious areas become more important. Finally, high runoff-producing zones were identified and a link between these and the urban sprawl has been illustrated by critical areas maps.

The precision of these results was discussed in each concerned section. Uncertainties are inevitably present but these results can be considered as acceptable.





## 7. FINAL CONCLUSION

This work consisted in the modelling of the rainfall-runoff relationships in the Upper Bukit Timah catchment in Singapore, in order to highlight the impacts of urbanisation on hydrology. The first hypothesis consisted in verifying that it is possible to build a watershed model using only few available data. This has been partly confirmed since the model only fitted the observed data of old storm events. The effects of urbanisation on the hydrograph shape, lag time, maximum discharge and high flow frequency were proved and quantified, confirming the second hypothesis. Next paragraphs show the major steps of the methodology implemented to tests these two hypotheses and the main final results. Uncertainties and limitations are then discussed and future research perspectives are proposed.

The Upper Bukit Timah basin, 6.8 km<sup>2</sup>, contains the highest point of Singapore (163 m) in its north part while the other parts of the basin are flat. The land use of the basin is variable, since 30 % of the catchment is constituted by the forests of the Nature Reserve of Singapore while other parts are much urbanised. The basin is mainly drained by concrete lined channels. The Upper Bukit Timah basin is a suitable area for this study since the urbanisation has occurred at a rapid pace, which has resulted in a high frequency of flood. Moreover, although the catchment has been studied extensively over the past, it is important to bring a new methodological approach which takes the current pattern into account of the area and which uses current powerful tools, like watershed models.

For the application of any watershed model, a large number of data is required. In this case, it was particularly difficult to obtain valuable data. The basic data, such as a DEM and a land use map, were obtained using the 2005 topographic map (1:25;000) and the 2009 Google Earth image. The new DEM, which has a resolution of 20 m, showed to be suitable for the study since a RMS error of 1.1 m was obtained. The RMS error of the ASTER GDEM, a DEM available at no charge which has a resolution of 30 m, was calculated at 10.1 m. Finally, comparison between the two DEMs showed divergences of more than 110 m. The new DEM was therefore used for the modelling. Land use data were obtained by digitising the 2009 Google Earth image, after defining each land use class as precisely as possible.

The SWMM model, a one-dimensional physically based model especially developed for urban areas, was mainly used. The parameters encoded into the model were determined by different means and several methods were used for their determination in order to assess their influence on the modelling. Observed discharge and rainfall data, essential to adjust the model, were determined either for old or current storm events. For old rainfall events, sixteen hyetographs and hydrographs of a variety of papers were georeferenced, digitised and their data extracted. For recent events, discharge data were determined from the water depth published on the PUB website while corresponding rainfall data were extracted from RADAR images. The adjustment of the model was firstly done using the old storm events. For each adjustment performed, the

model was evaluated using the Nash-Sutcliffe coefficient and a graphical analysis of the observed and modelled hydrographs. With a mean Nash-Sutcliffe coefficient of 0.482, and a simulated discharge matching the observed discharge fairly well, the SWMM model was considered as usable. For recent storm events, however, the low quality of the rainfall and discharge data, due to their indirect methods of determination, does not allow the adjustment of the model. Therefore, the assumption that the SWMM final model gives acceptable results for old and recent data was taken for the rest of this work.

Using the final adjustment of the SWMM model, a diachronic analysis was performed in order to present the effects of urbanisation on runoff. Our approach was to characterise the land use pattern of the Upper Bukit Timah basin for different dates (non-urbanised catchment, 1950, 1959, 1973, 1986, 2009, 2020), in order to characterise the catchment in terms of imperviousness, roughness and infiltration. For past dates, old land use maps were used. For the projection of 2020, the relationship between population density and imperviousness was determined using three empirical formulas. Then, in order to compare hydrographs of different periods of return, thirty synthetic design hyetographs of different duration and return period were constructed using the arithmetical mean of 103 observed storm event (NUS 5-minutes rainfall data). The results showed that urbanisation involve changes on the hydrographs shapes, with a significant increase of discharge and a decrease in lag time from date to date. From 1950 to 2009, the model showed a diminution in lag time by 8 minutes. The effects in peak flow are also noticeable, with, for example, a mean increase of more than 89 % from 1950 to today. The peak discharge-frequency curves generated for each storm duration also showed the effect of urban sprawl. For a 10-year return period storm event, for example, the peak discharge for a 50 % impervious catchment is more than the triple of what is produced by a non-urbanised catchment. Finally, high runoff-producing areas were identified using the runoff generated by each subcatchment of the Upper Bukit Timah basin. Critical areas maps were constructed for each date. They showed an increase in runoff from date to date for the whole basin, with a mean runoff depth of 1.80 mm for a non-urbanised catchment to a projected runoff volume of 6.05 mm in 2020. The most critical areas, constituted by downstream subcatchments, have an average production of runoff of 8 to 10 mm. The north part of the catchment, constituted by forests, is a low runoff-producing zone (0-4 mm).

Uncertainties and limitations of the methods were discussed along the work, in their corresponding sections. It is evident that with more precise valuable data, the model would have been easier to implement and to calibrate. The first uncertainties were linked to the DEM creation. Although the new DEM showed to be hydrologically correct, it is evident there are errors inherent to its creation. A LIDAR DEM would have been more suitable for this study. The quality of digitisation is also uncertain, mainly due to the subjectivity in the class choices as well as in the determination of the areas. Uncertainties in the SWMM parameters determination are also present, particularly for the width of each subcatchment. However, these parameters were adjusted to obtain results which fit observed data. This approach is common, since the calibration of a watershed model involves the modification of some parameters. The major limitations come from the determination of recent rainfall and discharge data, necessary to verify the model for recent land use pattern. Although as many RADAR images as possible were used, the too low resolution of the images and the approximate technique for the determination of rainfall intensity involved many errors. The best solution is to dispose of direct rainfall

measurements from weather stations within the catchment. Unfortunately, only NUS data were available. Then, the impossibility to dispose of a rating curve impeded the possibility to transform the water depth into discharge. These two datasets were therefore not valuable. However, the final adjustment of the SWMM model showed good agreement between observed and modelled discharge for old storm events and was therefore considered as acceptable. Concerning the diachronic analysis, the old land use maps used have been compiled approximately by Chuah (1987), lowering the quality of the data. Although the method used to calculate the predicted percentage of imperviousness is empirical, it is valuable to illustrate what would be the future projected impact of urbanisation on the Upper Bukit Timah basin. Finally, the results for low frequency storm event of high intensity may be underestimated because of the limitations of the one-dimensional model and the fact that this one was calibrated using low amplitude storms events.

There are some improvements which can be implemented in the future. First of all, providing valuable long term data could bring a verification of the model and its results, as well as a better adjustment. Indeed, data used to calibrate model simulations have a direct effect on the validation and evaluation of results. With continuous long-term rainfall and discharge data, it could be possible to automatically calibrate the model to fit the observed data. Rainfall data of several gages across the catchment could also be useful to take into account the spatial variability of rainfall during a storm event. An ideal model calibration would use a large range of data, with storm events of different duration, intensities and periods in order to « activate » all model parameters during calibration. It would also include uncertainty analysis, which allows the quantification of the level of confidence in a watershed model simulation output from a large number of relevant data. Uncertainty can be evaluated through the quantification of the quality and amount of observed data available, the absence of measured data, the lack of knowledge about the area of study, the approximations in the mathematical equations used in the model and the quality of the calibration. Also, precise data on catchment characteristics, such as channels dimensions, depression water storage, infiltration and so on, could surpass the problem linked to the one-dimension of the model and its impossibility to take into account overbanking water. For example, the SWMM model is able to take into account the effect of storage of water in surface depressions and its re-introduction into the system after a certain time. Dividing the basin into more uniform subcatchments could also be, in a lesser extent, interesting to improve the results.

Numerous applications can start from this work if data are available. For example, SWMM model is able to compute water quality around the considered catchment. This can be useful to quantify pollution generated from several sources (industry, used water, etc.). Another emerging challenge in urban areas is global warming, potentially leading to climate change. The model could be used to define the impacts of an eventual global increase of rainfall intensity for example. Moreover, data about infiltration and aquifers can also be used in SWMM to quantify the groundwater recharge reduction. This can be useful to estimate groundwater depletion and estimate the consequences of both urbanisation and eventually pumping. Finally, it has been seen that Singapore is a wealthy country, where floods are generally localised and of brief duration thanks to the flood alleviation schemes performed throughout the country. The situation would be different in countries that cannot afford fully engineered systems for flood mitigation. The application of the methodology showed here could therefore be useful to define the needs for flood control in such countries.

In conclusion, this research has reached its principal objective to provide a framework that can easily be reused in the future. It helps to understand the hydrological processes that take place in an urban environment and shows that a variety of indirect data can be useful for a watershed model application. If other valuable data are introduced, the constructed model can be used for other applications than the quantification of the effects of urbanisation on the hydrologic environment.

# BIBLIOGRAPHY

AHMAD, M.M., GHUMMAN, A.R., AHMAD, S. 2009. Estimation of Clark's instantaneous unit hydrograph parameters and development of direct surface runoff hydrograph, *Water Resources Management*, **23**(12), 2417-2435.

AKAN, O.A. 1993. *Urban stormwater hydrology: A guide to engineering calculations*, Lancaster (CA): Technomic Publishing.

ANCTIL, F., ROUSSELLE, J. AND LAUZON, N. 2005. *Hydrologie: cheminements de l'eau.*, Montréal (CA): Presses internationales Polytechnique.

Alicime, 2008. Pourquoi utiliser l'information radar? [Online]. Available at: <http://www.alicime.com/Radar.htm>. [Accessed in July 2011].

ASCE (American Society of Civil Engineers). 1996. *Hydrology Handbook*, ASCE Manuals and Reports of Engineering Practice No. 28.

ASTER GDEM Validation Team, 2009. *ASTER Global DEM Validation Summary Report*. [Online]. Available at: [http://www.ersdac.or.jp/GDEM/E/image/ASTERGDEM\\_ValidationSummaryReport\\_Ver1.pdf](http://www.ersdac.or.jp/GDEM/E/image/ASTERGDEM_ValidationSummaryReport_Ver1.pdf). [Accessed in November 2010].

BENABDESSELAM, T. AND HAMMAR, Y. 2009. Estimation de la réponse hydrologique d'un bassin versant urbanisé, *European Journal of Scientific Research*, **29**(3), 334-348.

BENGTSON, H. 2010. *The rational method for calculation of peak storm water runoff rate*. [Online]. Available at: <http://www.brighthub.com/engineering/civil/articles/60842.aspx#ixzz1Uo48StG4>. [Accessed in August 2010].

BENNIS, S. 2007. *Hydraulique et hydrologie*. 2<sup>nd</sup> ed. Québec: Presses de l'Université du Québec.

BEVEN, K. 2004. Robert E. Horton's perceptual model of infiltration processes, *Hydrological Processes*, **18**, 3447-3460.

BHAWAN, J.V. 1998. *Rainfall-runoff modelling of Morel catchment for design flood estimation*, National Institute of Hydrology, Roorkee (IN).

BLÖSHL, G. and SIVAPALAN, M. 1995. Scale issues in hydrological modeling: A review, *Hydrological Processes*, **9**, 251-290.

BOONSTRA, J. 1994. Estimating Peak Runoff Rates. In: RITZEMA, H.P. ed. 1994. *Drainage Principles and Application*. 2<sup>nd</sup> ed. Wageningen: International Institute for Land Reclamation and Improvement (ILRI). Ch. 4.

BRABEC, E., SCHULTE, S. RICHARDS, P.L. 2002. Impervious surfaces and water quality: A review of current literature and its implications for watershed planning, *Journal of Planning Literature*, **16**(4), 499-514.

Bukittimah.net, 2011. *CCTV Monitoring Trial Along Flood-prone Bukit Timah Canal*. [Online]. Available at: <http://www.bukittimah.net/page/5/>. [Accessed in July 2011].

BUTLER, D. and DAVIES J. W. 2004. *Urban Drainage*. 2<sup>nd</sup> ed. London (UK): Spon Press.

CANTONE, J.P. 2010. *Improved understanding and prediction of the hydrological response of highly urbanized catchments through development of the Illinois Urban Hydrologic Model (IUHM)*. Ph.D., Graduate College of the University of Illinois at Urbana-Champaign, USA.

Campbell, R.W., 2008. *Singapore: 1973, 1990, 2000, 2002. Earthshots: Satellite Images of Environmental Change*. U.S. Geological Survey. [Online]. Available at: <http://earthshots.usgs.gov/Singapore/Singapore>. [Accessed in May 2011].

Channelnewasia, 2009. *Heavy rain causes knee-high floods in Bukit Timah*. [Online]. Available at: <http://www.channelnewsasia.com/stories/singaporelocalnews/view/1019285/1/.html>. [Accessed in May 2011].

Channelnewasia, 2011. *CNA: Flash flood hits Singapore again*. [Video online]. Available at: <http://www.youtube.com/watch?v=RZ7-wZfefUA>. [Accessed in June 2011].

CHATTERJEA, K. 1989. *Observations on the fluvial and slope processes in Singapore and their impact on the urban environment*. Ph.D., Department of Geography, National University of Singapore, Singapore.

CHATTERJEA, K. 1994. Dynamics of fluvial and slope processes in the changing geomorphic environment of Singapore, *Earth Surface Processes and Landforms*, **19**, 585-607.

CHECK, L.M. 1997. Drainage planning and control in the urban environment. The Singapore experience, *Environmental Monitoring and Assessment*, **44**, 183-197.

CHENGTAI, D. 1996. An approach to theory and methods of urban geomorphology, *Chinese Geographical Science*, **6**(1), 88-95.

CHIA, E.H. 1979. *A computer simulation model of hydrological response in the Upper Bukit Timah Watershed*. B.A., Department of Geography, National University of Singapore, Singapore.

CHING, N.G.S. 1997. *Drainage canals in Singapore: flood control and other uses*. B.A., Department of Geography, National University of Singapore, Singapore.

CHOI, K.-S., BALL, J.E. 2002. Parameter estimation for urban runoff modeling, *Urban Water*, **4**, 31-41.

CHUAH, G.C.M. 1987. *The hydrological impact of landuse changes on runoff in the Upper Bukit Timah Basin*. B.A., Department of Geography, National University of Singapore, Singapore.

CHUA, L.H.C., and WONG, T.S.W. 2010. Improving event-based rainfall–runoff modeling using a combined artificial neural network–kinematic wave approach, *Journal of Hydrology*, **390**, 92-107.

County of San Diego, Department of Planning and Land Use, 2008. *Impervious Surface Coefficients for General Land Use Categories for Application within San Diego County*. [Online]. Available at: [http://www.sdcountry.ca.gov/dpw/watersheds/watershedpdf/impervious\\_surface\\_coefficients\\_2008.pdf](http://www.sdcountry.ca.gov/dpw/watersheds/watershedpdf/impervious_surface_coefficients_2008.pdf). [Accessed in January 2011].

DASSARGUES, A. 2010. *Hydrogéologie*. Université de Liège, Lecture notes, unpublished.

DONNAY, J.P. 2010. *Cartographie*. Université de Liège, Lecture notes, unpublished.

DONNAY, J.P. 2011. *Introduction aux sciences géographiques. Partim: Géomatique*. Université de Liège, Lecture notes, unpublished.

DUNNE, T. and LEOPOLD, L.B. 1978. *Water in Environmental Planning*. New York (USA): W.H. Freeman and Company.

EPA (US Environmental Protection Agency), 2008. *Watershed Modeling*. [Online]. Available at: <http://www.epa.gov/owow/watershed/wacademy/acad2000/modeling/index.html>. [Accessed in January 2011].

ESRI (Environmental Systems Research Institute), 2009. *ArcGIS Desktop 9.3 Help*. [Online]. Available at: <http://webhelp.esri.com/arcgisdesktop/9.3/index.cfm?TopicName=welcome>. [Accessed in 2011].

EXUM, L.R., BIRD, S.L., HARRISSON, J., PERKINS, C.A. 2005. Estimating and projecting impervious cover in the Southeastern United States, US Environmental Protection Agency (EPA), EPA/600/R-05/061, Ecosystems Research Division, National Exposure Research Laboratory, Athens, USA, 133p.

FANG, X., THOMPSON, D.B., CLEVELAND, T.G., PRADHA., P.D.E. and MALLA, R. 2008. Time of concentration estimated using watershed parameters determined by automated and manual methods, *Journal of Irrigation and Drainage Engineering*, 202-211.

FOO, S.Y. 1986. *Floods in Singapore: A general appraisal*. B.A., Department of Geography, National University of Singapore, Singapore.

GIRONÀS, J., ROESNER, L.A., and DAVIS, J. 2009. *Storm Water Management Model Applications Manual*, US Environmental Protection Agency (EPA), EPA/600/R-09/077, Department of Civil and Environmental Engineering, Colorado State University, Fort Collins, USA, 179p.

GOPI, S. 2005. *Global Positioning System: Principles and Applications*, New Delhi (IN): Tata McGraw-Hill.

GUO, J.C.Y. 2003. *Urban storm water design*. Colorado (USA): Water Resources Publications, LLC.

GUPTA, A. 1982. Observations on the effects of urbanization on runoff and sediment production in Singapore, *Singapore Journal of Tropical Geography*, **3**(2), 137-146.

GUPTA, A. 1994. Floods and sediment production in Singapore. In: GUPTA, A. and PITTS, J. ed. 1994. *Physical adjustments in a changing landscape: the Singapore story*. Singapore (SG): Singapore University Press. Ch. 10.

GUPTA, A. and PITTS, J. ed. 1994. *Physical adjustments in a changing landscape: the Singapore story*. Singapore (SG): Singapore University Press.

GUPTA, A. RAHMAN, A., WONG, P.P. and PITTS, J. 1987. The Old Alluvium of Singapore and the extinct drainage system to the South China Sea, *Earth Surface Processes and Landforms*, **12**, 259-275.

HORDON, R.M. 1977. Water supply as a limiting factor in developing communities: endogenous vs. Exogenous sources, *Journal of the American Water Resources Association*, **13**(5), 933-939.

HUTCHINSON, M.F. 1996. A locally adaptive approach to the interpolation of digital elevation models. In: NCGIA. 1996. *Proceedings of the Third International Conference/Workshop on Integrating GIS and Environmental Modeling*. Santa Barbara, CA: National Center for Geographic Information and Analysis. [Online]. Available at: [http://www.ncgia.ucsb.edu/conf/SANTA\\_FE\\_CD-ROM/sf\\_papers/hutchinson\\_michael\\_dem/local.html](http://www.ncgia.ucsb.edu/conf/SANTA_FE_CD-ROM/sf_papers/hutchinson_michael_dem/local.html). [Accessed on July 2011].

JACOBSON, C.R. 2011 (in press). Identification and quantification of the hydrological impacts of imperviousness in urban catchments: A review, *Journal of Environmental Management*, 1-11.

JAVAHERI, H. 1998. *Automatic calibration of urban runoff models using global optimization techniques*. Ph.D., Department of Civil Engineering and Applied Mechanics, McGill University, Canada.

KAUR, S. 1981. *Rainfall-runoff relationships of the Upper Bukit Timah Catchment area*. B.A., Department of Geography, National University of Singapore, Singapore.

KHU, S.T. and WERNER, M.G.F. 2003. Reduction of Monte-Carlo simulation runs for uncertainty estimation in hydrological modeling, *Hydrology and Earth System Sciences*, **7**(5), 680-292.

Leopold, L.B. 1968. Hydrology for urban land planning – A guidebook on the hydrologic effects of urban land use, *Geological Survey Circular*, **554**, 1-18.

LIONG, S-Y., CHAN, W.T., and LAW, C.L. 1991. An expert system for Storm Water Management Modelling and its application, *Engineering Applications of Artificial Intelligence*, **4**(5), 367-375.

LIONG, S-Y. GAUTAM, T.R., KHU, S.T., BABOVIC, V. KEIJZER, M. and MUTTIL, N. 2002. Genetic Programming: A new paradigm in rainfall runoff modeling, *Journal of the American Water Resources Association*, **38**(3), 705-718.

LIONG, S-Y. IBRAHIM, Y., CHAN, W.T. and LAW, C.L. 1993. Computer-aided catchment-calibration model, *Advances in Engineering Software*, **17**, 147-154.

LMNO Engineering, Research, and Software. 2000. Trapezoidal Open Channel Design Calculation. [Online]. Available at: <http://www.lmnoeng.com/Channels/trapezoid.htm>. [Accessed in May 2011].



LMNO Engineering, Research, and Software. 2003. Time of Concentration Calculator. Compute watershed time of concentration using FAA equation (rational method), Kirpich equation, or Kerby equation. [Online]. Available at: <http://www.lmnoeng.com/Hydrology/TimeConc.htm>. [Accessed in April 2011].

MAREK, M.A.P.E. 2009. *Hydraulic Design Manual*, Texas Department of Transportation, Design Division, (512) 302-2453, 451p.

MASON, B., and KNIGHT, R. 2001. *Sensitive habitat inventory and mapping*, Community Mapping Network, M. Johannes: Vancouver, British Columbia, Canada. Module 7 Imperviousness, 247-279.

McCuen, R.H. 2004. *Hydrological analysis and design*. 3<sup>rd</sup> edition. Upper Saddle River (USA): Pearson Prentice Hall.

MDDEP (Développement durable, de l'Environnement et des Parcs) and MAMROT (ministère des Affaires municipales, des Régions et de l'Occupation du territoire). 2002. *Guide de gestion des eaux pluviales. Stratégies d'aménagement, principes de conception et pratiques de gestion optimales pour les réseaux de drainage en milieu urbain*, Québec (CA).

MERWADE, V. 2010. *Creating SCS Curve Number Grid using HEC-GeoHMS*, School of Civil Engineering, USA, Purdue University, 27p.

MORIASI, D.N., ARNOLD, J.G., VAN LIEW, M.W. BINGNER, R.L., HARMEL, R.D., and VEITH, T.L. 2007. Model evaluation guidelines for systematic quantification of accuracy in watershed simulations, *American Society of Agricultural and Biological Engineers*, **50**(3), 885-900.

MUJUMDAR, P.P. 2001. Flood Wave Propagation, The Saint Venant Equations, *Resonance*, 66-73.

National Environment Agency, 2002. *Rain Areas Animation*. [Online]. Available at: [http://app2.nea.gov.sg/rain\\_animation.aspx](http://app2.nea.gov.sg/rain_animation.aspx). [Accessed in May and June 2011]

National Environment Agency, 2009. *WEATHERWise, Singapore*. [Online]. Available at: <http://app2.nea.gov.sg/data/cmsresource/20090721544571208250.pdf>. [Accessed in August 2010].

National Environment Agency, 2011. Weather Statistics. [Online]. Available at: [http://app2.nea.gov.sg/weather\\_statistics.aspx](http://app2.nea.gov.sg/weather_statistics.aspx). [Accessed in August 2010].

NICKLOW, J.W., BOULOS, P.F., and MULETA, M.K. 2004. *Comprehensive sewer collection systems analysis handbook for engineers and planners*, Pasadena (CA): MWH Soft.

PICOUET, C., HINGRAY, B. MUSY, A. 2003. *Calcul d'une pluie de projet de temps de retour donné selon différentes methods dérivant des courbes IDF ou des pluies observes – Application au bassin de la Seymaz à Pont Bochet (GE, Suisse)*, Hydrothèque, base de données d'exercices en Hydrologie, Exercice n°HA 0301 – Corrigé, Ecole Polytechnique Fédérale de Lausanne (SWZ).

Pikes Peak Area Council of Governments (PPACG), 2005. *Fountain Creek Watershed. Impervious surface area and watershed health analysis*.

PITT, R., LILBURN, M., DURRANS, R.S., BURIAN, S. NIX, S., VOORHEES, J., MARTINSON, J. and FAN, C.-Y. 1999. *Guidance Manual for Integrated Wet Weather Flow (WWF) Collection and Treatment Systems for Newly Urbanized Areas (New WWF Systems)*, US Environmental Protection Agency (EPA), National Risk Management Research Laboratory, Office of Research and Development, Cincinnati, USA.

PUB. 2010. *Drainage design and considerations*. [Online]. Available at: <http://www.pub.gov.sg/general/code/Pages/SurfaceDrainagePart2-7.aspx>. [Accessed in September 2010].

PUB. 2011. *Water Level Sensors*. [Online]. Available at: <http://www.pub.gov.sg/MANAGINGFLASHFLOODS/WLS/Pages/WaterLevelSensors.aspx> [Accessed in April 2011]

Public Works Department Singapore. 1976. *Geology of the Republic of Singapore*, Singapore: Public Works Department.

RAHARDJO, H., AUNG, K.K., LEONG, E.C., and REZAUR, R.B. 2004. Characteristics of residual soils in Singapore as formed by weathering, *Engineering Geology*, **73**, 157-169.

RAHMAN, A. 1990. Near surface hydrological processes under changing land use in humid-equatorial conditions, *IAHS Publication*, **187**, 331-340.

ROSSMAN, L.A., 2010. *Storm Water Management Model User's Manual Version 5.0*, US Environmental Protection Agency (EPA), EPA/600/R-05/040, Water Supply and Water Resources Division, National Risk Management Research Laboratory, Cincinnati, USA.

SELVALINGAM, S. LIONG, S.Y. and MANOHARAN, P.C. 1987. Use of RORB and SWMM models to an urban catchment in Singapore, *Adv. Water Resources*, **10**, 78-86.

SERVAT, E. and DEZETTER, A. 1991. Selection of calibration objective functions in the context of rainfall-runoff modelling in a sudanese savannah area, *Hydrological sciences*, **36**(4), 307-330.

SIEN, C.L. and FOOK, F.S. 1991. Climate and weather. In: SIEN, C.L., RAHMAN, A. and TAY D.B.H. ed. 1991. *The Biophysical Environment of Singapore*. Singapore: Singapore University Press. Ch. 2.

Singapore Department of Statistics, 2010. *Population Trends 2010*. Ministry of Trade & Industry, Republic of Singapore. [Online]. Available at: <http://www.singstat.gov.sg/pubn/popn/population2010.pdf>. [Accessed in June 2011].

SINGH, V.P. and WOOLHISER, D.A. 2002. Mathematical Modeling of Watershed Hydrology, *Journal of Hydrologic Engineering*, 270-292.

SMITH, A.A. 2010. *Hydrological Theory. Calculating Runoff. SWMM-RUNOFF Algorithm*. [Online]. Available at: <http://www.miduss.com/theory-Calculating-Runoff-SWMM-RUNOFF-Algorithm.htm>. [Accessed in June 2011].

STANESCU, V.A., AND MUSY, A. 2006. Design Storm. In: Stanescu, V.A. (Module leader) 2006. *Virtual Campus In hydrology and water REsources management (VICAIRE)*. Ch. 1b.2.

Strait Times, 2010. *All eyes on flood hot spot Orchard*. [Online]. Available at: <http://wildsingaporenews.blogspot.com/2010/07/flooding-in-singapore-comments.html>. [Accessed in May 2011].

STRAUB, T. D., MELCHING, C. S. and KOCHER, K.E. 2000. *Equations for estimating Clark Unit-Hydrograph parameters for small rural watersheds in Illinois*, USGS, Water-Resources Investigations Report 00-4184.

Testech, n.d. *WLS01 Water Level And Flood Monitoring System*. [Online]. Available at: <http://www.testech-elect.com/m2m/wls01.htm>. [Accessed in May 2011].

The Weather Channel, 2011. *Monthly Averages for Singapore*. [Online]. Available at: <http://www.weather.com/weather/wxclimatology/monthly/SNXX0006>. [Accessed in May 2011].

THOMPSON, D.B., 2006. *The rational method, regional regression equations, and site-specific flood frequency relations*, Texas Tech University, TechMRT Report 0-4405-1.

US Army Corps of Engineers. 2008. *Hydrologic Modeling System HEC-HMS. Applications Guide*, Hydrologic Engineering Center, March 2008.

US Army Corps of Engineers. 2010. *Hydrologic Modeling System HEC-HMS. User's manual*, Hydrologic Engineering Center, August 2008.

USDA (U.S. Department of Agriculture). 1986. *Urban Hydrology for Small Watersheds*, Technical Release 55 (TR-55), Natural Resources Conservation Service, Conservation Engineering Division. [Online]. Available at : <http://www.cset.sp.utoledo.edu/~nkisoff/pdf/CIVE-3520/Modified-tr55.pdf>. [Accessed in March 2011].

USGS (U.S. Geological Survey), 2010. *What is hydrology and what do hydrologists do?*. [Online]. Available at: <http://ga.water.usgs.gov/edu/hydrology.html>. [Accessed in May 2011].

WASHBURN, B. YANCEY, and K. MENDOZA, J. 2010. *User's Guide for the California Impervious Surface Coefficients*, California Environmental Protection Agency (EPA), Ecotoxicology Program, Office of Environmental Health Hazard Assessment, USA, 56p.

WEI, T.D. 2011. *PUB to speed up improvement works*. The Strait Times. [Online]. Available at: [http://www.straitstimes.com/BreakingNews/Singapore/Story/STIStory\\_679019.html](http://www.straitstimes.com/BreakingNews/Singapore/Story/STIStory_679019.html). [Accessed in July 2011].

Wisconsin Department of Transportation, 2007. *Facilities Development Manual. Chapter 13: Drainage*. [Online] Available at: <https://trust.dot.state.wi.us/static/standards/fdm/13/tc13.pdf>. [Accessed in February 2011]

WONG, S.T. 1975. *Runoff analysis of the Upper Bukit Timah catchment area, Singapore*. B.A., Department of Geography, National University of Singapore, Singapore.

YEE, Y.W., DING, L.Y., and JIAN, C.S. 2010. *Rebasing of Singapore's National Accounts to Reference Year 2005*, Statistics Singapore Newsletter, Economic Accounts Division, Singapore Department of Statistics, September 2010.



# TUTORIAL

Section 1. Georeferencing .....	121
Section 2. DEM realisation .....	124
Section 3. Land use digitisation .....	130
Section 4. SWMM subcatchments parameters determination .....	134
Section 5. Old hyetograph and hydrograph: data extraction .....	141
Section 6. Data extraction from RADAR images .....	144
Section 7. Determination of HEC-HMS parameters .....	148
Section 8. Synthetic design hyetographs determination.....	151





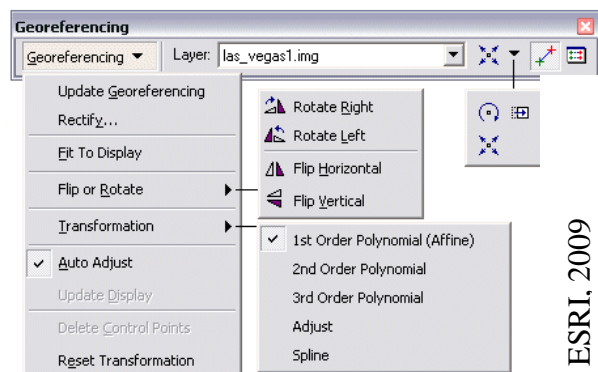
## Section 1. Georeferencing

### Topographic sheets details

- Published by Mapping Unit, Ministry of Defense, Singapore, 2005.
- Compiled by Mapping Unit from the following sources:
  - Series L802, Edition 9 SMU (2000),
  - 1:5,000 Topo plans, 2002 and 2003 / Aerial Photography Oct 2003,
  - PSA SP1 Chart – 18 March 1998,
  - MPA (Port limit) Notification 1997.
- Series L802, Sheets 1 and 4, Edition 10 SMU.
- Scale: 1:25,000.
- Contour interval 10 meters, supplementary contour 5 meters.
- Projection: Rectified Skew Orthomorphic (Metric Grid).
- Spheroid: Everest.
- Origin: 4°00 N., 102°15' E.

### Topographic sheets georeferencing

- Add the *Georeferencing* toolbar to the view (*View > Toolbars > Georeferencing*);
- Click the *Add Control Point* tool ;
- Click the mouse pointer on a junction of the projection lines;
- Right click *Input X and Y* and enter the coordinates indicated along the border;
- Repeat the operation for each junction;
- Click *View Link Table* tool  which shows residual error for each links and the RMS error in a tabular form to evaluate the transformation;
- Click *Georeferencing > Rectify* in order to permanently transform the topographic sheet;
- Repeat the operation for each photo.




ESRI, 2009

The *Adjust* transformation has been used. According to the ESRI (2009), the adjust transformation optimizes for both global least square feature algorithm and local accuracy. It is built upon an algorithm that combines a polynomial transformation and TIN interpolation techniques. Each area inside the triangular network is then adjusted by bilinear interpolation. Typically, the adjust transformations give a RMS of near zero or zero (however, this does not mean that the image will be perfectly georeferenced but this method allows the user to give reference points their exact location on the final image).

An example of *Link Table* obtained for the DSCN0643 photo is shown below.

Dscn0643

X Source	Y Source	X Map	Y Map
138.419747	-180.003254	642000.000000	148395.000000
1749.150813	-1346.678696	644000.000000	147000.000000
2608.371289	-539.463804	645000.000000	148000.000000
3642.108180	-250.853861	646250.000000	148395.000000
3443.345430	-560.004754	646000.000000	148000.000000
2604.472669	-1363.929588	645000.000000	147000.000000
3457.964992	-1382.159726	646000.000000	147000.000000
871.990078	-2177.531299	643000.000000	146000.000000
901.536971	-1329.208172	643000.000000	147000.000000
70.907075	-1314.070425	642000.000000	147000.000000
117.678280	-495.916771	642000.000000	148000.000000
952.052887	-187.042794	643000.000000	148395.000000
936.949304	-504.938144	643000.000000	148000.000000
1771.997937	-525.170948	644000.000000	148000.000000
29.977275	-2156.926623	642000.000000	146000.000000
1728.050099	-2199.220139	644000.000000	146000.000000
2594.137964	-2220.518867	645000.000000	146000.000000
3467.033900	-2239.394361	646000.000000	146000.000000
1781.199536	-207.713012	644000.000000	148395.000000
2610.442402	-224.927288	645000.000000	148395.000000
3436.207542	-245.779575	646000.000000	148395.000000
3651.525202	-565.003662	646250.000000	148000.000000
3667.208104	-1387.431581	646250.000000	147000.000000
3684.313158	-2244.006241	646250.000000	146000.000000

- In *ArcToolbox*  use the *Define Projection* function (*Data Management Tools > Projections and Transformation > Raster > Define Projection*) to assign the projection *Kertau RSO Malaya Meters (Projected Coordinate System > National grids > Malaysia)* to the georeferenced topographic sheets. This projection corresponds to the characteristics shown on the map. Its characteristics are resumed below.
- In *ArcToolbox* use the *Project* function (*Data Management Tools > Projections and Transformations > Feature > Project*) to change the Malaysian coordinate system to the UTM coordinate system (*Projected Coordinate System > UTM > WGS 1984*). Singapore corresponds to the UTM Zone 48 N. The characteristics of the projection are resumed below.

## Topographic sheets assembling

Use *Erdas Imagine Software* to assemble the four georeferenced images of topographic sheets. This software allows the creation of a seamless (automatic or user controlled) mosaic.

## Google Earth image georeferencing

The date of the Google Earth image that has been used is the 14<sup>th</sup> of March, 2009, the last available accurate image acquired with the Quickbird satellite (original panchromatic resolution: 0.61 m).



- Proceed as explained above and:
- When using the *Add Control Point* tool, input the X and Y figuring on Google Earth;
- The *View Link Table* tool showed an acceptable RMS with 35 ground control points;
  - The Google Earth image is projected in UTM (Zone 48 N).

## Projection characteristics: Kertau RSO Malaya Meters

```

Projection: Rectified_Skew_Orthomorphic_Natural_Origin
False_Easting: 804671.299775
False_Northing: 0.000000
Scale_Factor: 0.999840
Azimuth: -36.974209
Longitude_Of_Center: 102.250000
Latitude_Of_Center: 4.000000
XY_Plane_Rotation: -36.869898
Linear Unit: Meter (1.000000)

Geographic Coordinate System: GCS_Kertau
Angular Unit: Degree (0.017453292519943295)
Prime Meridian: Greenwich (0.000000000000000000)
Datum: D_Kertau
Spheroid: Everest_1830_Modified
Semimajor Axis: 6377304.063000000100000000
Semiminor Axis: 6356103.038993154700000000
Inverse Flattening: 300.801699999999980000

```

## Projection characteristics: UTM Zone 48 N

```

Projection: Transverse_Mercator
False_Easting: 500000,000000
False_Northing: 0,000000
Central_Meridian: 105,000000
Scale_Factor: 0,999600
Latitude_Of_Origin: 0,000000
Linear Unit: Meter (1,000000)




Geographic Coordinate System: GCS_WGS_1984
Angular Unit: Degree (0,017453292519943295)
Prime Meridian: Greenwich (0,000000000000000000)
Datum: D_WGS_1984
Spheroid: WGS_1984
Semimajor Axis: 6378137,000000000000000000
Semiminor Axis: 6356752,314245179300000000
Inverse Flattening: 298,257223563000030000

```

## Section 2. DEM realisation

### Digitisation

Contour lines:

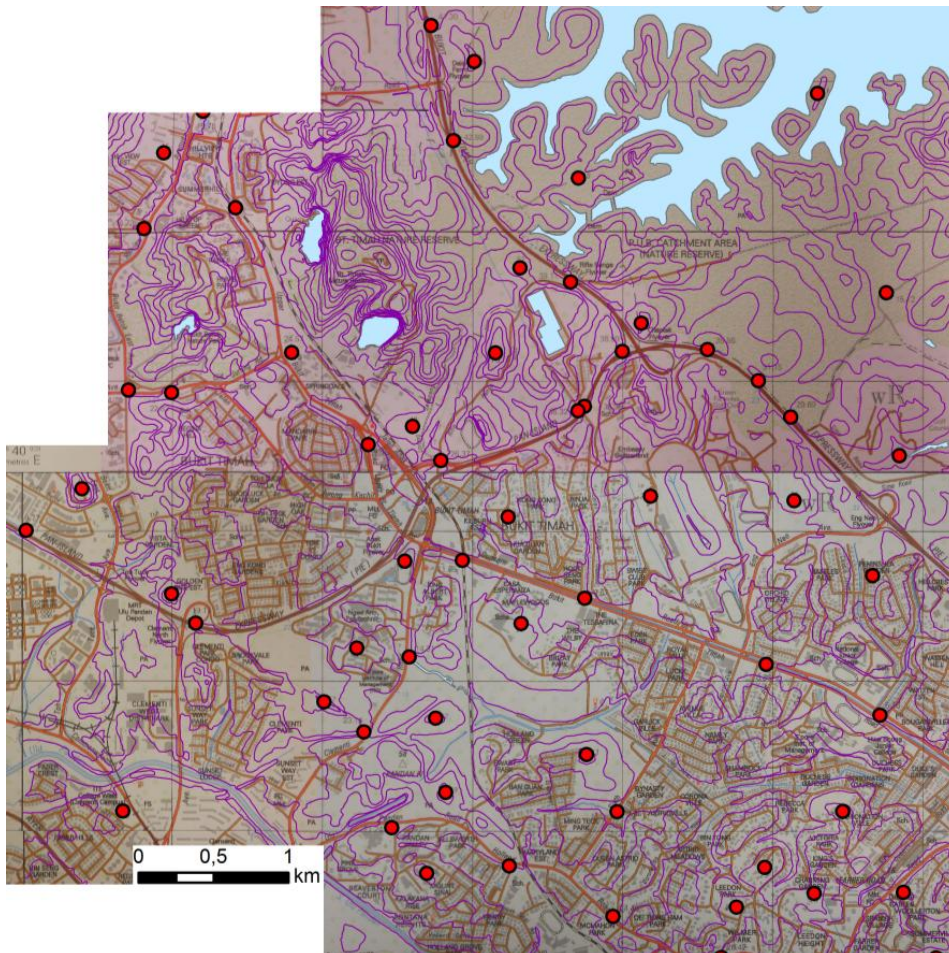
- Open *ArcCatalog*  and create a *New Shapefile* (*File > New > Shapefile*). Set the feature type as *Polyline* and define the spatial reference (UTM 48 N);
- Set the *Properties* by adding a *Field* named *Elevation* (*Data type: Double*);
- Add the new shapefile to *ArcMap*;
- Add the *Editor Toolbar* to *ArcMap*;
- Edit the shapefile (*Editor > Start Editing*) by creating a *New Feature*;
- Use the pencil  to digitise each contour line of the topographic map and enter manually the elevation value in the *Attributes Table* ;
- *Save Edits* when needed.

Quoted points:

- Repeat the same steps, but create a *Point* shapefile instead of a *Polyline* shapefile.

Lakes:

- Repeat the same steps, but create a *Polygon* shapefile.



## First test with the *Topo to Raster* function

- In *ArcToolbox*, use the *Topo to Raster* function (*ArcToolbox* > *3D Analyst Tools* > *Raster Interpolation* > *Topo to Raster*) to create a DEM;
- Input the lakes, contour lines and quoted points as feature layers as shown below.

- Test the *Flow Direction* function (*ArcToolbox* > *Arc Hydro Tools* > *Terrain Preprocessing* > *Flow Direction*) by using the DEM.

The *FlowDir* output raster shows the direction of flow out of each cell. It is an integer raster whose values range from 1 to 255 (ESRI, 2009). The values for each direction from the center are:

32	64	128
16		1
8	4	2

- Test the function *Flow Accumulation* (*ArcToolbox* > *Arc Hydro Tools* > *Terrain Preprocessing* > *Flow Accumulation*) by using the DEM and the *FlowDir* raster.

The *FlowAcc* output represents the number of upslope cells that flow into each cell, assuming that all rain became runoff and there was no interception, evapotranspiration or loss to groundwater (ESRI, 2009).

- The result of this function is not accurate enough. Optimization is needed and is explained below.

## Streams digitisation and characteristics (→ water system in 2D)

- Create a *New Shapefile*. Set the feature type as *Polyline* and define the spatial reference;
- Georeference the Chuah & Wong's sketch of the Upper Bukit Timah catchment. It constitutes a first reference for the drains position. The second reference is Google Street View;
- From both sources, digitise the drains of the catchment (in forested areas, Chuah & Wong's sketch is the reference; in built areas, Street View is the used tool);
- Modify the *Attributes Table* by adding the following fields:  
 State\*\* (aerial, subterranean or unknown), *Text*;  
 Channel type\* (concrete line channel or earth channel), *Text*;  
 Manning's coefficient\*, *Double*;  
 Length\*, *Double*;  
 Slope\*, *Double*;  
 Channel shape\*\*\* (trapezoidal, wide rectangular or triangular), *Text*;  
 Width\*, *Double*;  
 Side slope\*, *Double*;  
 Upstream flow\*, *Text*.
- Edit the *Attributes Table* manually for each field (Sources: \* Chuah & Wong (2010); \*\* Google Earth, Google Street View, and fieldwork; \*\*\* Chuah & Wong (2010), Google Street View and fieldwork). A part of the *Attributes Table* is shown below.

FID	Shape *	Id	Etat	Channel ty	Manning co	Length	Slope	Channel sh	Width	Side slope	Upstream f
0	Polyline	170	Aerien	Concrete line channel	0,013	710	0,003	Trapezoidal	3,5	1	C130, C160
1	Polyline	0	Aerien		0	0	0		0	0	
2	Polyline	0	Aerien		0	0	0		0	0	
3	Polyline	250	Aerien	Concrete line channel	0,013	210	0,003	Trapezoidal	4,5	1	C170, C210, C240
4	Polyline	130	Aerien	Concrete line channel	0,013	630	0,003	Wide rectangular	7,5	0	C120
5	Polyline	120	Aerien	Concrete line channel	0,013	300	0,005	Wide rectangular	4,8	0	C70, C110
6	Polyline	70	Aerien	Concrete line channel	0,013	460	0,005	Wide rectangular	4,2	0	C20, C40, C60
7	Polyline	260	Souterrain	Earth channel	0,03	420	0,025	Triangular	0	1,5	
8	Polyline	270	Aerien	Concrete line channel	0,013	470	0,01	Wide rectangular	2	0	C260
9	Polyline	220	Inconnu	Concrete line channel	0,013	440	0,011	Wide rectangular	2,5	0	
10	Polyline	230	Aerien	Concrete line channel	0,013	790	0,011	Wide rectangular	2,5	0	C220
11	Polyline	240	Aerien	Concrete line channel	0,013	670	0,011	Wide rectangular	2,5	0	C230
12	Polyline	210	Aerien	Concrete line channel	0,013	530	0,005	Wide rectangular	3,5	0	C200
13	Polyline	200	Aerien	Concrete line channel	0,013	330	0,01	Wide rectangular	1,5	0	C190
14	Polyline	190	Aerien	Concrete line channel	0,013	330	0,02	Triangular	0	0,5	C180
15	Polyline	180	Inconnu	Earth channel	0,03	800	0,035	Triangular	0	1,5	

- For the depth, make a sketch of the drains with their respective depth using Google Street View (eg. One step ~ 20 cm, 10 steps ~ 2 m) when more accurate data is not available. This will be used later.


## Transformation of the streams into points (→water system in 3D)

### Drains:

- Add the *ET GeoWizard* toolbar and use the *Create Station Point* function;
- Input the waterways shapefile (in *Source Polyline Layer*) and set the distance between stations to 50 m. This function creates a point every 50 m on the waterways;
- Edit the *Attributes Table* by encoding the elevation of each point manually :
  - The first point elevation is known: 7.62 m (9.67 m as noted on the topographic map minus the drain depth of about 2 m (determined in Google Street View and personal field photos)).

- Drain depth, drain slopes and distance between points are also known.
- The other elevations are determined by rule of three and the upstream propagation of this calculation.

#### Drain sides:

- Create a point shapefile to create new points on the bank of all drains;
- Use the *Copy Parallel Tool*  (*Editor > Copy Parallel*) to copy the 'central drain' on the bank position for both sides (the width of each drain is known) into the created shapefile;
- Edit the *Attributes Table* by encoding the elevation of each point. The elevation value is calculated from the width (which is known) and from the depth (determined with Google Street View).

#### Second test with the *TIN* function

- In *ArcToolbox*, find the *TIN Creation* tab and create a *TIN* (*3D Analyst Tools > TIN Creation > Create a TIN*);
- Then, use the *Edit TIN* function. The inputs are the contour lines, the quoted point, the 'central drain' shapefile and the 'drain sides' shapefile;
- It gives accurate results for the drains areas but not for the remaining zones.

#### Transformation of the *Station Points*


- The *Create Station Point* function (*ET GeoWizard*) is rerun with the *Source Polyline Layer* being the waterways shapefile and the distance between stations set to 5 m;
- Transform the *TIN* layer into a raster (*TIN to Raster* function);
- In *ArcToolbox* find the *Extract Value to Point* function (*Spatial Analyst Tools > Extraction > Extract Value to Point*) and enter the *TIN* raster and the *Station Points* shapefile as inputs in order to associate the *TIN* elevation value to each created point.



#### Rerun the *Topo to Raster* function as many times as necessary

- Reuse the *Topo to Raster* function to create a DEM. In addition to all the inputs used in the previous test, add the *Station Point* (every 5 m) shapefile;
- Test the *Flow Direction* function;
- Test the *FlowAccumulation* function;
- Create a new shapefile and define the *Pour Point* (outlet) using the *FlowAcc* layer;
- Create a new *Polygon* shapefile and digitise the Upper Bukit Timah watershed of the Chuah and Wong's article;
- Test the function *Watershed* with the *Pour Point* and *Flow Direction* layers as inputs;
- Check the different layers created; compare the modelled watershed with the real one;
- Rerun the operation as many times as necessary after each modification.

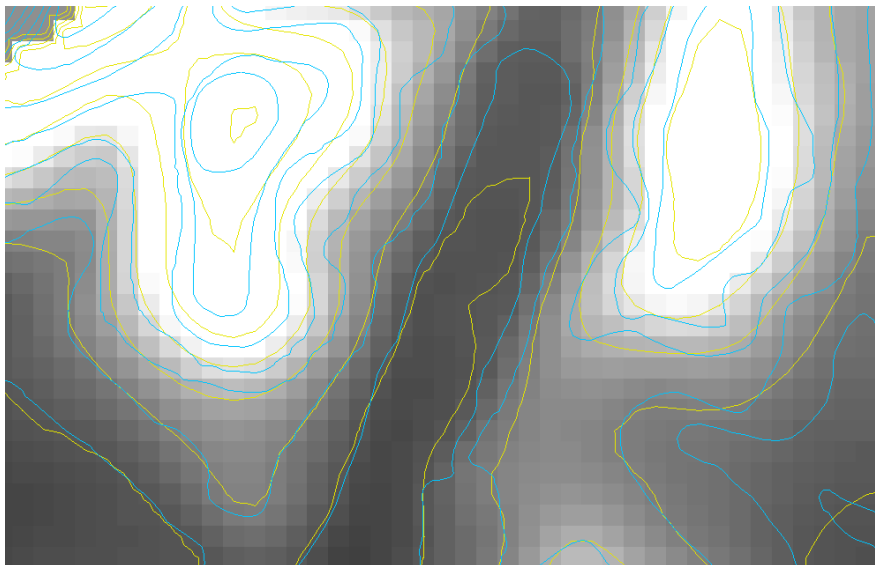


- The modifications made to the inputs layers between tests are:
  - Delete problematic parts of contour lines: *Edit* the shapefile, use the *Split Tool*  (*Editor Toolbar*) to create the feature which has to be deleted. Select it and delete it using the *Attributes Table*. Repeat the operation as many times as necessary.
  - Delete problematic contour lines (*Editor Toolbar*).
  - Redigitise some contour lines (see above).
  - Change the resolution of the created DEM (several tests with 10, 15, 20, 30 m).
- After numerous tests (~ 40), the *FlowAcc* layer looks hydrologically correct and the *Watershed* looks like the Chuah and Wong's Upper Bukit Timah catchment.

## Evaluation of the DEM

### Contour lines:

- Reconstitute the contour lines of the newly created DEM by using the *Raster to Polyline* function (*ArcToolbox* > *Conversion Tools* > *From Raster* > *Raster to Polyline*);
- Compare the reconstituted contour lines (blue) with the actual ones (yellow).



### Drainage system

- Visually compare the *FlowAcc* output with the shapefile of drains created from different sources of the literature.

### RMS error

- Use the *Extract Value to Point* function (*ArcToolbox* > *Spatial Analyst Tools* > *Extraction* > *Extract Values to Point*) to extract the value of quoted points from the new DEM;
- Clip them with the polygon representing the basin limits (*ArcToolbox* > *Analysis Tools* > *Extract* > *Clip*) ;

- Clip the known quoted point with the polygon representing the basin limits too;
- Report the *Attributes Tables* in Excel and determine the RMS error from the following expression:

$$RMS\ error = \sqrt{\frac{\sum_{i=1}^N (p_i^{interpolated} - p_i^{real})^2}{N}}$$

Where,  $p_i^{interpolated}$  refers to the  $i^{th}$  interpolated point value,  $p_i^{real}$  refers to the  $i^{th}$  known quoted point and N is the number of sample points.

## Comparison with ASTER GDEM

- Clip both DEMs with the basin limits (*ArcToolbox > Data Management Tools > Raster > Raster Processing > Clip*);
- Use the *Single Output Map Algebra* function to subtract the ASTER GDEM from the new DEM (*ArcToolbox > Spatial Analyst Tools > Map Algebra > Single Output Map Algebra*):

FINAL\_MNT\_Clip1.img - ASTGTM\_N01E103\_dem\_Clip.img

- The layer properties show the statistics data of the layer obtained.
- To calculate the RMS error of the ASTER GDEM in order to compare it with the previously calculated RMS error, repeat the steps described above.

## Section 3. Land use digitisation

### Shapefiles creation


- Create a new shapefile. Set the feature type as *Polygon* and define the spatial reference (UTM 48 N) for each land use classes:
  - Forests
  - General vegetation
  - Railroad
  - Car parks
  - Industrial
  - Commercial & educational
- Single-family dwellings
- Multiple-family dwellings, detached
- Multiple-family dwellings, attached
- Apartment buildings
- Construction sites

NB1: Lakes digitisation has already been done with the DEM creation ([Appendix II](#)).


NB2: For roads, see below.

- Add all shapefiles to ArcMap;
- Add the *Editor Toolbar* to ArcMap.

### Land use classes creation

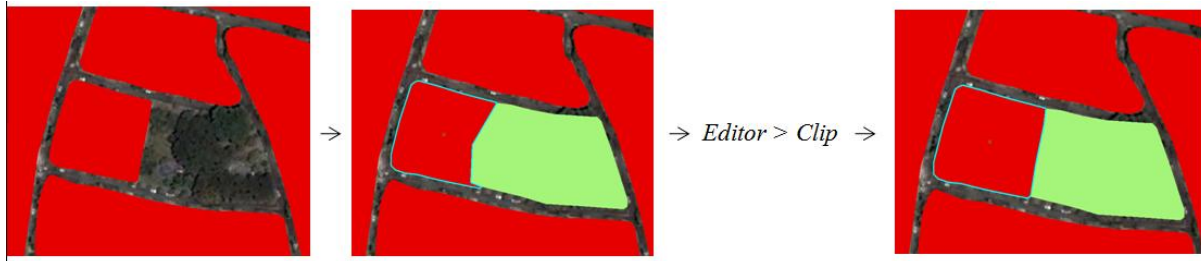
- Start an editing session (*Editor > Start Editing*), set the *Task* field to *Create New Feature*, choose the land use class you want to digitize (*Target*) and click on the pencil  to start the digitisation. Finish the sketch (*Right click > Finish sketch*) when the polygon is done.




### Useful tools

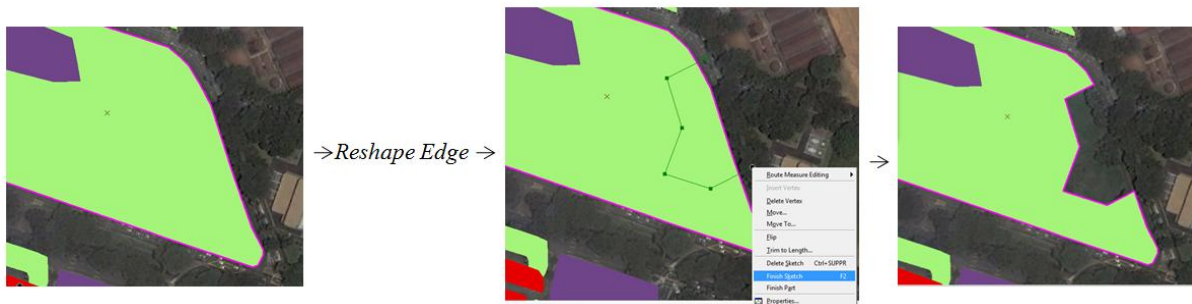
- Use the *Clip* tool (*Editor > Clip*) when two adjacent polygons should share a border in order to avoid digitising the border twice or having overlaps or spaces between polygons:
  - Digitise the first polygon;
  - Digitise the second one, insure it overlays the first one;
  - Select  the first one and clip it.


NB: You can also use the *Auto-CompletePolygon* task







- Use the *Merge* tool (*Editor > Merge*) when two polygons of the same class need to be merged:
  - Select  the two polygons and merge them.
- To reshape a polygon, follow these steps:
  - Build a *Map Topology* by clicking the topology icon  and select all the land use classes;
  - Use the *Topology Edit* tool  to select the polygon to be reshaped. It is selected in magenta;
  - Set the task to *Reshape Edge*;
  - Use the pencil to draw a sketch of the reshaped line, make sure that the sketch intersects the polygon at least two times;
  - Finish the sketch.



- To create a hole in a polygon (eg. forest surrounding a lake):
  - Digitise the outer boundary of the polygon, right-click and click *Finish Part*;
  - Sketch the inner boundary, right-click and click *Finish Sketch*.
- To split an existing polygon into two or more features:
  - Click the *Edit* tool ;
  - Set the *Cut Polygon Features* task;
  - Use the pencil to construct a line that cuts the original polygon as desired;
  - Finish the sketch.

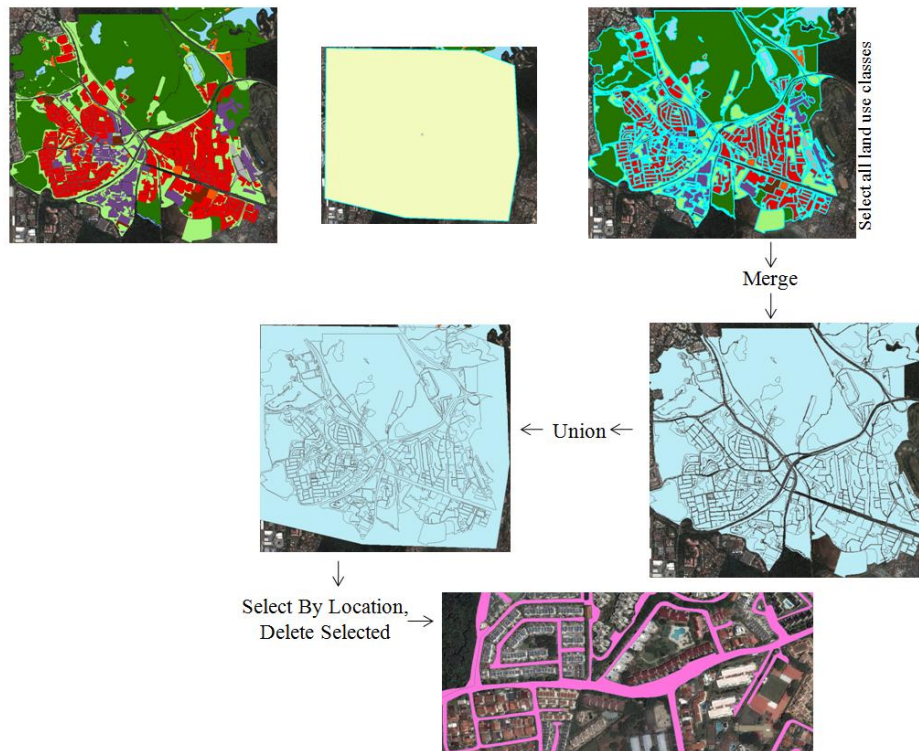


## Other tips

- To add or delete a vertex, click the *Edit* tool and double-click the polygon you want to modify, right click and click *Insert Vertex* or *Delete Vertex*.
- The *Trace* tool  helps you create segments that follow along existing segments.
- The *Intersect* command (*Editor > Intersect*) creates a new feature from the common areas or edges of any two selected features of the same geometry type.
- To separate a multipart feature, click the *Explode* tool .

## A special case of land use class: the roads

- Create a *New Polygon Shapefile* encompassing all the Upper Bukit Timah area;
- Use the *Merge* tool of the *ArcToolbox* (*ArcToolbox > Data Management Tools > General > Merge*) to merge all the land use classes previously created (all the classes except the roads). It creates a new shapefile which regroups all the classes except the roads;
- Use the *Union* tool (*ArcToolbox > Analysis Tools > Overlay > Union*) to join the big polygon with the 'Merge' shapefile. This function computes a geometric intersection of the input features. All features are assembled in a new shapefile with the attributes from the input features;
- Use the *Select By Location* tool (*Selection > Select By Location*) in order to select the features from the 'Union' shapefile that are equal to the features from the of 'Merge' shapefile;
- Delete the selected features (via the *Attributes Table*).



### Add details to the *Attributes Tables*

- For each land use class layer, set the *Properties* by adding two *Fields* named *Type* (*Data type: Text*) and *Surface* (*Data type: Double*).
- Edit each layer manually: add the type of land use and the surface of each polygon (in the *Attributes Table*, *Right Click* on the top of the column 'Surface', select *Calculate Geometry* and choose the *Area* property).

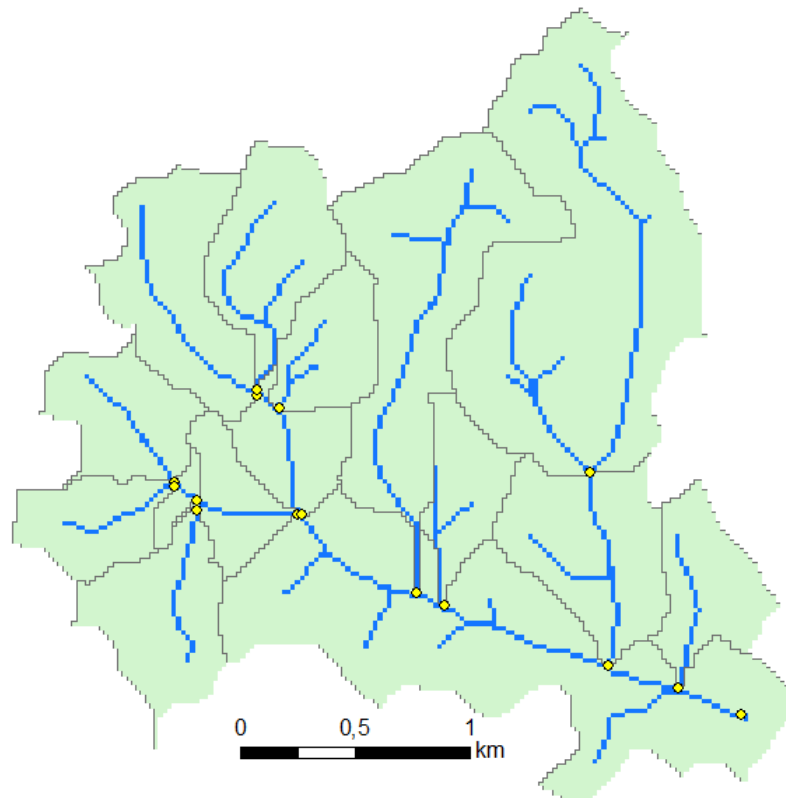
### Create one layer regrouping all land use classes

- The *Merge* function combines input features from multiple input sources into a single one. Use it to merge all land use classes and obtain a new shapefile. This procedure assumes that every empty spaces within the digitisation area are classified as road network. No distinction is made between the different types of highways, freeways and local roads.

## Section 4. SWMM subcatchments parameters determination

### Delimitation

- Using the *FlowAcc* raster, create a stream network by applying a threshold value (100 cells) to select cells with high accumulated flow. To do so, use the *Reclassify* function (*ArcToolbox* > *3D Analyst Tools* > *Raster Reclass* > *Reclassify*) to assign the value of one to all cells that have more than 100 cells flowing into them, and *NoData* to all other cells;
- From the created layer determine a pour point for each subcatchment (create a *Point New Shapefile*, and edit it). On the figure below, pour points are presented in yellow;
- Using this new shapefile, use the *Watershed* function;
- A raster layer representing the subcatchments is created.



- Use the *Reclassify* function to create a mask for each subcatchment: assign the value of one to all cells contained into a given subcatchment and the value of *NoData* to all other cells;
- 15 raster files are created;
- Use the *Raster To Polygon* function (*ArcToolbox* > *Conversion Tools* > *From Raster* > *Raster to Polygon*) to convert the raster features to polygon features (*simplify polygon* box not checked).

## Area

- To determine the area of each subcatchment, open the *Attributes Table*, and note the number of pixels contained in it. Since the resolution is 20 m, each pixel represents 400 m<sup>2</sup>,
- Multiply the number of pixels by that value and transform the result into hectares.



## Width

### Longest flow path method:

According to the SWMM user's manual (2010) and SWMM applications manual (2009), the width can be defined as the subcatchment's area divided by the length of the longest overland flow path that water can travel.

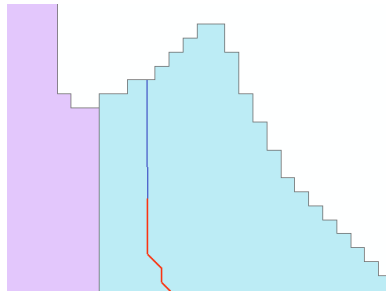
- Add the *HEC-GeoHMS Main View 9* and *HEC-GeoHMS Project View 9* toolbars to *ArcMap*;
- Use the *Merge* function to combine all the subcatchment polygons;
- Add a column in the *Attributes Table* of that new layer named 'HydroID' and assign the subcatchment number to each polygon (necessary step for the use of *HEC-GeoHMS*);
- Use the *Longest Flow Path* function (*Watershed Processing > Longest Flow Path*);
- In Excel, divide the value of the longest flow path by the subcatchment's area.

Several tests have been done in applying this approach by excluding the channelized flow as part of the flow path.

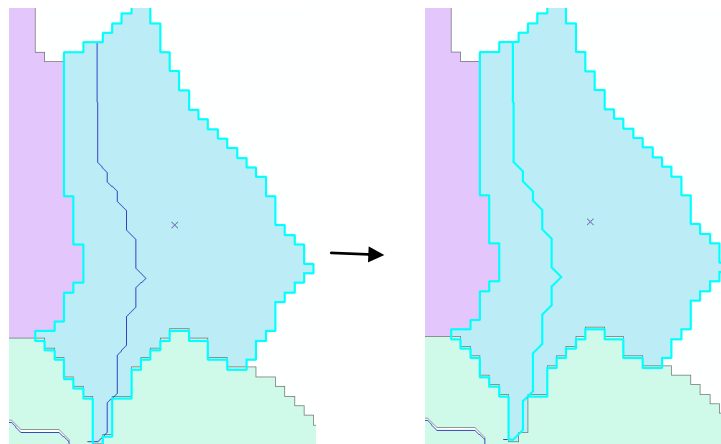
- Open the reclassified *FlowAcc* shapefile (considered as the 'channelized flow') and the *Longest Flow Path* shapefile;
- Start an editing session with the *Longest Flow Path* shapefile as a target;
- Use the *Split* tool  (click the *Edit* tool , set the *Cut Polygon Features* task) to cut the *Longest Flow Path* shapefile where it meets the channelized flow;
- Recalculate the length of each segment (via the *Attributes Table*);
- In Excel, divide that value by the subcatchment's area.

### Skew factor method:

- Transform the reclassified *FlowAcc* output into a polyline shapefile using the function *Raster to Polyline* (*ArcToolbox > Conversion Tools > From Raster > Raster to Polyline*);
- Created an edit session for this layer and lengthen the main channel in order to form two parts of the subcatchment (*Double Click* on the polyline feature which has to be lengthened and move the vertex across the limits of the subcatchment as showed below: in blue the modified polyline which will separate the subcatchment in two parts; in red the original polyline);



- Split the polygon by the overlapping line feature : select the polygon, set the *Task* to *Cut Polygon Features*, use the pencil tool to *Right Click* the line and select *Replace Sketch* and then *Finish the sketch* ;
- The subcatchment is split in two parts along the main channel.



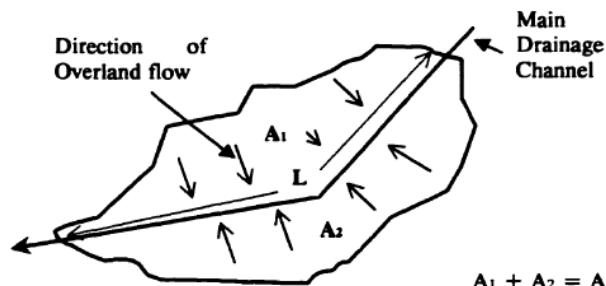
- Recalculate the surface of each part of each subcatchment;
- From the reclassified *FlowAcc* shapefile created above, calculate the length of each main channel within each subcatchment;
- The width can now be determined by:

$$W = (2 - \gamma) \times L$$

Where  $L$  is the length of the main drainage channel and  $\gamma$  is the skew factor (comprised between 0 and 1) calculated as:

$$\gamma = \frac{A_2 - A_1}{A}$$

Where,  $A_1$  is the area to one side of the main channel,  $A_2$  is the area to the other side of the main channel and  $A$  is the total area of the subcatchment ( $A = A_1 + A_2$ ).



Javaheri, 1999

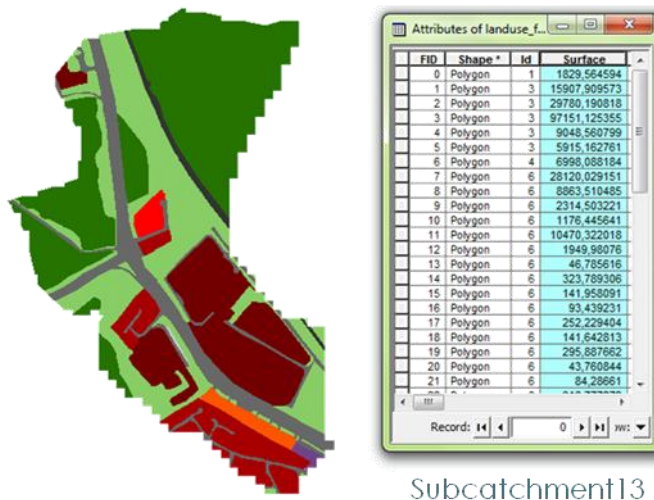


## Slope (%slope)

- Use the *Slope* function (*ArcToolbox* > *3D Analyst Tools* > *Raster Surface* > *Slope*) to determine the slope (in percents) of the DEM;
- Multiply each subcatchment mask by the *Slope* raster layer using the *Raster Calculator* (*Spatial Analyst* > *Raster Calculator*). This creates a raster layer for each subcatchment;
- Note the *Mean* value of the slope for each subcatchment (*Right click* on the layer > *Properties* > *Source* > *Mean*).

## Percent of impervious area (%Imperv)

- Use the *Clip* function (*ArcToolbox* > *Analysis Tools* > *Extract* > *Clip*) to extract the part of the land use layer that overlays the subcatchment features: *Input Features* = land use layer, *Clip features* = subcatchment polygons;
- 15 shapefiles are created;
- For each subcatchment, determine the surface occupied by each polygon of land use (via the *Attributes Table*, select the *Calculate Geometry* function);
- In Excel, copy and paste the *Attributes Table* of each subcatchment and calculate the proportion of each land use classes contained in it;
- From the imperviousness coefficients of each land use classes, determine the percent of imperviousness of each subcatchment.



## Infiltration model (Curve Number method)

Create a Curve Number (CN) Grid using *HEC-GeoHMS* (according to Merwade, 2010):

- Preparing land use data for CN Grid: use the *Reclassify* function on the land use raster dataset to create three classes of land use: water (1), medium residential (2) containing developed open space and developed land from low to high intensity, and forest (3);

- Convert the reclassified land use grid into a polygon feature class (*Raster To Polygon* function);
- Create an empty field named “LandUse” (*Data Type: Short Integer*) and equal it to the GRIDCODE column (representing the land use class) via the *Field Calculator*.
- Create a soil map from Chuah (1989): georeferencing, digitalisation of the soil classes (see sections 1 and 3);
- Create an empty field for storing soil group data named ‘SoilCode’ (*Data type: Text*). Edit the field by adding the SoilCode associated to each type of polygon (C for Rengam and red variant Rengam series, D for Tengah series).
- SCS classification of soils:
- 

Soil code	Characteristics	Examples
A	Soils having high infiltration rates (low runoff potential), well to excessively-drained sands or gravels	Sand, sandy loam, aggregated silts
B	Soils having moderate infiltration rates (moderately low runoff potential), moderately fine to moderately coarse textures	Silt loam, loam
C	Soils having slow infiltration rates (moderately high runoff potential), soils with a layer that impedes downward movement of water, or soils with moderately fine to fine texture	Soils high in clay, sandy clay loam
D	Soils having very slow infiltration rates (high runoff potential), soils with a clay layer at or near the surface, soils with permanently high water tables	Clay loam, silty clay loam, sandy clay, silt

Sources: Marek (2009), SWMM User’s manual (2010), NRCS (1986)

- Create four more fields named PctA, PctB, PctC, and PctD (*Data type: Short Integer*) for each feature (polygon). PctA will define what percentage of area within the polygon has soil group A (100 %), PctB will define what percentage of area within the polygon will have soil group B (100 %) and so on;
- Use the *Union* tool (*ArcToolbox > Analysis Tools > Overlay > Union*) to combine soil and land use data. The result of *Union* features inherits attributes from both feature classes;
- Delete the features that have attributes from only one feature class (*via the Attributes Table*).
- Create a table named ‘CNLookUp’ (*ArcCatalog > File > New > dBASE Table*),
- Create six fields in it (in *ArcCatalog*, *Right Click* on the table > *Properties*), representing the Curve Numbers associated to each land use class for each land use soil group:
  - LUValue (*Data Type: Short Integer*)
  - Description (*Data Type: Text*)
  - A (*Data Type: Short Integer*)
  - B (*Data Type: Short Integer*)



C (Data Type: Short Integer)

D (Data Type: Short Integer)

- Start the Editor to edit the table and fill it as shown below:

OBJECTID *	LUValue	Description	A	B	C	D
1	1	Water	100	100	100	100
2	2	Medium Residential	57	72	81	86
3	3	Forest	30	58	71	78
4	4	Agricultural	67	77	83	87

Record: 4 Show: All Selected Records (0 out of 4)

Merwade, 2010

- Use *HEC-GeoHMS* to create the curve number grid click on *Utility > Generate CN Grid*: use the DEM, the soil and land use layer and the CN Lookup table as inputs;
- Use the *Int* function (*ArcToolbox > 3D Analyst Tools > Raster Math > Int*) to convert it to integer;
- Apply the *Raster To Polygon* function;
- Use the *Clip* function to clip it with each subcatchment;
- Within each subcatchment, *Merge* the features of the same CN, add the field 'Surface' (Data Type: Double);
- From the surface and the CN associated to each subcatchment, calculate a weighted CN in Excel.
- To obtain a more precise CN Grid, repeat these steps using all the land use classes. The CN associated to them are described in the table below:
- Thus, the CN Lookup table is:

OID	LUValue	Descriptio	A	B	C	D
0	1	Commercial & Educational	89	92	94	95
1	2	Construction site	76	85	89	91
2	3	Woodland	30	55	70	77
3	4	Industrial	81	88	91	93
4	5	Water	100	100	100	100
5	6	General vegetation	39	61	74	80
6	7	Car Park	98	98	98	98
7	8	Apartment	85	85	90	92
8	9	Multiple-family, attached	77	85	90	92
9	10	Multiple-family, detached	77	85	90	92
10	11	Road	98	98	98	98
11	12	Single-family	57	72	81	86

## Manning's coefficient (*N-Imperv* & *N-perv*)

- From the Excel table containing the proportion of each land use class in each subcatchment, calculate a weighted Manning's coefficient for the impervious areas (industrial, car park and road) and the pervious areas (others). The Manning's coefficients are noted below:


	Manning's coefficient
Apartment	0,05
Multiple-family, attached	0,05
Multiple-family, detached	0,05
Single-family	0,05
Commercial & Educational	0,05
Industrial	0,011
General vegetation	0,24
Woodland	0,6
Car park	0,012
Road	0,011
Construction site	0,05

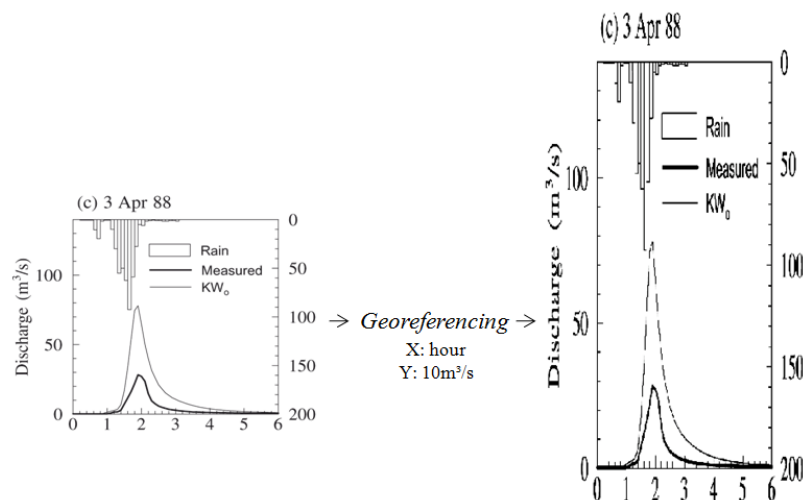
(Source: Rossman (2010), USDA (1986))

## Section 5. Old hyetograph and hydrograph: data extraction

### Georeferencing

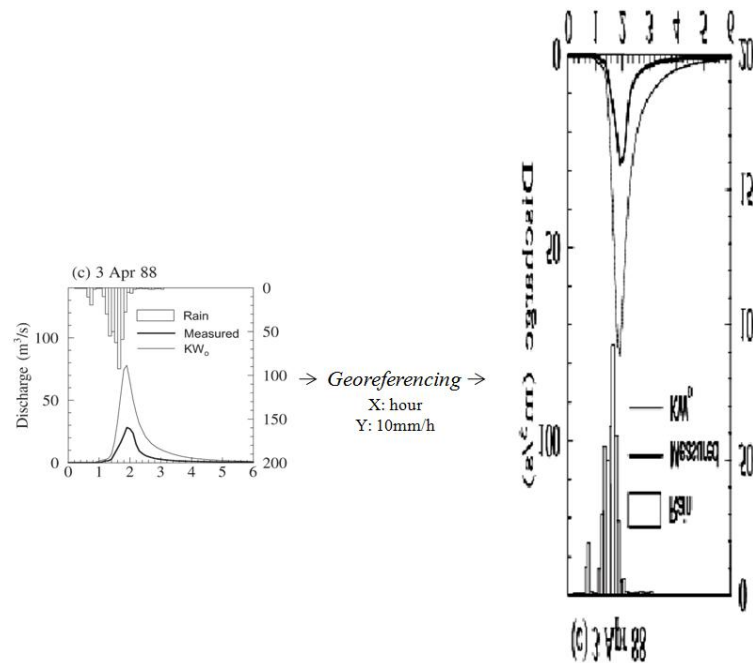
Discharge:

- Add the *Georeferencing* toolbar to the view;
  - Click the *Add Control Point* tool ;
  - Click the mouse pointer on a graduation on the X axis;
  - Right click *Input X and Y* and enter the coordinates of the considered point (values in hour, Y = 0);
  - Repeat the operation as many times as possible along the X axis.
  - Repeat these steps for the Y axis (values in  $\text{m}^3/\text{s}$  or  $10\text{m}^3/\text{s}$ , 0).
- NB: Multiply the graph unit per ten is useful to not overstretch it.
- Click *Georeferencing* > *Rectify* in order to permanently transform the image.



### Precipitation

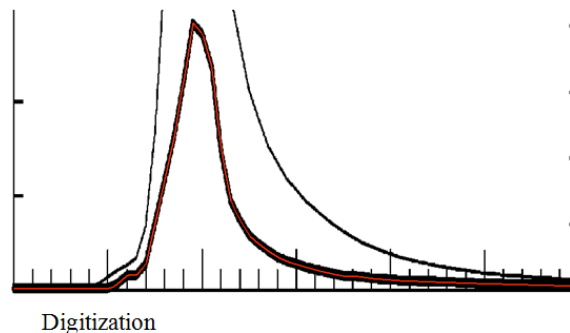
- Add the initial graph on the view;
- Repeat the previous steps (X values in hour, Y values in mm, 10mm, mm/h or 10mm/h).



## Data extraction

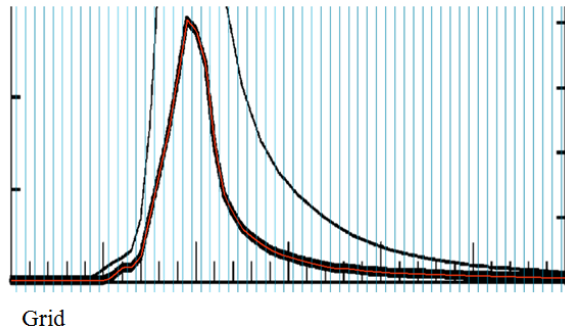
### Discharge

- Create a new shapefile. Set the feature type as *Polyline*;
- Add it to ArcMap;
- Start an editing session and digitize the discharge curve (*Task: Create New Feature*).

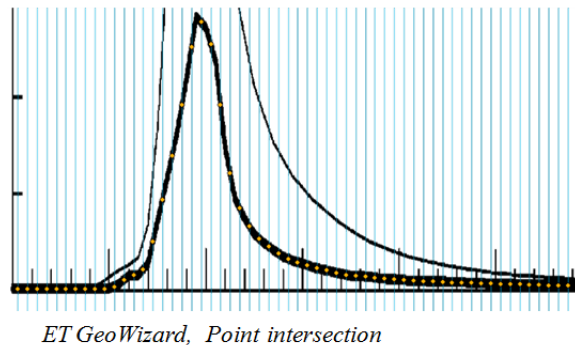


- Create a *New Shapefile (Polyline)* called 'grid';
- Draw manually several lines spaced by a width equal to the width between the center of two bars of precipitation (0,10 = 6 min between two records of precipitation, 0,4 = 15 min...).

To do so, *Right Click* on the polyline created > *Properties* and enter the coordinates of both ends. Then, copy and paste 1, 2, 4, 16... polylines and move them on the right place.



- In *ET GeoWizard*, use the *Point Intersection* function to create a point feature class with the intersection points of the grid and the digitized discharge curve.



- In the *Attributes Table* of the newly created shapefile, add two fields named X and Y and fill them with the X and Y coordinates (*Calculate Geometry*).
- In Excel, multiply the Y values per ten if necessary.

## Precipitation


- Use the *Create Station Point* function in *ET GeoWizard* to create a layer of points spaced by a width equal to the width between the center of two bars of precipitation;
- Start an editing session and modify that layer by deleting the useless points and by moving the remaining points on the top of the histogram bars;
- In the *Attributes Table*, add two fields named X and Y and calculate the X and Y coordinates (*Calculate Geometry*).
- In Excel, multiply the Y values per ten if necessary.

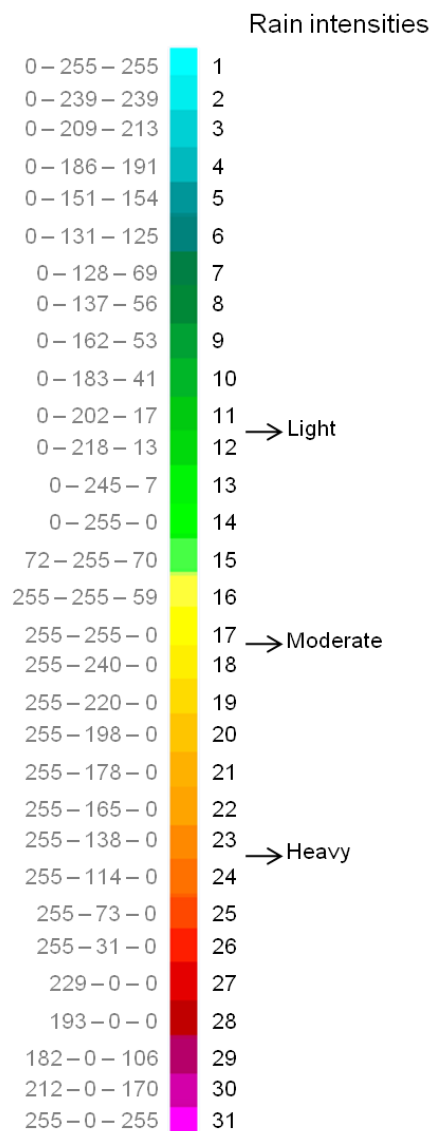
## Section 6. Data extraction from RADAR images

### NUS weather station

- Records from August, 2003 to present;
- Hourly data or 5-minute data;
- Coordinates: 103° 46' 41''E, 1° 17' 40'' N
- Distance between the centre of the Upper Bukit Timah and the NUS weather station: about 5.5 km.

### Pre-treatments in *Corel Photo Paint* software

- For each color figuring on the color palette and the image background, find the RGB code using *Corel Photo Paint* software (using the *Eyedropper* tool ) and associate it a class number;



- Choose the interesting RADAR images and convert them into tif (gif → tif) with *Corel Photo Paint* software (*File > Batch process*, load the files to convert, save as type tif). “8-Bit paletted” images are created.
- Convert the colors of every image with a *Corel Photo Paint* script in order to obtain the same value in the RVB code (eg. 151 – 151 – 151, 152 – 152 – 152...): *File > Batch process*, load the files and add the script previously created.  
The “8 Bit paletted” image has new colors (associated to a new RGB code), each of them being associated with a number of the palette, different for each image;
- In order to obtain a same value associated to a given colour for every image, create a script converting the “8 Bit paletted” image into a “24 Bit RGB” image.

## Georeferencing

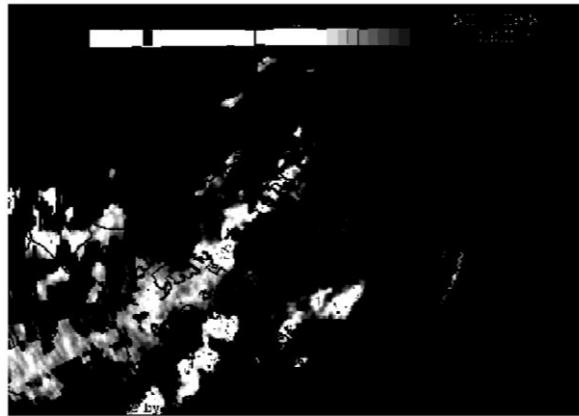
See section 1 for details

- Georeference a first image in *Arcmap*, and save the *Link Table* (figuring below). In our case, the RMS equalled 50, which is acceptable since the resolution of the RADAR images is around 220 m. Project it into UTM 48N;
- Open all the RADAR images of a given event and build a new macro using *Workspace Macro Pro*, in order to automatically georeference all the following images;
- Use the same macro for all events (an event contains between 6 and 43 images, taken every 10 min).

X Source	Y Source	X Map	Y Map
1.668511	2.107182	348231.000000	145247.000000
4.273237	2.497541	389463.000000	151507.000000
3.334294	1.864586	374680.000000	141482.000000
2.965693	3.200807	368845.000000	162372.000000

## Qualitative values extraction – weather station

- Create a new point shapefile representing the NUS weather station. Set its coordinates to 363748 m E, 143135 m N (Projection UTM 48N). Transform that shapefile into a raster layer using the *Point to Raster* function (*ArcToolbox > Conversion Tools > To Raster > Point To Raster*);
- Use the *Reclassify* function to create 31 classes representing each colour of the qualitative scale, the remaining (background, title...) being set at 0 (see an example of reclassified image below). Save the reclassification table (figuring below);



Old values	New values				
		161	11	173	23
0-130	0	162	12	174	24
151	1	163	13	175	25
152	2	164	14	176	26
153	3	165	15	177	27
154	4	166	16	178	28
155	5	167	17	179	29
156	6	168	18	180	30
157	7	169	19	181	31
158	8	170	20	182-255	0
159	9	171	21		
160	10	172	22		
		NoData	NoData		

- Use the *Zonal Statistics as Table* function (*ArcToolbox > Spatial Analyst Tools > Zonal > Zonal Statistics as Table*) in order to extract the qualitative value of the rainfall in the NUS weather station (mean). An example of table is showed below;

VALUE	COUNT	AREA	MIN	MAX	RANGE	MEAN	STD	SUM	VARIETY	MAJORITY	MINORITY	MEDIAN
1	1	48130,30000000000	22	22	0	22,00000000000	0,00000000000	22,00000000000	1	22	22	22

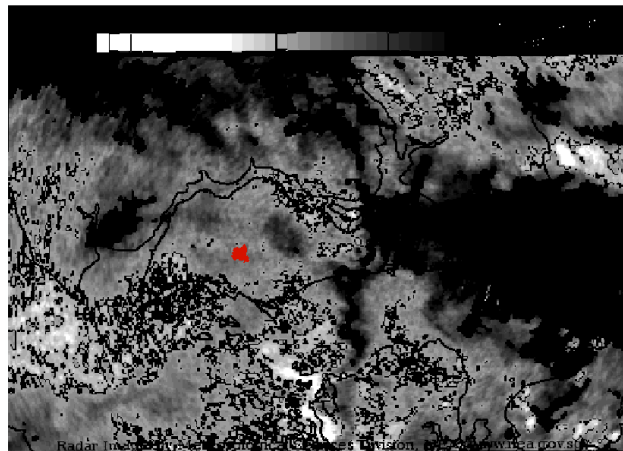
- For each image, repeat these last two steps (using *Workspace Macro Pro*);
- For each event, report the qualitative values of rainfall in an Excel file and associate them to the measured values of precipitation;
- Find the best polynomial relation ( $R^2 > 0.8$ ) between the qualitative and measured values (deleted aberrant points if necessary);
- From all polynomial equations, find the “mean” relationship between them and calculate the values of precipitation for the different classes of the qualitative scale.

## Qualitative values extraction – Upper Bukit Timah Basin

- A relation is now established between the qualitative scale and the quantity of rainfall. Use the *Zonal Statistics as Table* function in order to extract the mean qualitative value of rainfall falling on the Upper Bukit Timah Basin (in red on the image below);



- Repeat that step for each image of the event;
- From the relationship between qualitative and quantitative data, calculate the quantity of rainfall falling on the basin during the event, every 10 min. A linear interpolation is needed between the values of the scale.



## Section 7. Determination of HEC-HMS parameters

Almost all parameters were previously determined to be encoded in the SWMM model, with the exception of the conduits slope, time of concentration and storage coefficient.

### Conduits slope

The elevation of the outlet and inlet of each conduit as well as its length were determined for the SWMM application. The slope of each conduit was simply determined using these data, in order to be sure the two models are identical.

### Time of concentration

Several parameters were needed to determine the time of concentration using the six empirical methods presented before. Among them, the runoff coefficient and the channel slope were not determined for the SWMM model. They are thus determined here.

- $C$ , runoff coefficient:

A runoff coefficient was attributed to each land use class. Then, a weighted coefficient was calculated for each subcatchment, depending on the surface of each land use class within the subcatchment.

Runoff coefficients associated to each land use class:

Land use class	$C^*$
Apartment	0.60
Multiple-family, attached	0.67
Multiple-family, detached	0.50
Single-family	0.40
Commercial + Educational	0.73
Construction site	0.50
Industrial	0.65
Grass	0.25
Woodland	0.15
Parking	0.86
Road	0.83
Railroad	0.30

\*Mean value from: Guo (2003), Wisconsin Department of Transportation (2007), McCuen (2004), and Dunnes and Leopold (1978).

Weighted runoff coefficient calculated for each subcatchment:

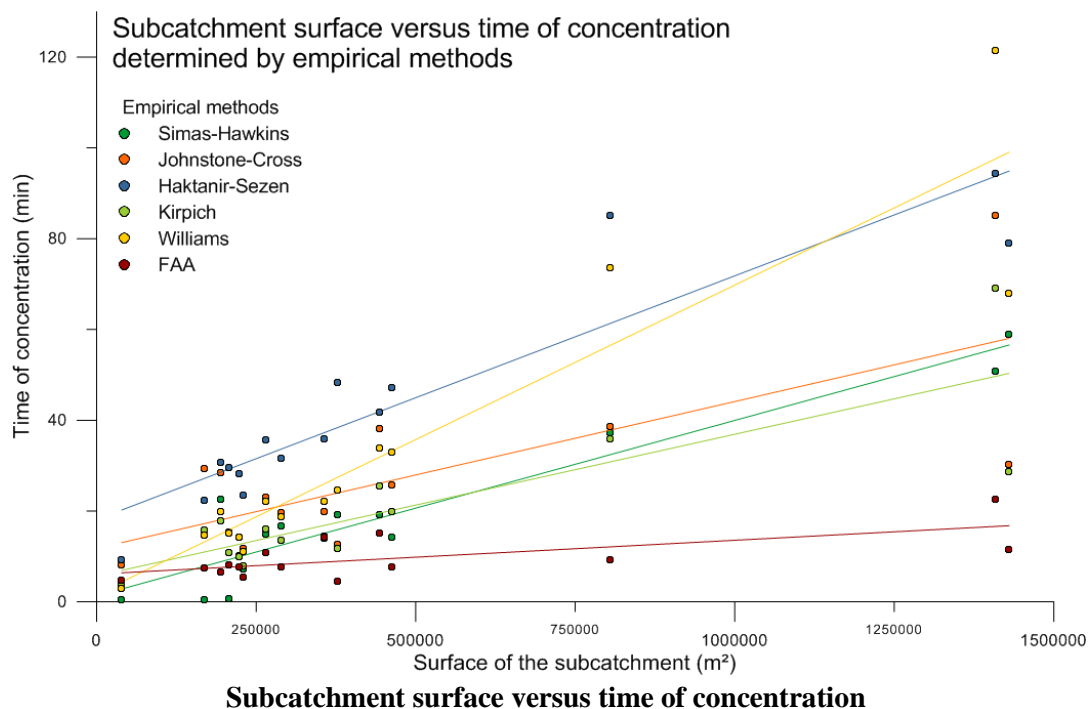
s1	s2	s3	s4	s5	s6	s7	s8	s9	s10	s11	s12	s13	s14	s15
0.53	0.58	0.50	0.46	0.23	0.68	0.57	0.62	0.59	0.53	0.57	0.23	0.39	0.17	0.30

- $S_c$ , channel slope (m/m):

All conduits situated in one specific subcatchment were regrouped. The channel slope was simply taken as the mean slope of these conduits.

Time of concentration (min) determined by four empirical methods

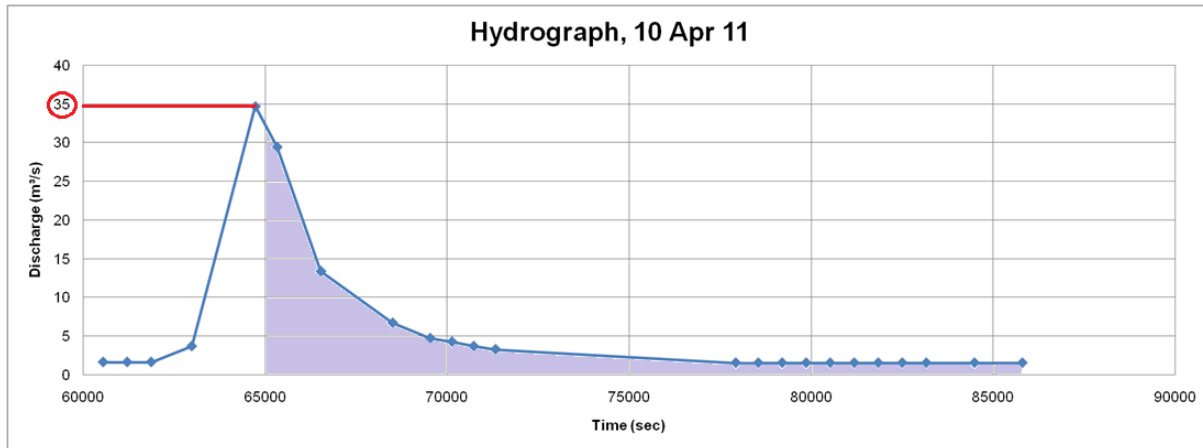
Sub id.	Surface (m <sup>2</sup> )	Methods of estimation					
		FAA	Williams	Kirpich	Haktanir-Sezen	Johnstone-Cross	Simas-Hawkins
s8	39200.000	4.756	3.027	3.881	9.235	8.063	0.426
s6	168007.866	7.552	14.610	15.742	22.288	29.427	0.435
s7	194400.000	6.559	19.942	17.724	30.665	28.397	22.492
s4	206799.957	8.182	15.182	10.883	29.460	15.435	0.605
s11	222785.150	7.677	14.271	10.001	28.279	14.172	10.247
s12	229199.833	5.412	11.068	7.883	23.411	11.640	7.183
s2	264708.486	10.793	22.126	16.109	35.639	22.938	14.888
s10	289200.000	7.650	18.771	13.506	31.586	19.603	16.646
s9	355978.811	14.170	22.037	14.492	35.964	19.887	13.947
s14	378131.725	4.473	24.494	11.655	48.261	12.582	19.216
s3	443200.713	15.050	33.944	25.548	41.643	38.061	19.258
s13	462798.873	7.753	32.858	19.948	47.209	25.617	14.235
s5	804693.938	9.229	73.604	35.827	84.976	38.640	37.133
s1	1408366.642	22.497	121.381	69.079	94.424	85.140	50.684
s15	1430033.518	11.401	67.963	28.721	79.098	30.259	58.999



## Storage coefficient

The storage coefficient is calculated by dividing the surface after inflection point (in purple on the example below) by the value of the flow at the point of inflection (in red).

The surface after inflection point was calculated by determining the surface formed by each trapezium under the curve and then summing all concerned surfaces.

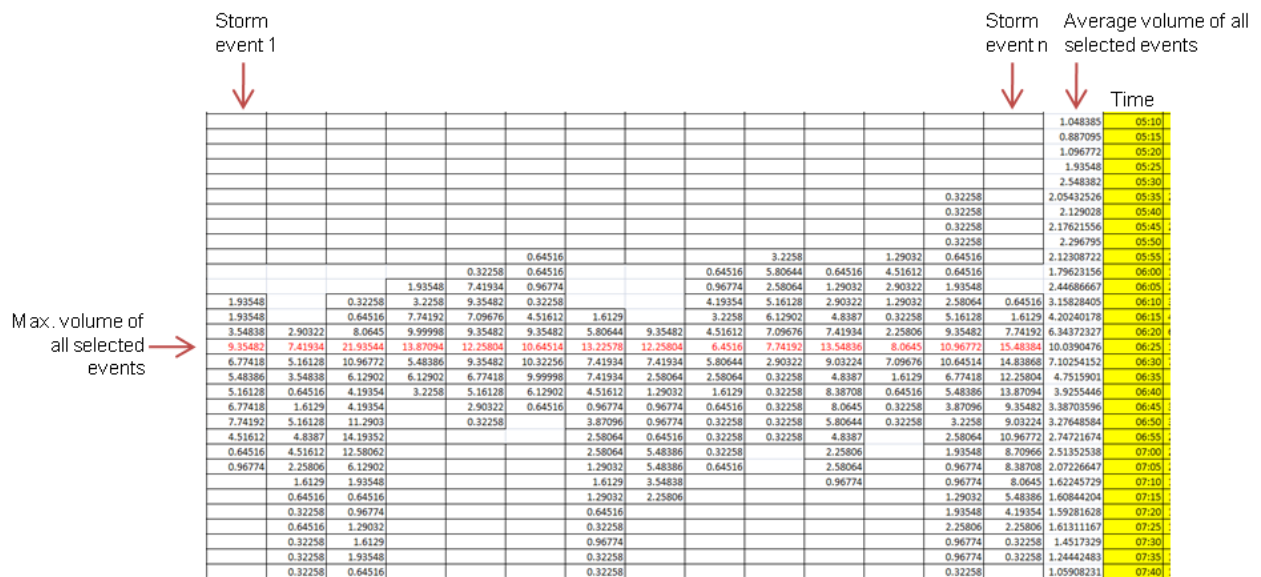


Two recent storm events (2<sup>nd</sup> of April, 2011, and 10<sup>th</sup> of April, 2011) for which the data provided from the PUB were used for the determination of the storage coefficient. Two old storm events (18<sup>th</sup> of April, 1989, 11<sup>th</sup> of July, 1988) were also used. The mean storage coefficient determined from these four events was encoded in the HEC-HMS model.

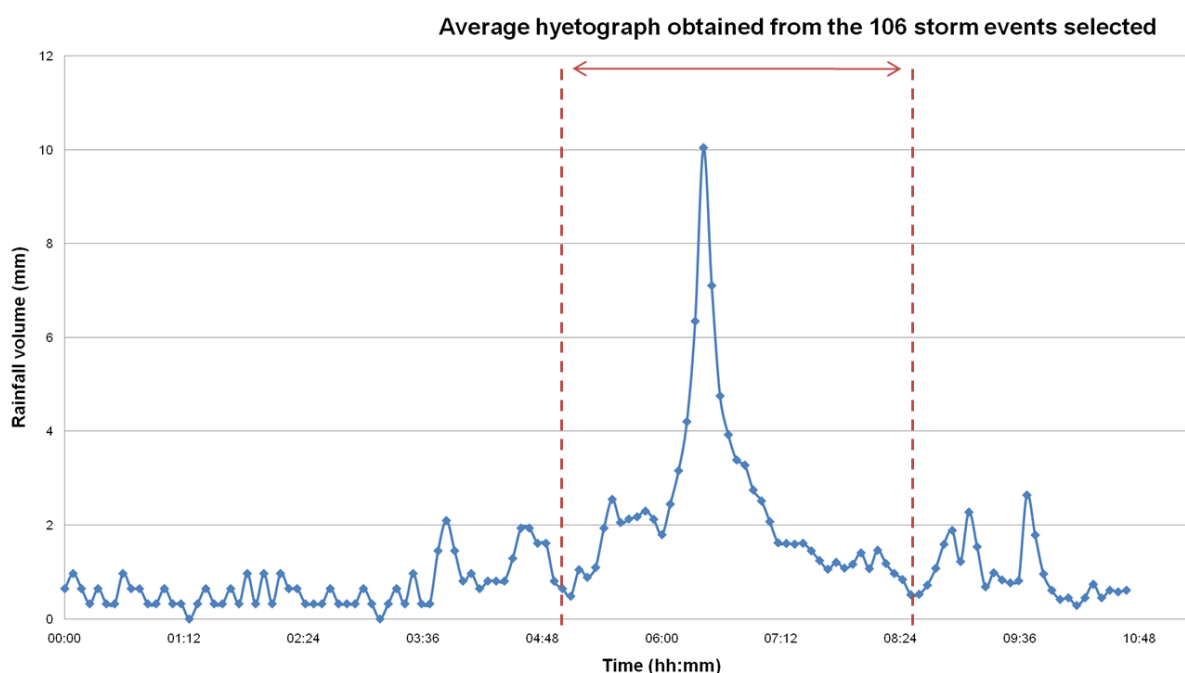
## Section 8. Synthetic design hyetographs determination

### Arithmetical mean derived from measured precipitation

- Select, from the NUS 5-minutes rainfall data, the storm events having a daily rainfall volume superior or equal to 50 mm;
- Translate the maximum intensity of each event in time in order to match all maximum intensities;
- Calculate the average volume of precipitation for all selected storm events.

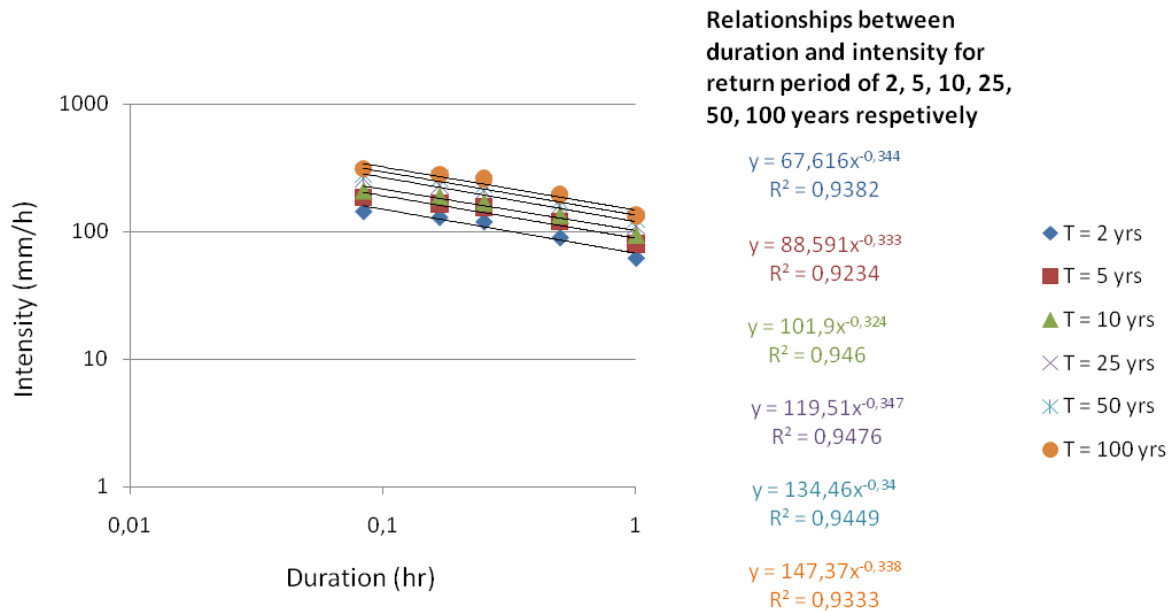


- The hyetograph obtained from the average volume of all selected events is presented below. The portion between 05:30 and 08:30 was selected to represent the design hyetograph shape.



- From the obtained mean hyetograph, express the volume as a percentage of the total depth;
- From the IDF curves, establish the relationships between intensity, duration and frequency of the storm. Several points of a given duration and return period were selected to determine the associated rainfall intensity (mm/h, in blue in the table below). Then the relationships were established, using these points.

Return period (yr)	Duration (hr)				
	0.083	0.166	0.25	0.5	1
2	145	130	120	90	62
5	185	165	155	120	80
10	210	190	170	135	94
25	260	230	210	160	110
50	285	260	235	175	125
100	310	280	260	195	135



- The duration of the hyetograph is 03:30. From the IDF curves, the total volume of precipitation can be determined, given the duration and return period of the storm (the intensity needs to be multiplied by the duration to be transformed into volume of precipitation). For a storm event having a duration of 03:30, the total volume of precipitation is:

Return period (years)	Volume (mm)
2	153.8
5	204.3
10	237.7
25	270.8
30	307.4

- In order to obtain design hyetographs of different duration the procedure is repeated by selecting the storm events of specific duration:
  - Between 20 and 40 minutes: 30-minutes design rainfall;
  - Between 50 and 70 minutes: 60-minutes design rainfall;
  - Between 80 and 100 minutes: 90-minutes design rainfall;
  - Between 110 and 130 minutes: 120-minutes design rainfall and;
  - Between 160 and 200 minutes: 180-minutes design rainfall.
- Thirty synthetic hyetographs are therefore created (see appendix 12).



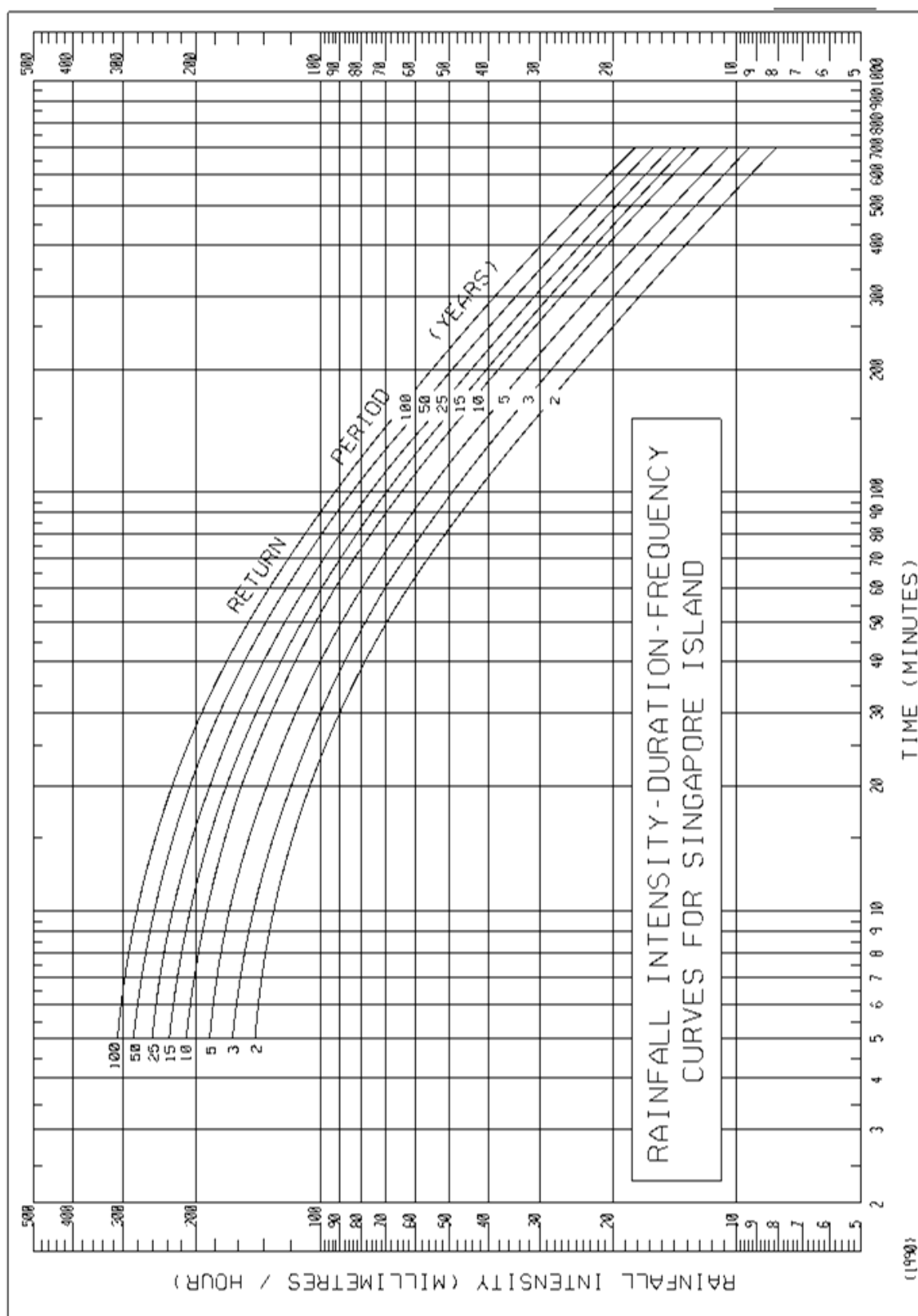


# APPENDICES LIST

Appendix 1. Intensity-duration-frequency curves for Singapore.....	157
Appendix 2. Major features of the Upper Bukit Timah basin.....	158
Appendix 3. Land use criteria .....	159
Appendix 4. SWMM pre-parameterisation hydrographs .....	167
Appendix 5. SWMM final adjustment hydrographs .....	191
Appendix 6. Correspondences between old maps legends and current map classification .....	211
Appendix 7. Influence SWMM parameters on the modelled discharge for recent events.....	212
Appendix 8. 3D iso-responses curves, 5 <sup>th</sup> of June, 2011. ....	224
Appendix 8. HEC-HMS: simulated versus modelled hydrographs .....	225
Appendix 9. Runoff coefficients .....	231
Appendix 10. Percentages of imperviousness (%) by subcatchment, from 1950 to 2020 .....	232
Appendix 11. Design synthetic hyetographs.....	233
Appendix 12. Design hydrograms for the return periods of 2, 10, 25, 50 and 100 years. ....	241
Appendix 13. Modelled peak discharge for each design rainfall event .....	246
Appendix 14. Graphs of imperviousness versus return period and peak discharge.....	247

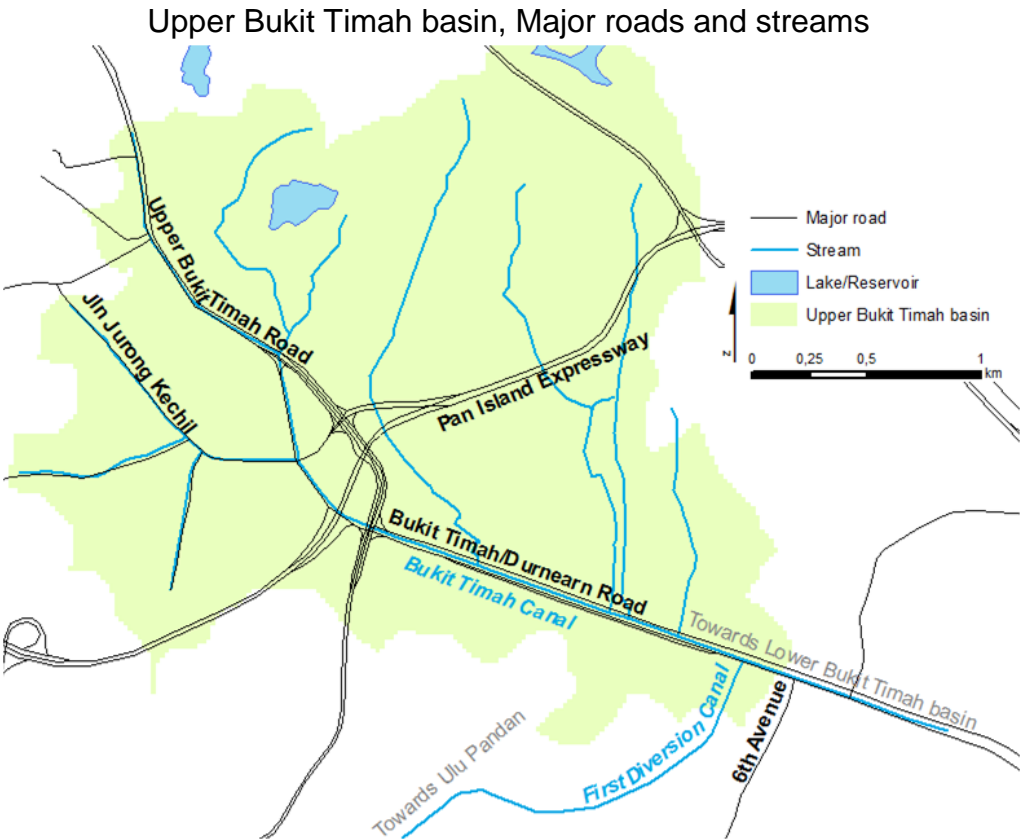


## Appendix 1. Intensity-duration-frequency curves for Singapore





Source: PUB, 2010



Appendix 2. Major features of the Upper Bukit Timah basin

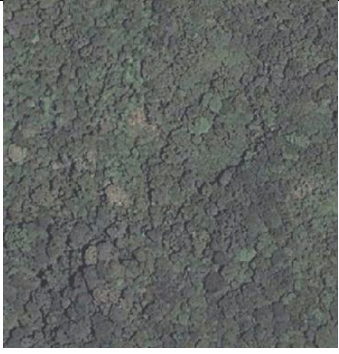

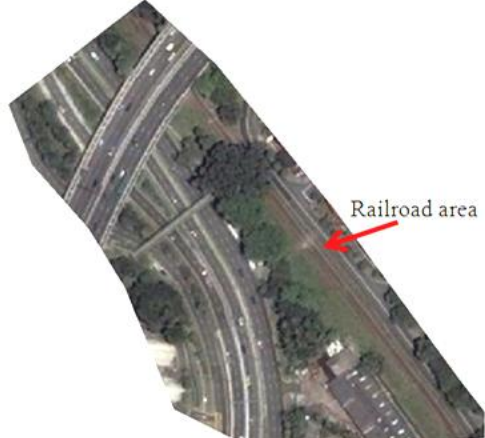


## Appendix 3. Land use criteria




Several criteria have been defined before the digitisation, in order to avoid or reduce any subjective selection in the land use classes. They are presented in the table below.

Land use Class	Definition	Example
<b>Residential</b>		
<b>Single-family dwellings</b>	<p>The term ‘single-family’ means that the building is usually occupied by just one household and consists of just one dwelling unit.</p> <p>This type of dwelling does not share any wall with any other house and has only outside walls. It does not touch any other dwelling.</p> <p>Commonly, there is a garden surrounding the house. In most of the cases, there is a swimming pool near the dwelling.</p>	
<b>Multiple-family dwellings, detached (= duplexes)</b>	<p>The term ‘multiple-family’ means that the building is occupied by two (or more) families. The term ‘detached’ means that the building consists of just one dwelling unit for two (or more) families.</p> <p>Duplexes commonly refer to two separate residences, attached side-by-side. The detached multiple family dwellings often looks like either two houses put together, or as a large single home with two different entrances.</p> <p>The difference between</p>	




	apartment building (see below) and duplexes is sometimes vague but generally, apartment buildings tend to be bigger whereas duplexes are usually the size of a normal house.	
<b>Multiple-family dwellings, attached (= row houses)</b>	<p>Row houses refer a style where a row of identical or mirror-image houses share side walls.</p> <p>Attached multiple family dwellings are inspired by the well-known British house design: they are multistory housing units that are at least consistent, if not identical, to all adjoining homes.</p>	
<b>Apartment buildings</b>	<p>Apartment buildings consist in a block of flats, multi-unit dwelling made up of several flats.</p> <p>In Singapore, apartment buildings are often Condominium, which are a form of ownership with individual apartment for everyone with common areas, such as lobbies, recreation rooms, swimming-pool, tennis courts... They are easily recognizable.</p>	
<b>Vegetation</b>		
<b>Forests</b>	Forested areas consist in a zone containing dense trees only (zone consisting in grass and sparse trees are	

	<p>regrouped in the 'general vegetation' class).</p> <p>They figure on the topographic map and the Street Directory book.</p>	
<p><b>General vegetation (parks, grass, green spaces, open spaces)</b></p>	<p>This class contains parks, grass, green spaces, open spaces... These features can be found around condominiums, on the sides of the road. They sometimes contain sparse trees.</p> <p>Parks generally figure on the Street Directory book.</p>	
<p style="text-align: center;"><b>Communication</b></p>		
<p><b>Roads</b></p>		
<p><b>Railroad</b></p>	<p>Railroad area has been identified on the topographic map and the Street Directory book.</p>	



<b>Car parks</b>	To avoid any subjectivity, only the car parks figuring in the Street Directory book have been classified.	
<b>Industrial, commercial &amp; educational</b>		
<b>Industrial</b>	<p>Few industrial areas are present in the Upper Bukit Timah Catchment.</p> <p>They consist in gasoil stations, car dealers and industries companies figuring on the Street Directory and on Google Earth information.</p> <p>Generally, they can be spotted by their concrete pavement and flat roofs.</p>	 <p>Nissan Motor Centre, Bukit Timah Road</p>
<b>Commercial &amp; educational</b>	<p>School and universities are easily identifiable thanks to their playgrounds, tennis courts and racetracks.</p> <p>Commercial areas are generally situated near an important road and consist in big infrastructure with surrounding car parks.</p> <p>All schools, shopping malls and shops have been listed in the class after confirmation with Google Earth and/or the Street Directory book.</p> <p>Chuah (1989) regrouped schools and commercial</p>	 <p>Bukit Timah Primary school (left) and Bukit Batok Secondary school (right)</p>



	<p>features in a same class, as schools zone tend to have little or no open space. This reinforced our choice to regroup them into a same class.</p> <p>NB: religious features such as churches and temples have been regrouped in this class.</p>	 <p>Bukit Timah Shopping Center</p>
<b>Others</b>		
<b>Lakes</b>	<p>These features can be easily identified on the topographic map as well as on Google Earth.</p>	
<b>Construction sites</b>	<p>Generally, construction sites are disturbed sites light coloured, depending on their current construction phase. They are identified easily.</p>	

Some photos taken on the field can illustrate the different land use classes used in this work. They are presented below.



**Forest:** Bukit Timah Nature Reserve (15/08/2010)



**General vegetation:** Open space near Bukit Timah Nature Reserve (15/08/2010)



**Industrial:** BMW at Dunearn Road (17/09/2010)





**Commercial:** Bukit Timah Shopping Center, Upper Bukit Timah road (18/09/2010)



**Apartments:** Upper Bukit Timah road (18/09/2010)



**Multiple-family dwellings, attached:** Kismis Green (13/08/2010)





**Multiple-family dwellings, detached:** Bukit Timah road (23/08/2010)



**Single-family dwelling:** Binjai Park (17/09/2010)



**Construction:** near Bukit Timah Nature Reserve (08/09/2010)

## Appendix 4. SWMM pre-parameterisation hydrographs

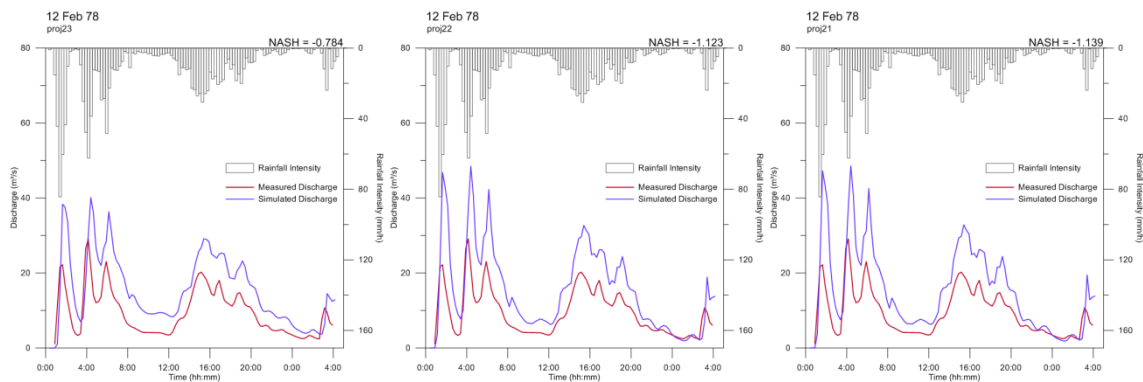
The graphs presented here are:

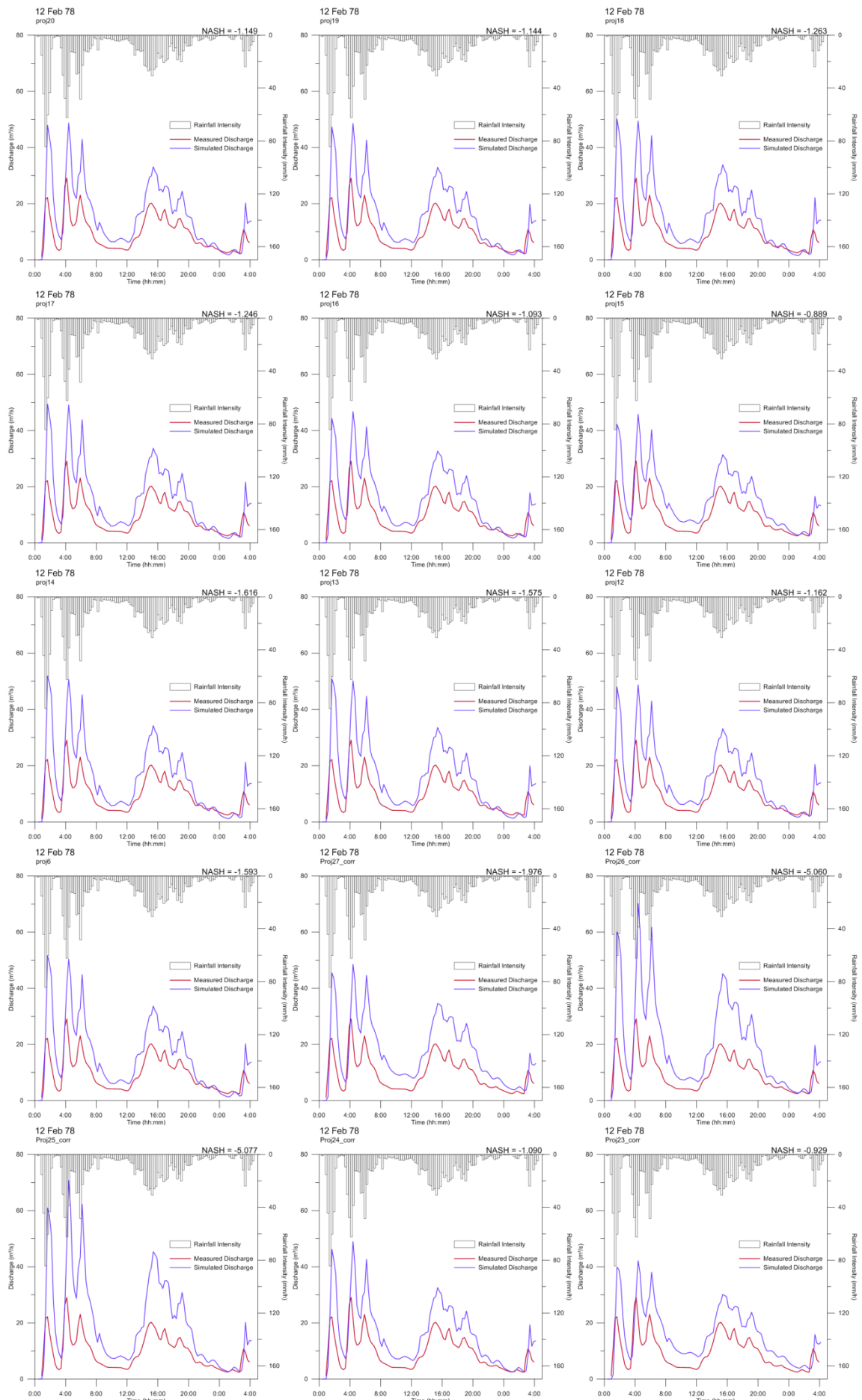
- 12 Feb 78;
- 01 Jun 79;
- 02 Mar 84;
- 02 Jul 84;
- 03 Jan 85;
- 18 Jun 86;
- 01 Aug 86;
- 07 Oct 86;
- 27 Nov 87;
- 15 Feb 88;
- 03 Apr 88;
- 03 Feb 84;
- 17 Apr 88;
- 11 Jul 88;
- 18 Apr 89
- 02 Dec 78.

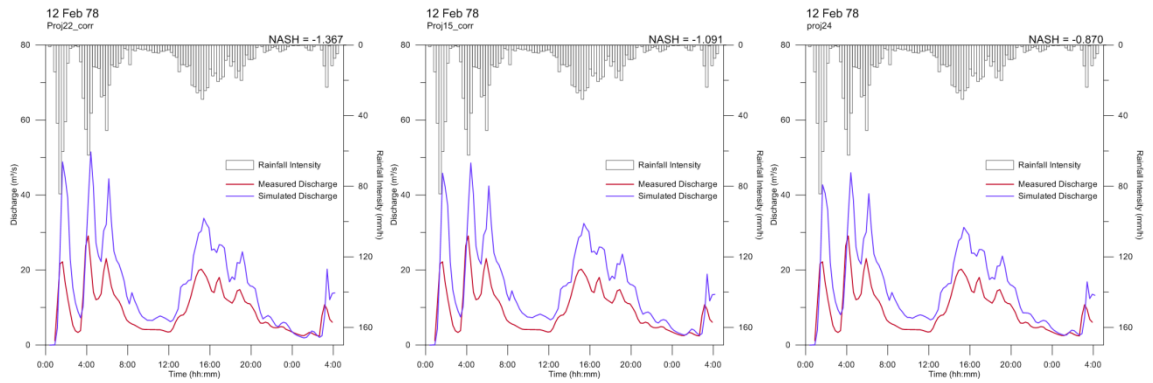
Time (hh:mm) figures on X axis, discharge ( $\text{m}^3/\text{s}$ ) figures on Y left axis and rainfall intensity (mm/h) figures on Y right axis. Measured discharge is in red, simulated discharge in blue. The Nash-Sutcliffe coefficient is noted on the right hand side of each graph.

In order to allow a global view of the curves and to save space, graphs presented here are reduced.

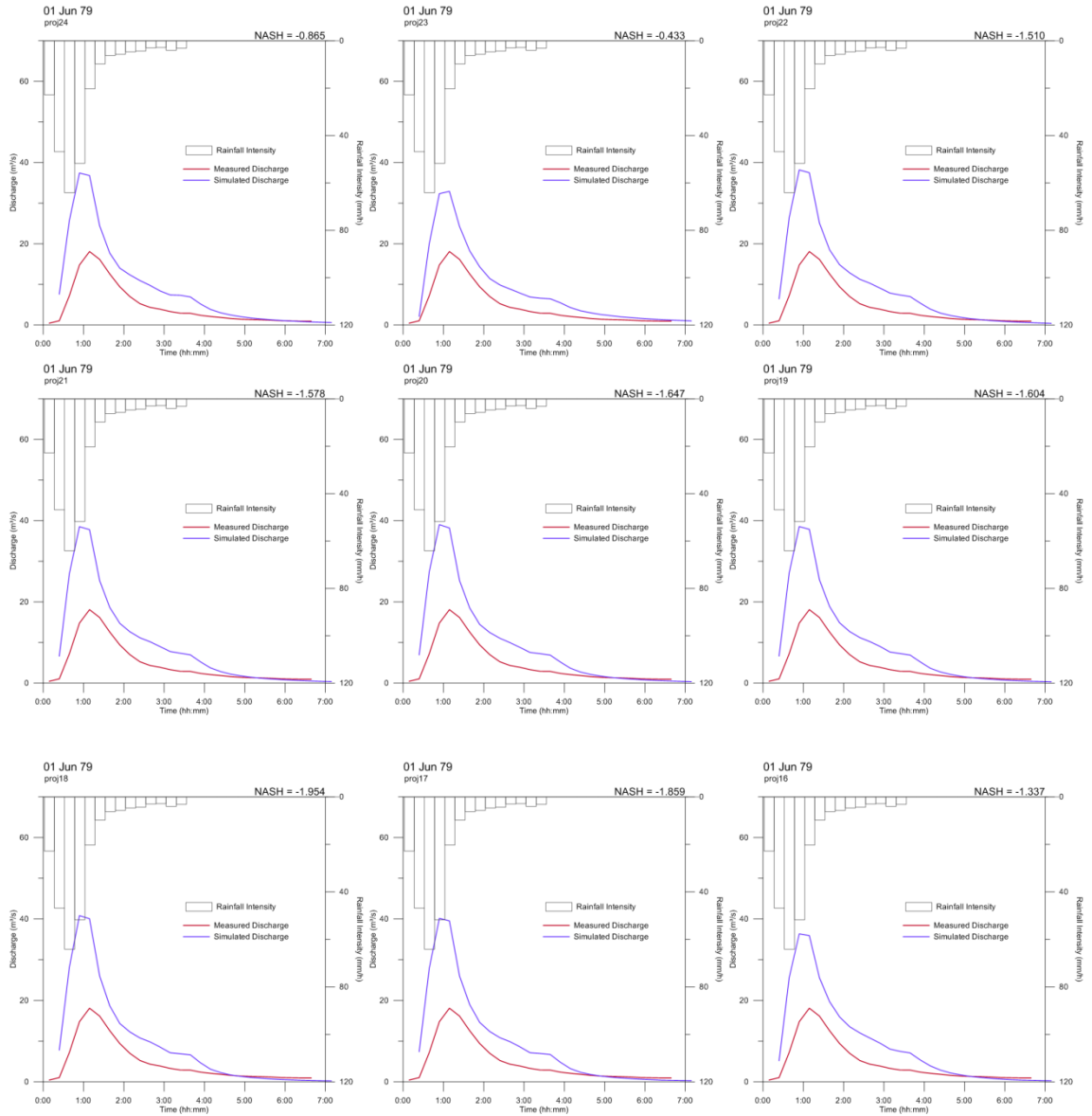
### 12 Feb 78

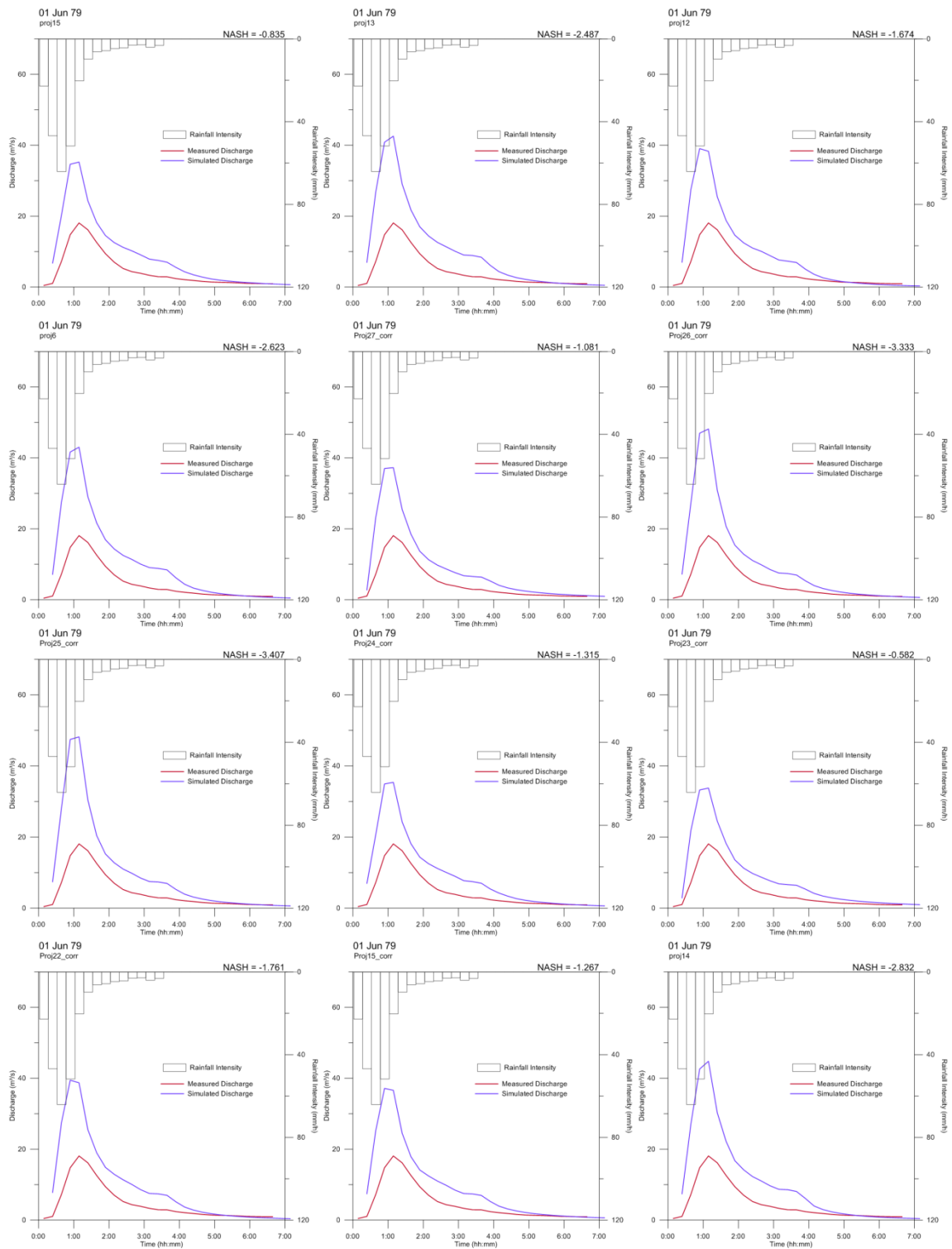




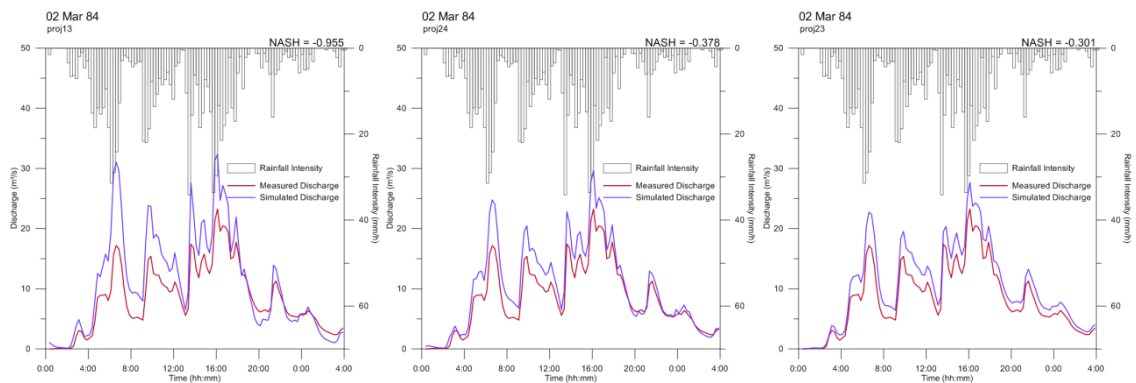


## 01 Jun 79

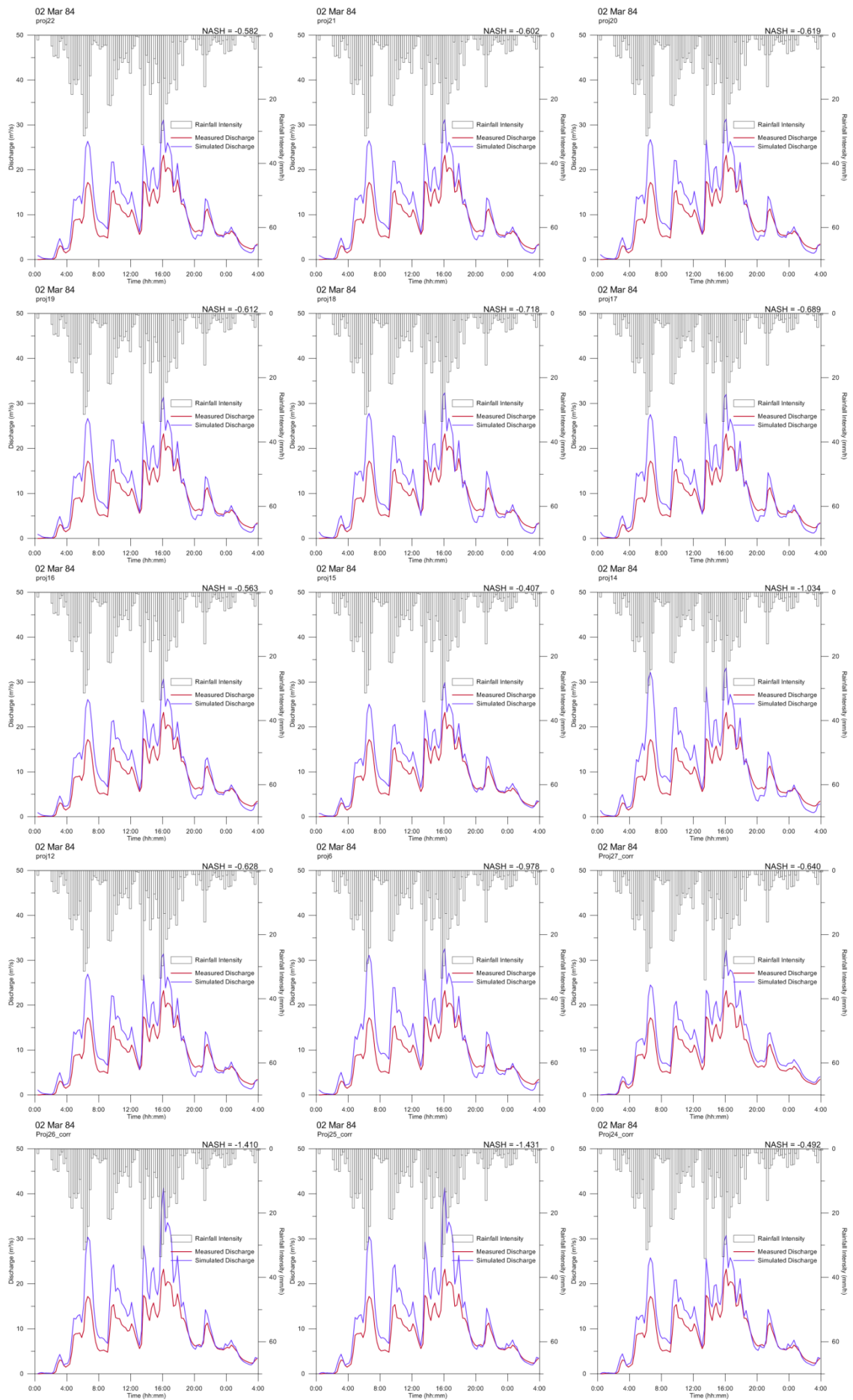


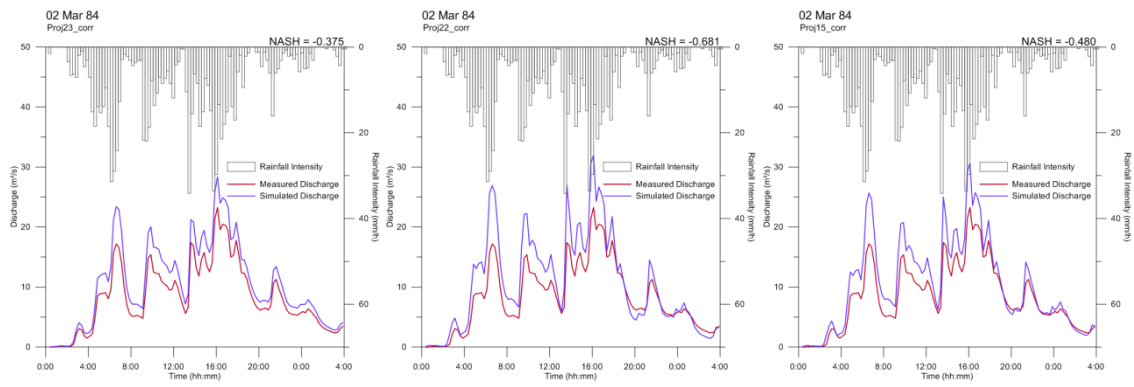


## 02 Mar 84

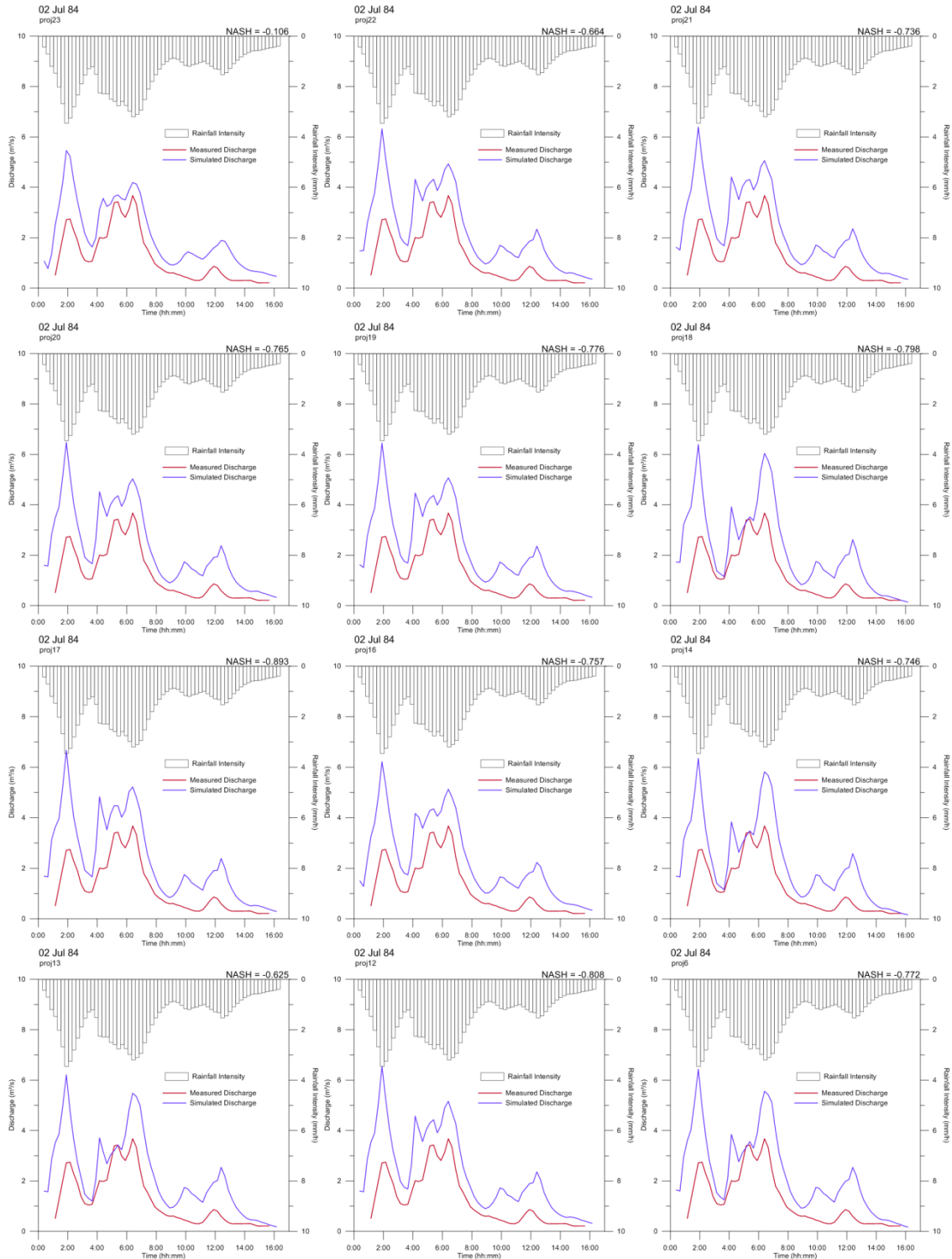


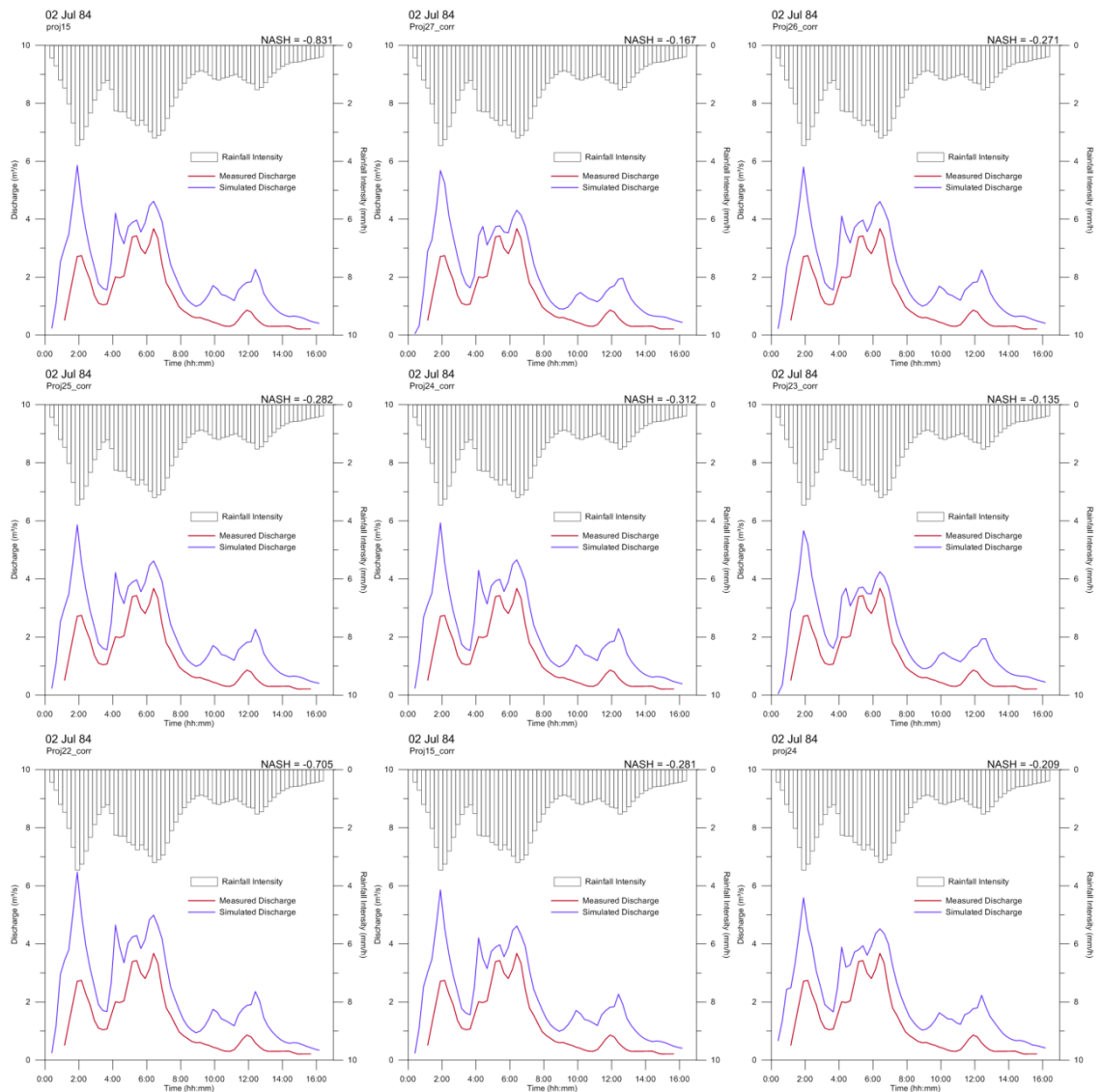




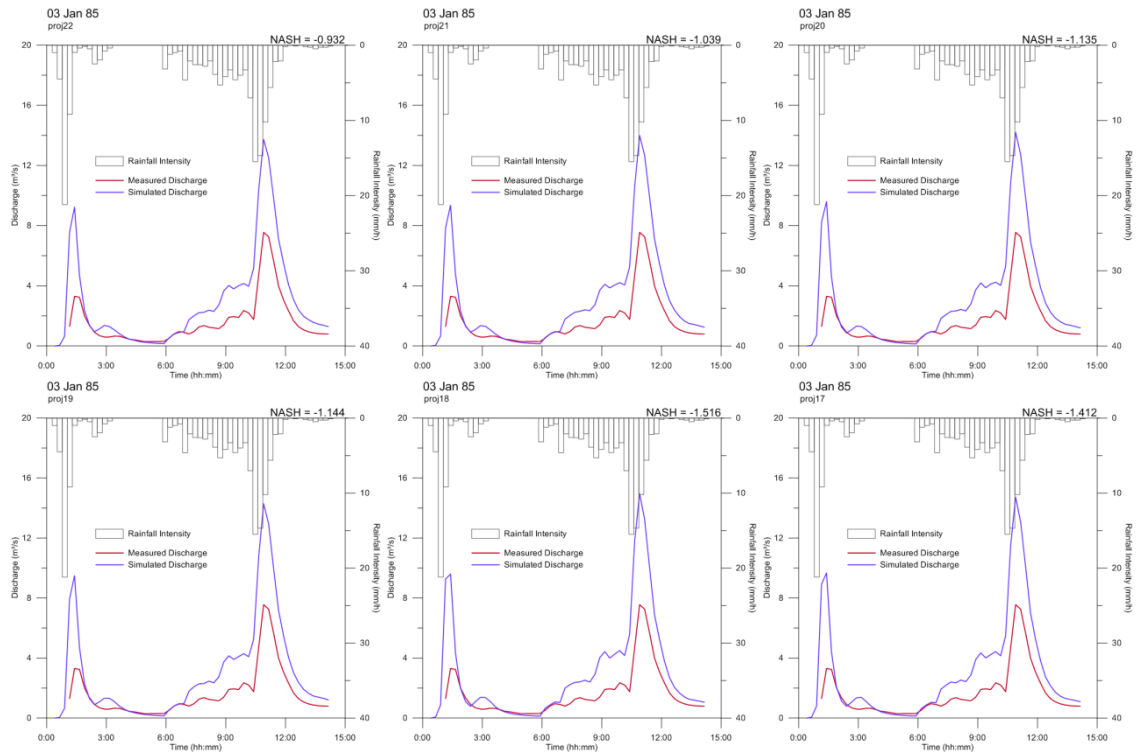


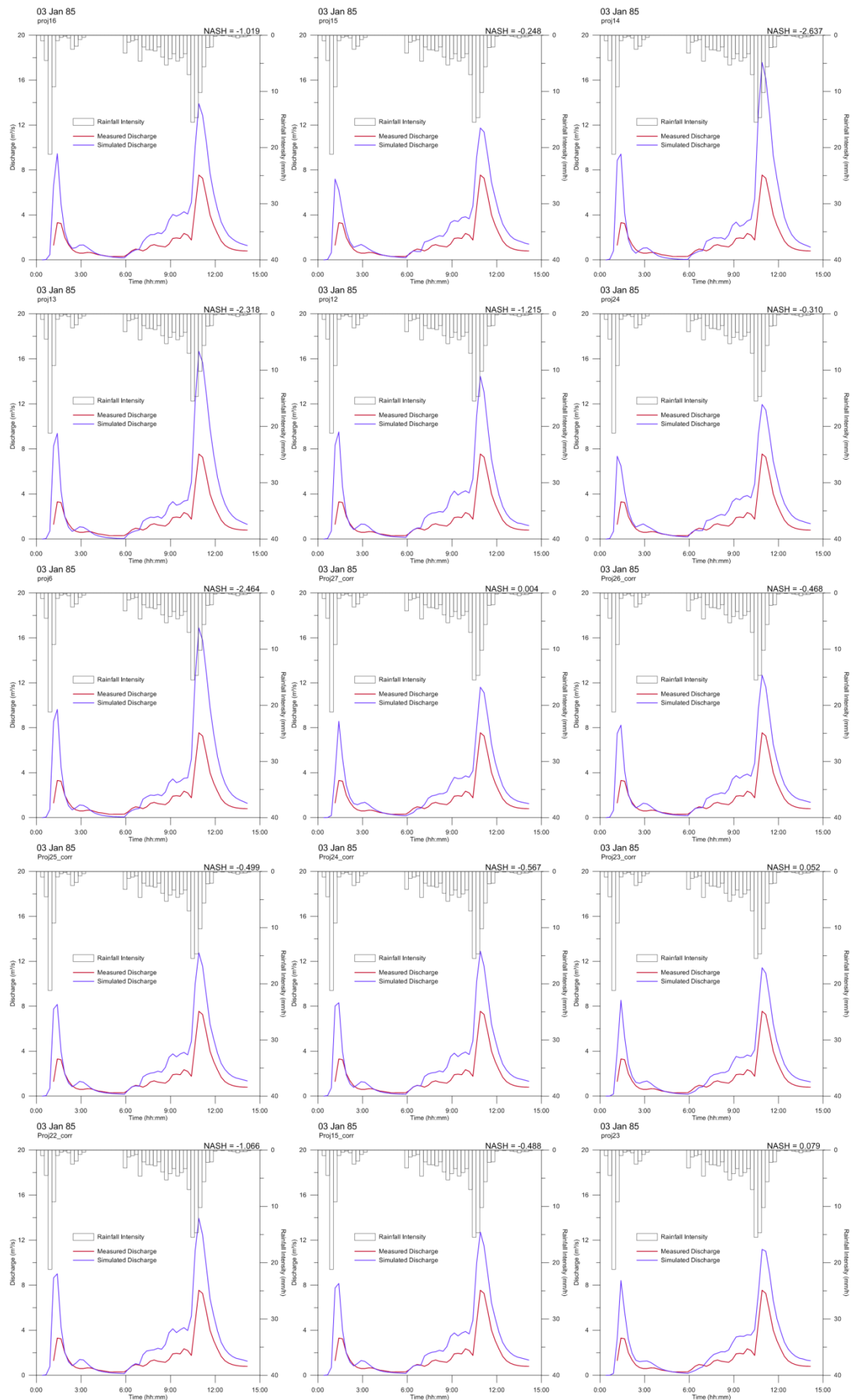
**02 Jul 84**



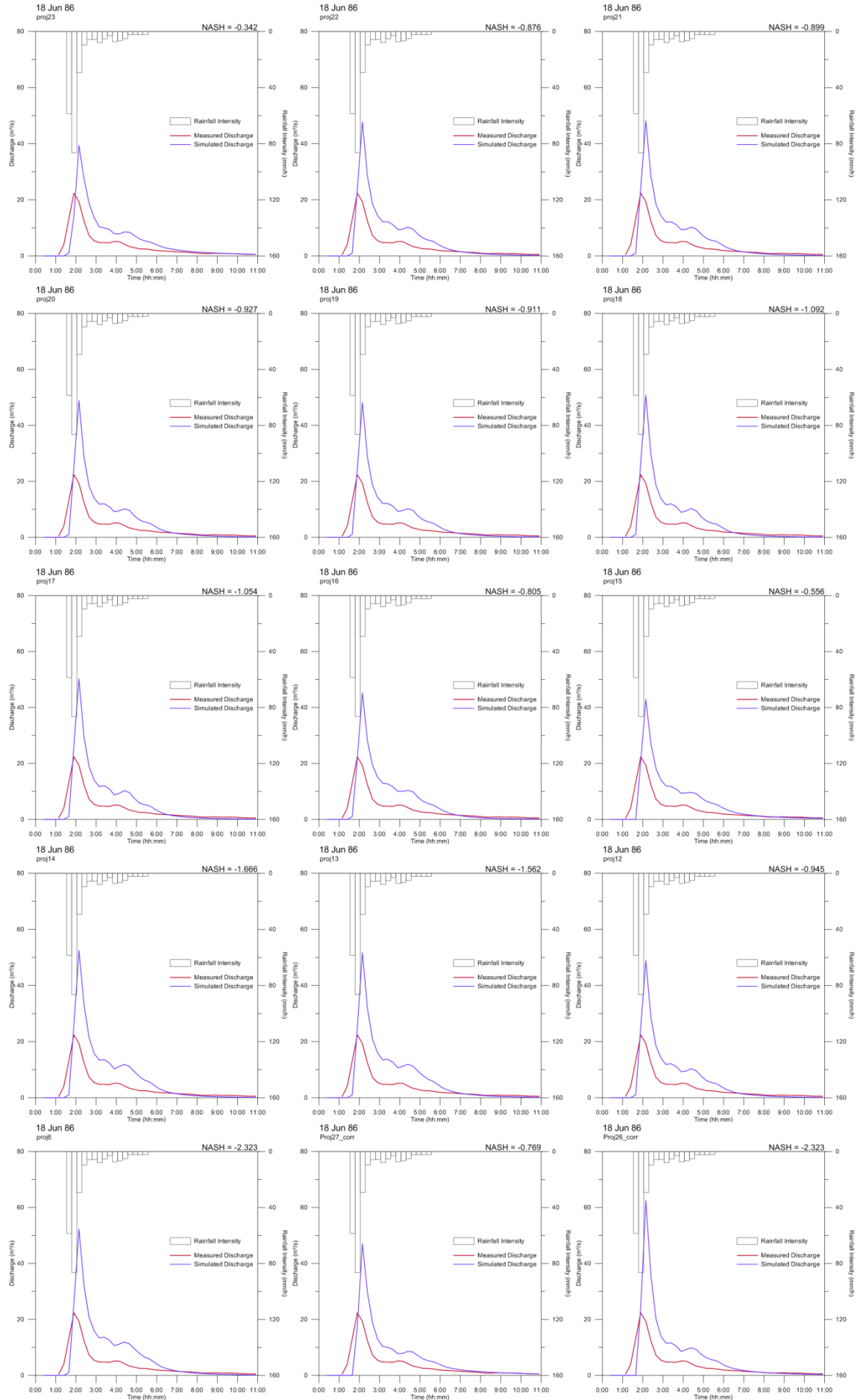


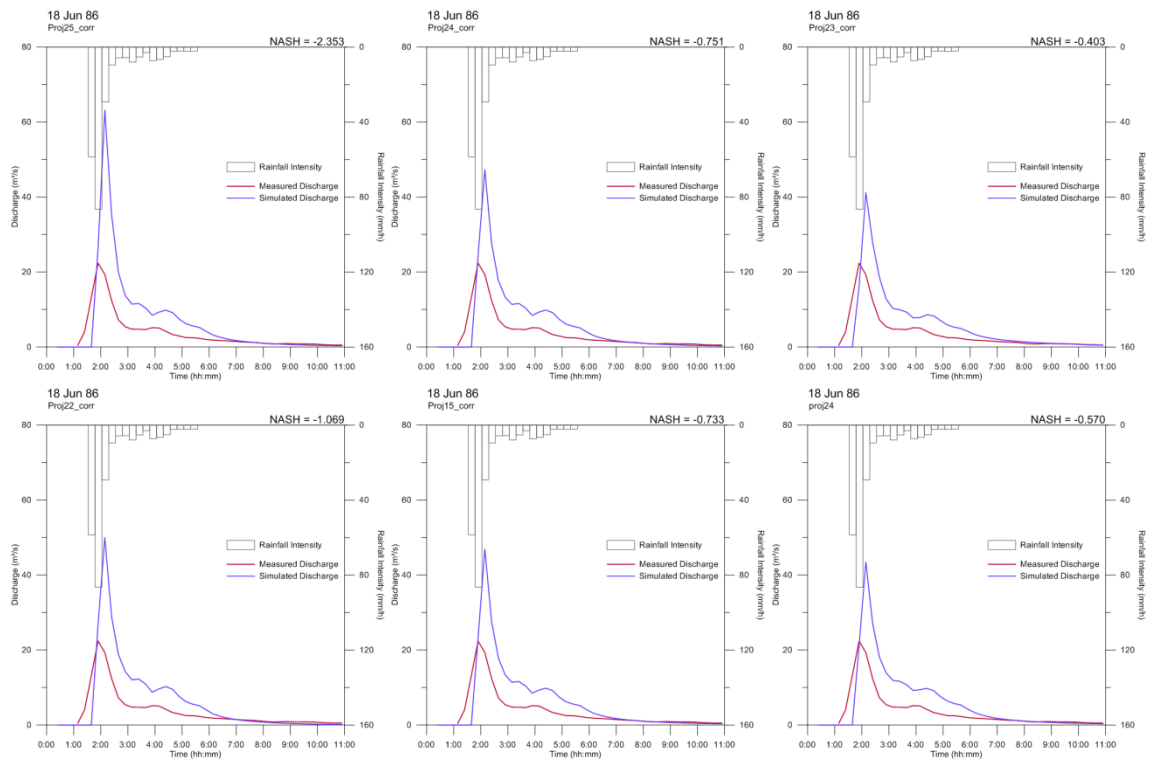
### 03 Jan 85



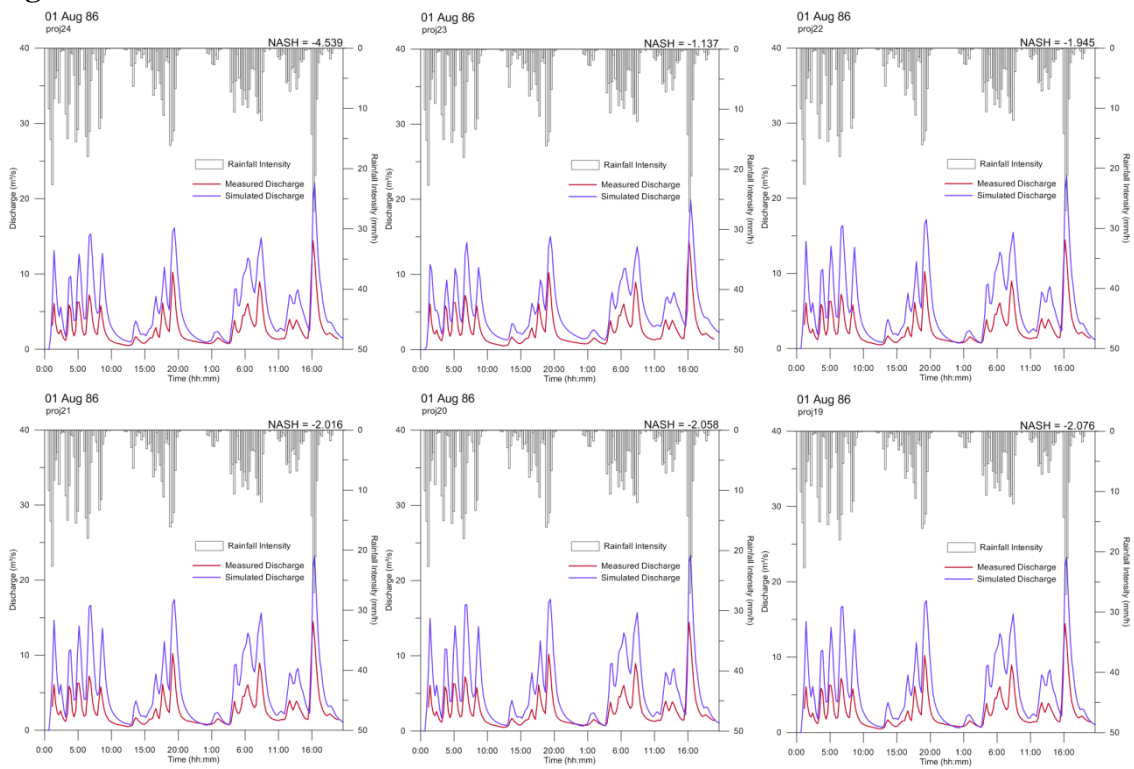


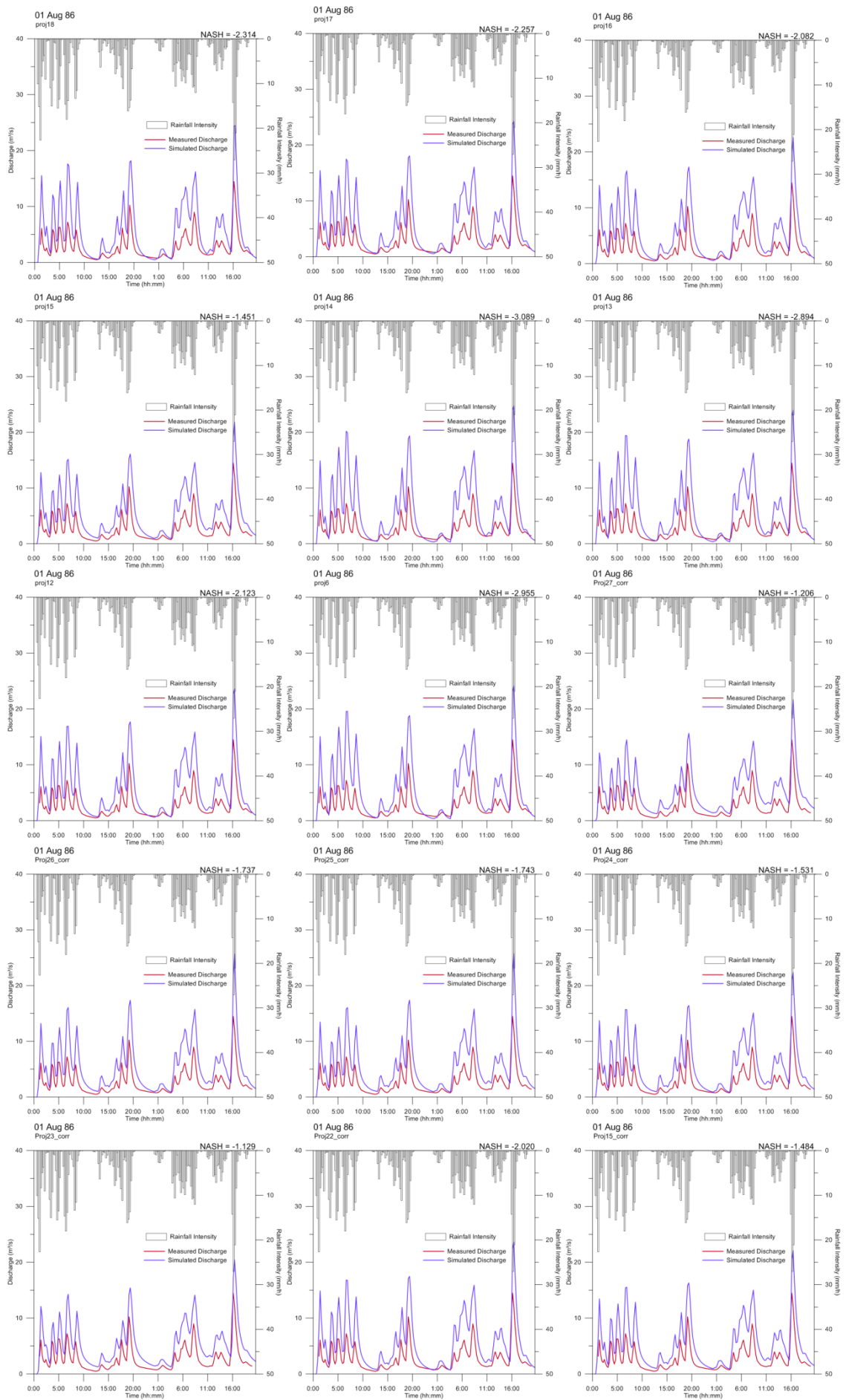
18 Jun 86



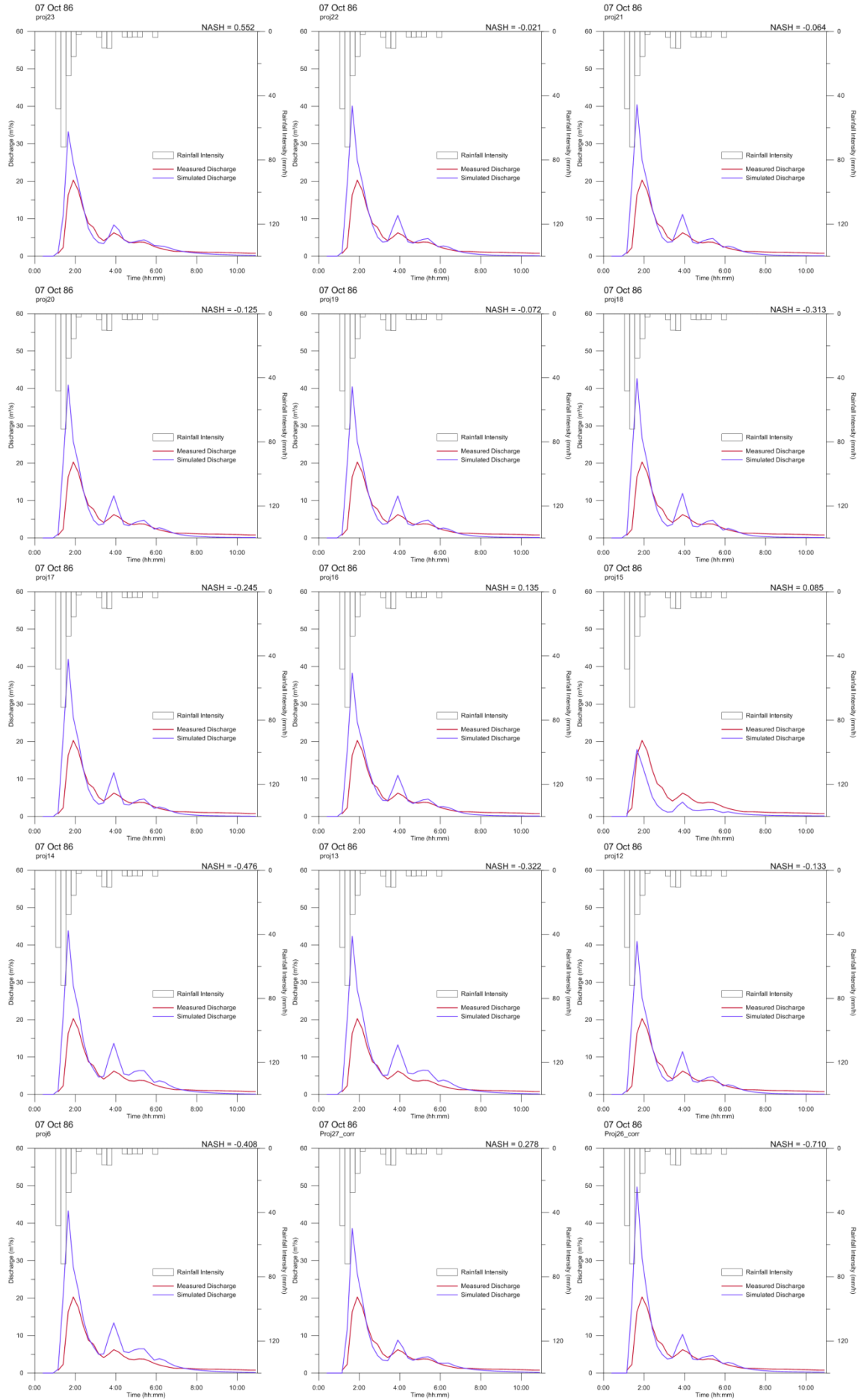


## 01 Aug 86

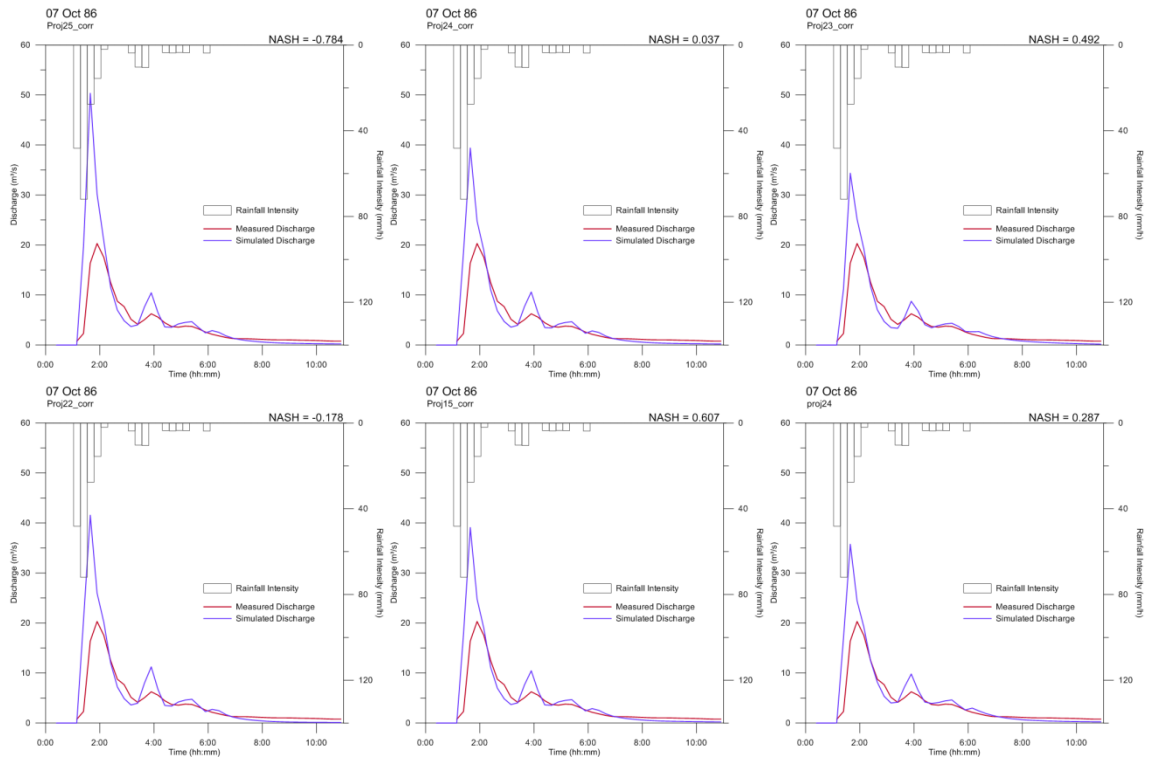




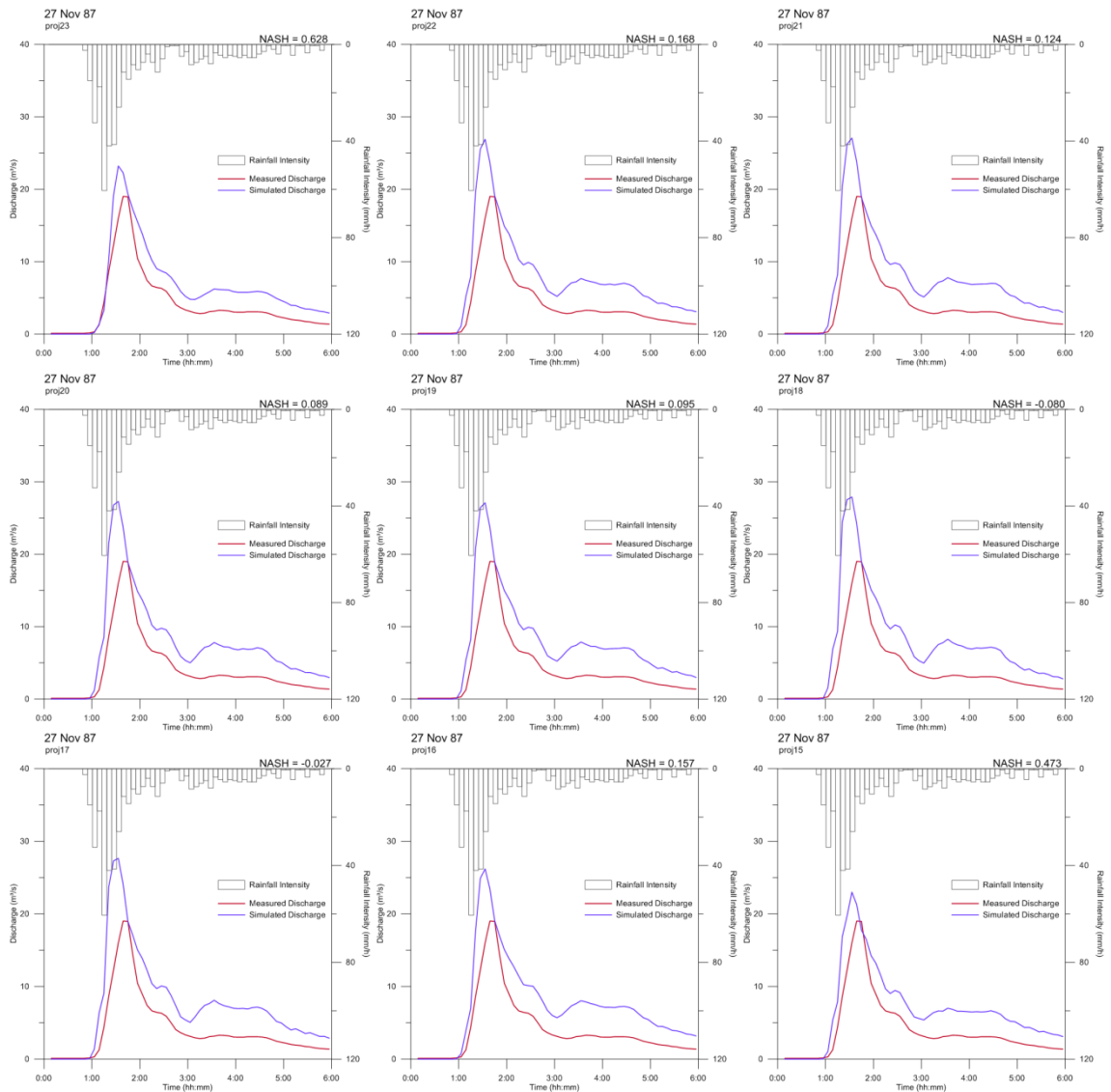
07 Oct 86

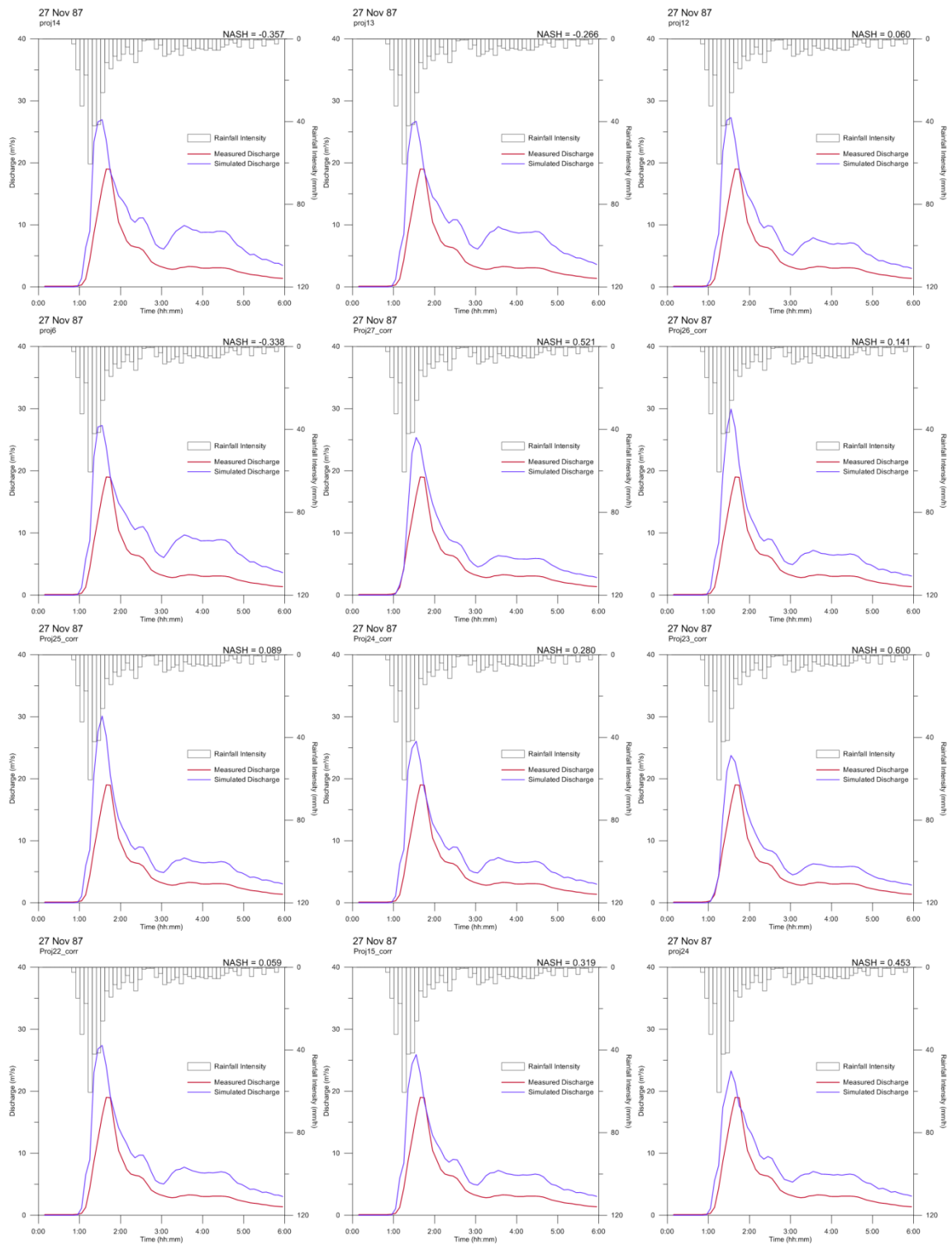




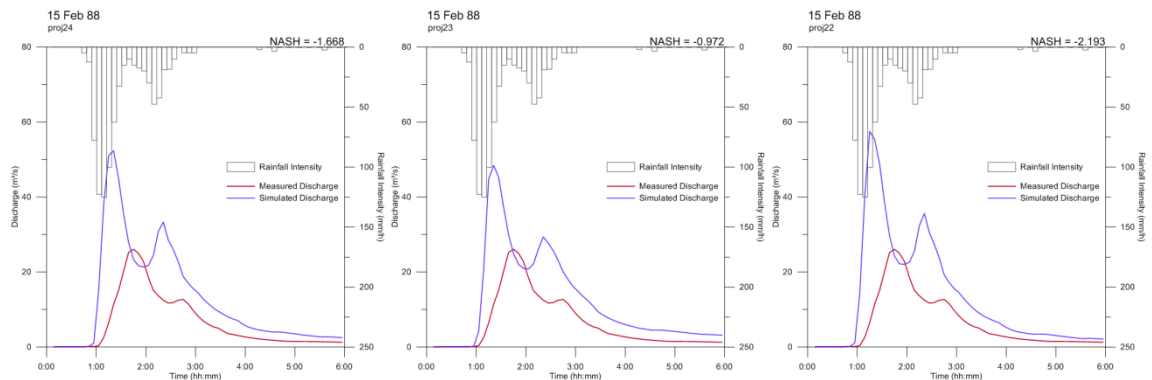


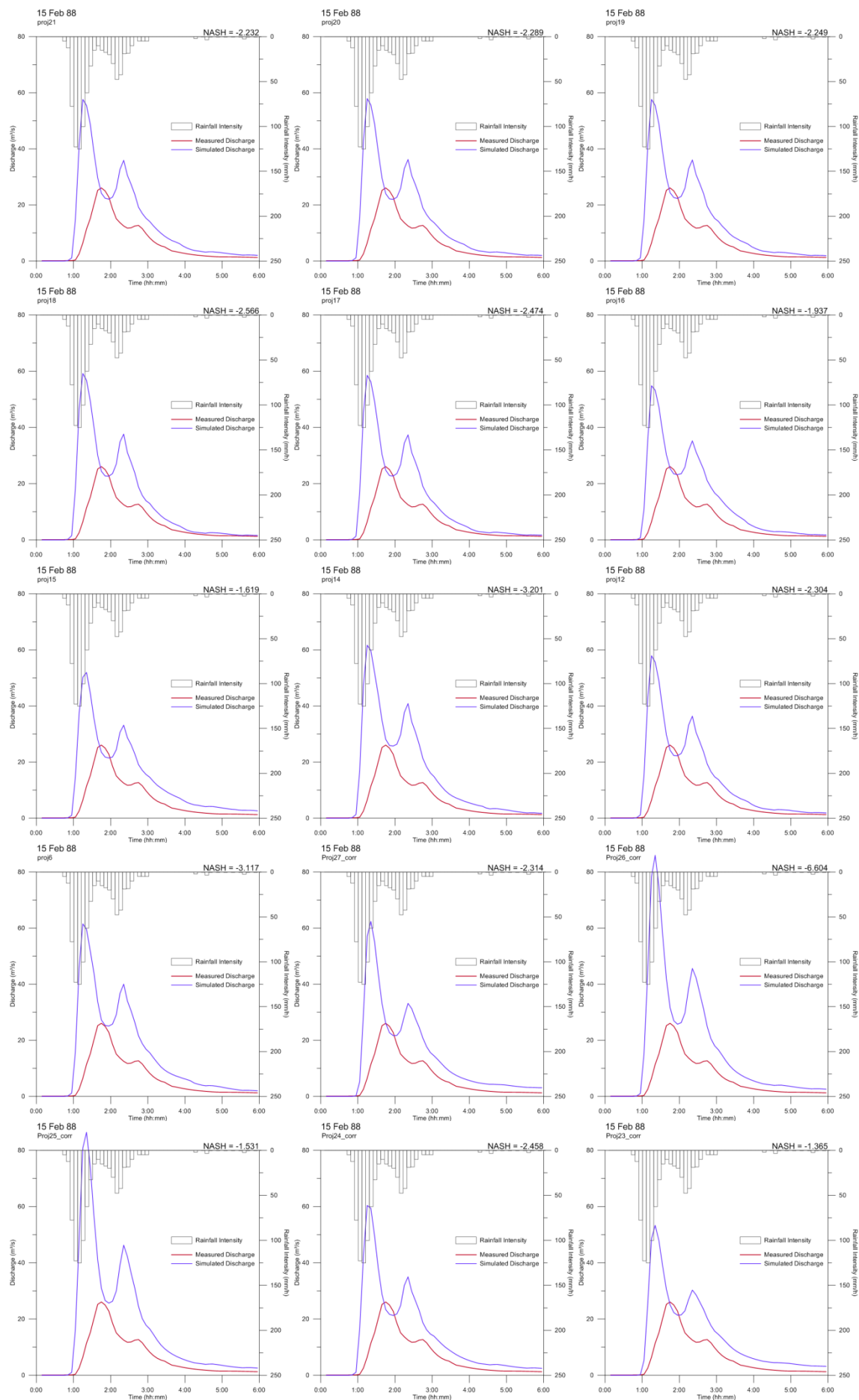
## 27 Nov 87

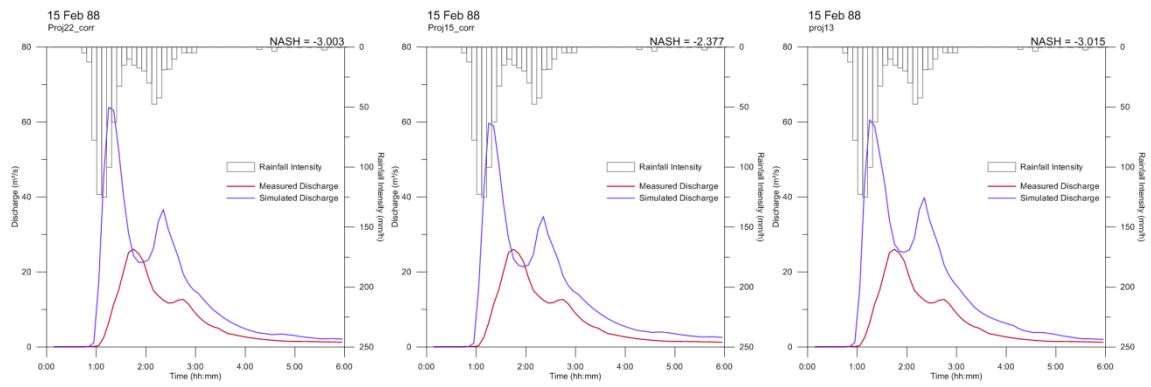




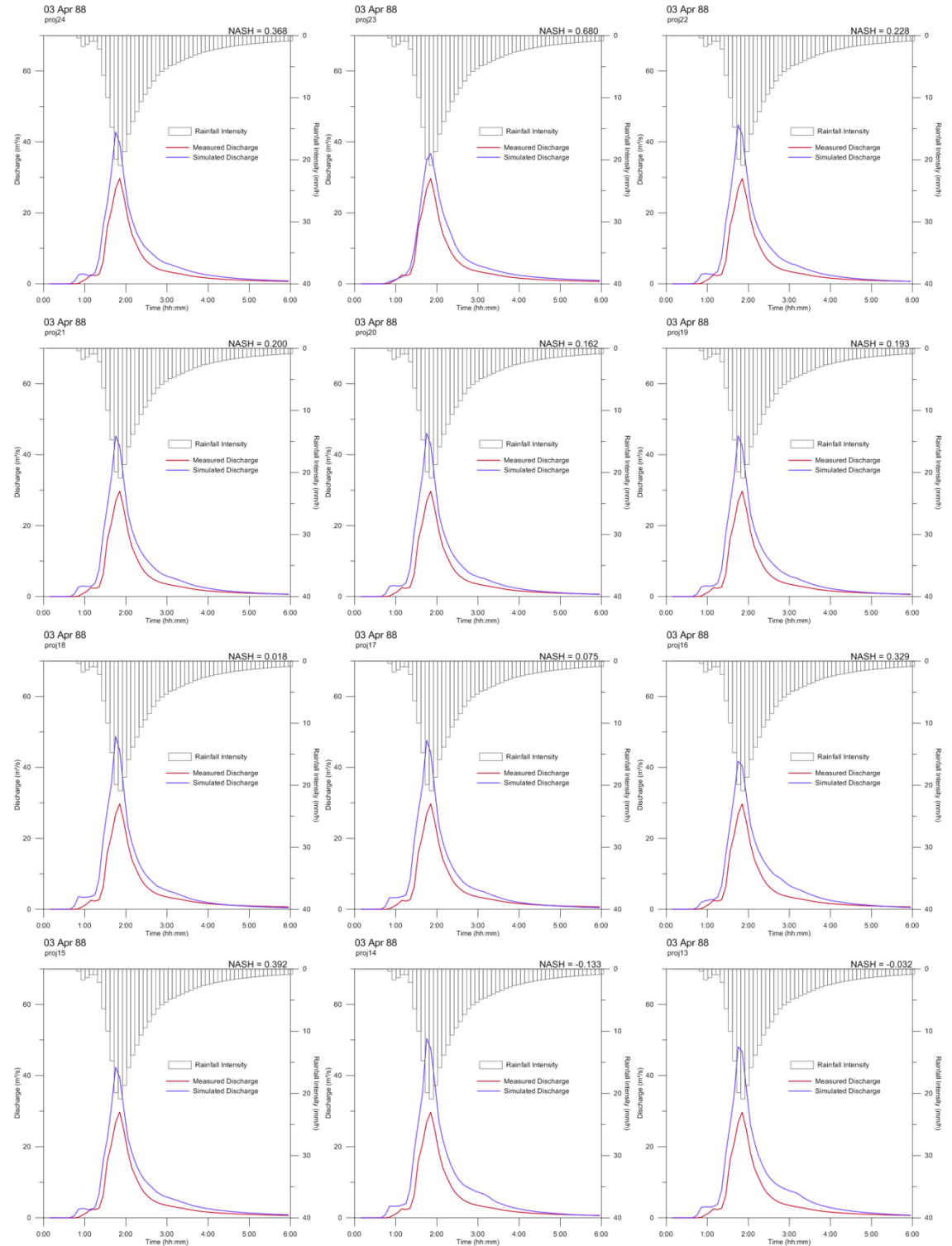
## 15 Feb 88

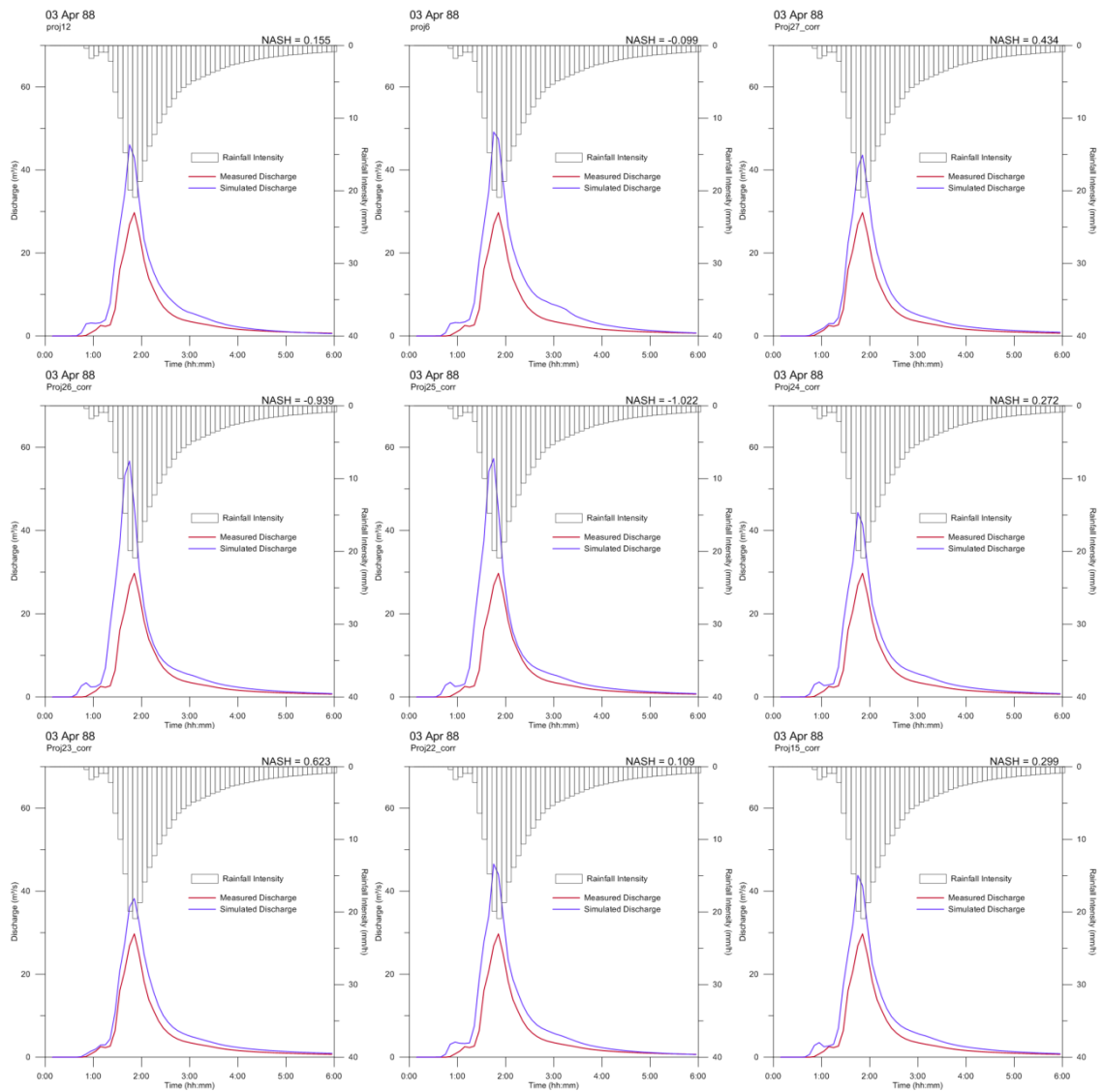




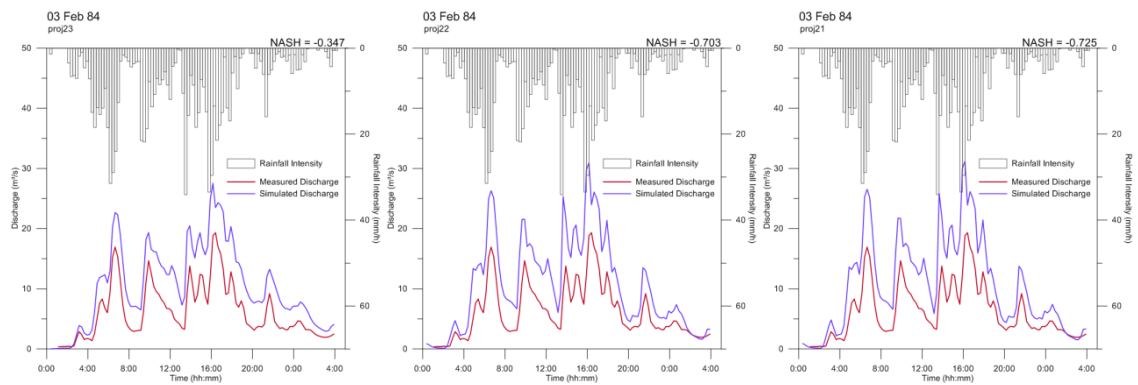


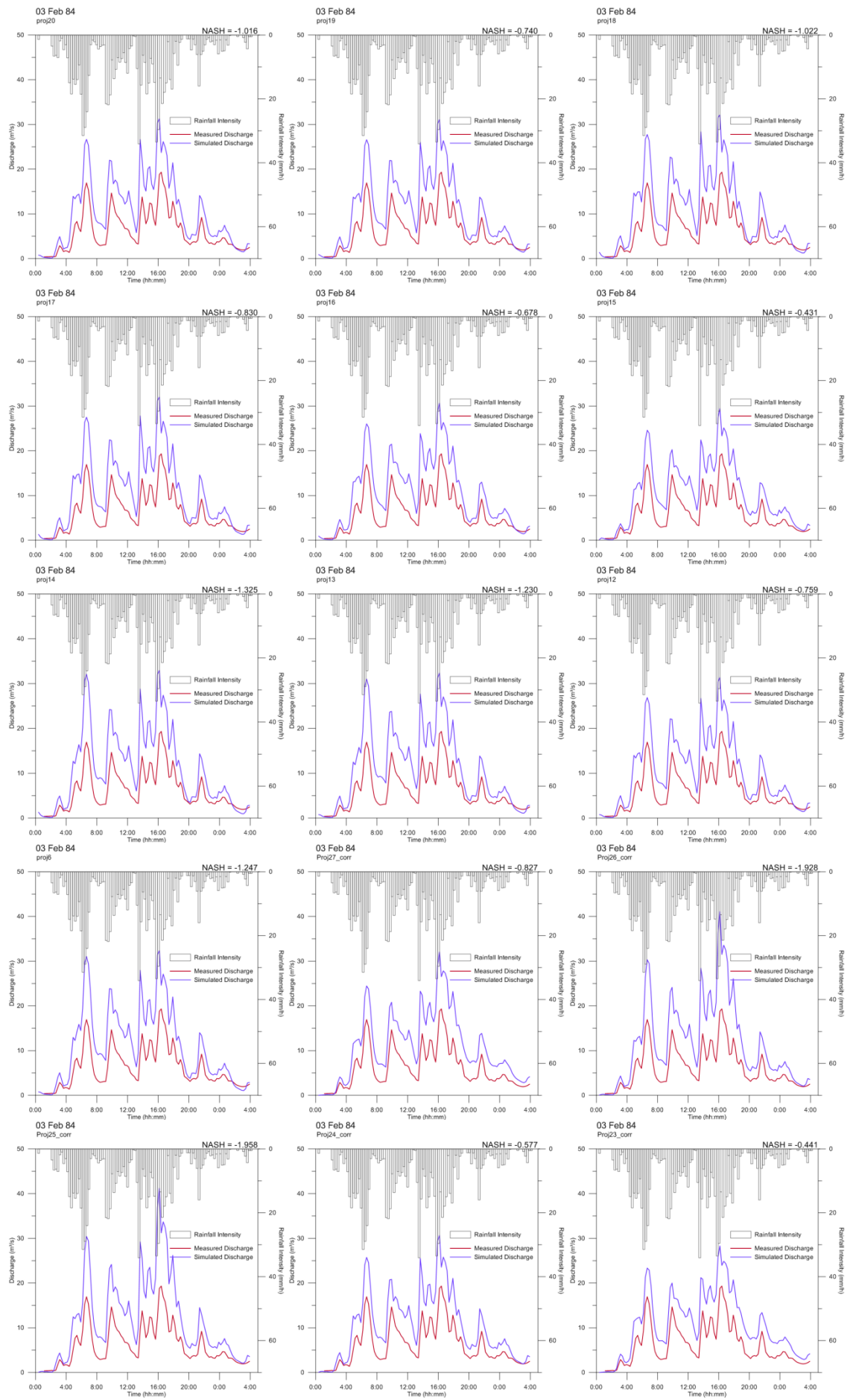
**03 Apr 88**

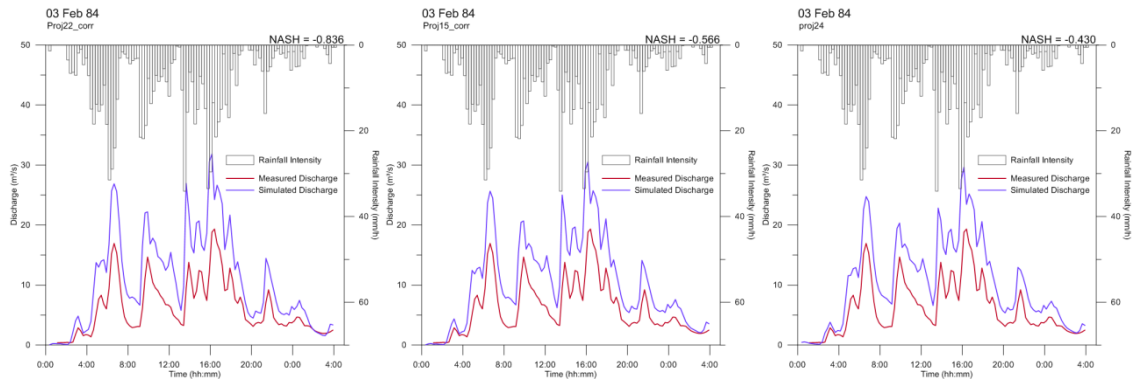




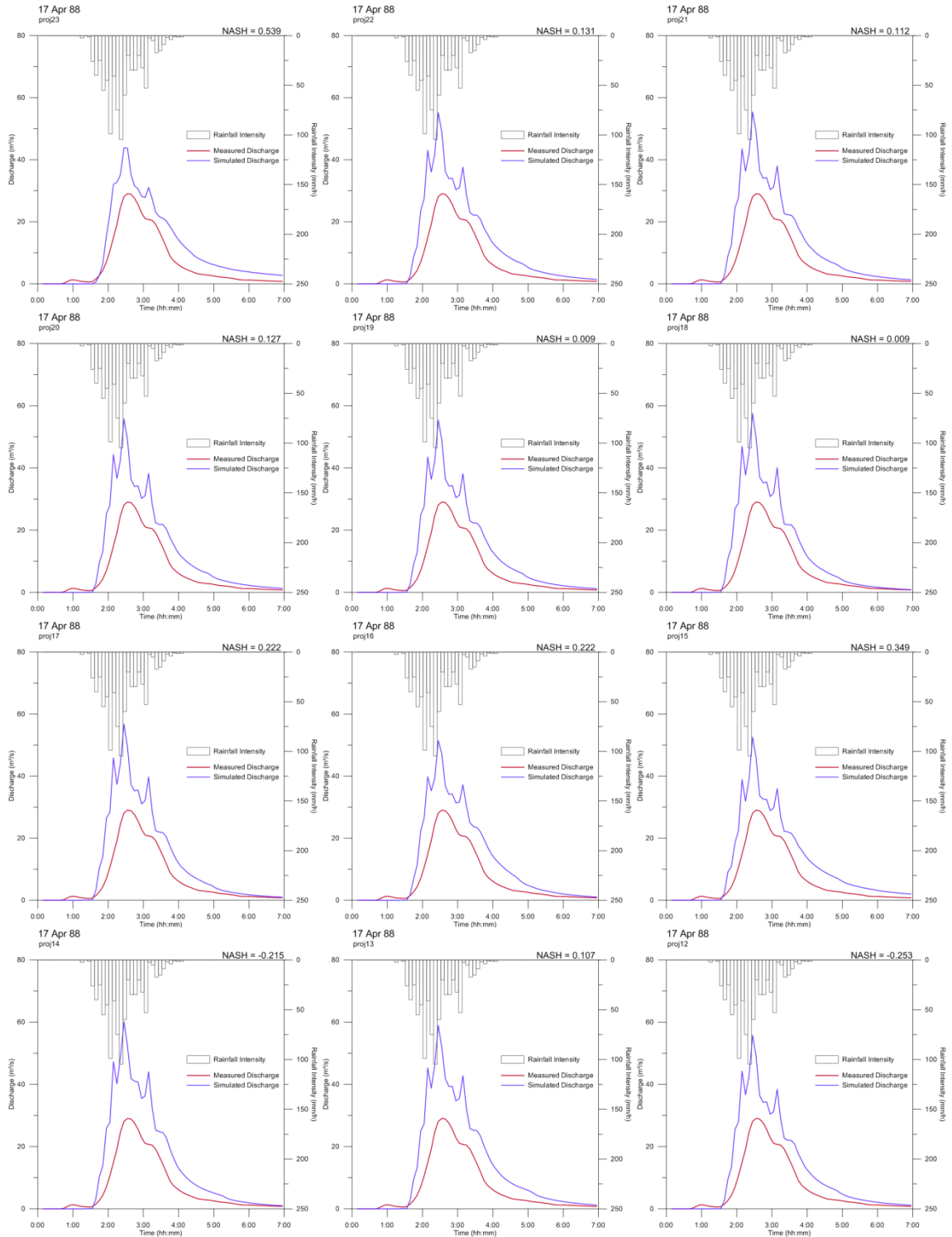
## 03 Feb 84

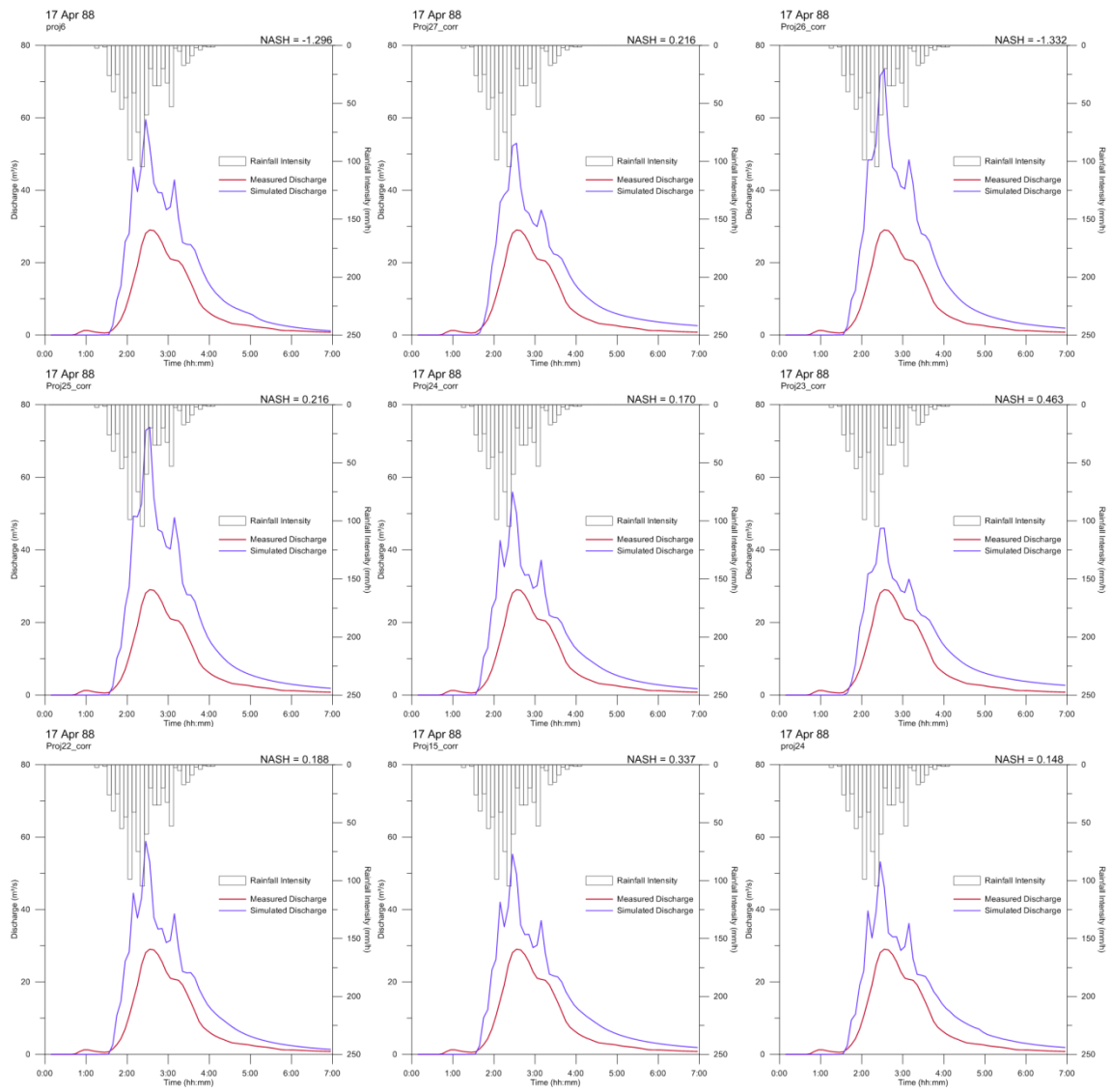




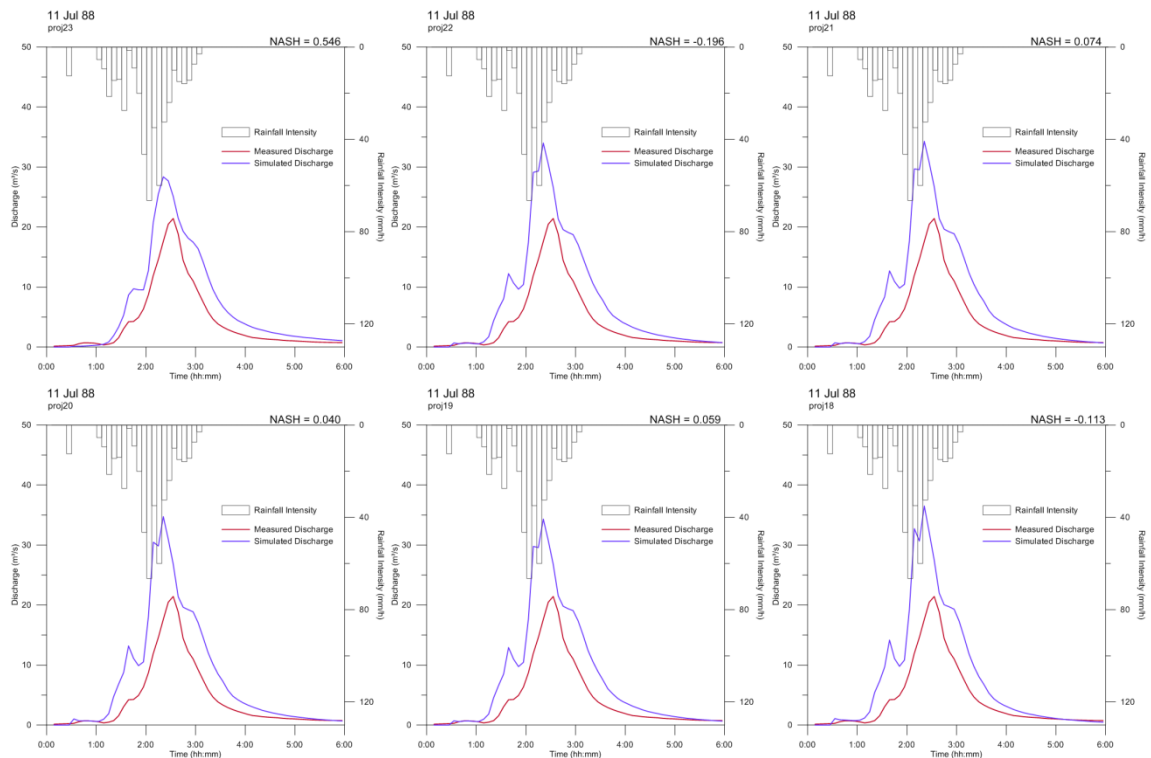


**17 Apr 88**

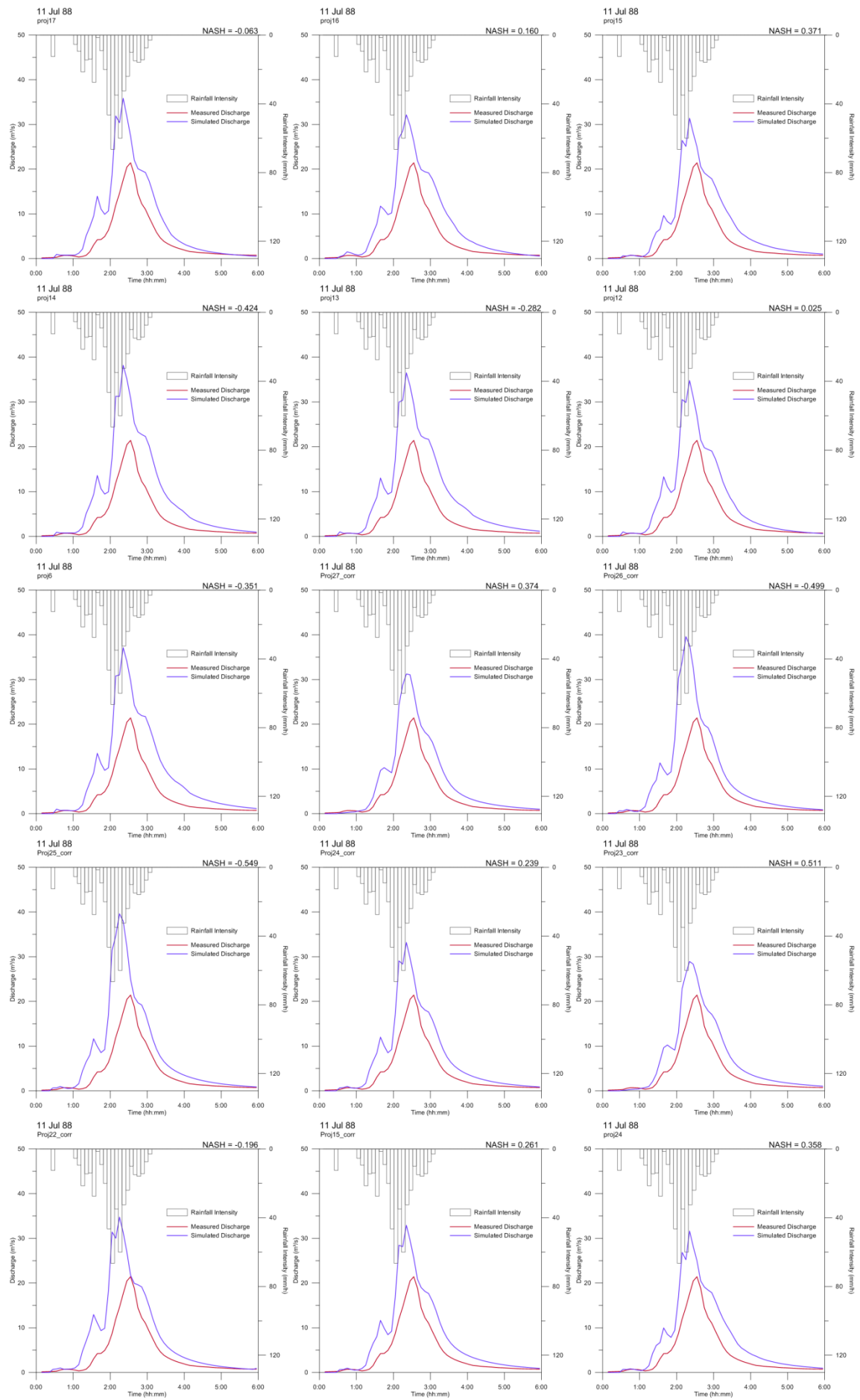




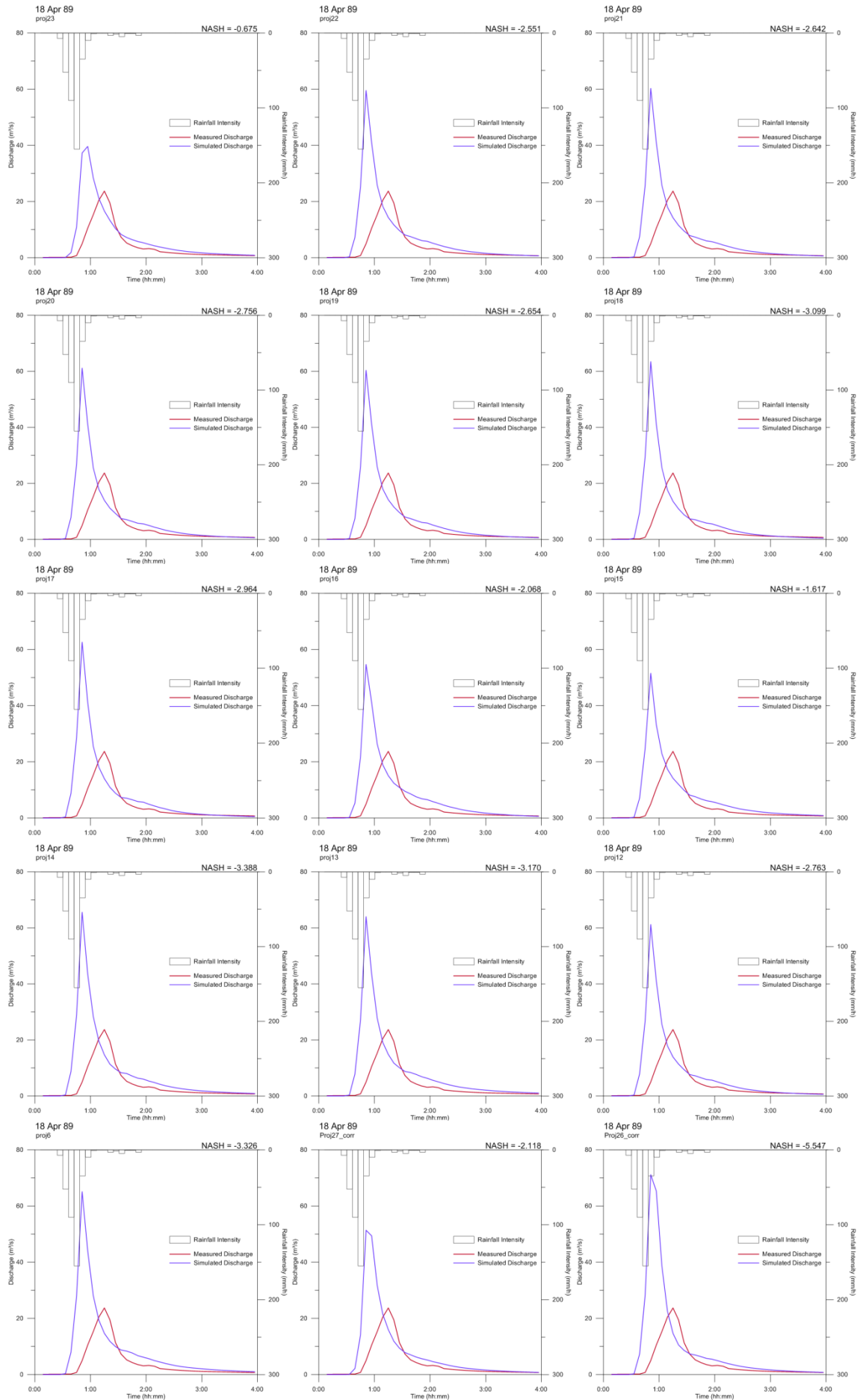
11 Jul 88

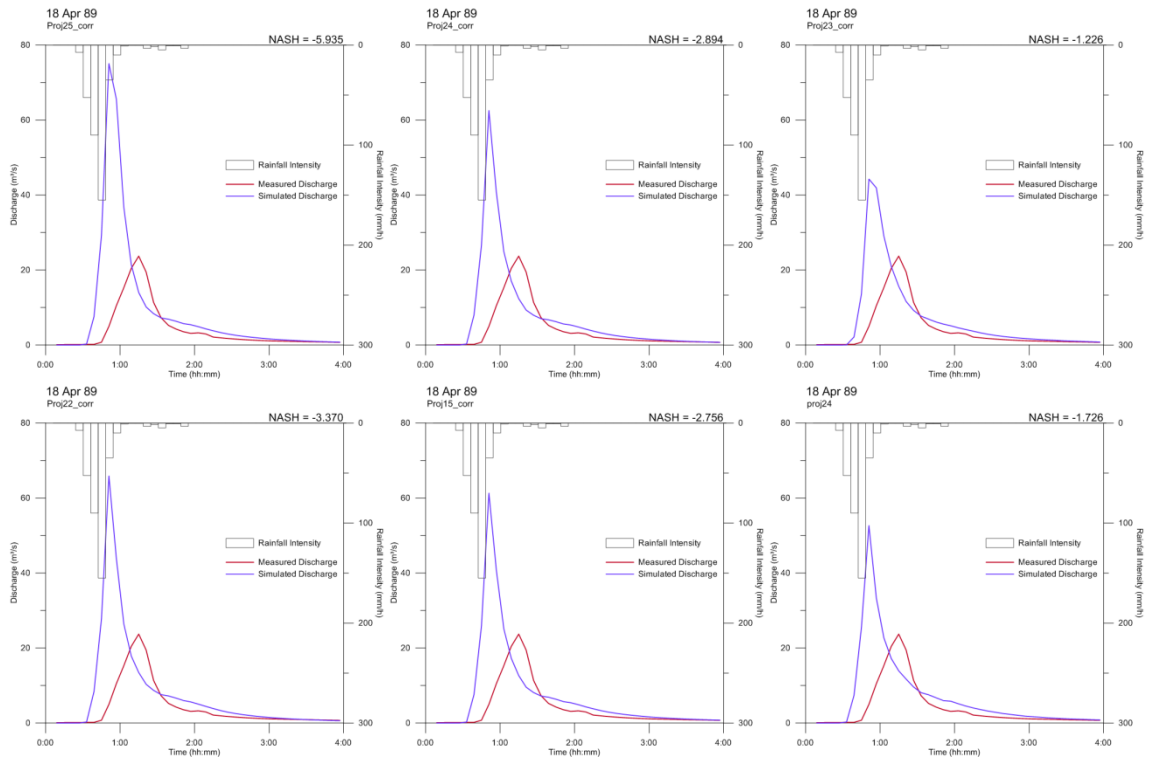




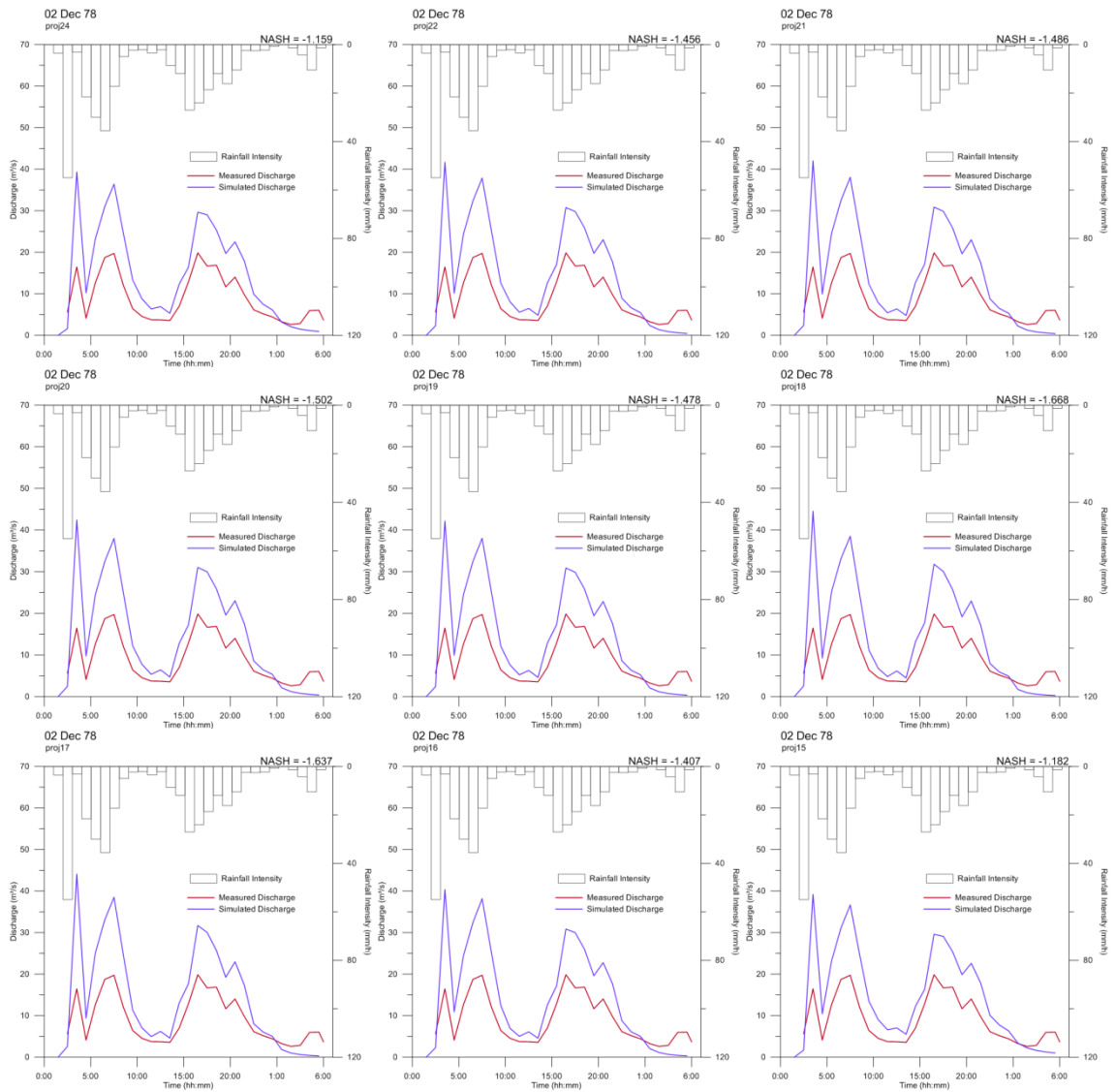


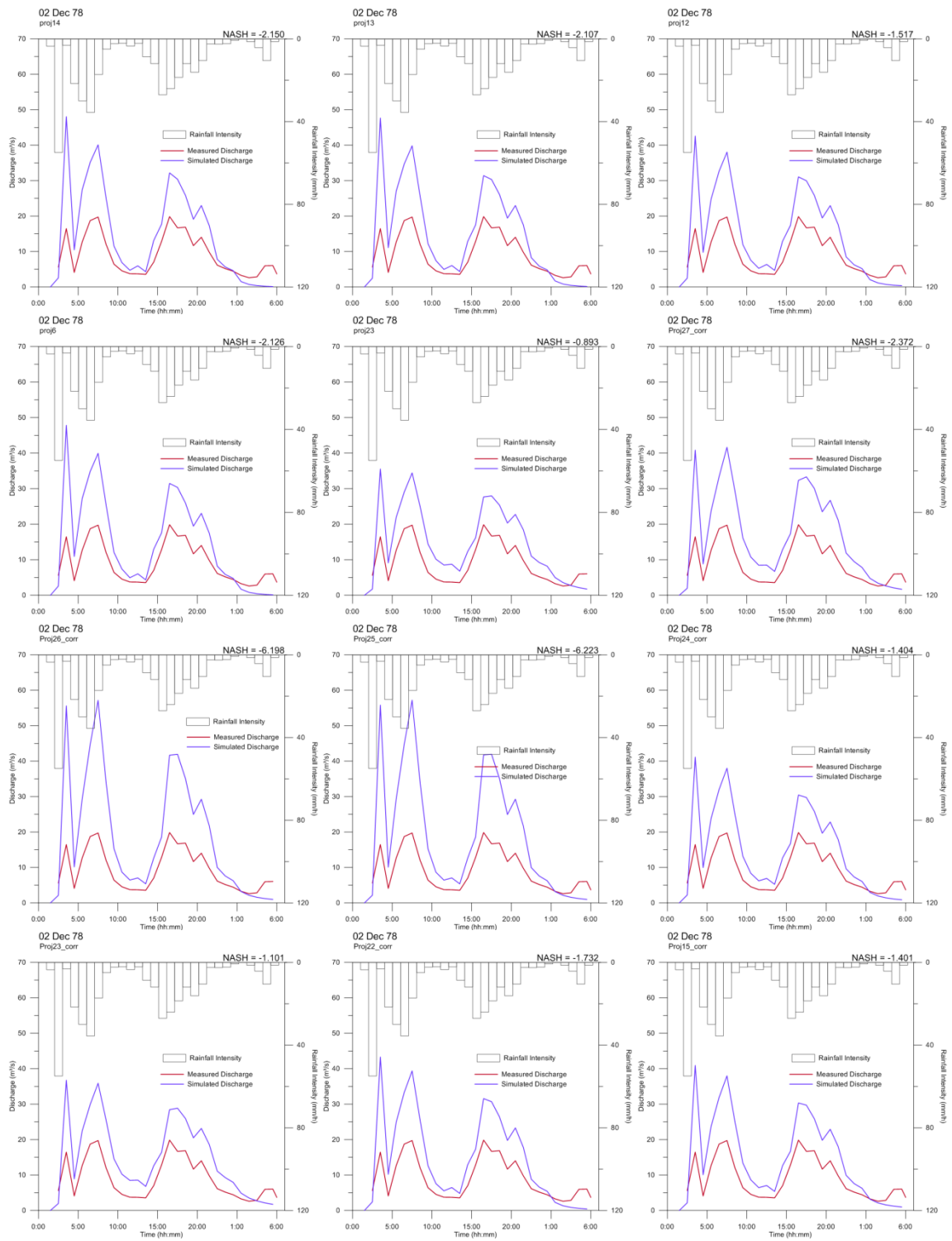
18 Apr 89





## 02 Dec 78





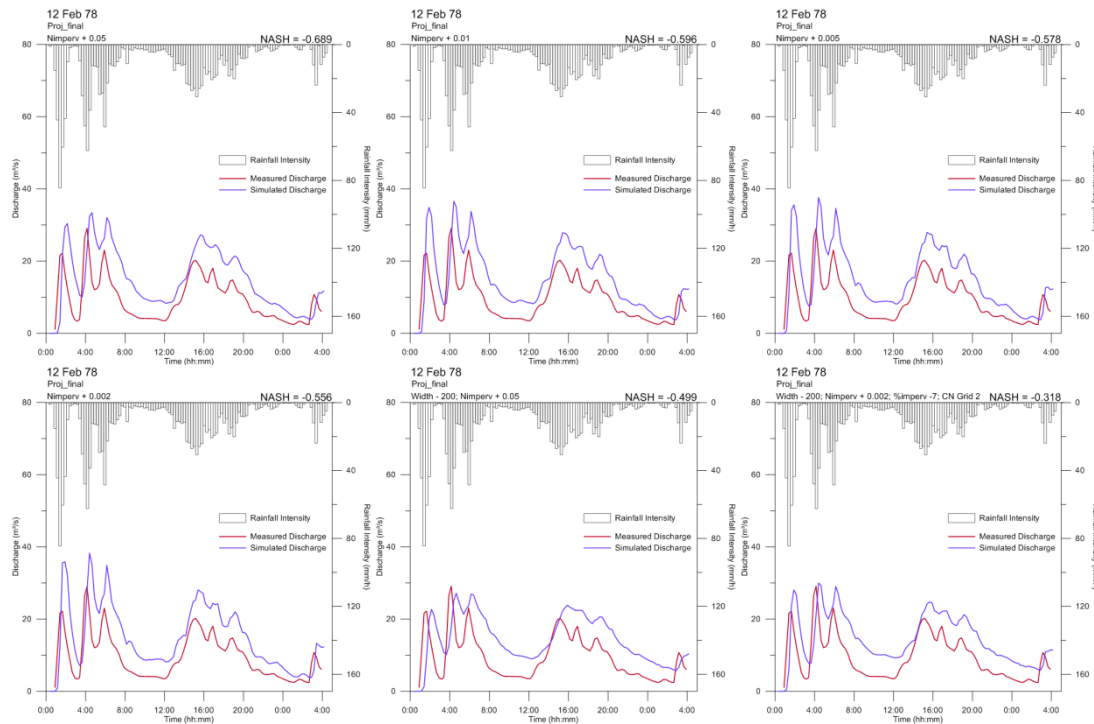
## Appendix 5. SWMM final adjustment hydrographs

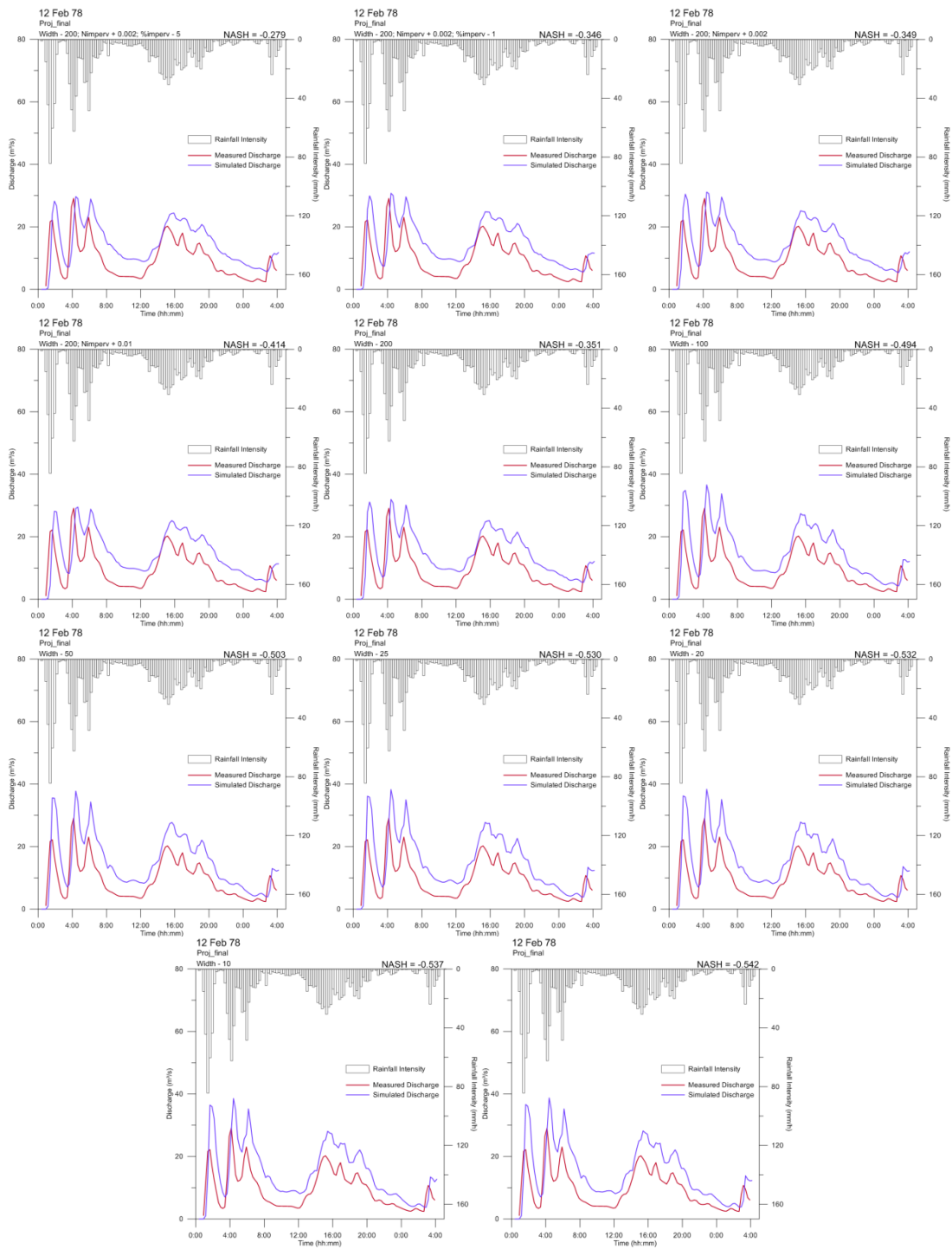
The graphs presented here are:

- 12 Feb 78;
- 01 Jun 79;
- 02 Mar 84;
- 02 Jul 84;
- 03 Jan 85;
- 18 Jun 86;
- 01 Aug 86;
- 07 Oct 86;
- 27 Nov 87;
- 15 Feb 88;
- 03 Apr 88;
- 03 Feb 84;
- 17 Apr 88;
- 11 Jul 88;
- 18 Apr 89
- 02 Dec 78.

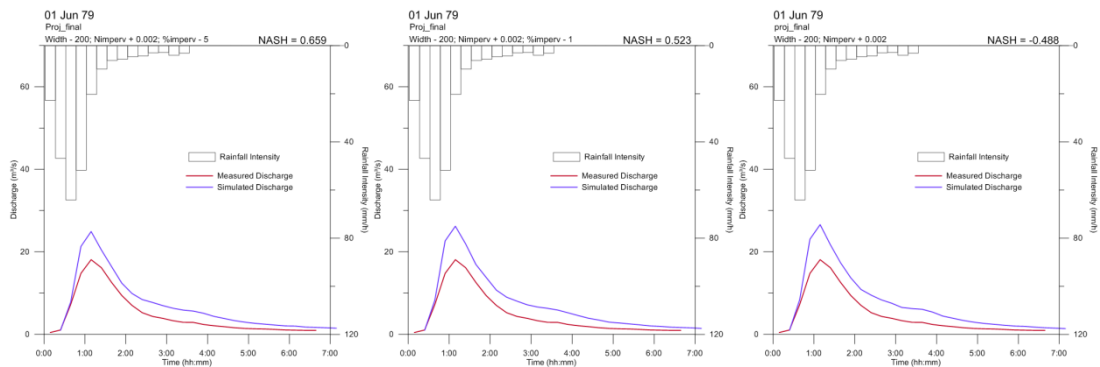
Time (hh:mm) figures on X axis, discharge ( $\text{m}^3/\text{s}$ ) figures on Y left axis and rainfall intensity (mm/h) figures on Y right axis. Measured discharge is in red, simulated discharge in blue. The Nash-Sutcliffe coefficient is noted on the right hand side of each graph. In order to allow a global view of the curves and to save space, graphs presented here are reduced.

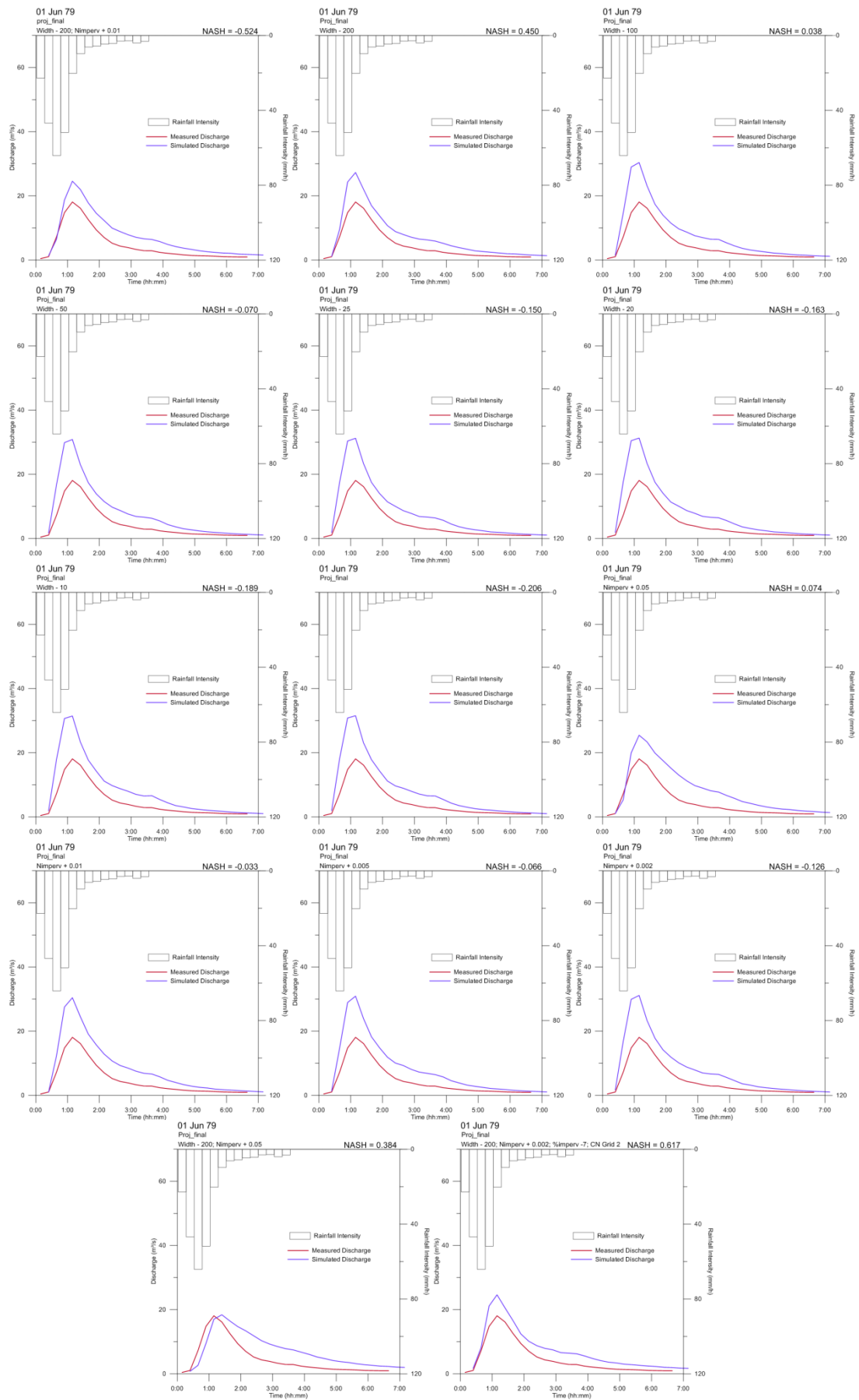
### 12 Feb 78



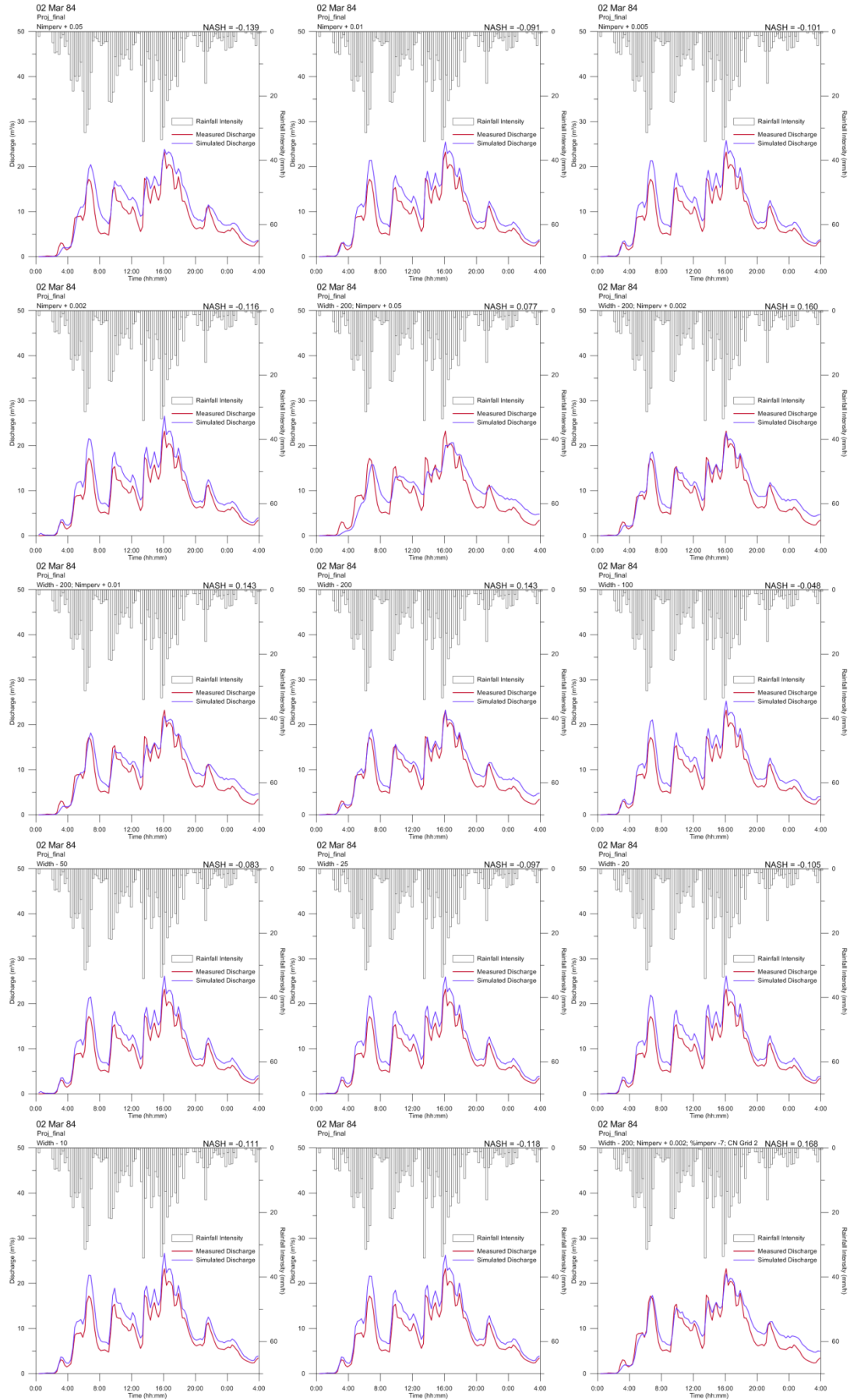


**01 Jun 79**

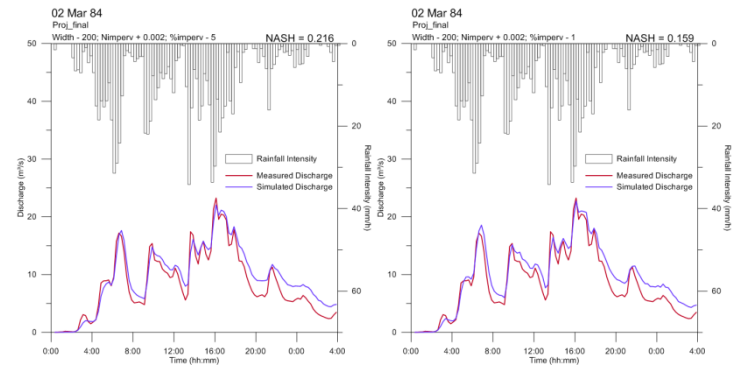




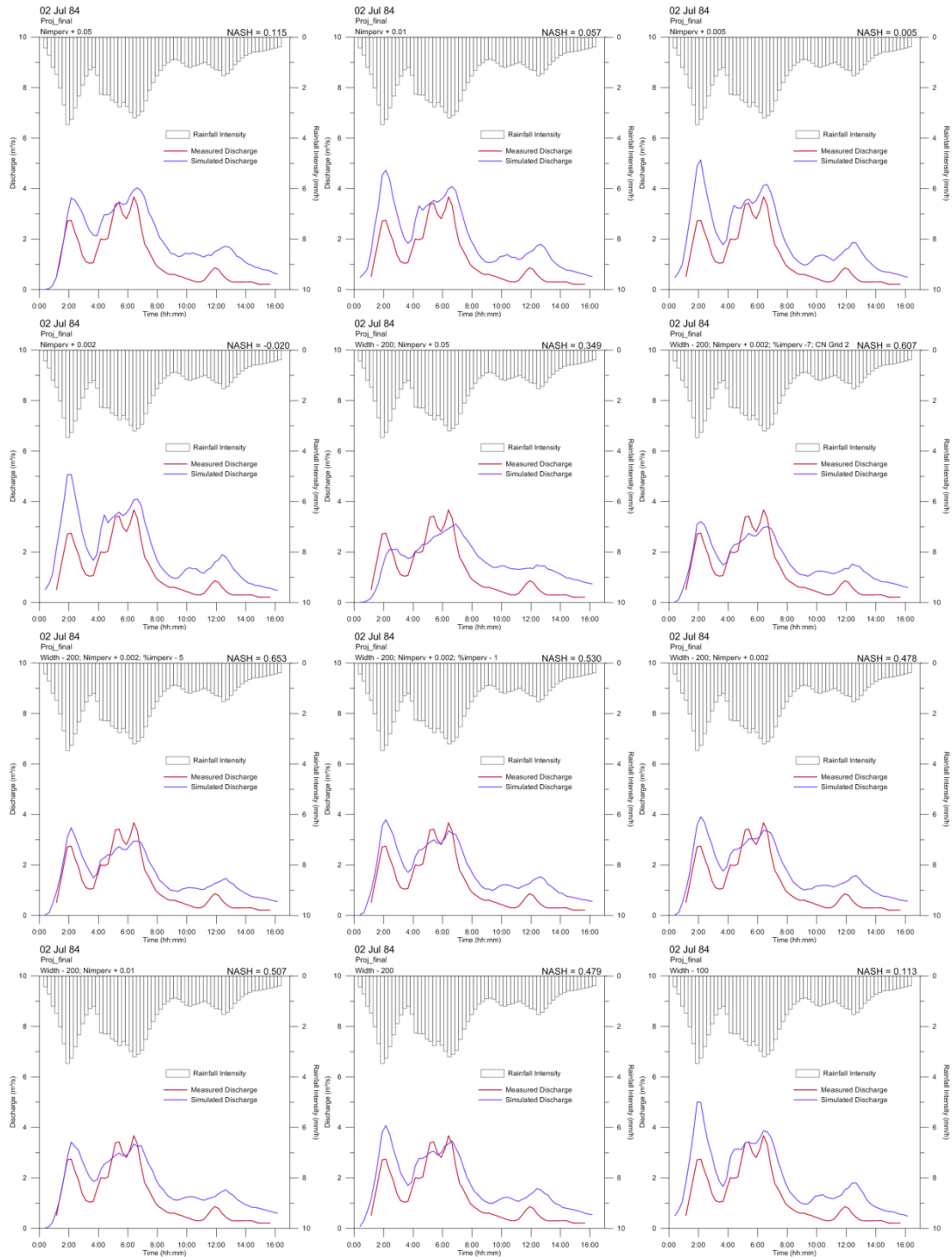
## 02 Mar 84

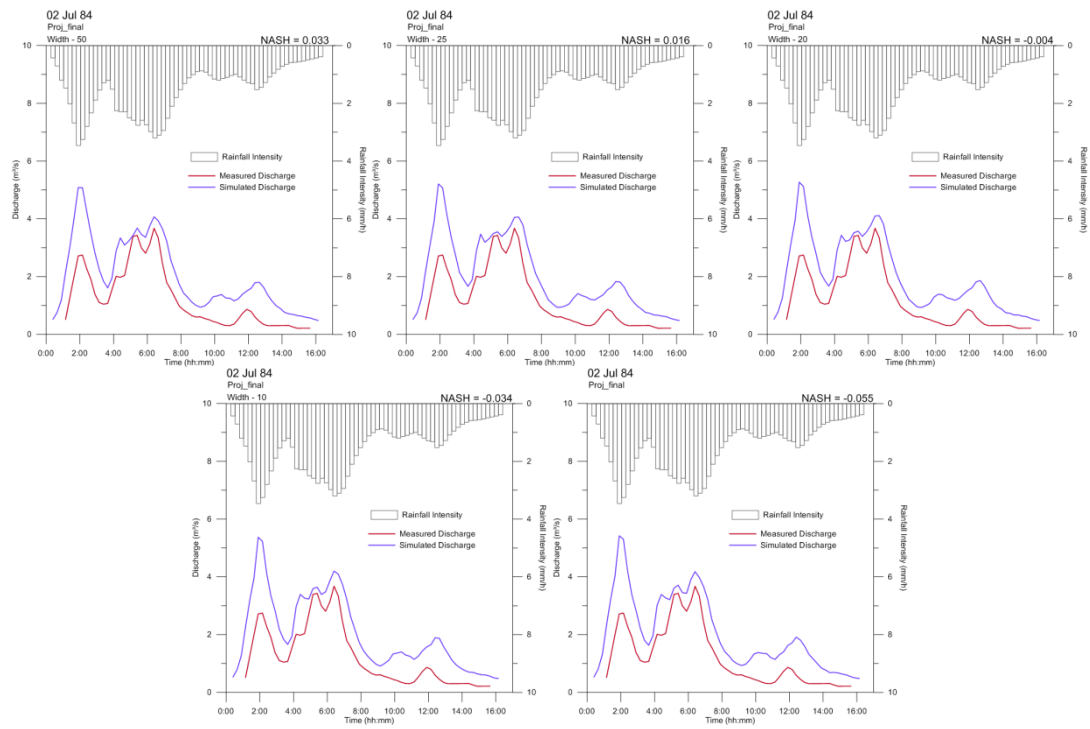




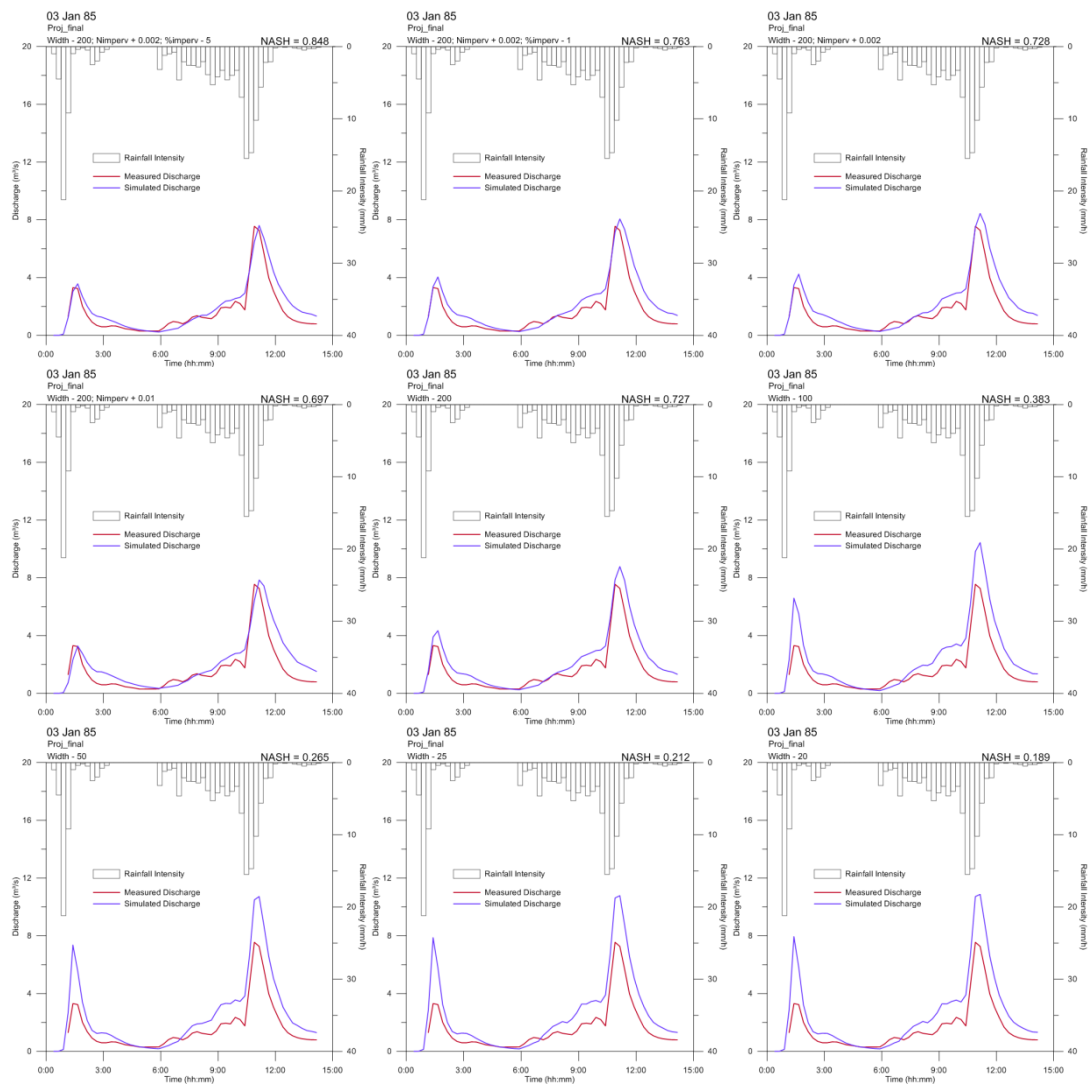


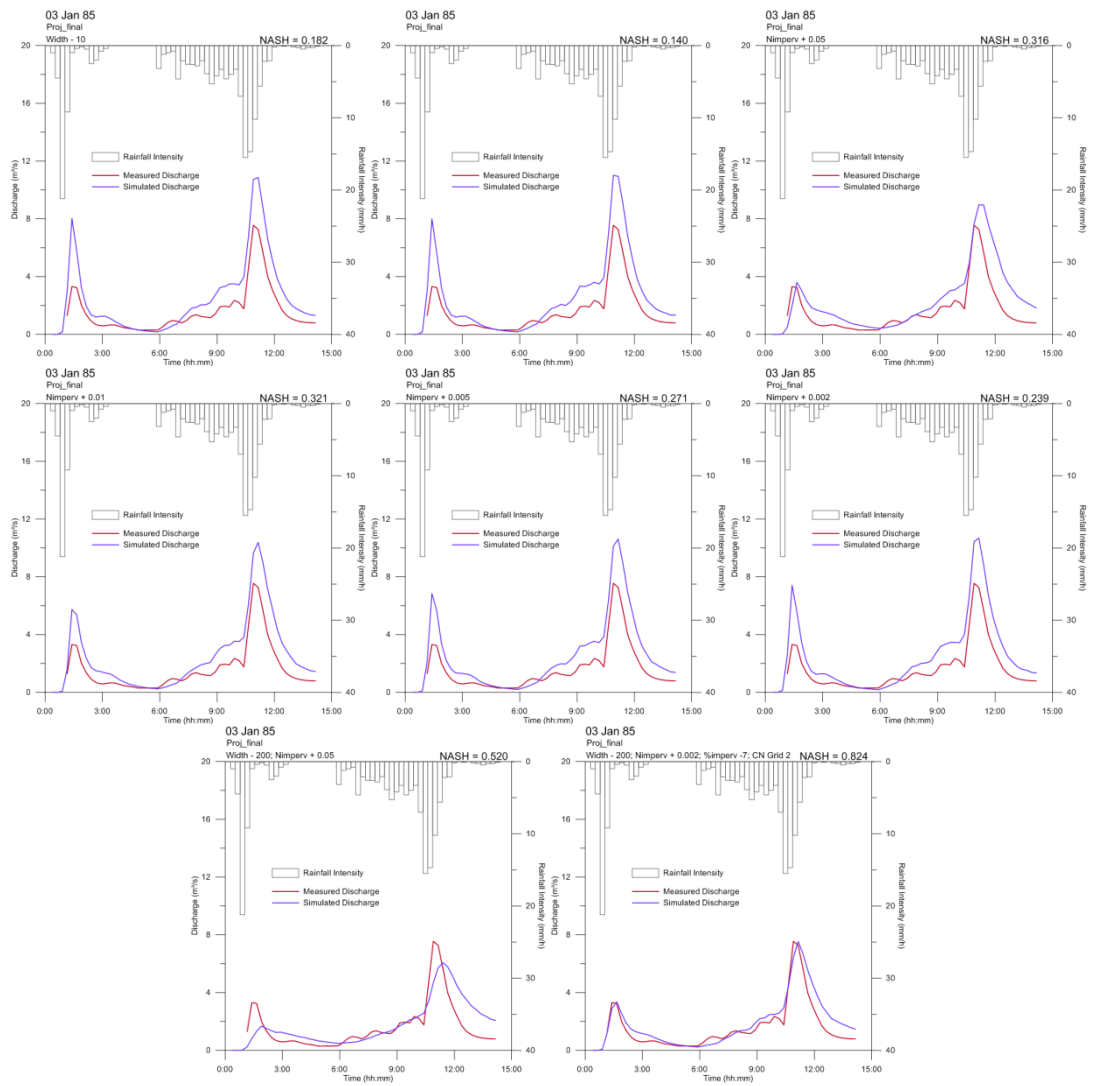
02 Jul 84



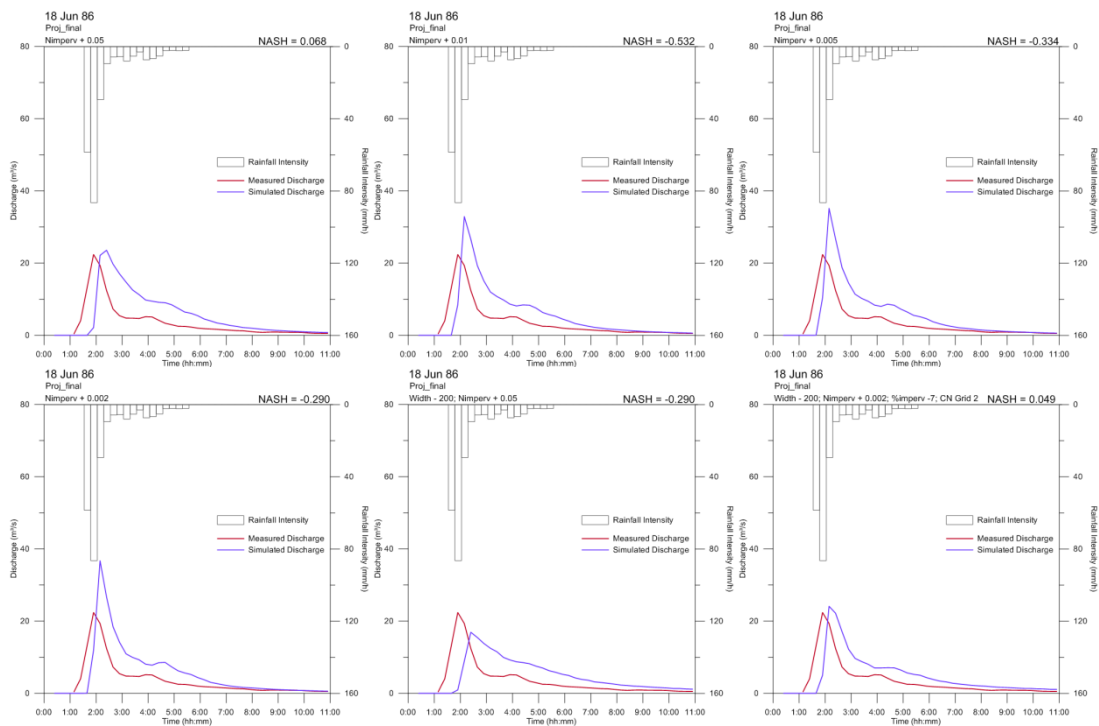


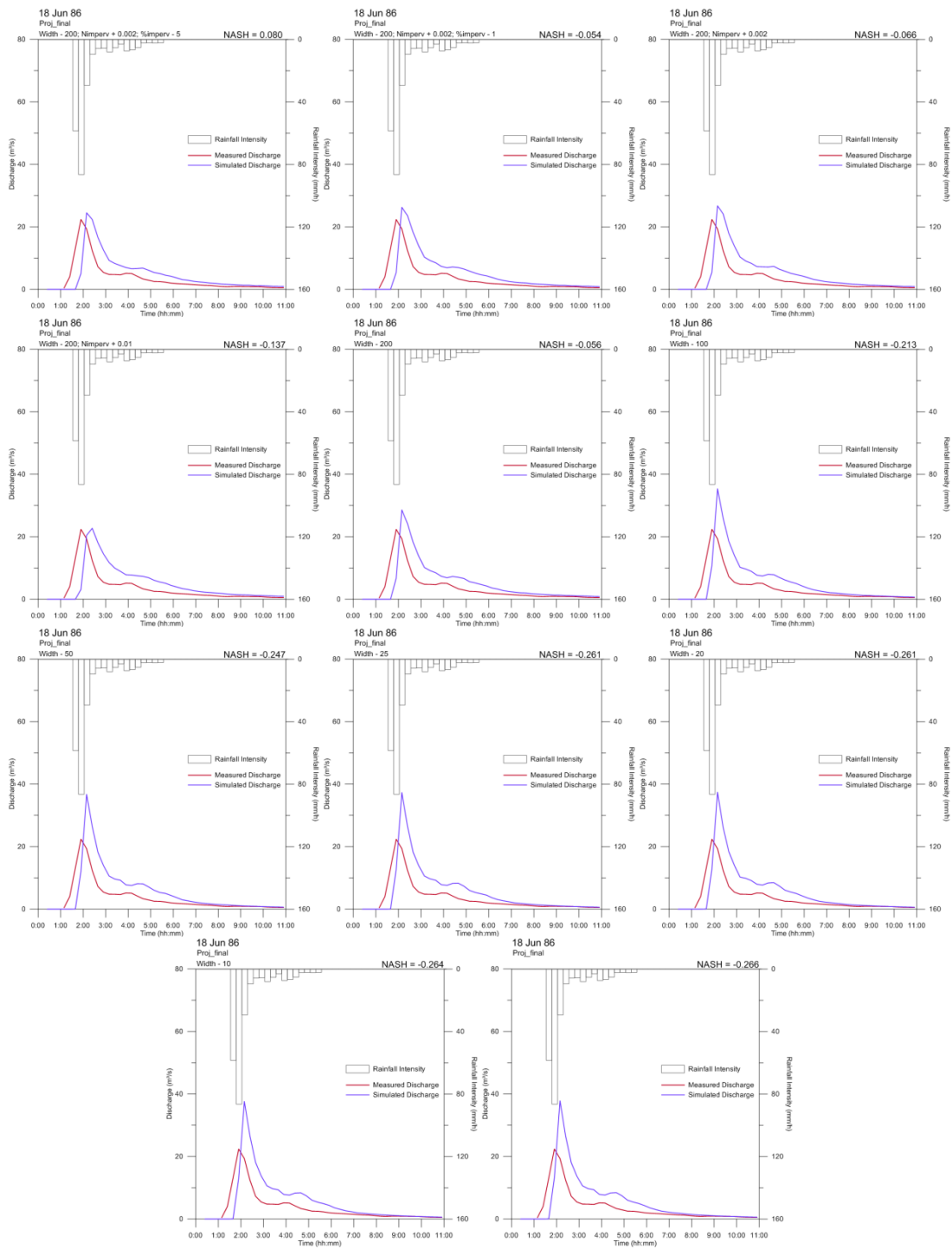
## 03 Jan 85



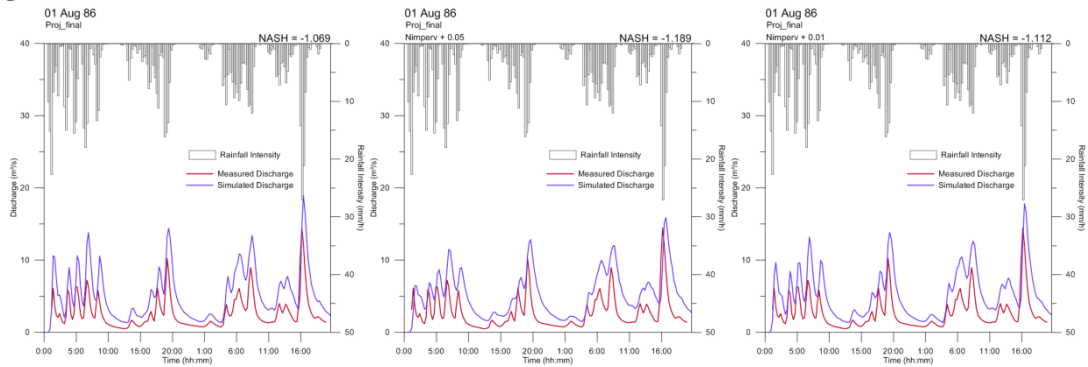


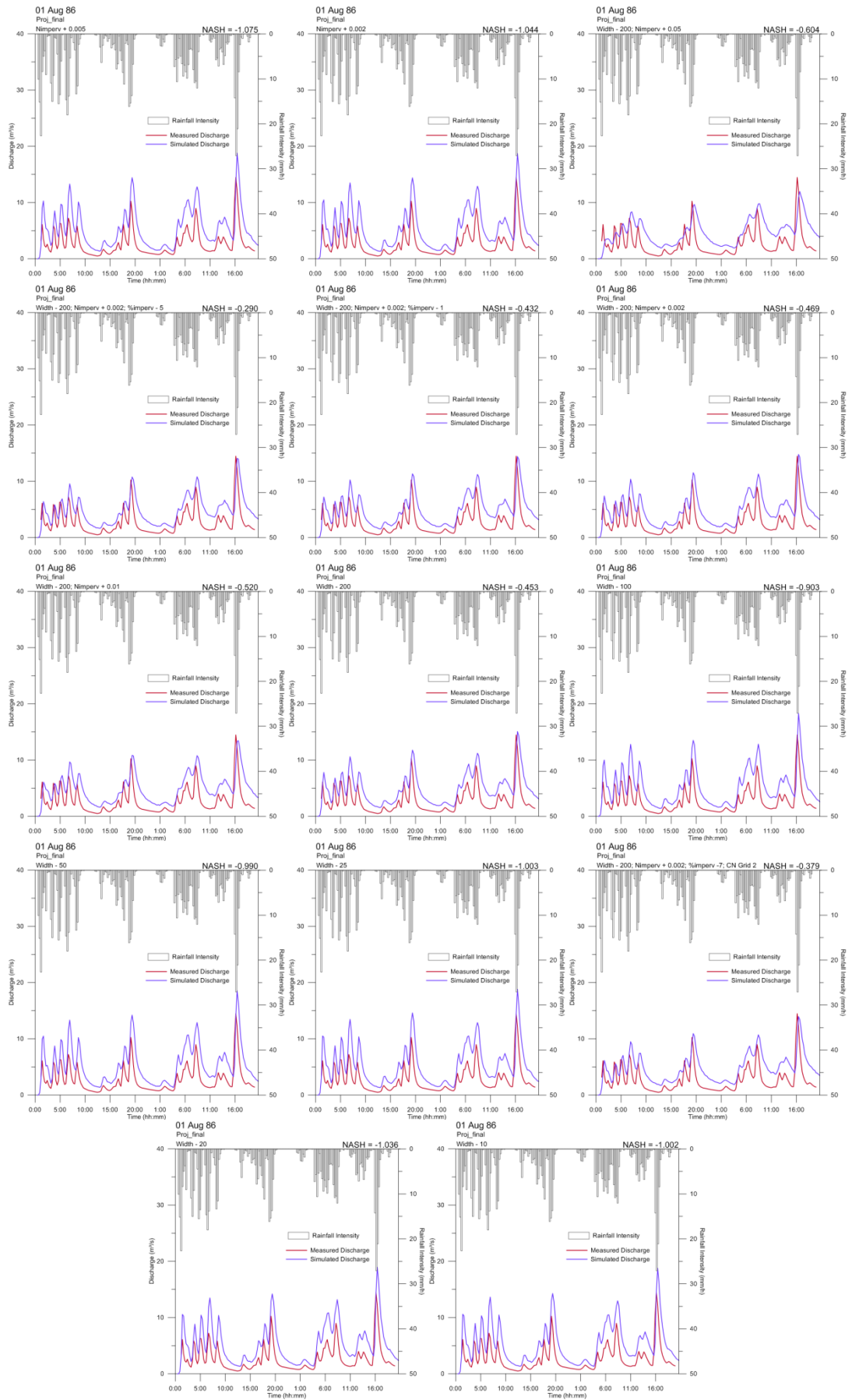
## 18 Jun 86



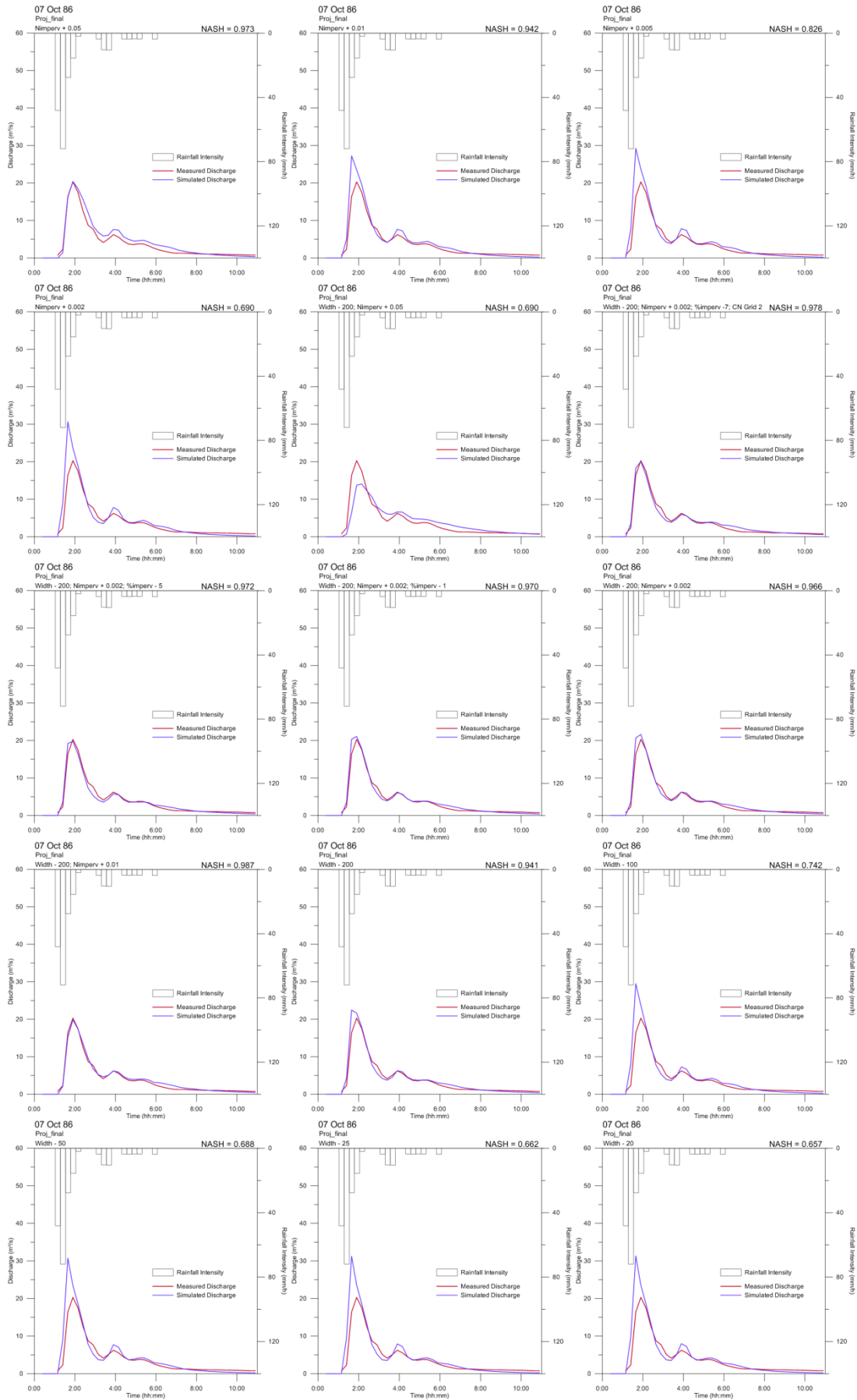


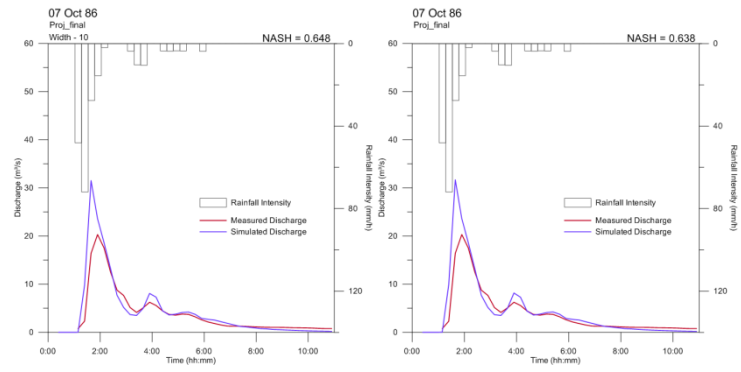
01 Aug 86



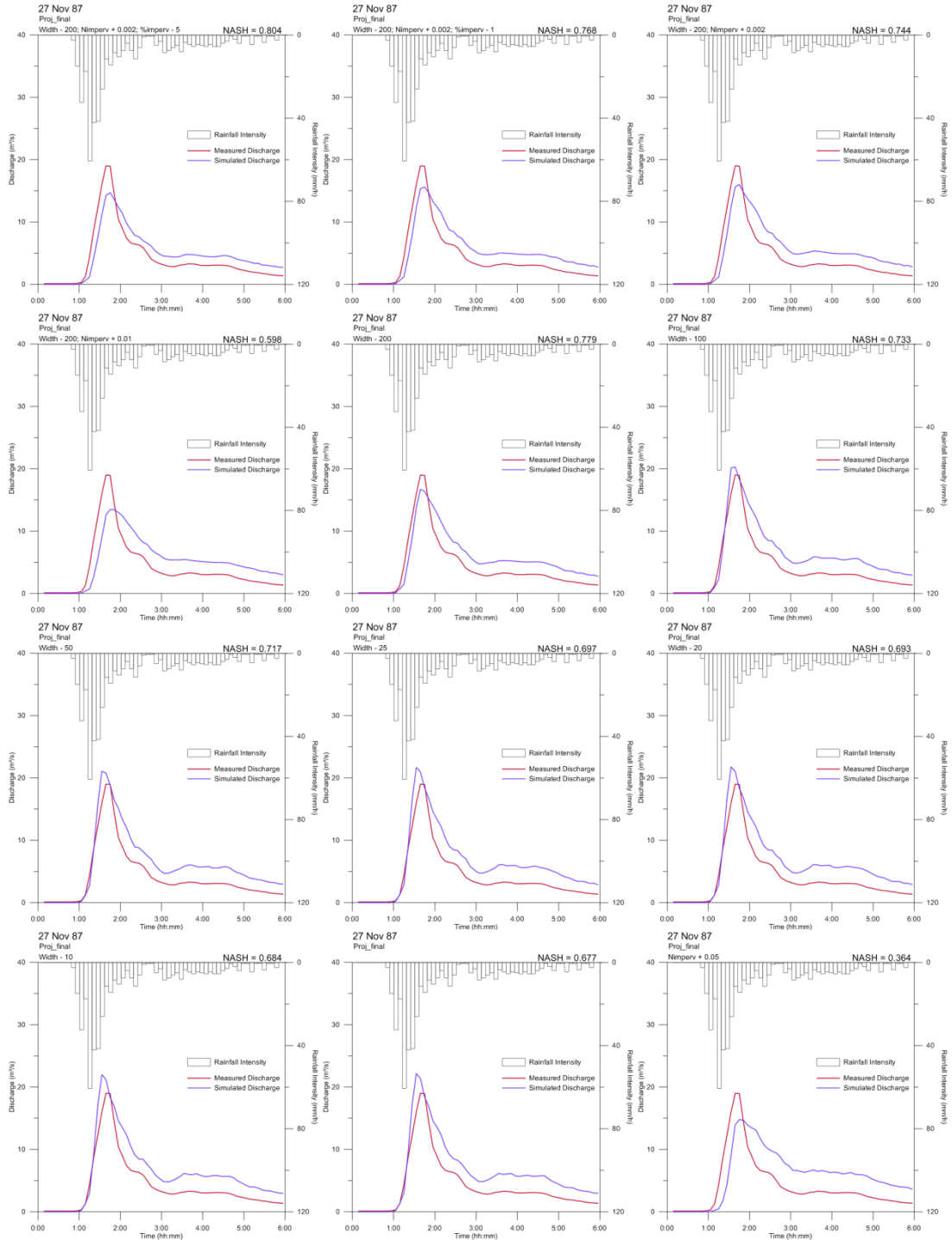


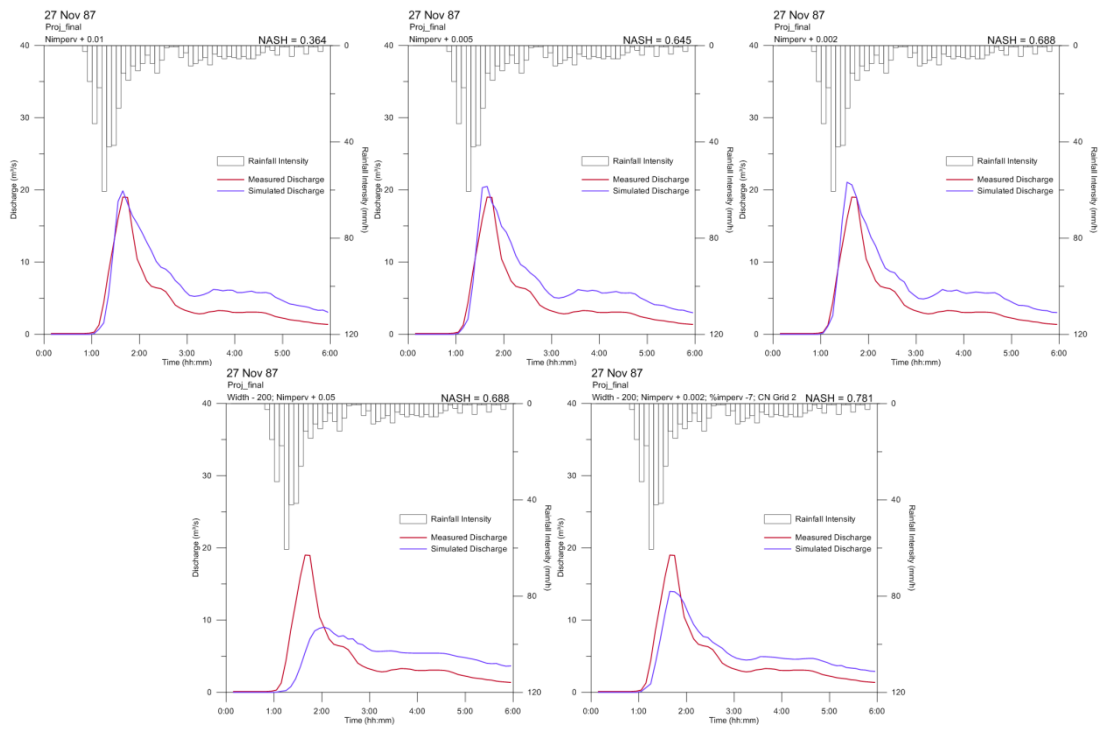
07 Oct 86



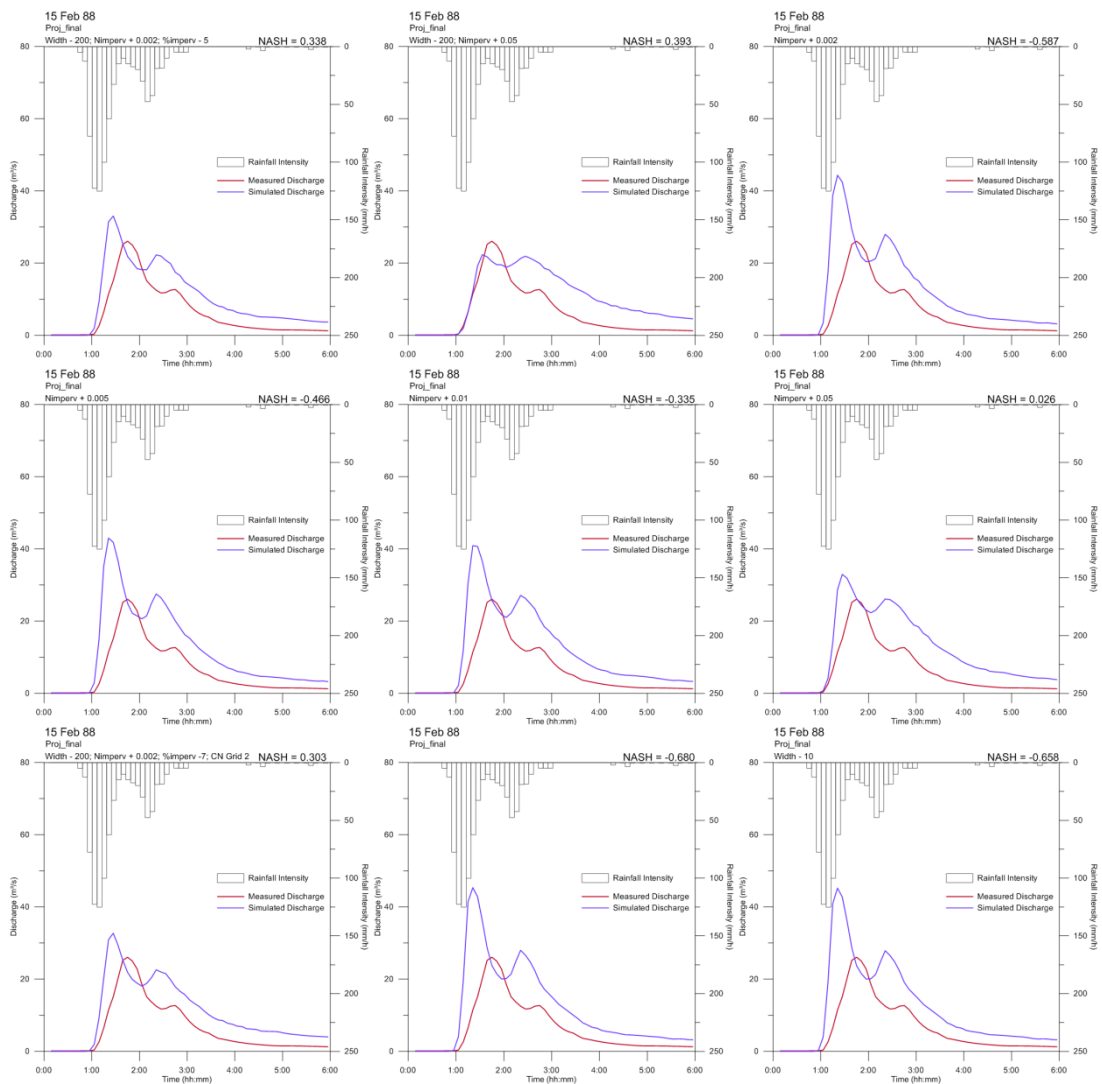


27 Nov 87

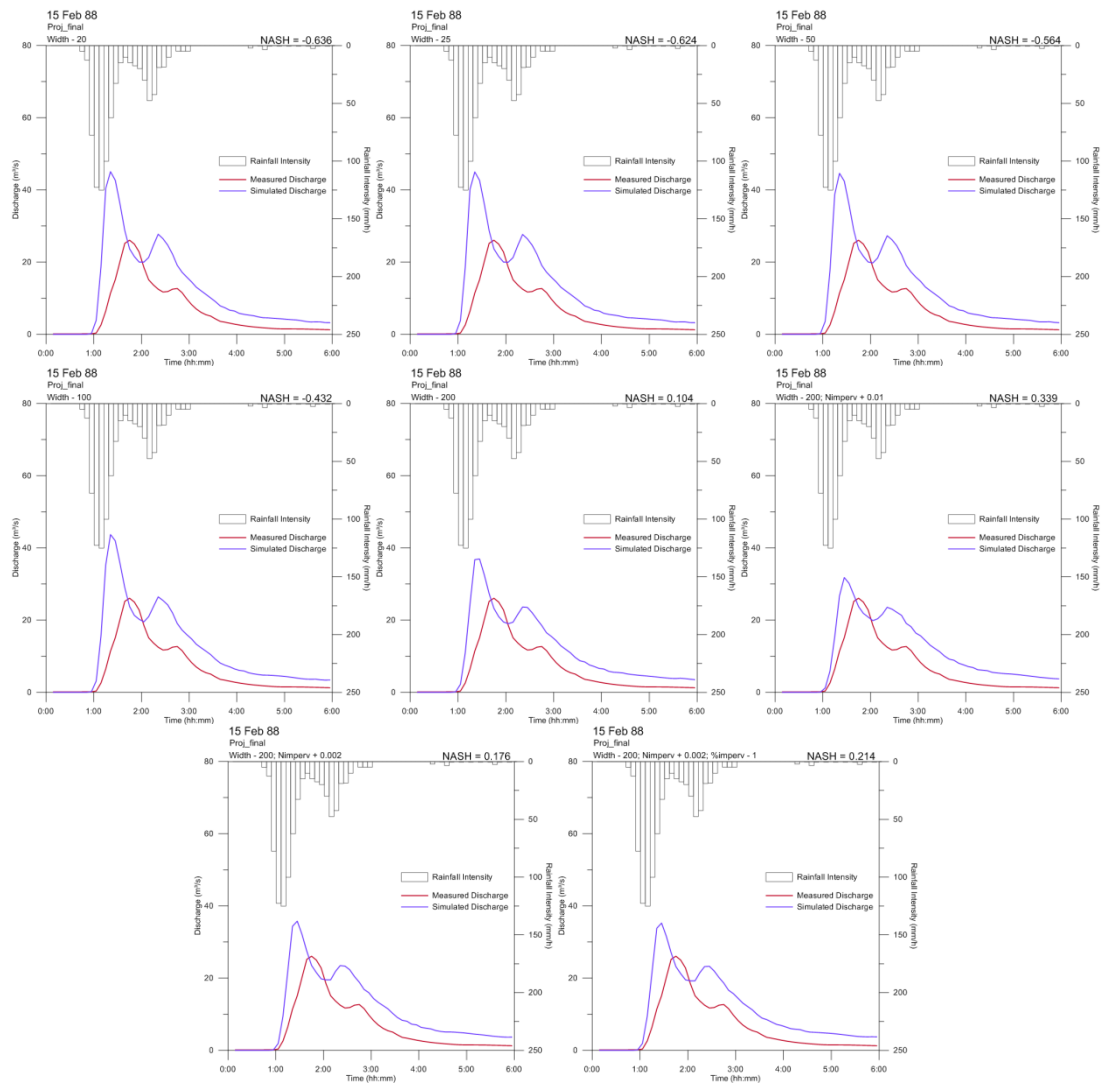




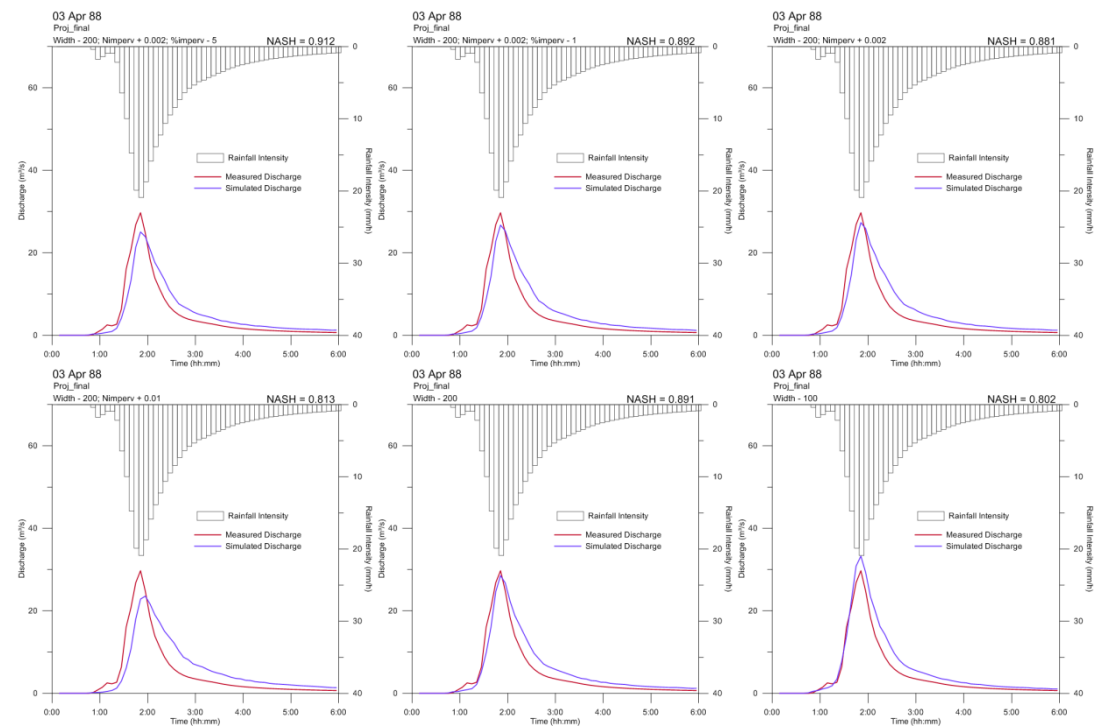
**15 Feb 88**

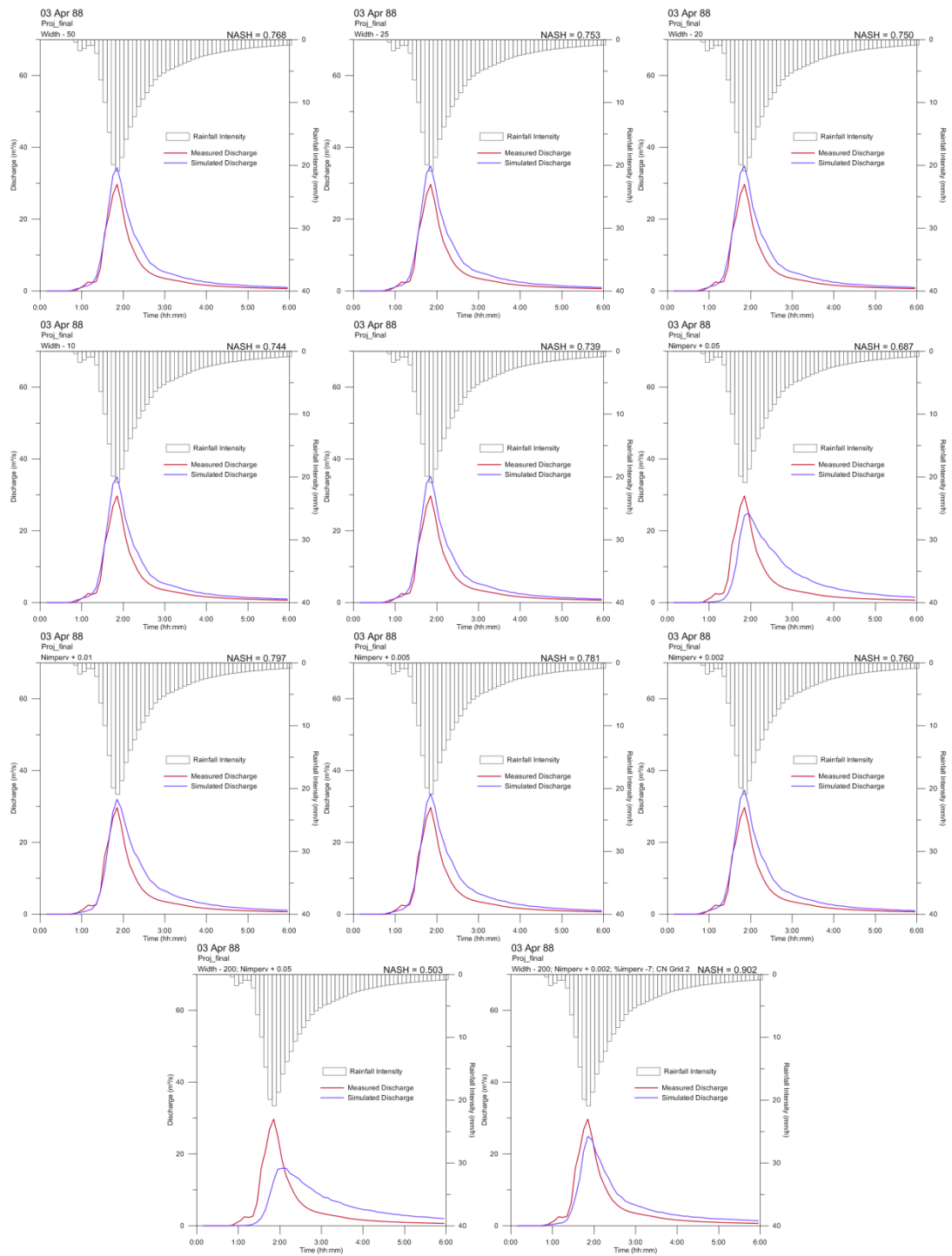




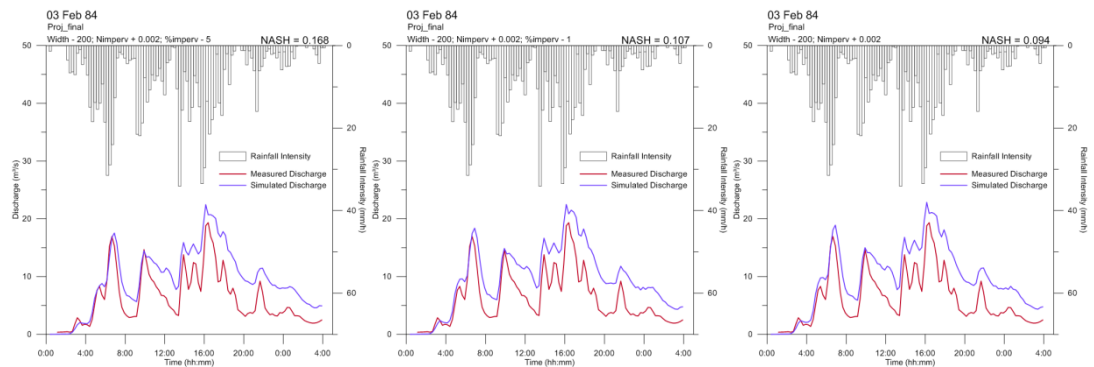


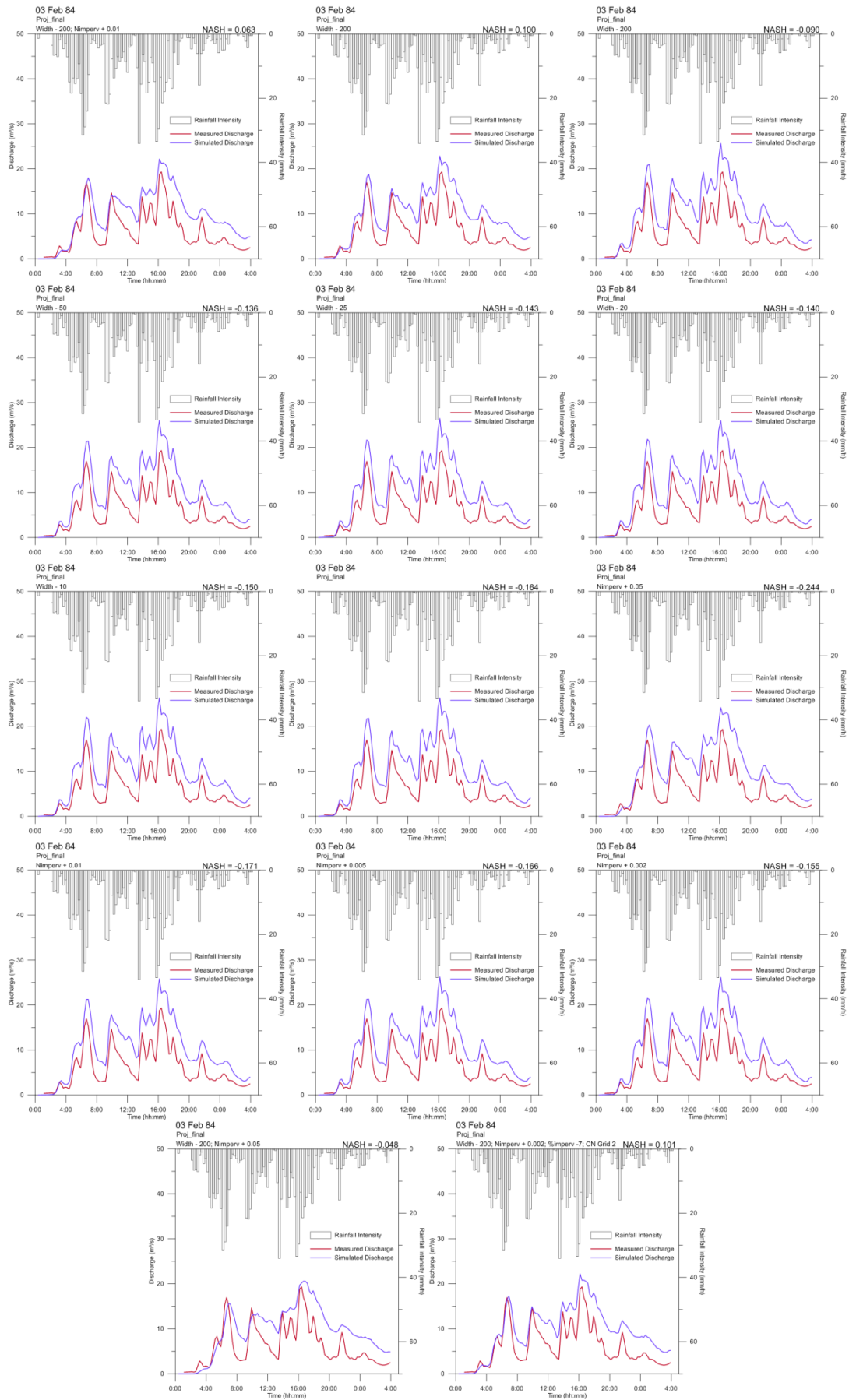
03 Apr 88



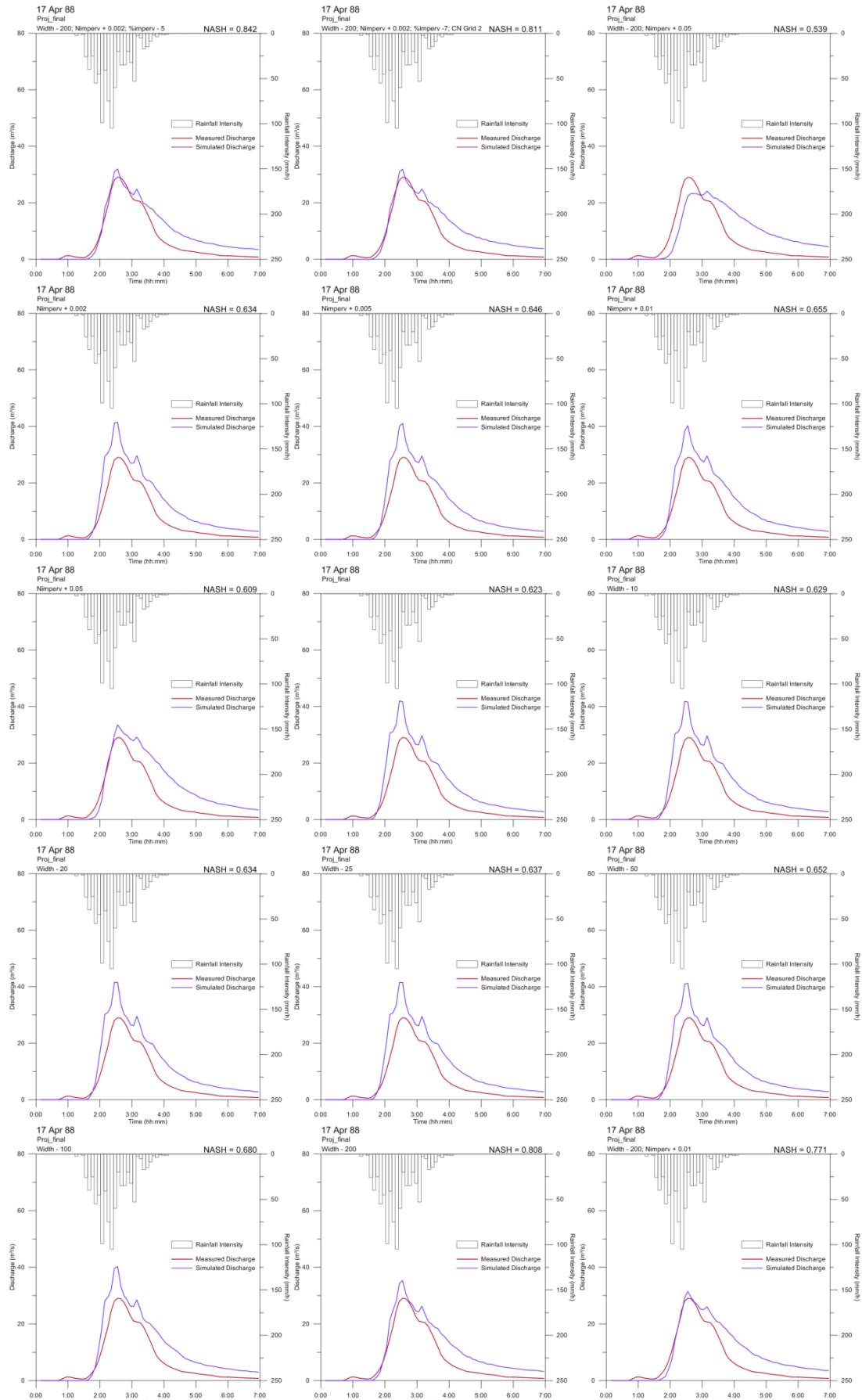


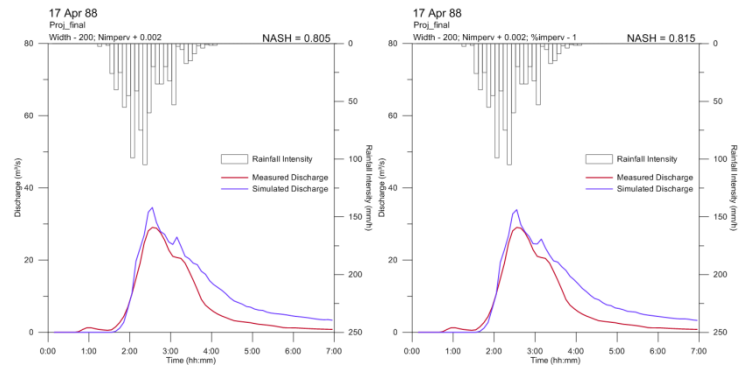
## 03 Feb 84



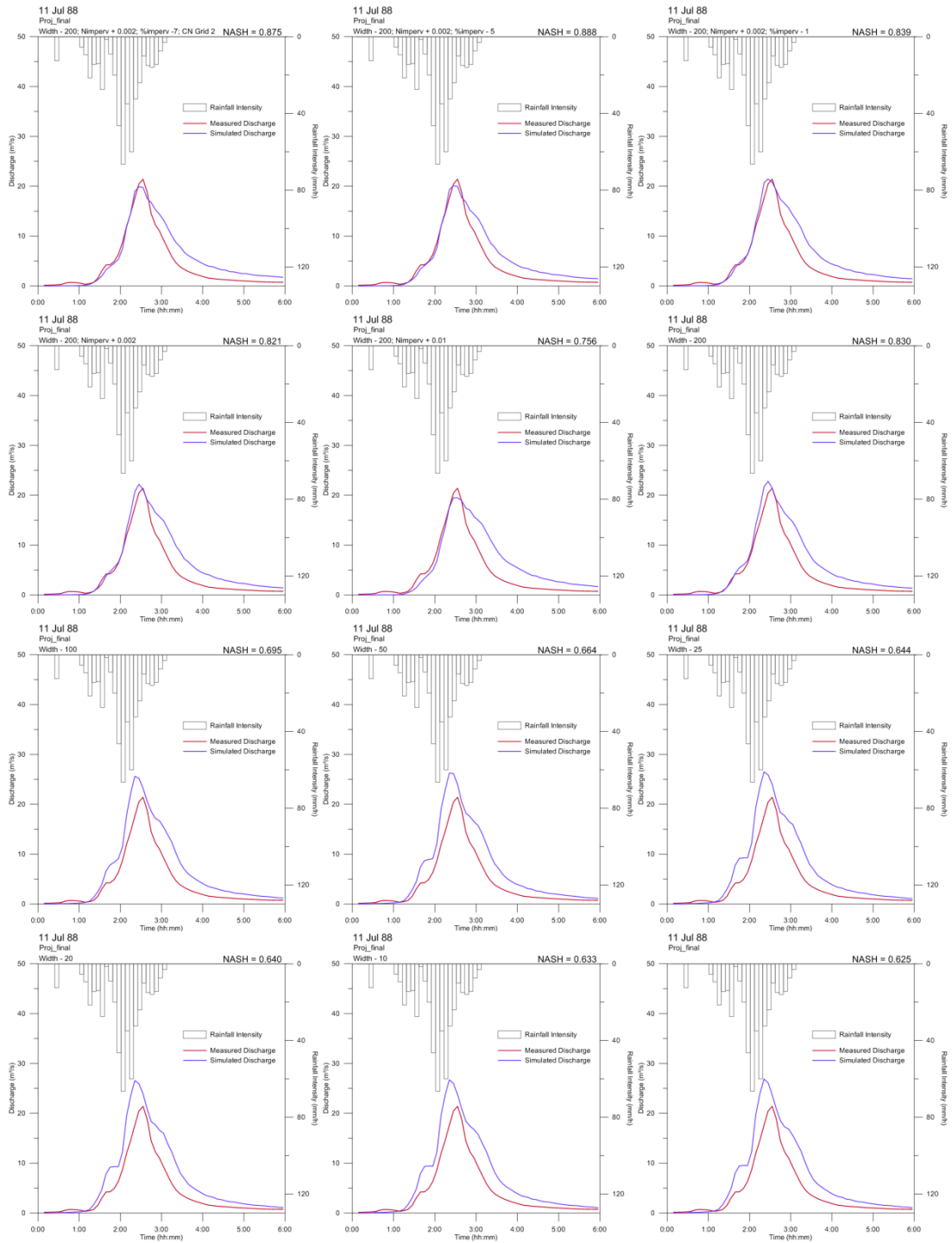


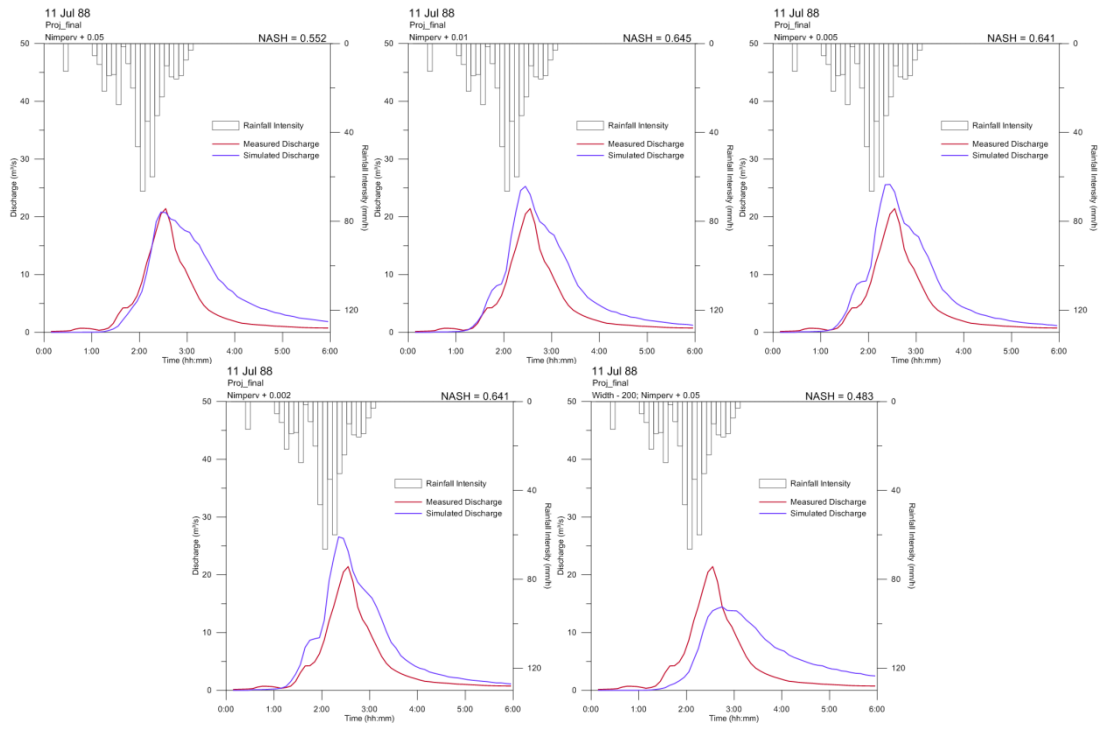
17 Apr 88



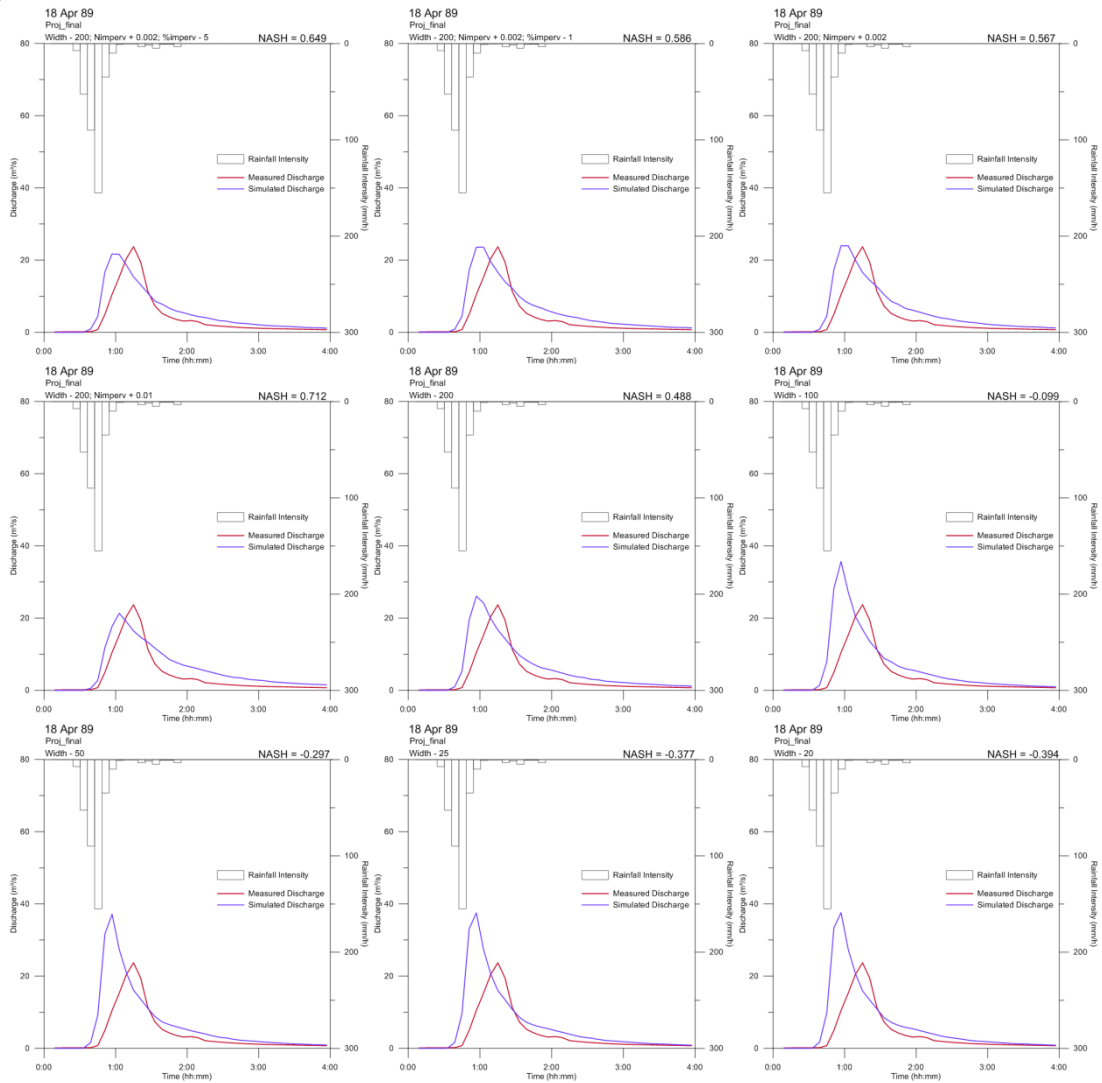


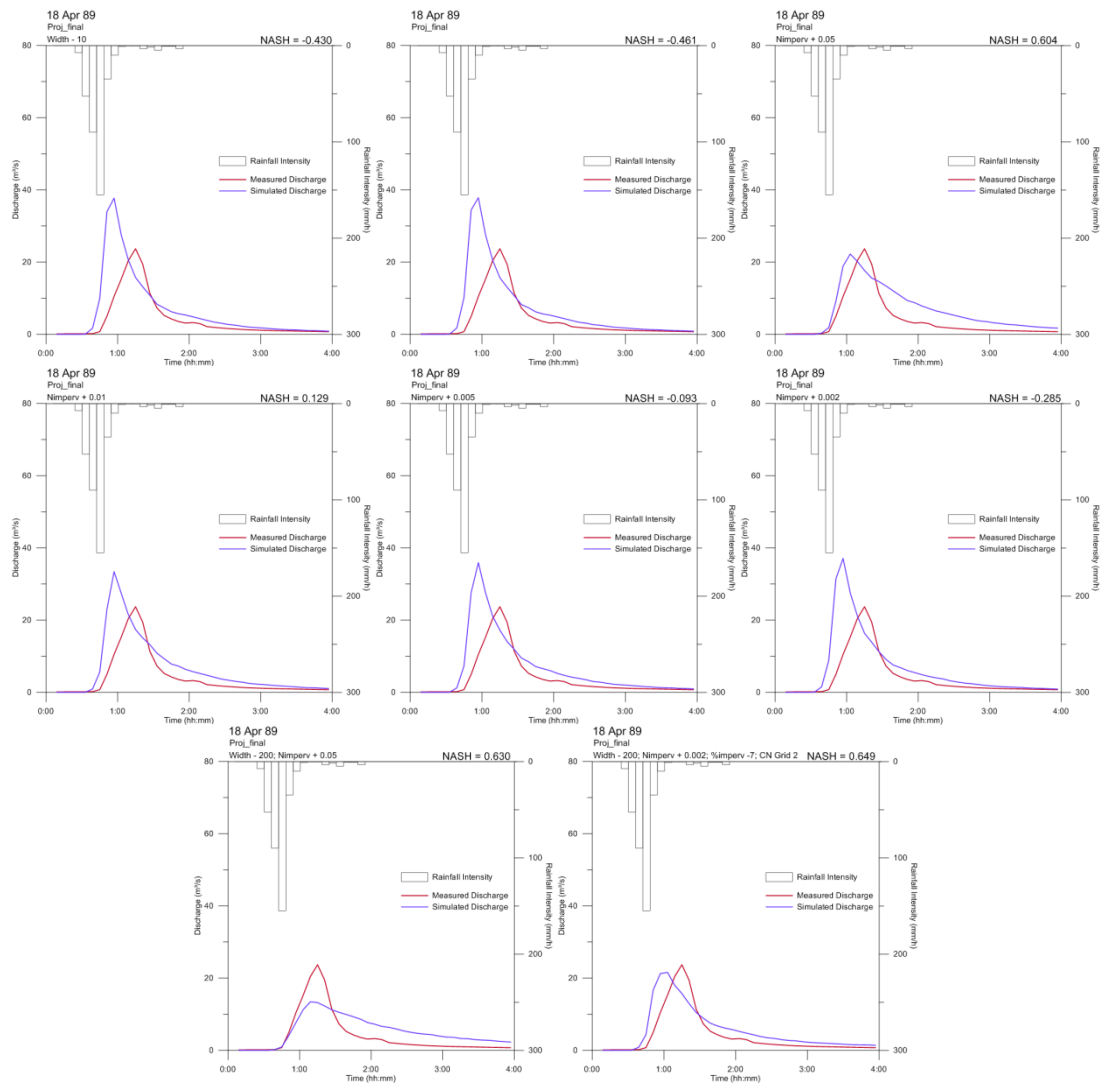
11 Jul 88



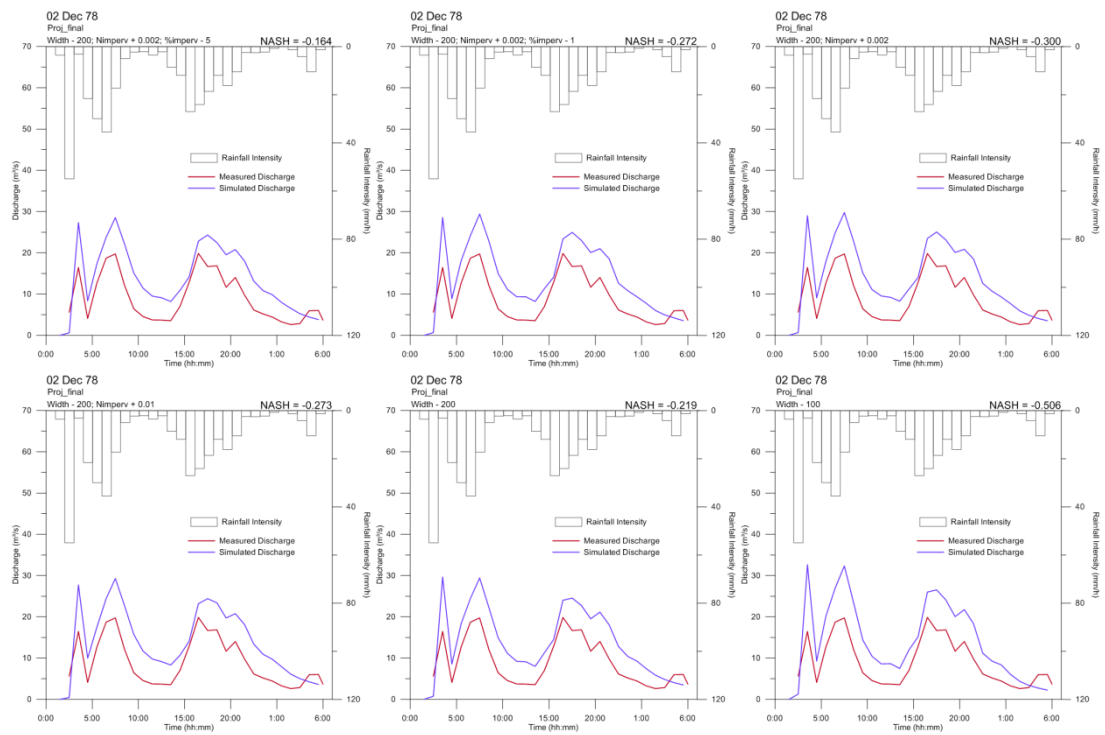


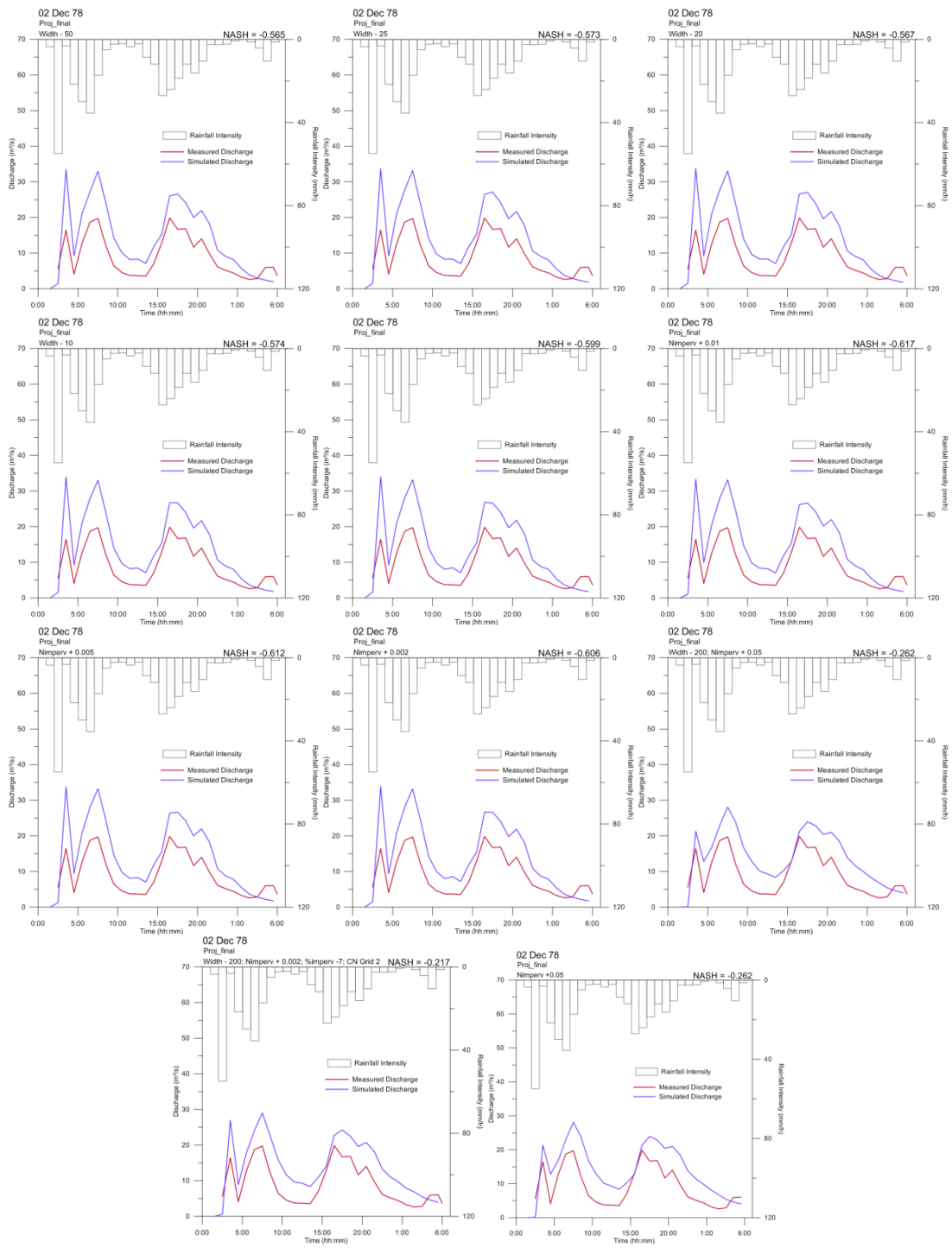
18 Apr 89





## 02 Dec 78







## Appendix 6. Correspondences between old maps legends and current map classification

Old legend	New legend, corresponding to the 2009 map classification
<b>1950</b>	
Sparse residential with open space	Single-family dwellings + Open space*
Forests	Forests
Sparse residential + secondary lowland vegetation	Single-family dwellings + Forests**
Lowland secondary vegetation	Forests
Built-up areas	Multiple-family dwellings + Apartment + Commercial & Educational + Industrial
Open space with little or no trees	Open space
Quarry	Construction site
Cemetery	Open space
<b>1959</b>	
Sparse residential with open space	Single-family dwellings + Open space*
Forests	Forests
Sparse residential + lowland secondary vegetation	Single-family dwellings + Forests**
Lowland secondary vegetation	Forests
Built-up areas	Multiple-family dwellings + Apartment + Commercial & Educational + Industrial
Open space with little or no trees	Open space
Quarry	Construction site
Cemetery	Open space
Murnane Reservoir	Lake
<b>1973</b>	
Lowland Rainforest	Forests
Tall Secondary Forest	Forests
Low Secondary Forest	Forests
Grass & Shrub	OpenSpace + Forests***
Suburban Gardens	Single-family dwellings + General vegetation**
Mown Grass	Open Space
Mixed Tree Crops	Forest
Urban	Multiple-family dwellings + Apartment + Commercial & Educational
Industrial	Industrial
Quarry	Construction site
Murnane Reservoir	Lake
<b>1986</b>	
Dense residential little open space	Multiple-family dwellings
Dense residential bigger open space	Single-family dwellings
Sparse residential + Lowland veget	Single-family dwellings + Forests**
Open space with little or no trees	Open space
Secondary lowland vegetation	Forests
Forests	Forests
Construction	Construction site
Quarry	Construction site
Commercial+Educational	Commercial + Educational
Industrial	Industrial
Service reservoir	Lake

### Assumptions:

\* 50% Single-Family dwellings, 50% Open space

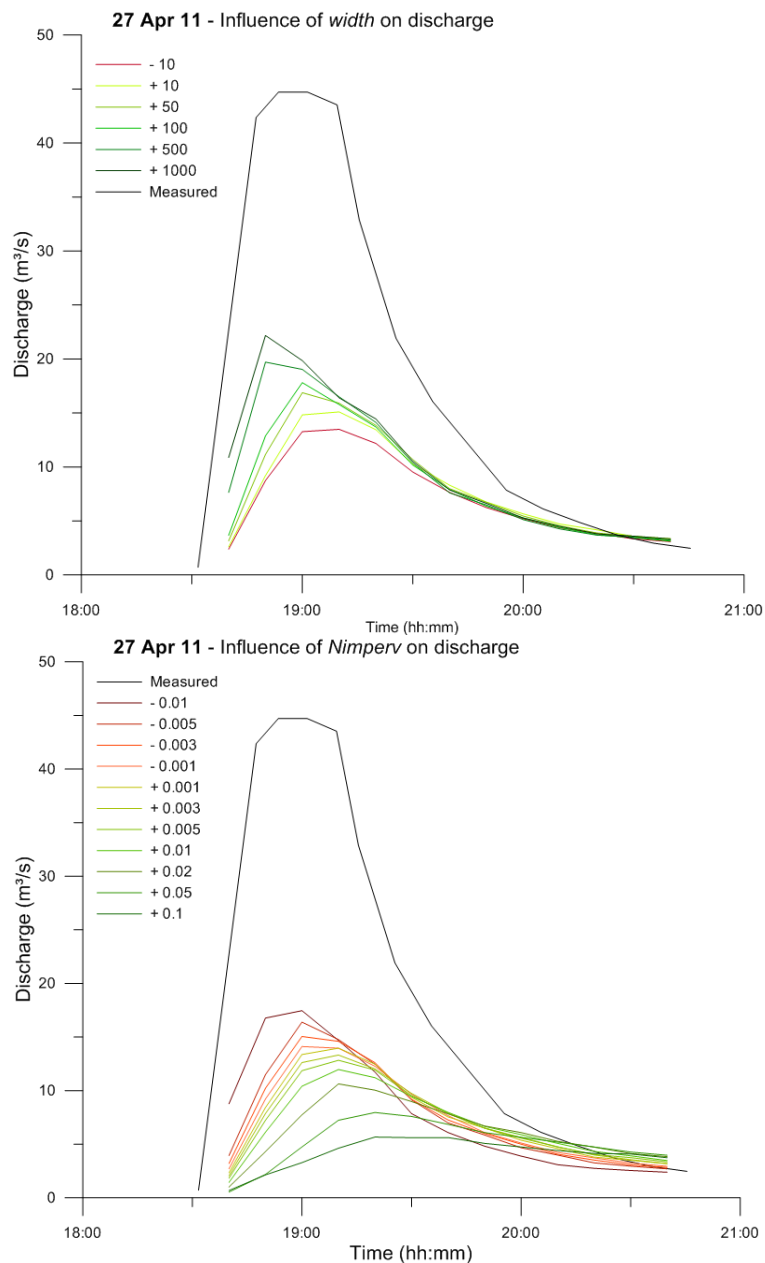
\*\* 20% Single-Family dwellings, 80% Forests (according to Chuah (1987), this class represents lowland secondary vegetation with scattered houses)

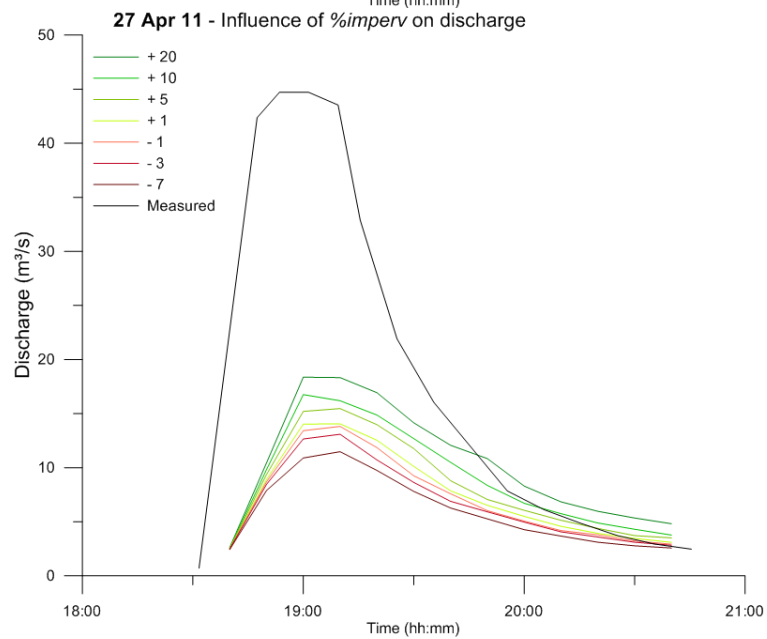
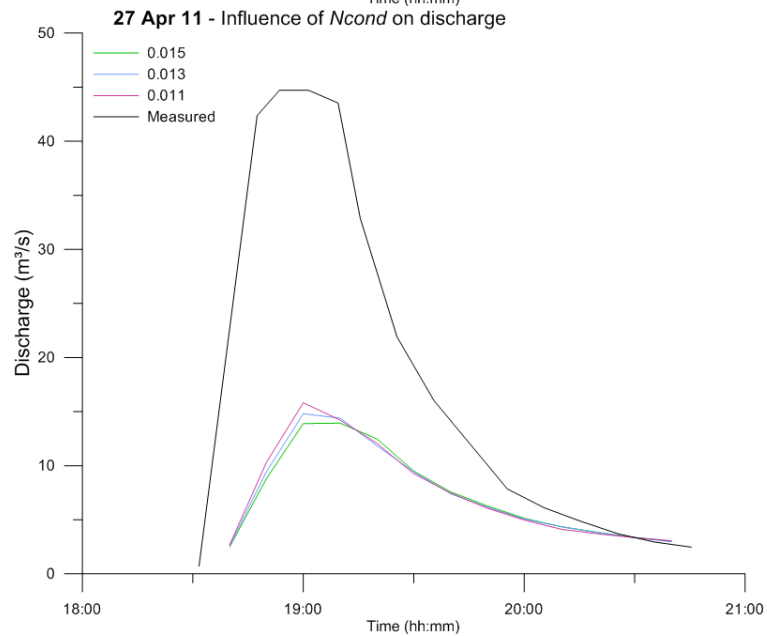
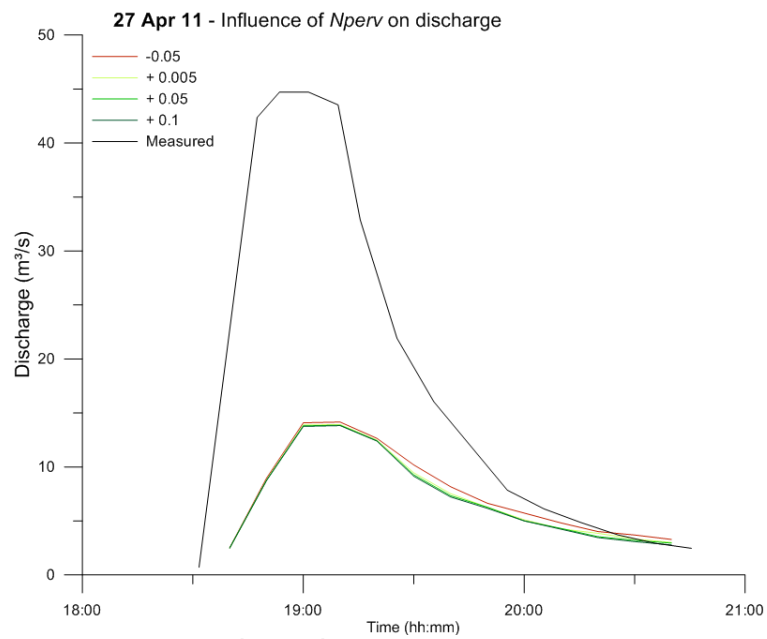
\*\*\* 50% Open space, 50% Forests

## Appendix 7. Influence SWMM parameters on the modelled discharge for recent events

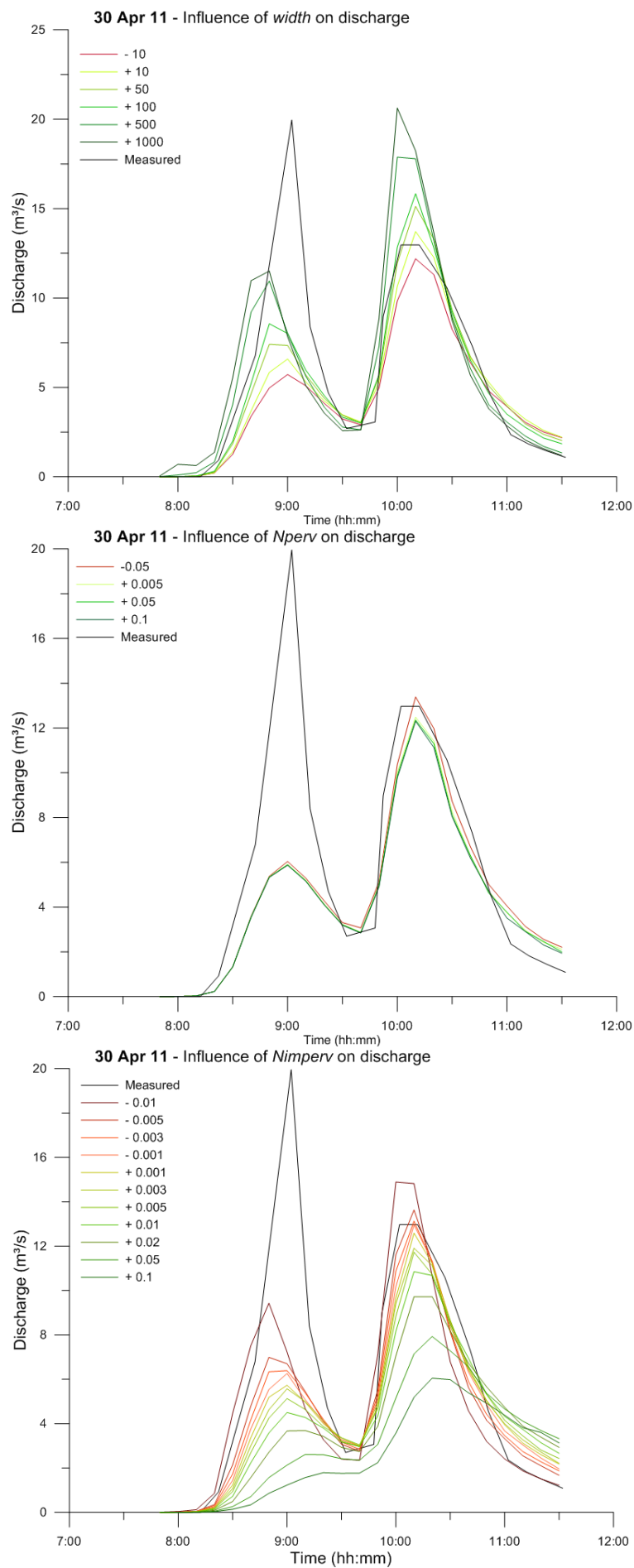
Parameters tested: width, Manning's coefficient of impervious/pervious areas ( $N_{imperv}/N_{perv}$ ), percentage of impervious areas ( $\%imperv$ ) and Manning's coefficient of concrete conduits ( $N_{cond}$ )

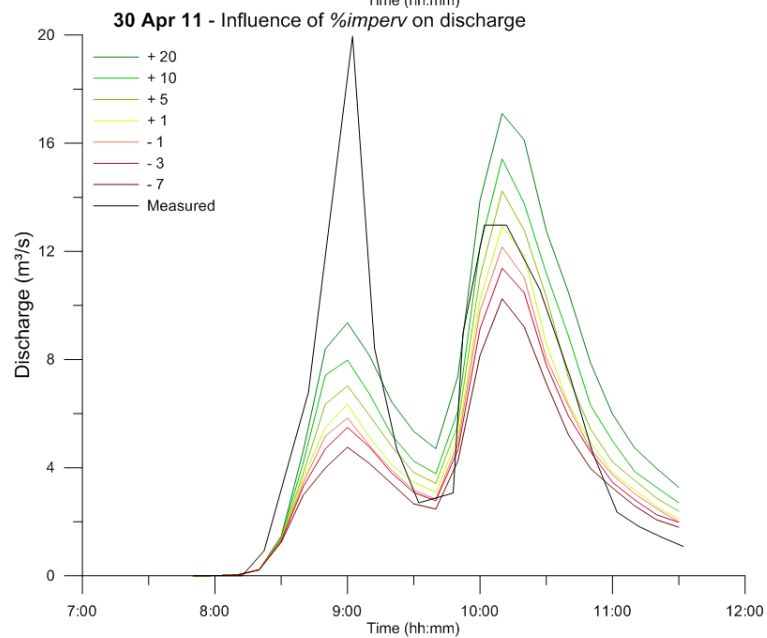
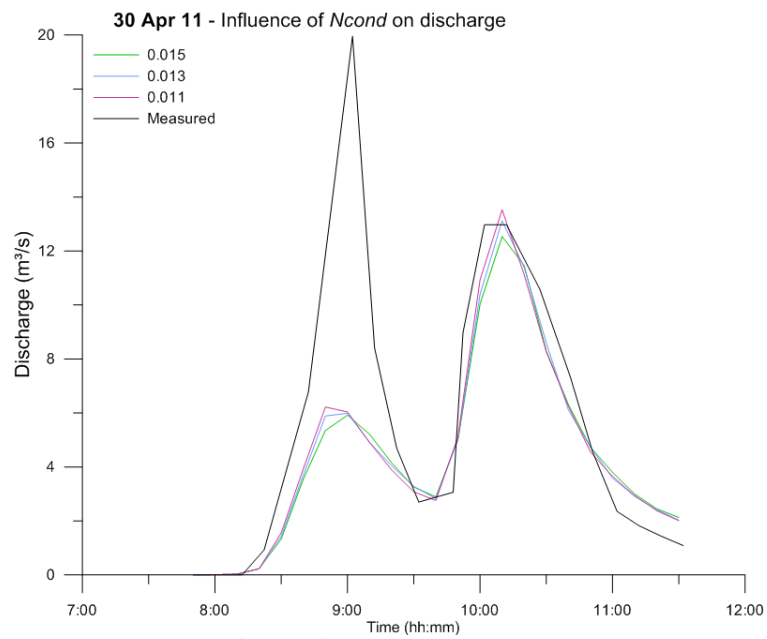
27<sup>th</sup> of April, 2011



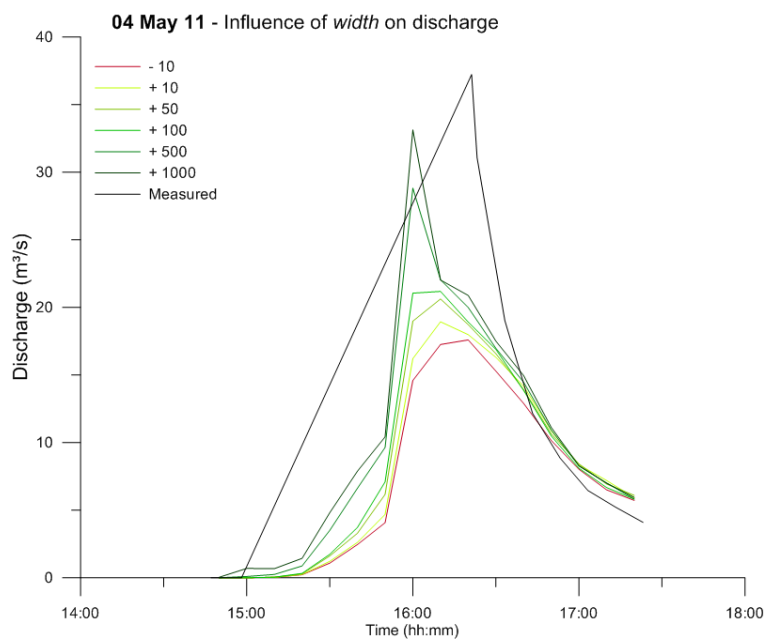


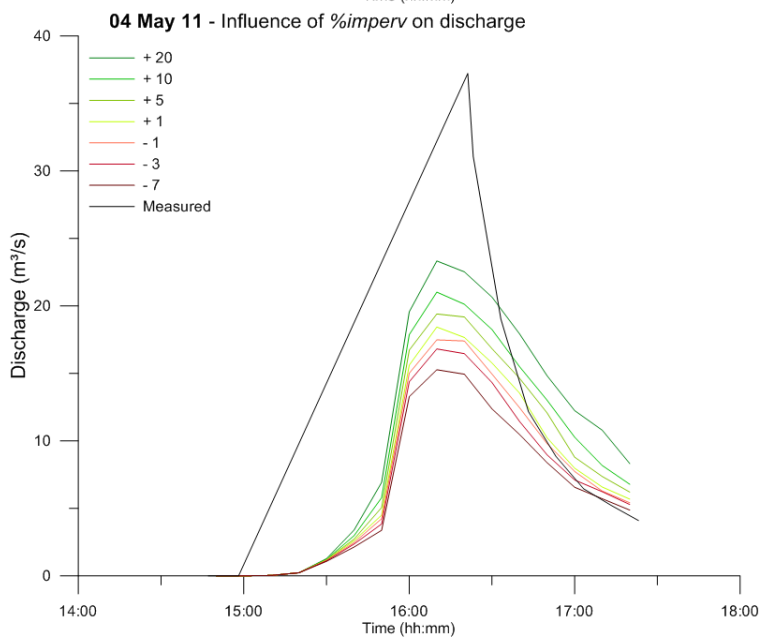
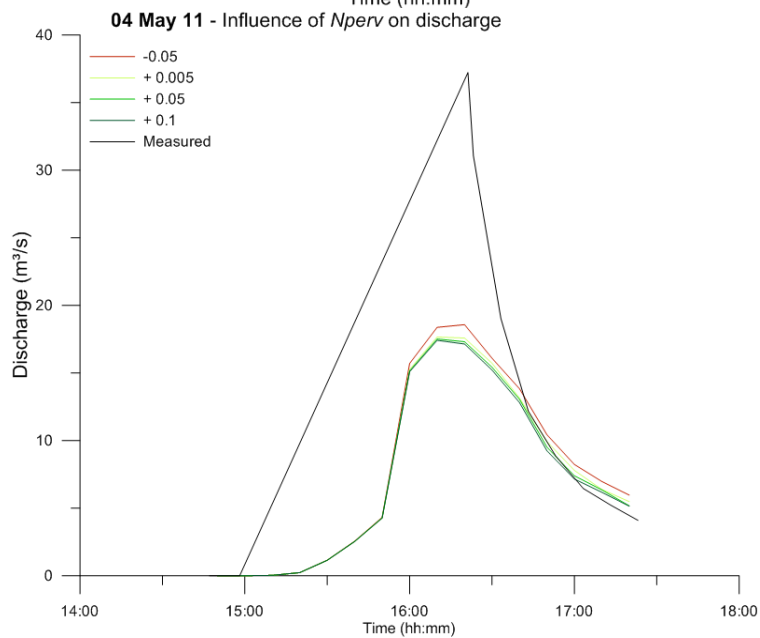
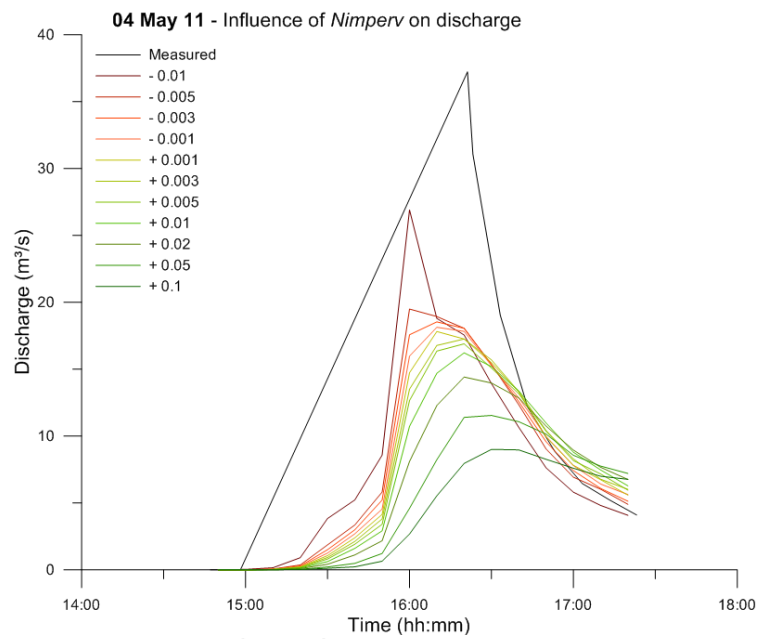
30<sup>th</sup> of April, 2011

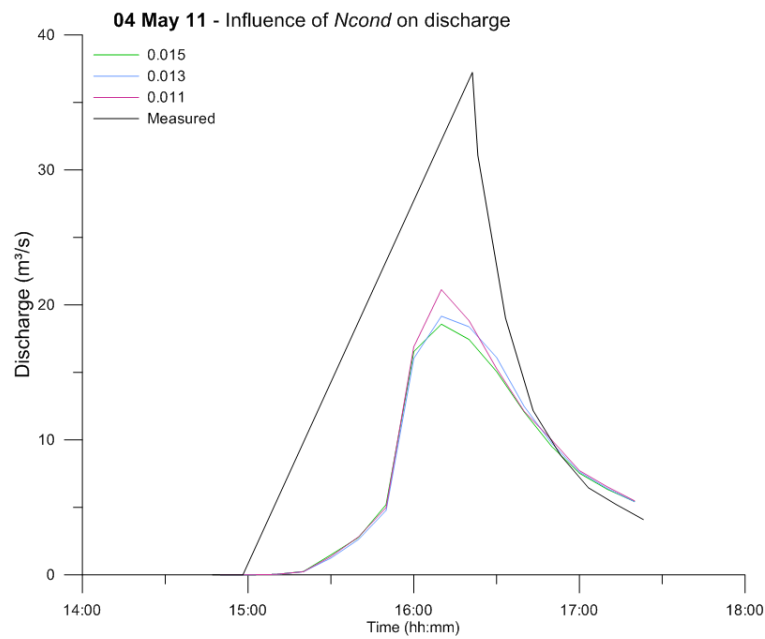




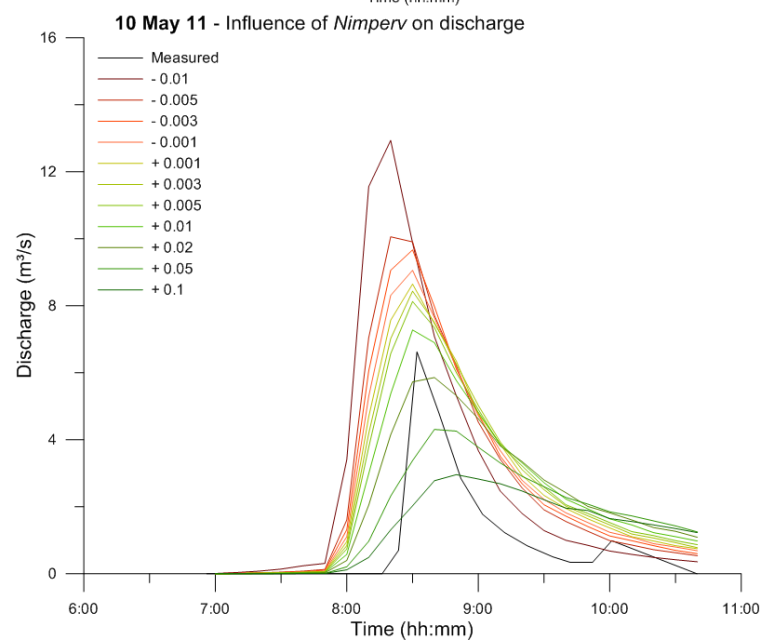
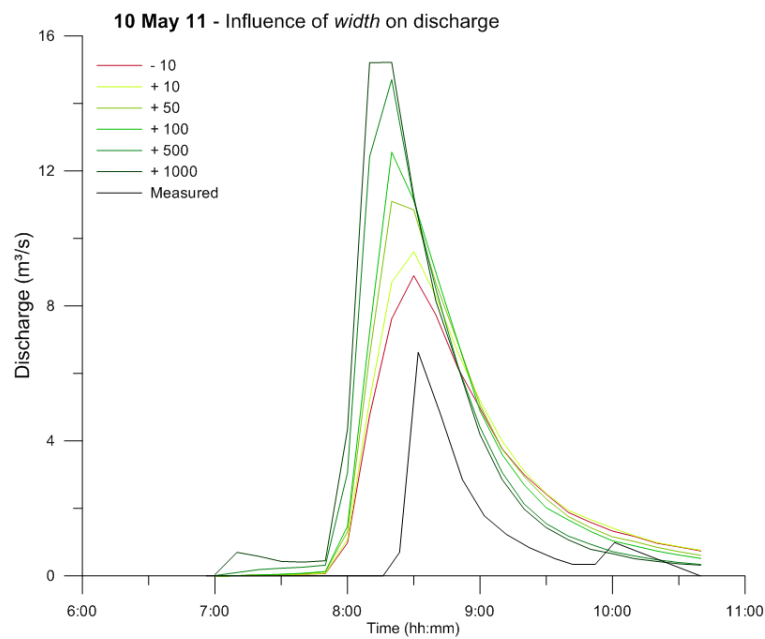
**4th of May 2011**

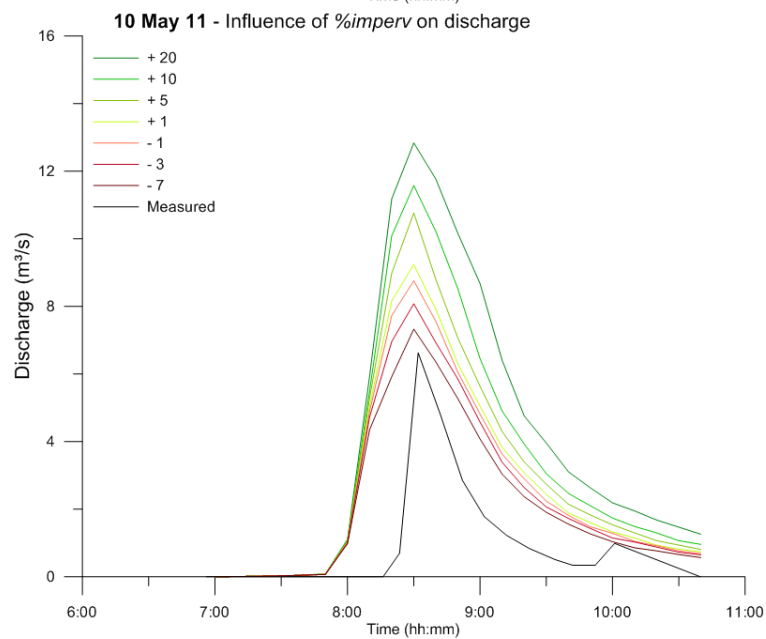
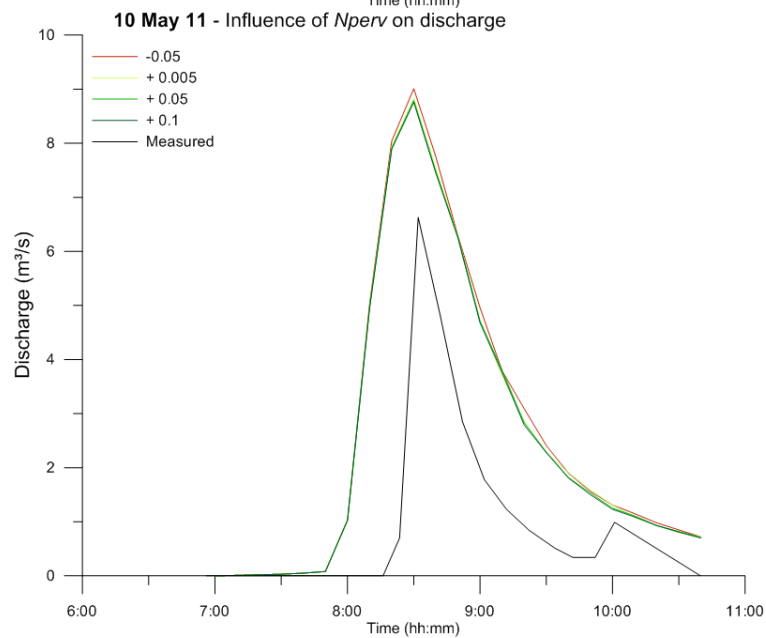
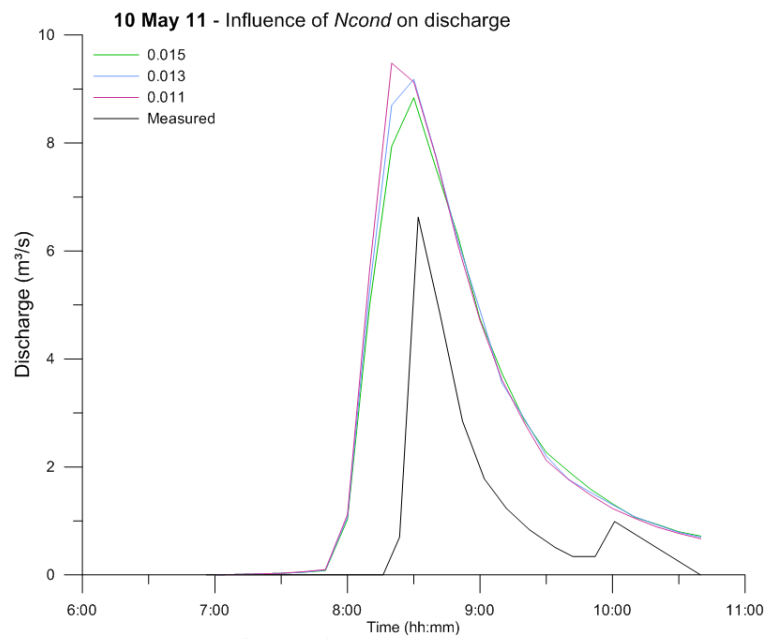






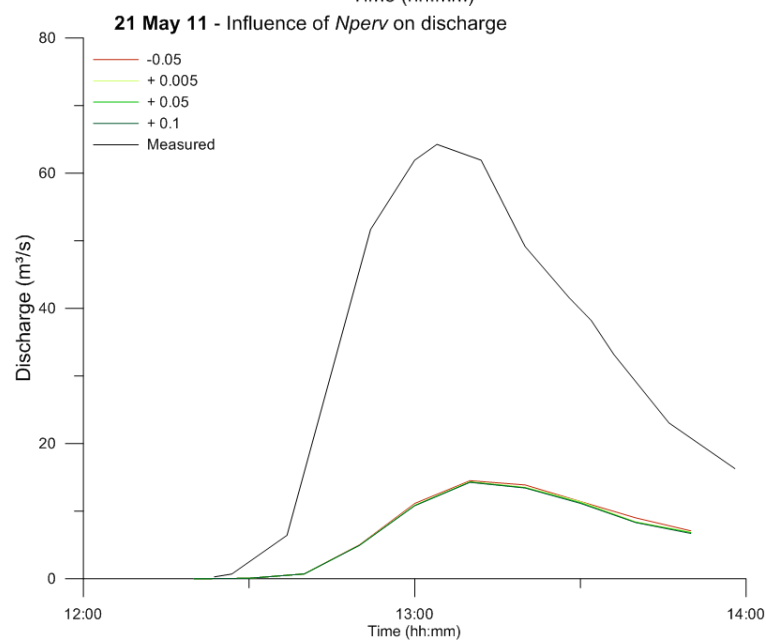
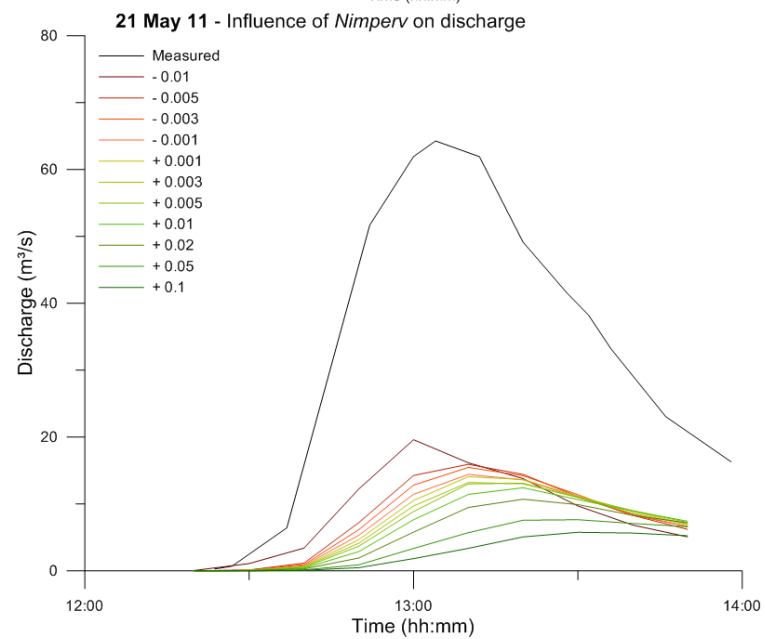
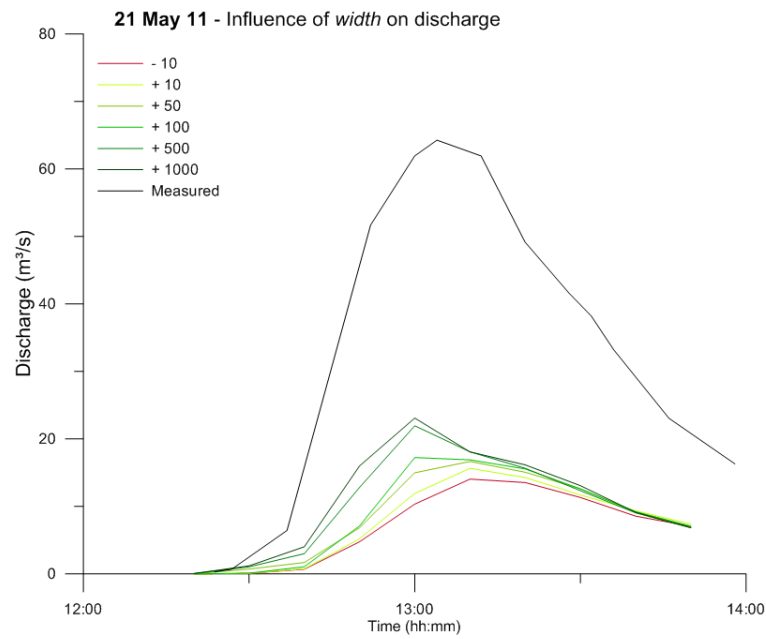
**10<sup>th</sup> of May, 2011**

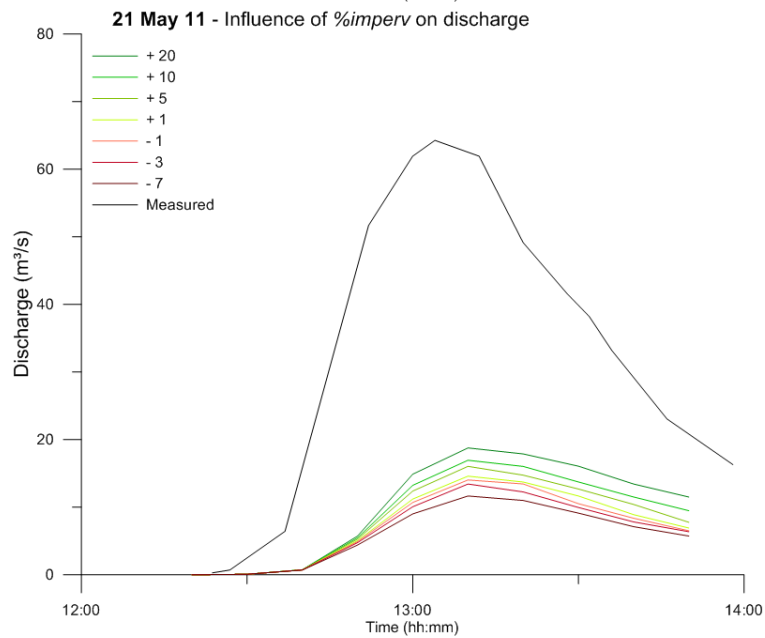
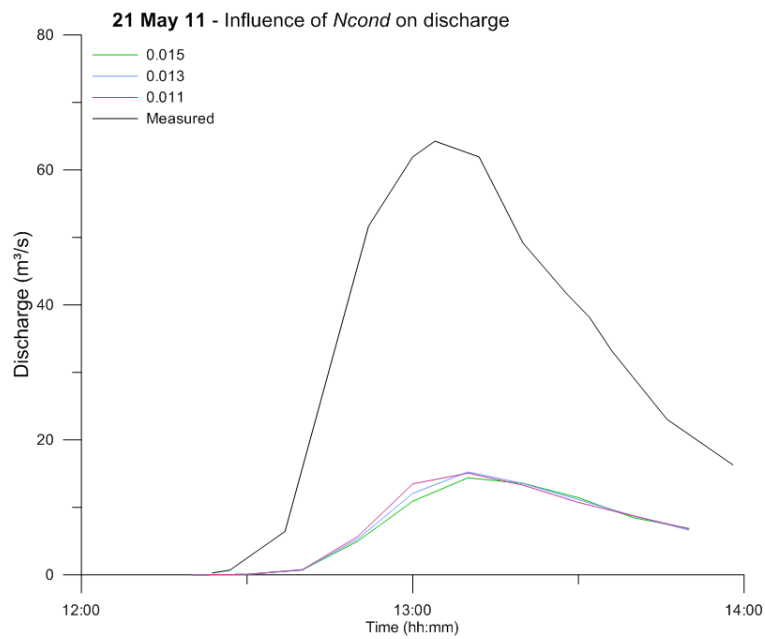




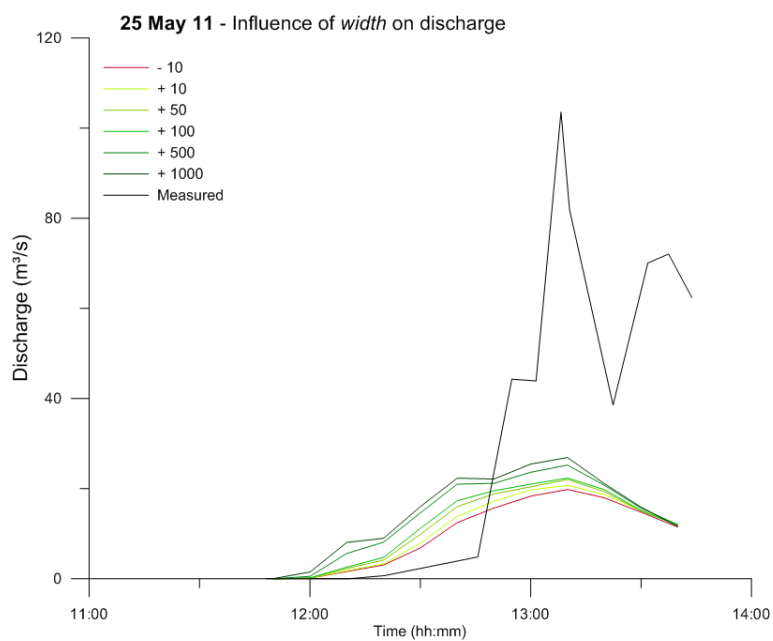


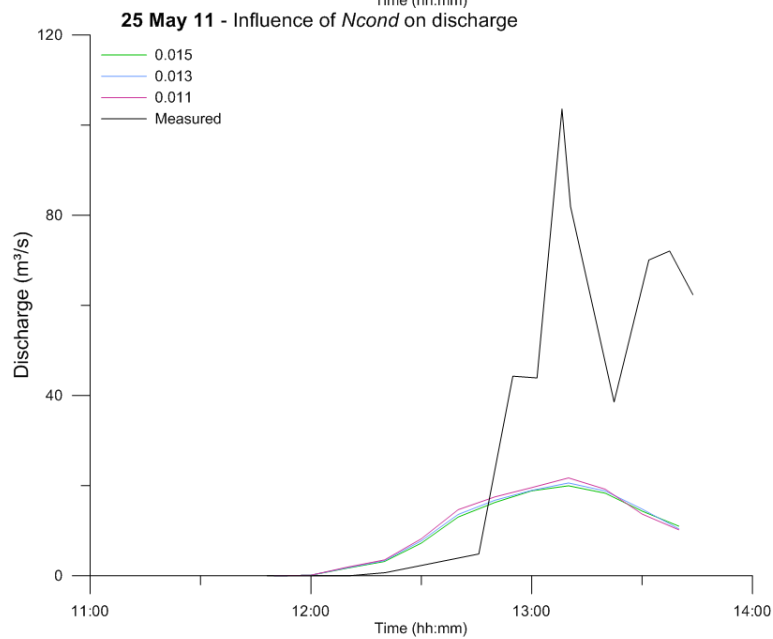
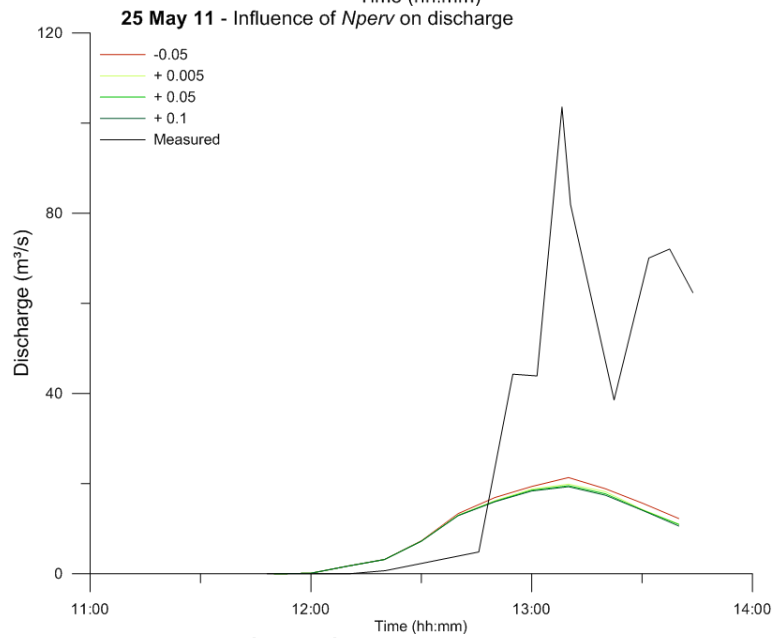
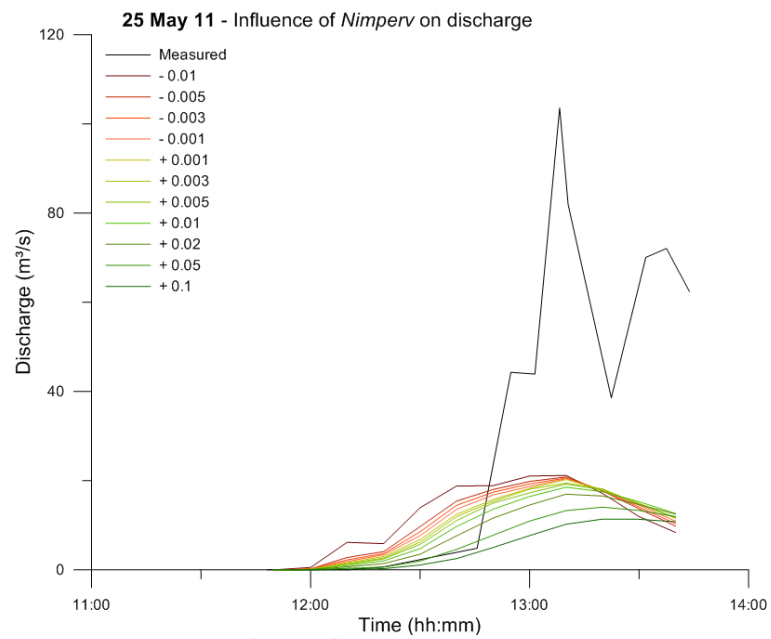
21<sup>th</sup> of May, 2011

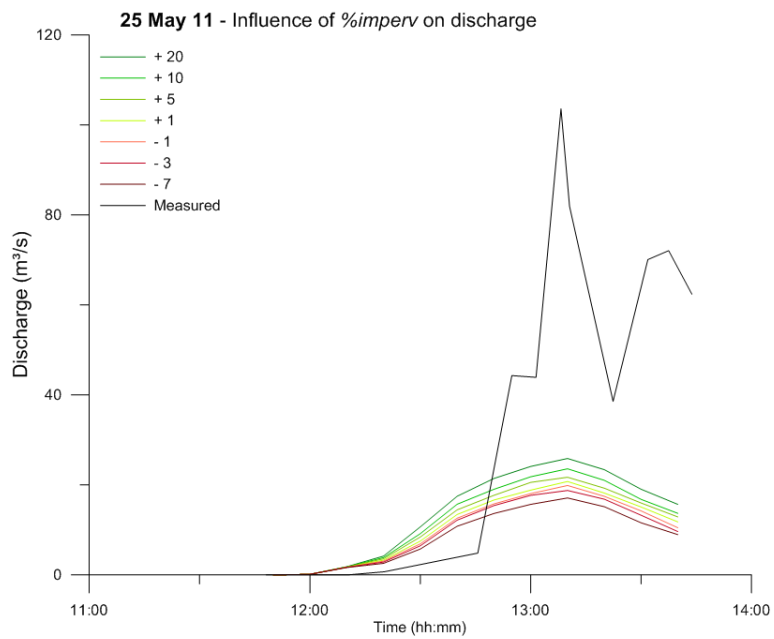




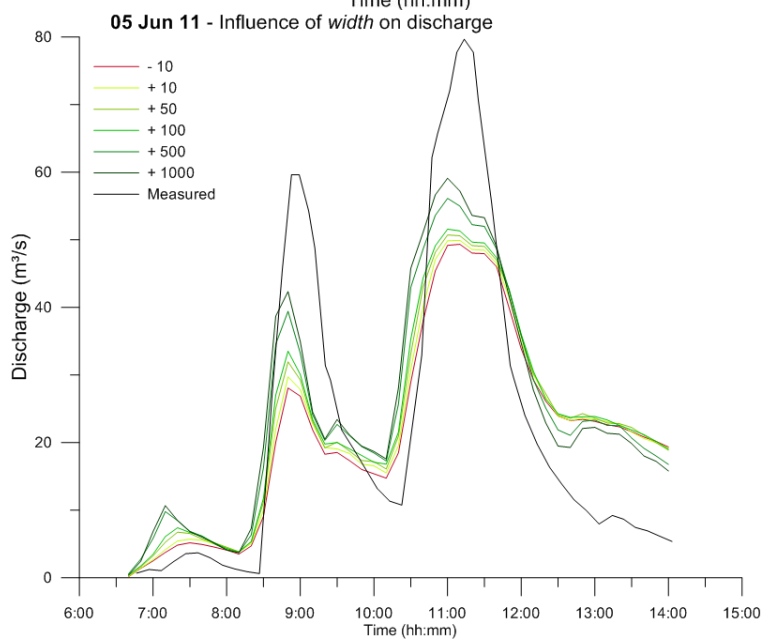
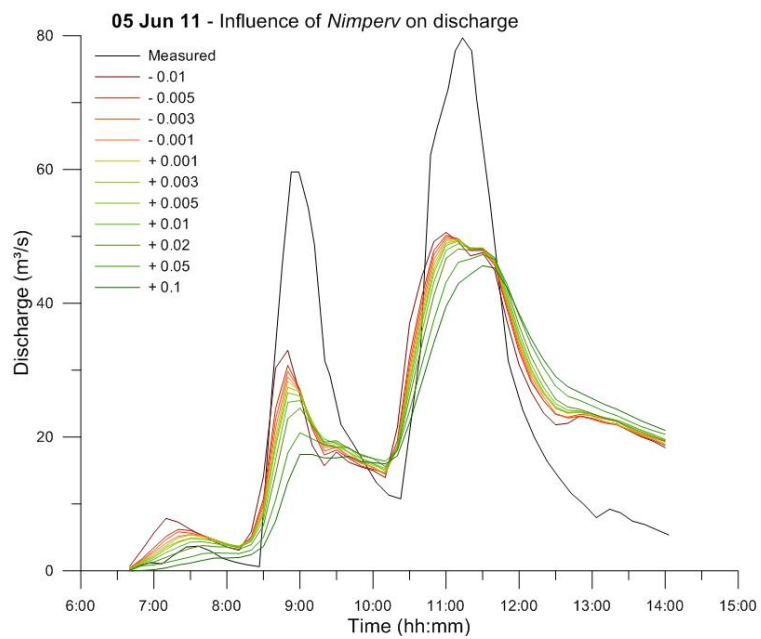
**25<sup>th</sup> of May, 2011**

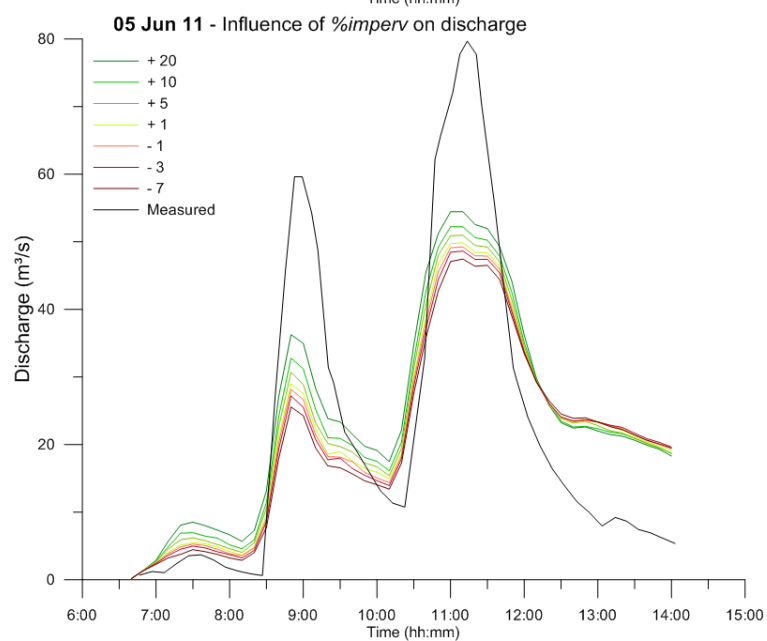
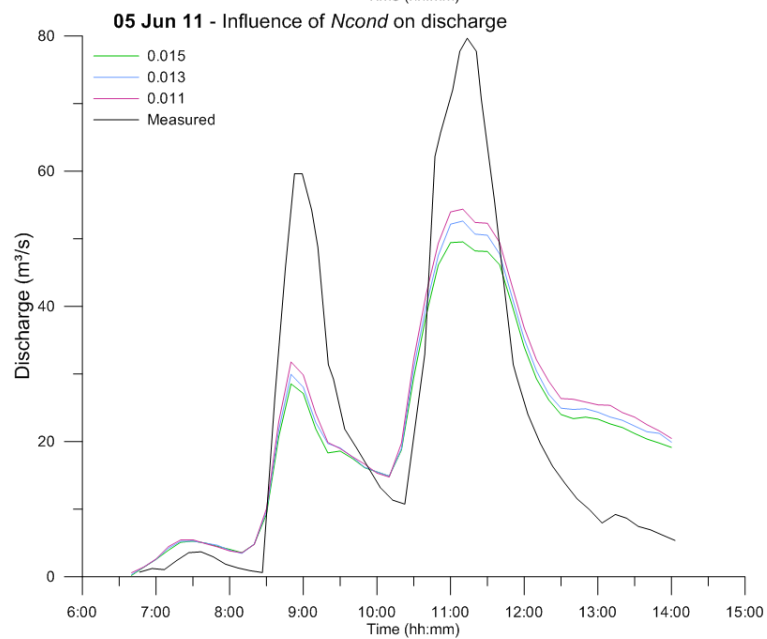
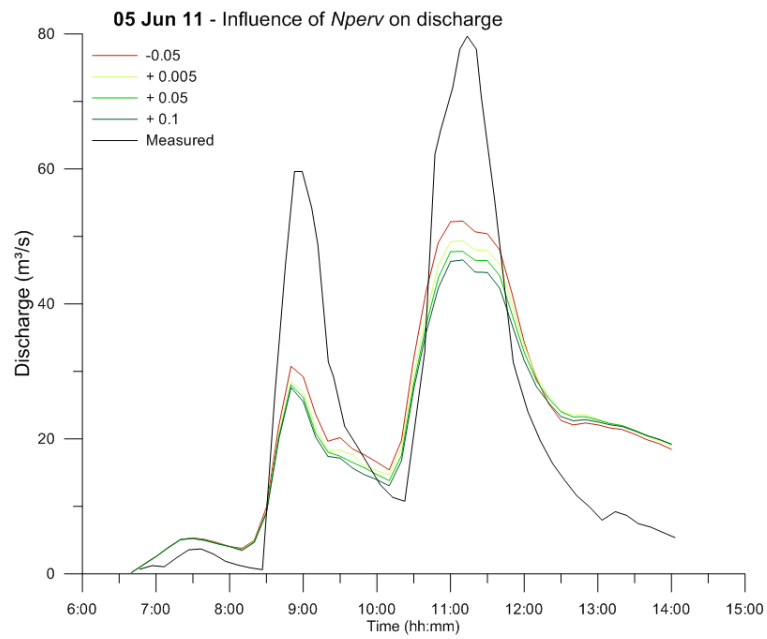




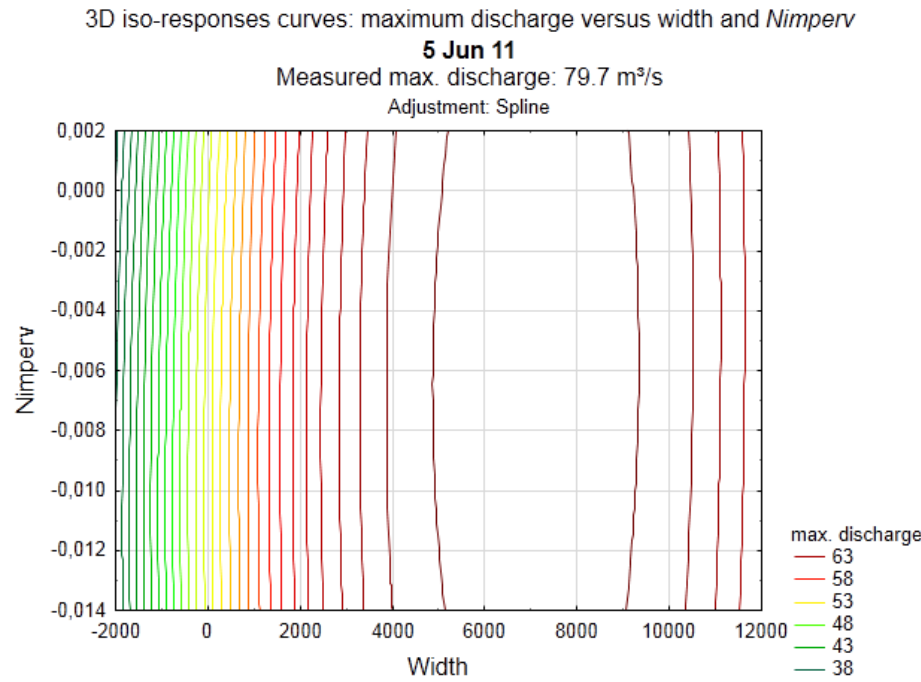


**5<sup>th</sup> of June, 2011**





Appendix 8. 3D iso-responses curves, 5<sup>th</sup> of June, 2011.



## Appendix 9. HEC-HMS: simulated versus modelled hydrographs

The graphs presented here are:

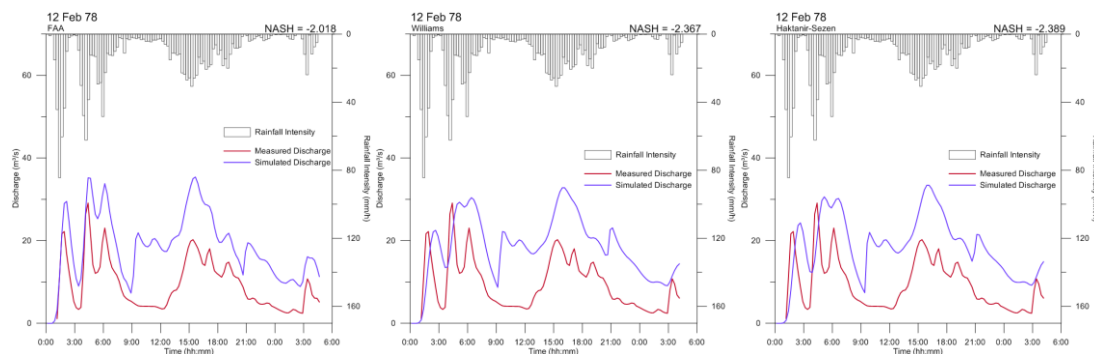
- 12 Feb 78;
- 03 Feb 84;
- 02 Jul 84;
- 03 Jan 85;
- 01 Aug 86;
- 27 Nov 87;
- 15 Feb 88;
- 03 Apr 88;
- 17 Apr 88;
- 11 Jul 88;
- 18 Apr 89;
- 02 Mar 84.

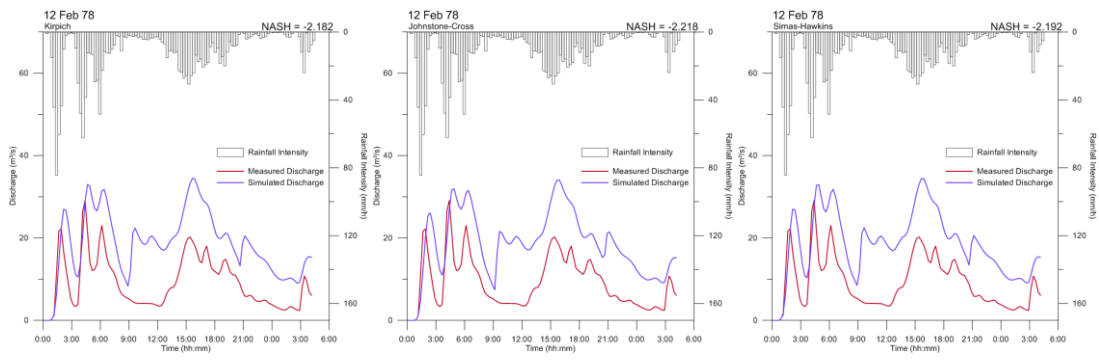
From left to right, top to the bottom, the methods for estimating the time of concentration are:

- FAA;
- Williams;
- Haktanir-Sezen;
- Kirpich;
- Johnstone- Cross and;
- Simas-Hawkins.

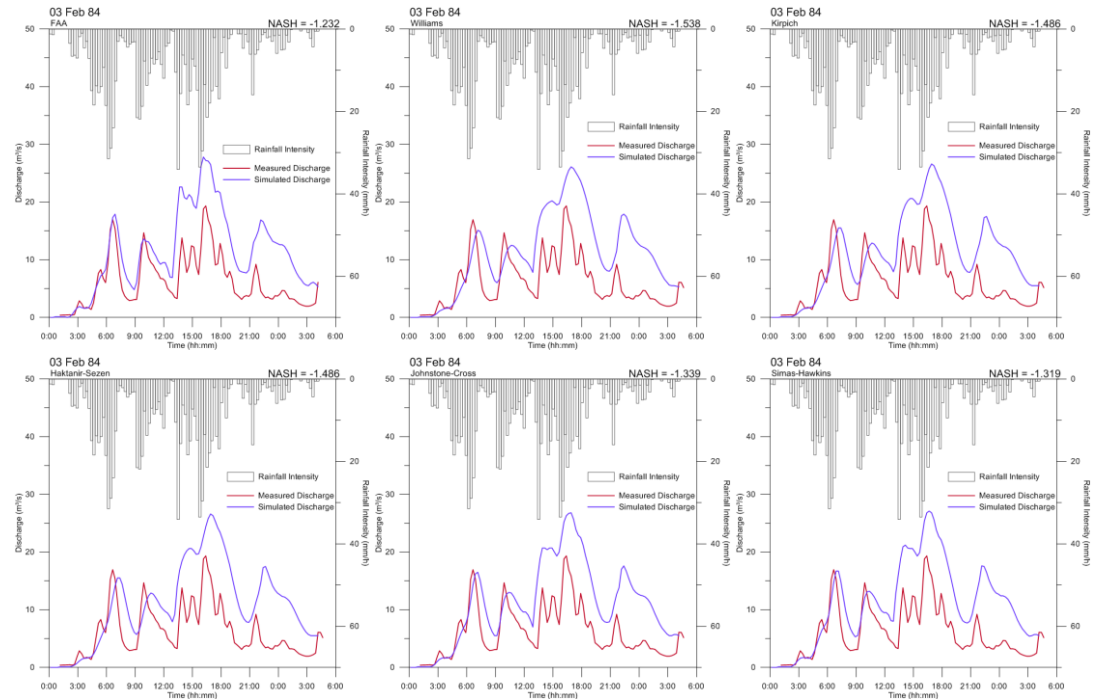
Time (hh:mm) figures on X axis, discharge ( $\text{m}^3/\text{s}$ ) figures on Y left axis and rainfall intensity (mm/h) figures on Y right axis. Measured discharge is in red, simulated discharge in blue. The Nash-Sutcliffe coefficient is noted on the right hand side of each graph. In order to allow a global view of the curves and to save space, graphs presented here are reduced.

### 12 Feb 78

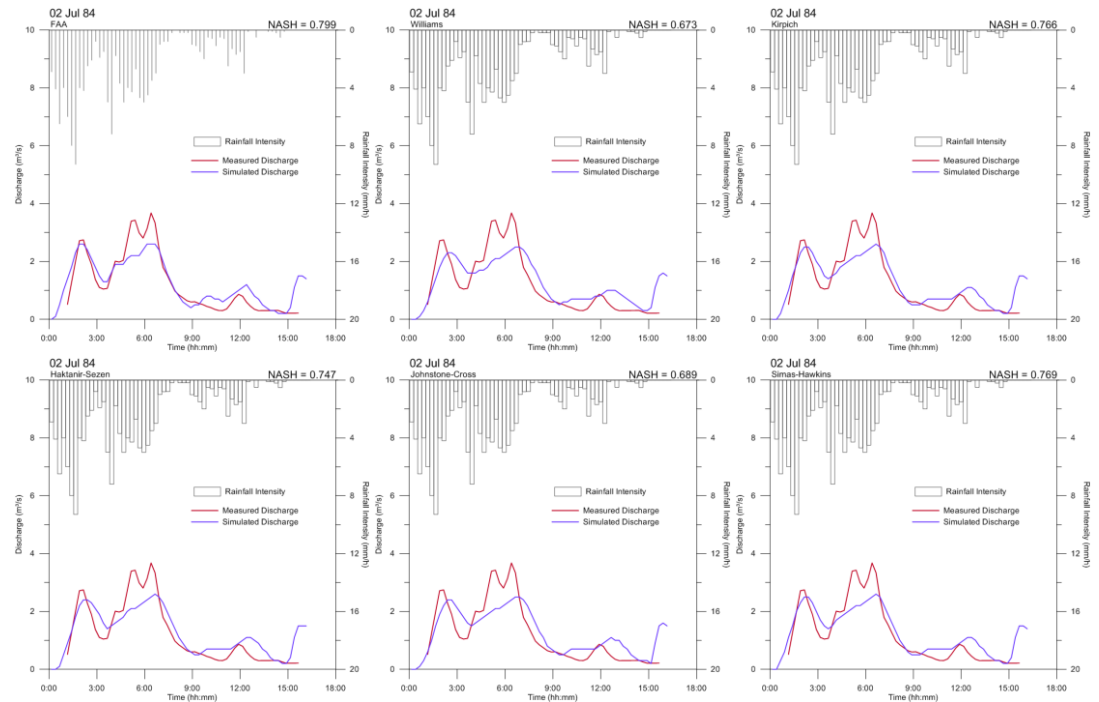




## 03 Feb 84

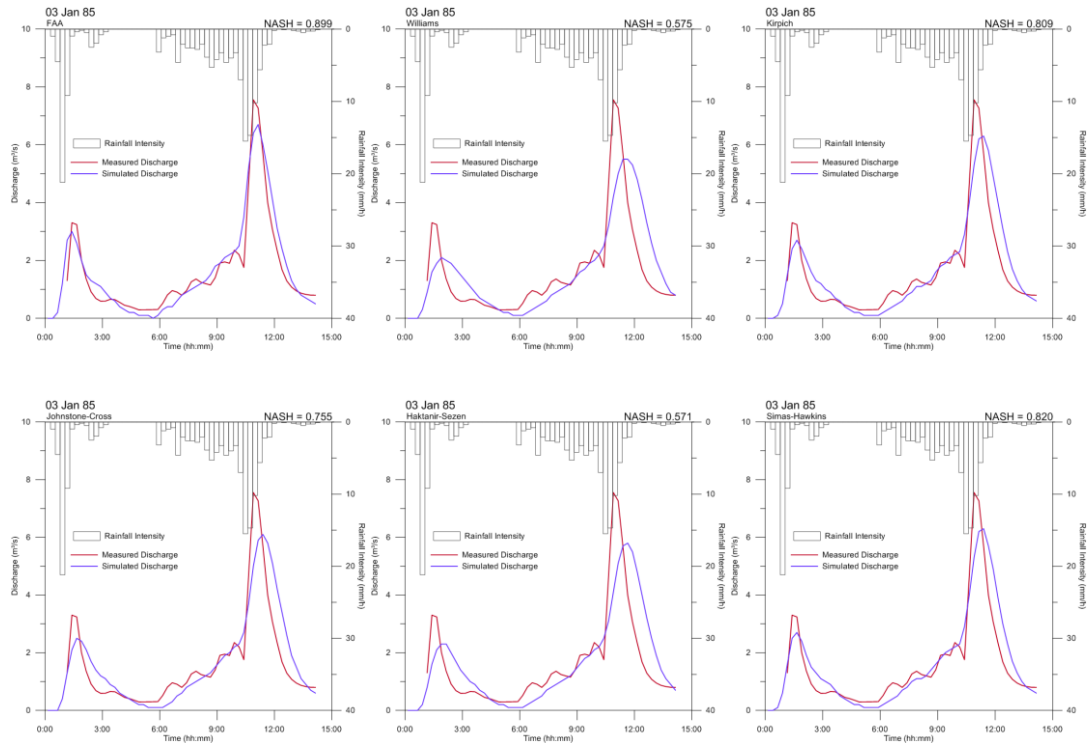


## 02 Jul 84

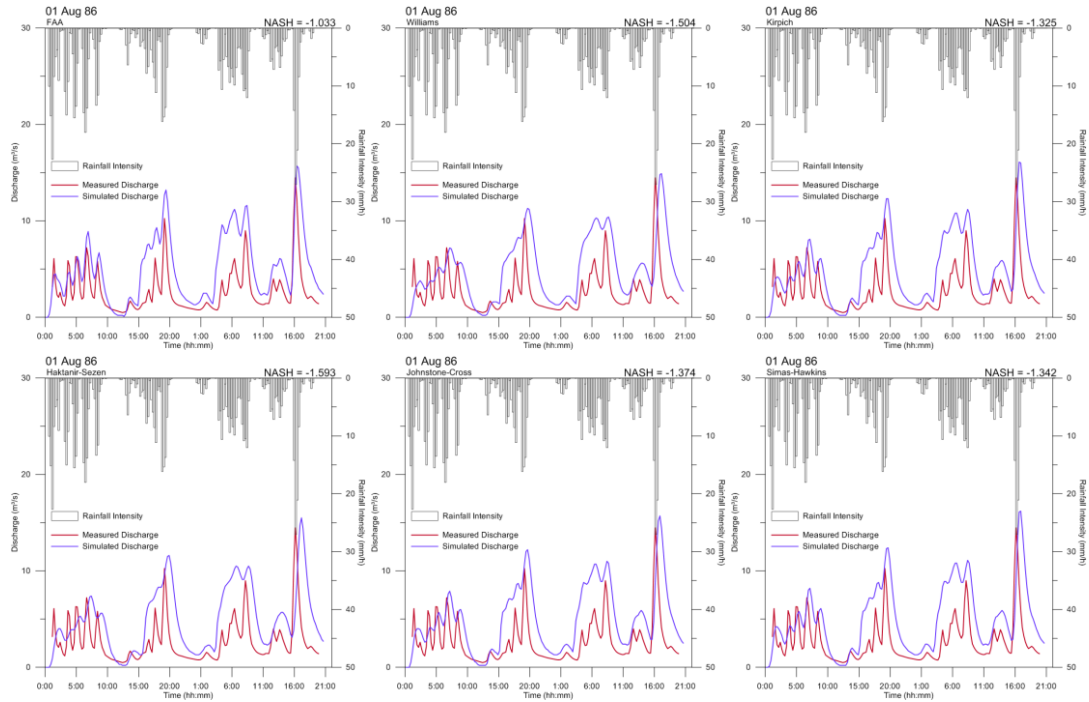




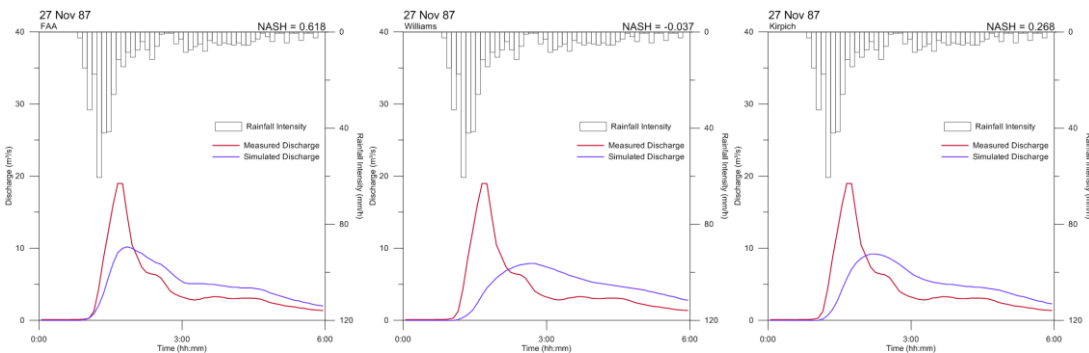
03 Jan 85

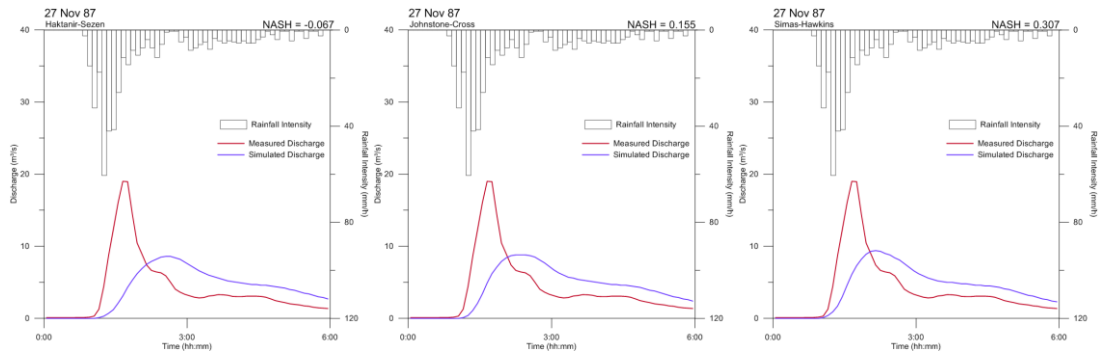


01 Aug 86

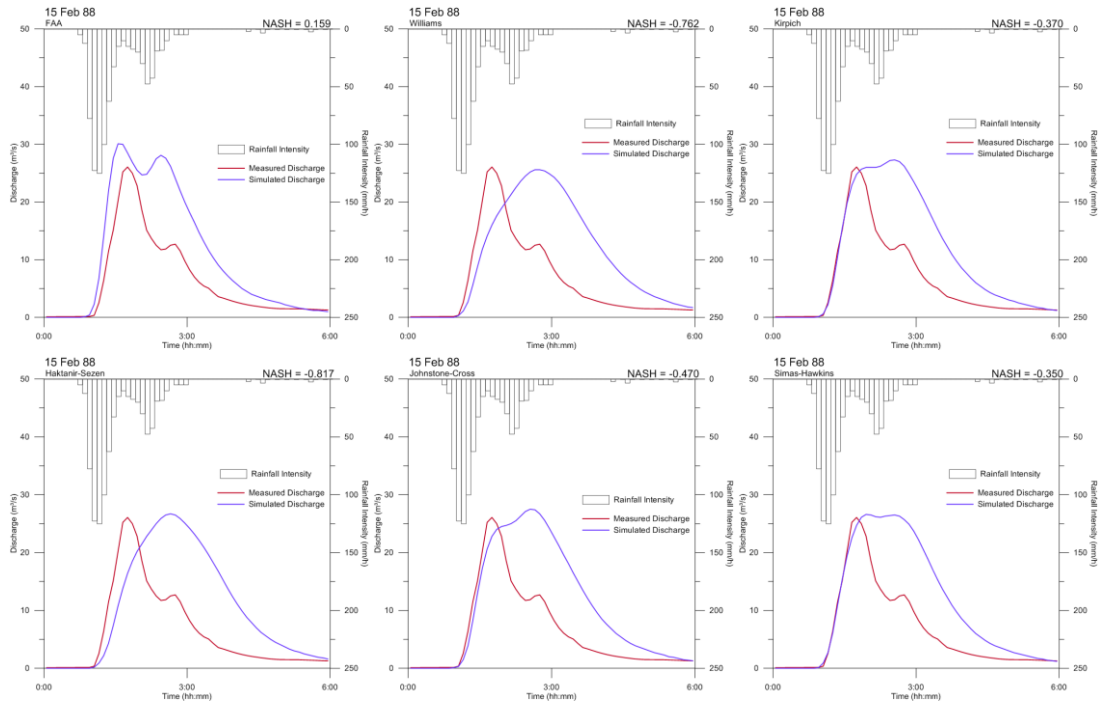


27 Nov 87

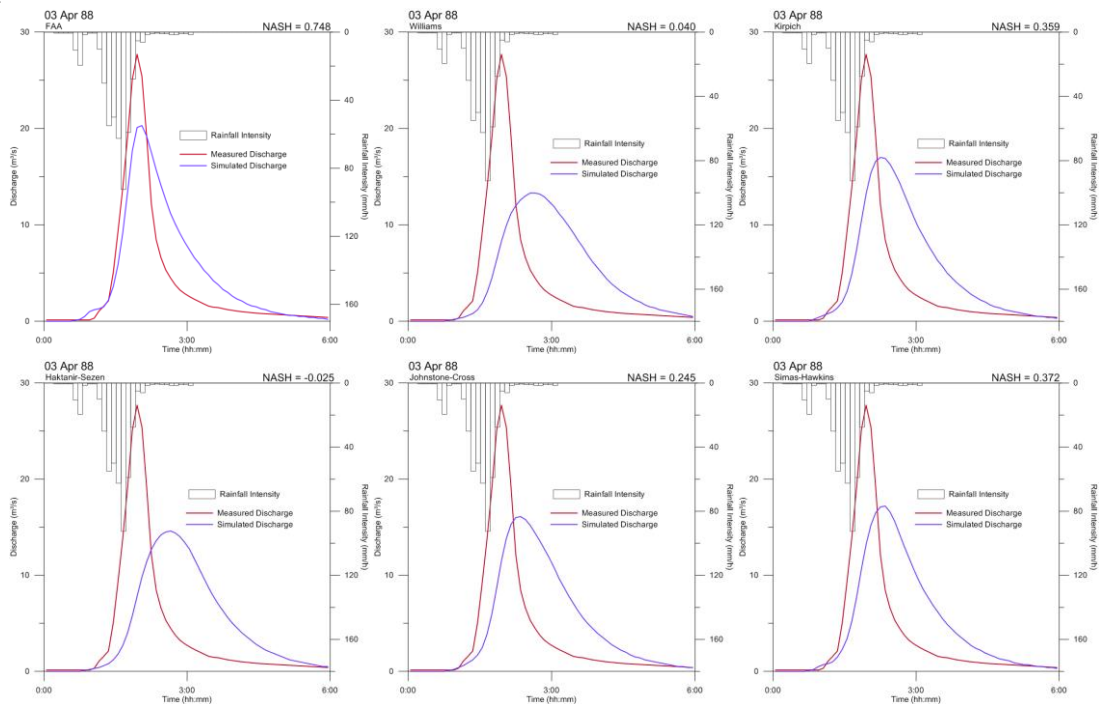




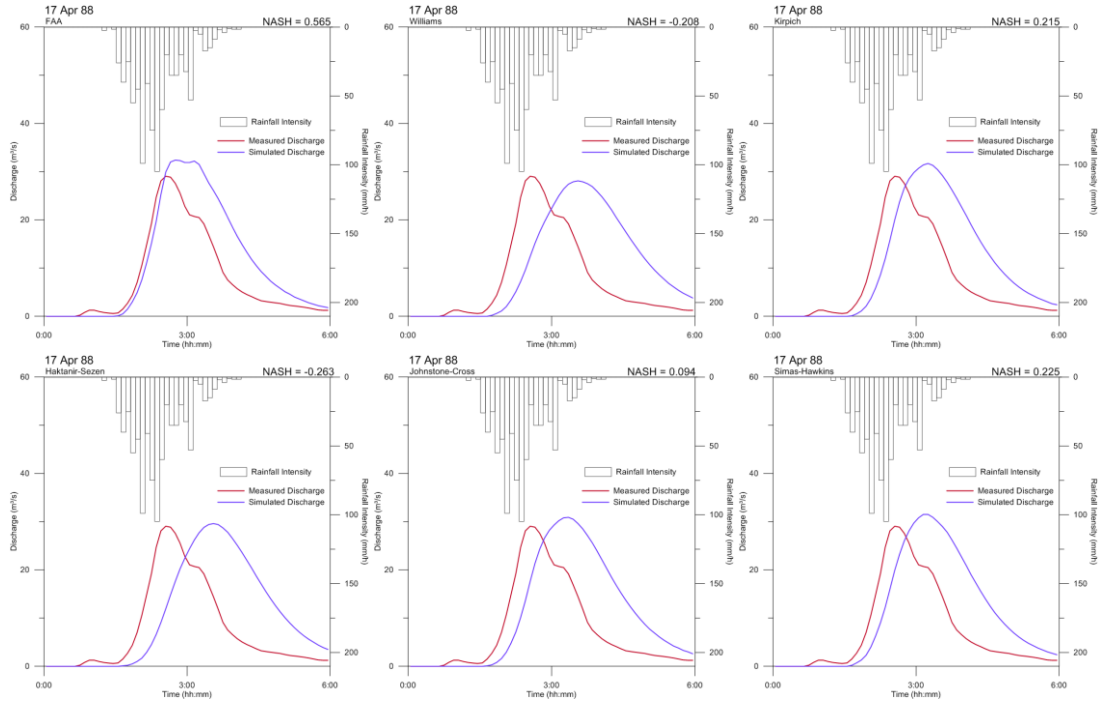
15 Feb 88



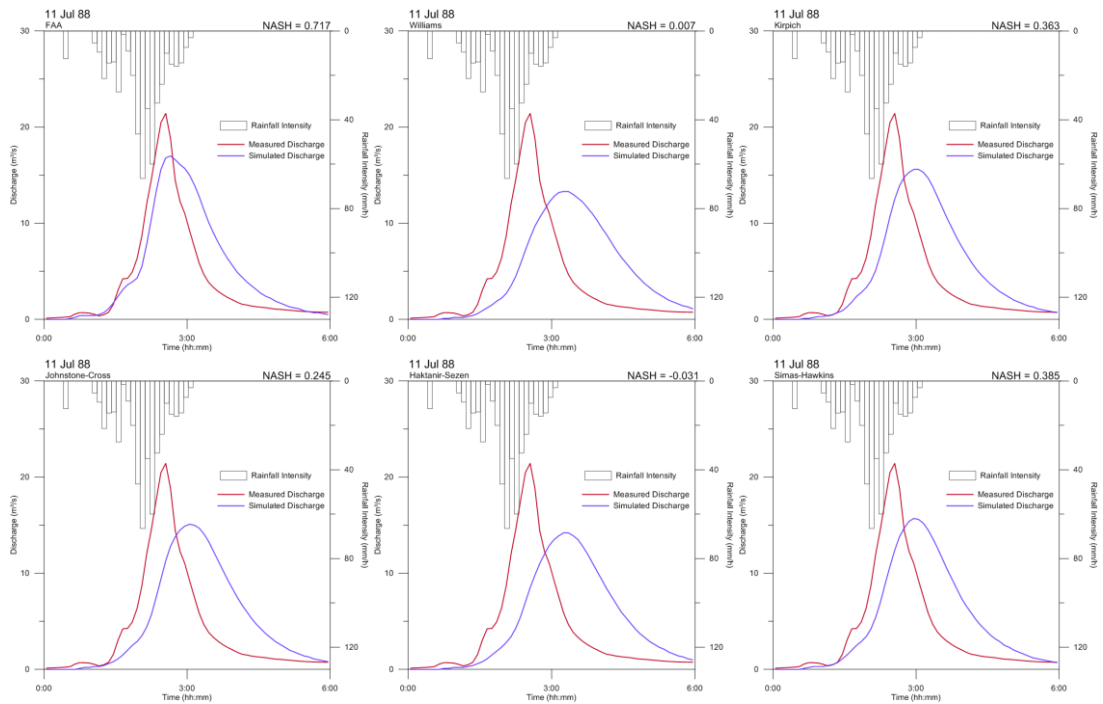
03 Apr 88



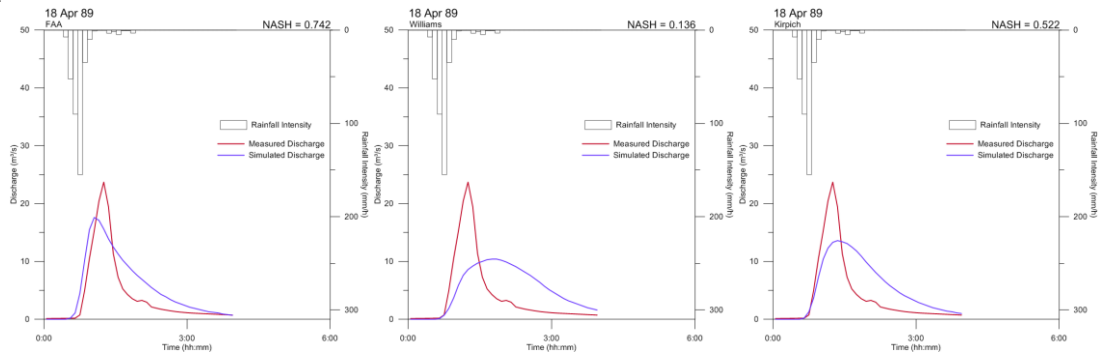
## 17 Apr 88

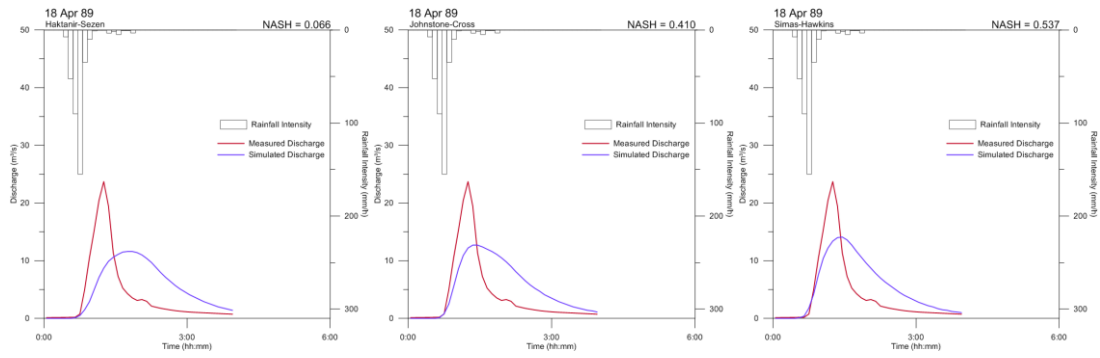


## 11 Jul 88

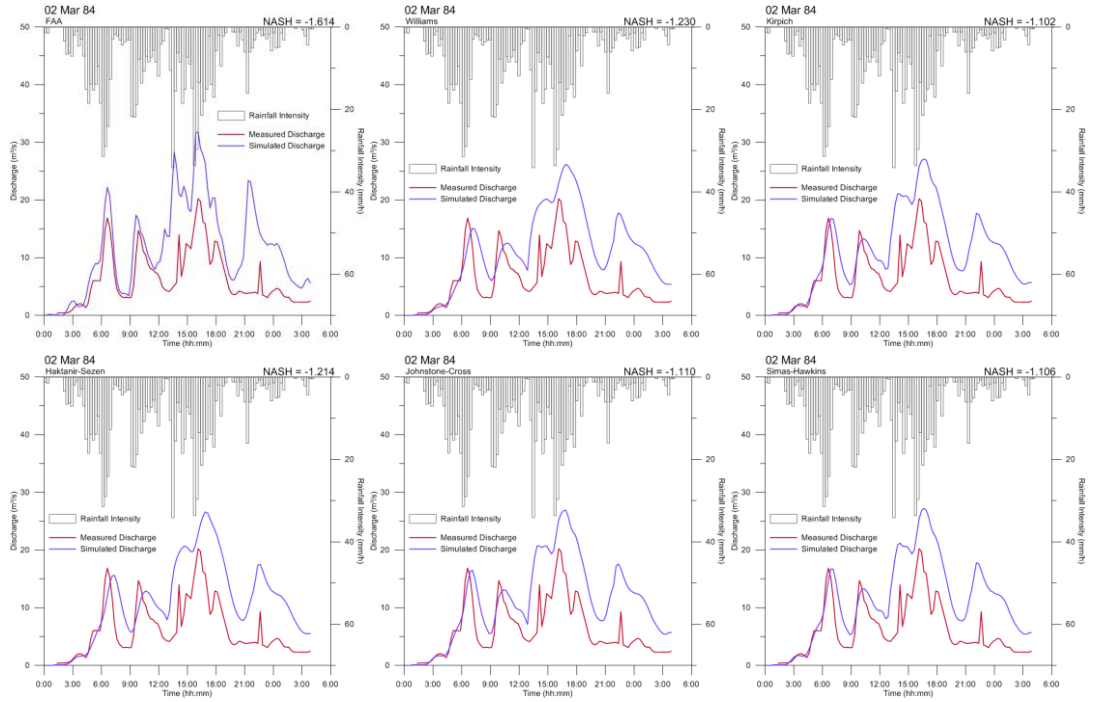


## 18 Apr 89





## 02 Mar 84



## Appendix 10. Runoff coefficients

Land use class	Runoff coefficient*
Apartment	0.60
Multiple-family dwellings, attached	0.67
Multiple-family dwellings, detached	0.50
Single-family dwellings	0.40
Commercial + Educational	0.73
Construction site	0.50
Industrial	0.65
Grass	0.25
Forest	0.15
Parking	0.86
Road	0.83
Railroad	0.30
Lake	0.00

\*Mean value from: Dunnes and Leopold (1978)

## Appendix 11. Percentages of imperviousness (%) by subcatchment, from 1950 to 2020

Calculated from the coefficients of imperviousness given by Guo (2003)

	1950*	1959*	1973*	1986*	2009**	2020***
s1	27.561	35.679	41.690	49.634	53.693	56.897
s2	20.464	43.188	34.360	33.604	55.096	58.300
s3	20.626	24.423	41.475	47.170	54.701	57.905
s4	20.775	20.142	39.311	39.753	44.546	47.750
s5	6.099	7.008	10.194	9.711	11.274	14.478
s6	29.452	34.915	34.456	61.317	69.894	73.098
s7	25.093	30.652	53.357	48.248	55.052	58.256
s8	28.013	25.733	36.984	60.978	62.634	65.838
s9	31.512	31.867	7.800	62.220	60.509	63.713
s10	23.042	30.876	37.448	52.836	56.258	59.462
s11	25.208	24.133	34.620	60.287	58.974	62.178
s12	13.774	15.248	7.912	10.253	12.290	15.494
s13	22.251	22.215	28.683	32.176	34.197	37.401
s14	12.502	10.479	14.345	15.973	6.007	9.211
s15	12.657	14.165	22.914	16.392	22.341	25.544

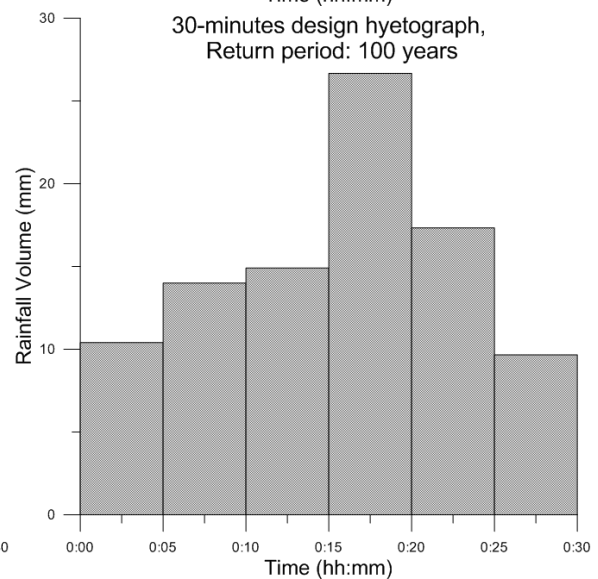
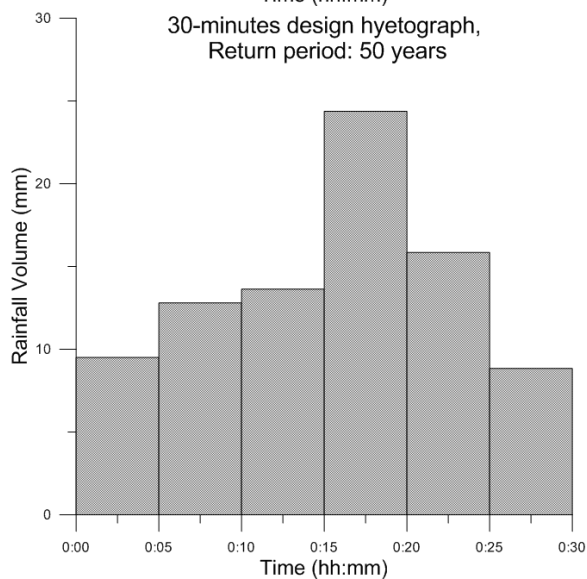
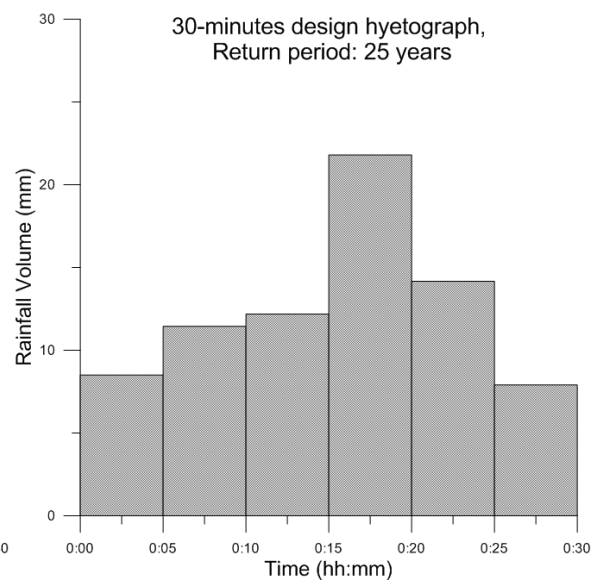
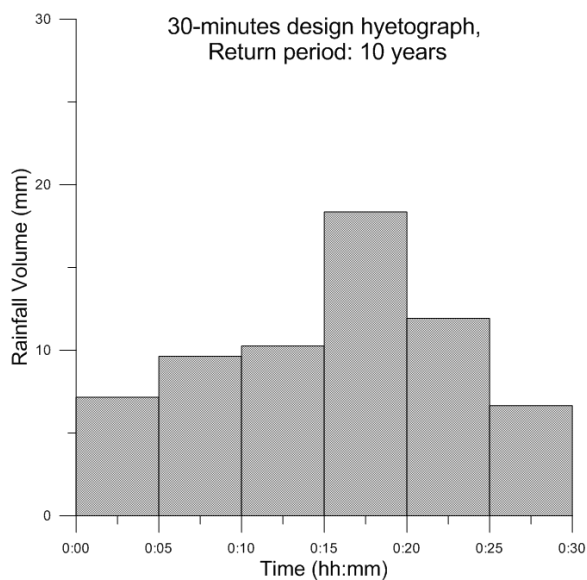
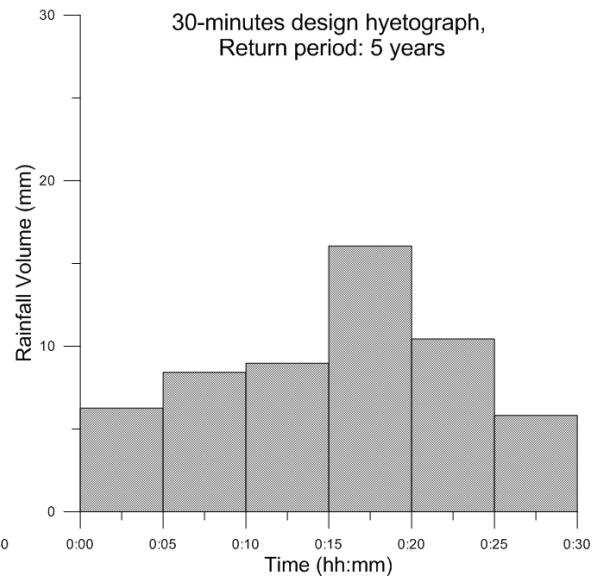
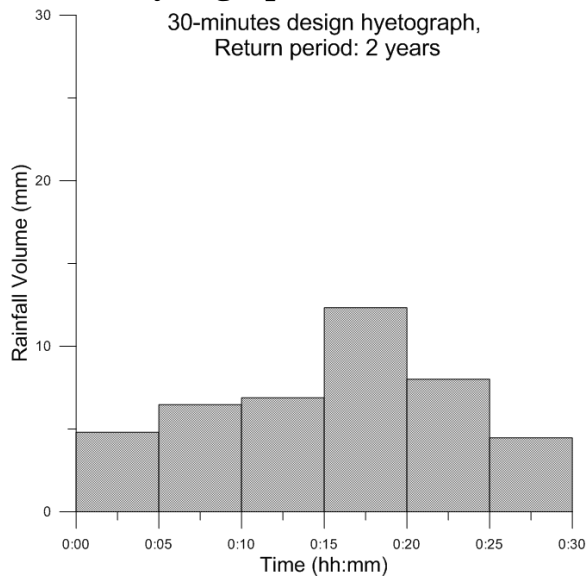
\*Calculated from Chuah's maps (1987)

\*\*Calculated from Google Earth (13/03/2009)

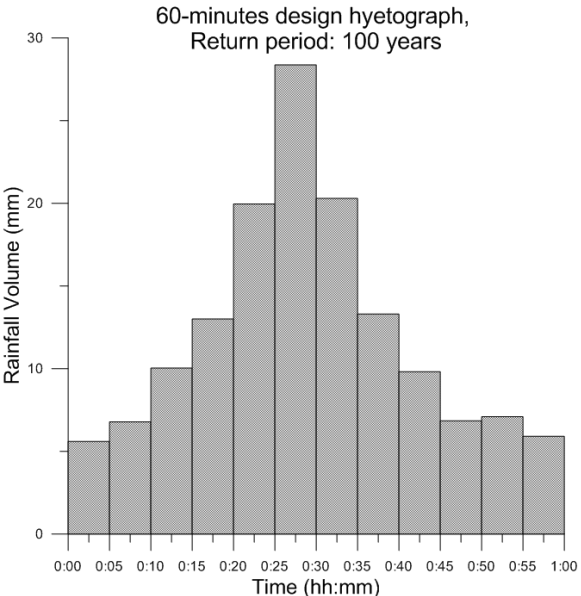
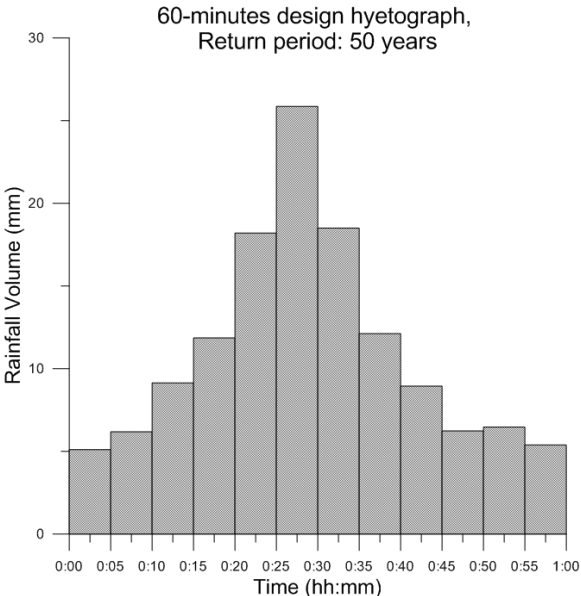
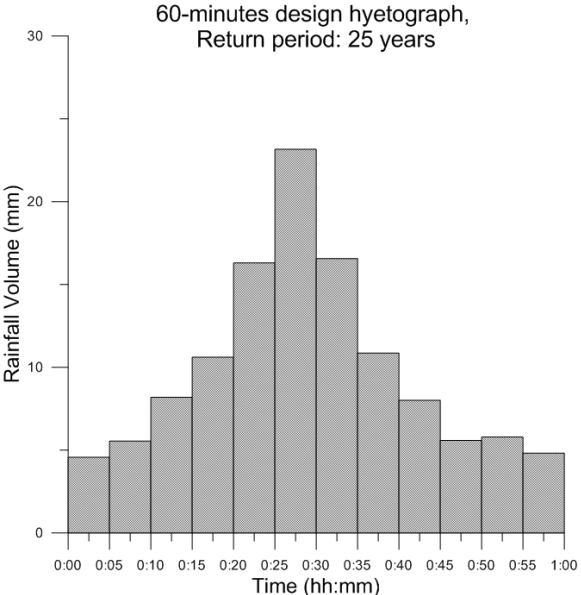
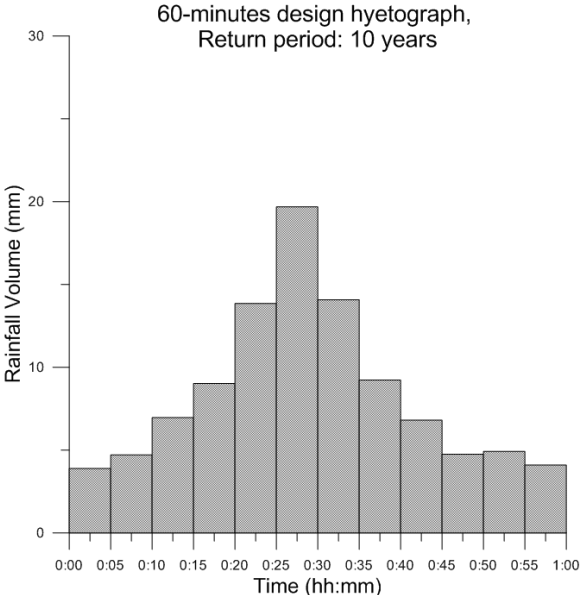
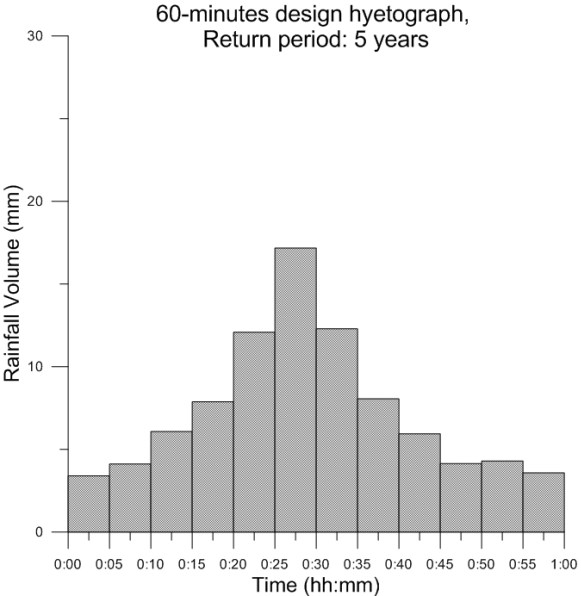
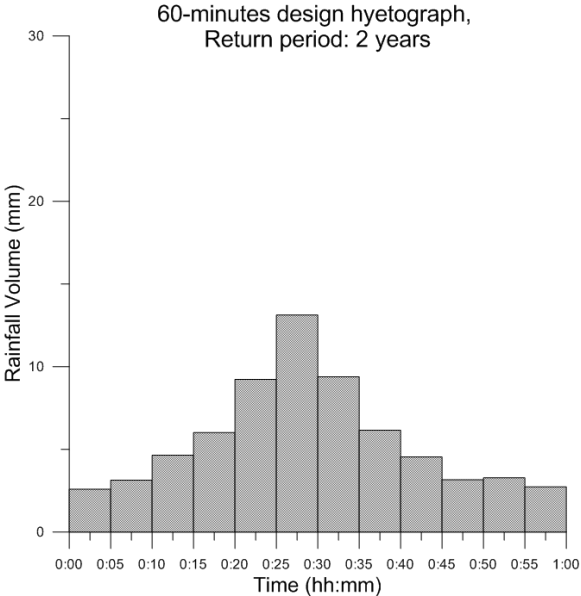
\*\*\*Estimated by empirical formula (1974)

## Appendix 12. Design synthetic hyetographs

### 30-minutes hyetographs

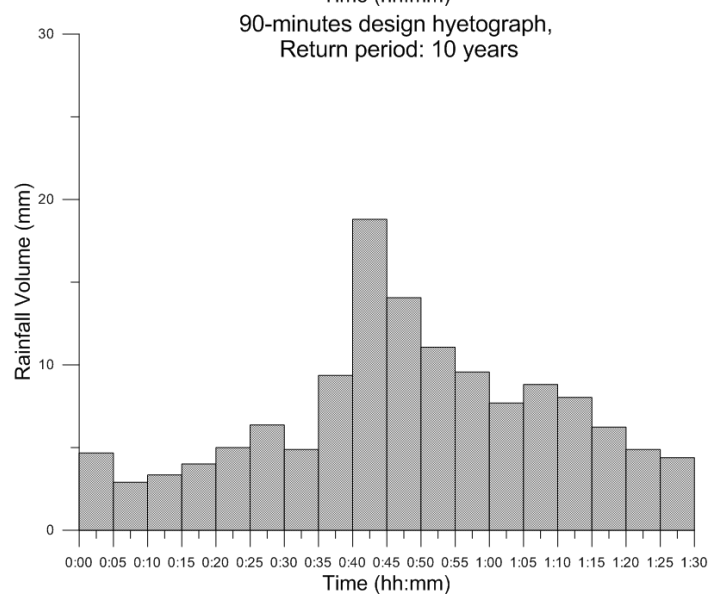
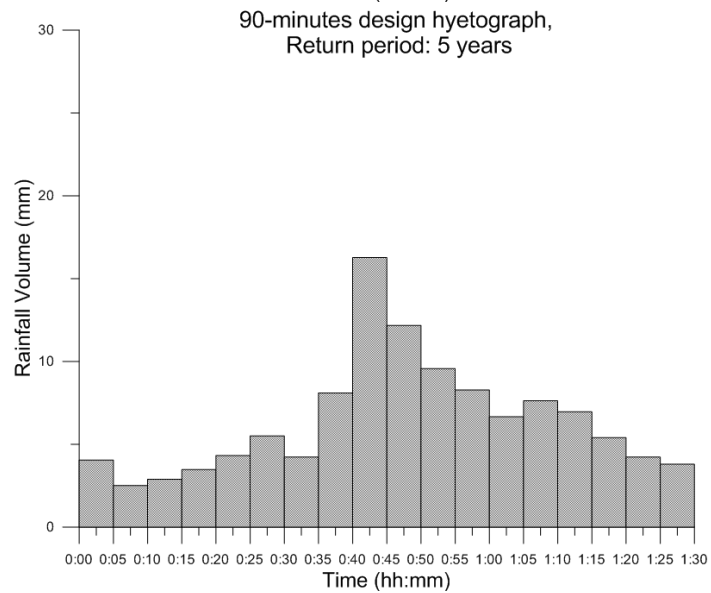
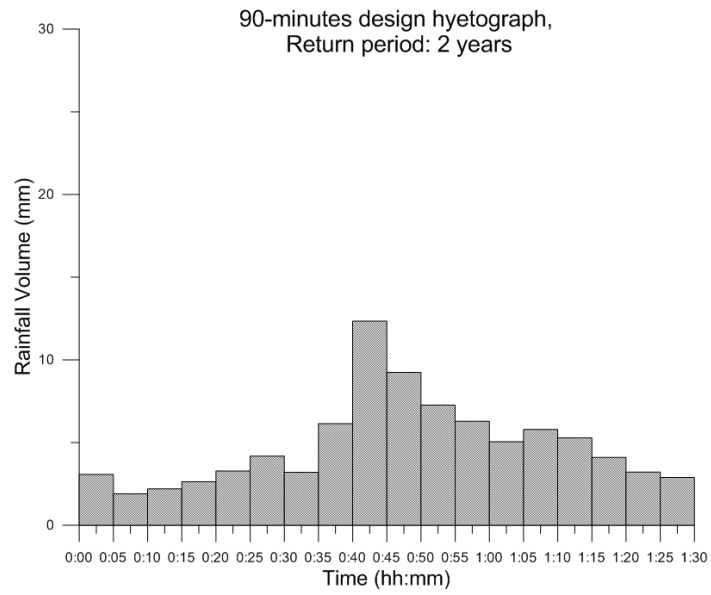


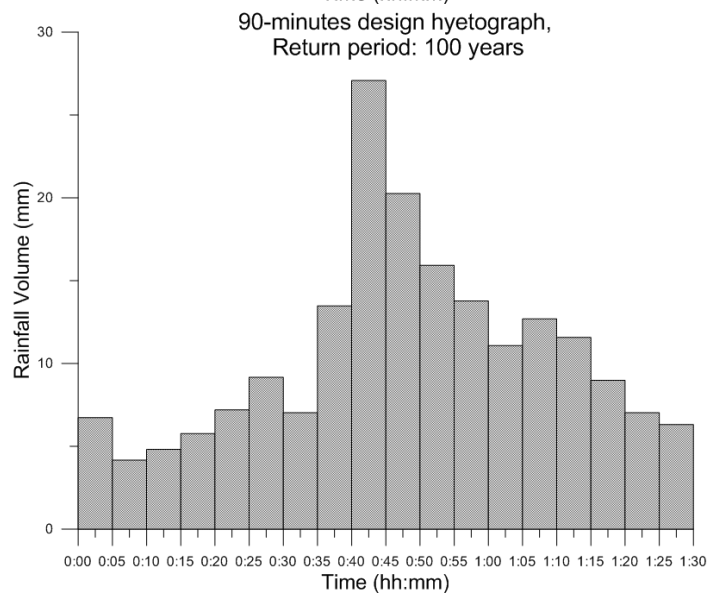
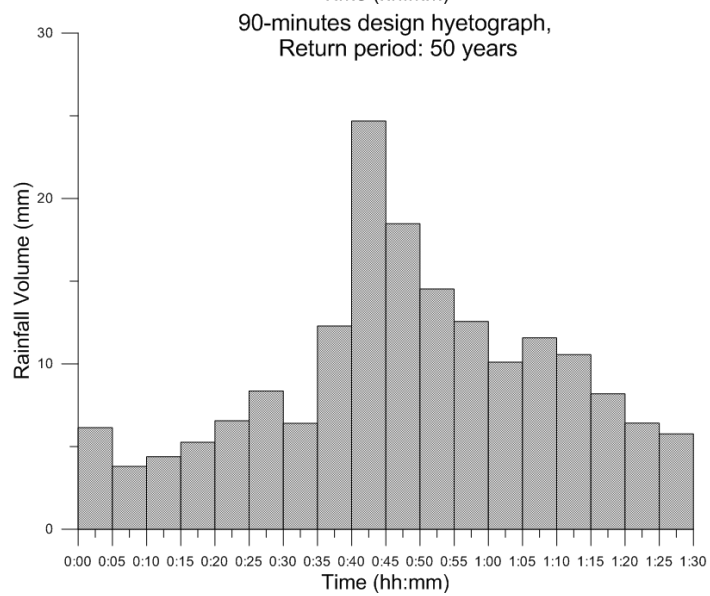
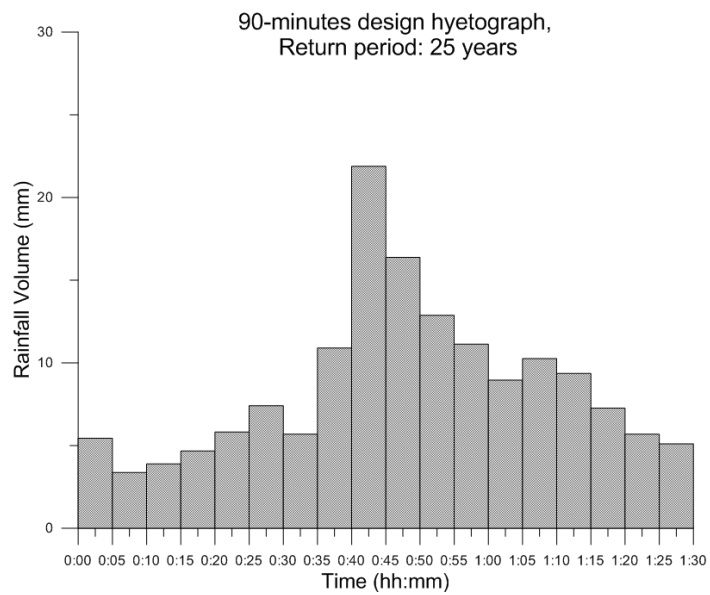
60-minutes hyetographs



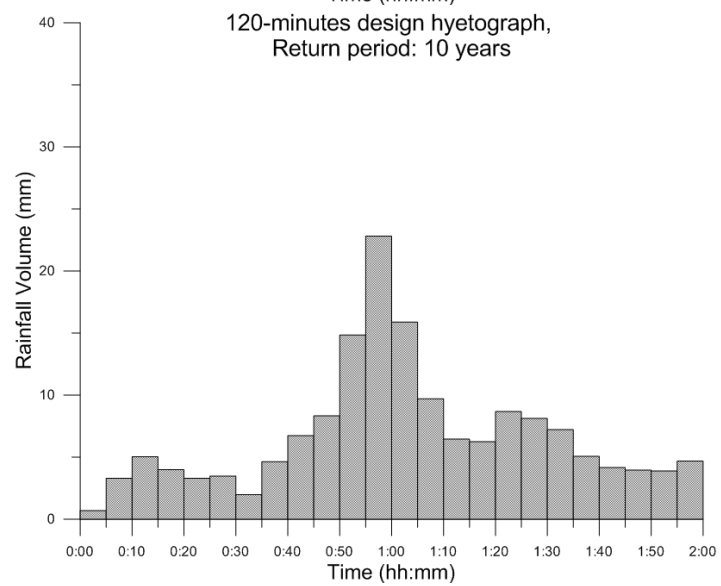
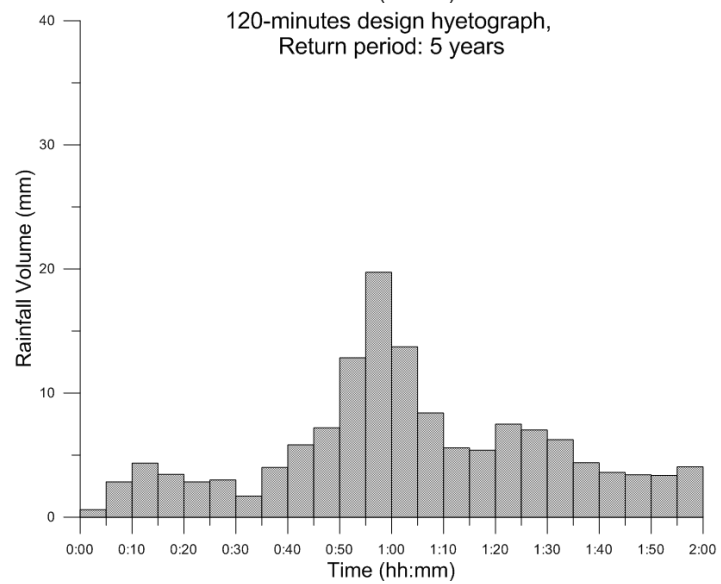
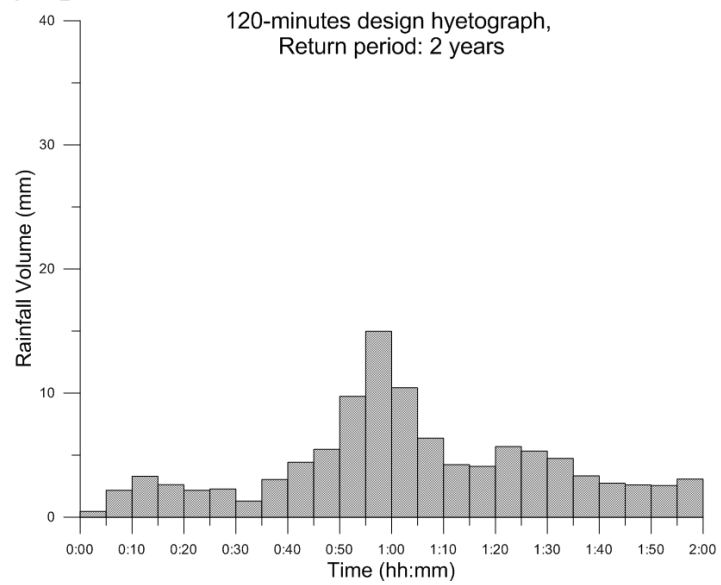


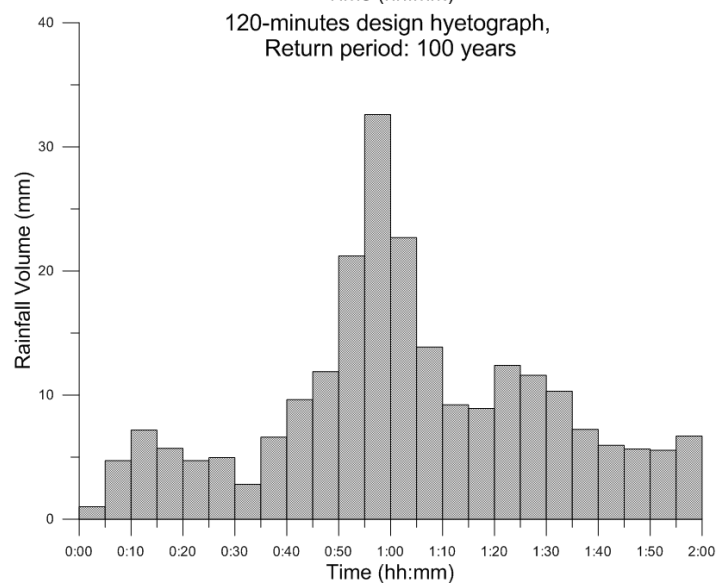
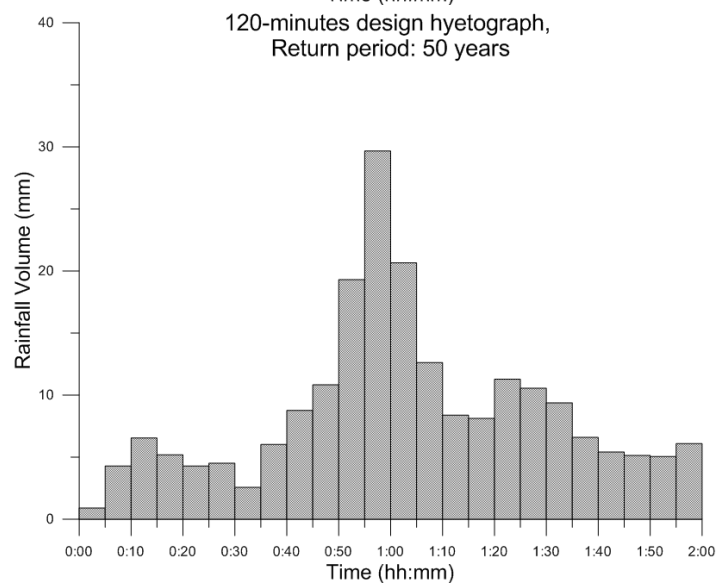
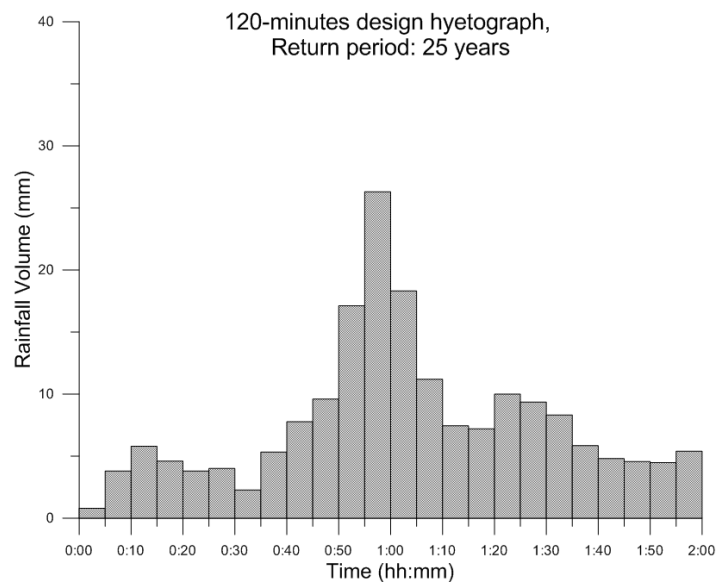
## 90-minutes hyetographs





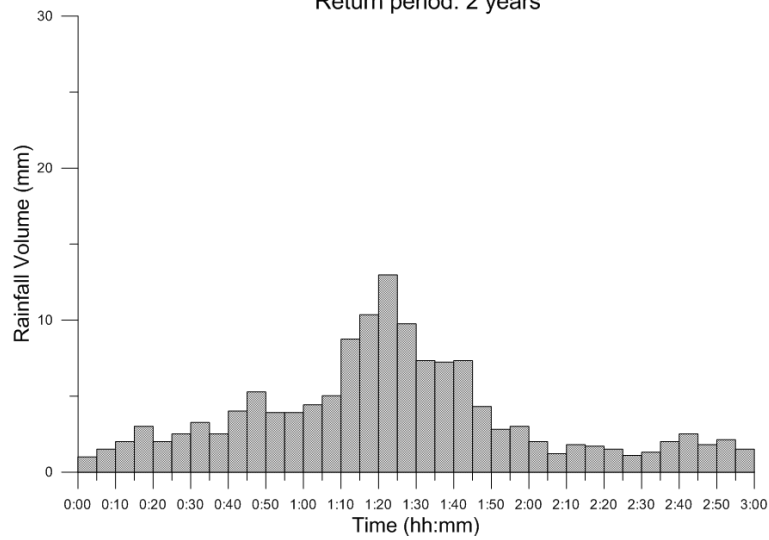
## 120-minutes hyetographs



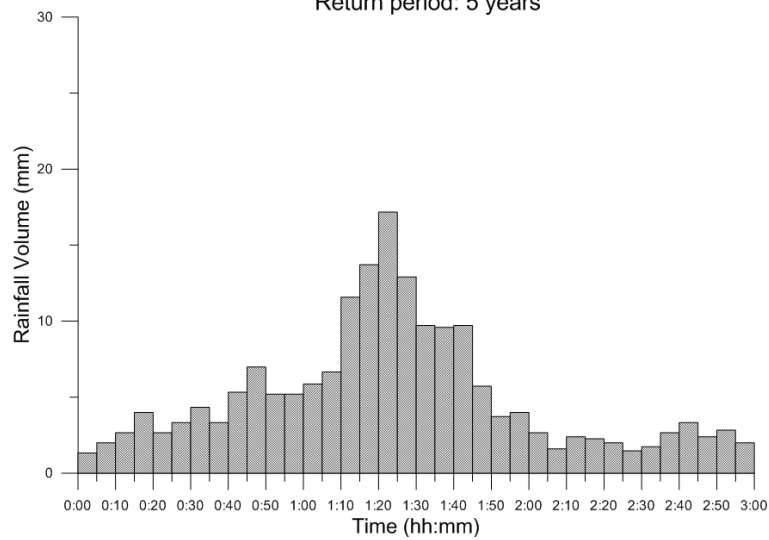


## 180-minutes hyetographs

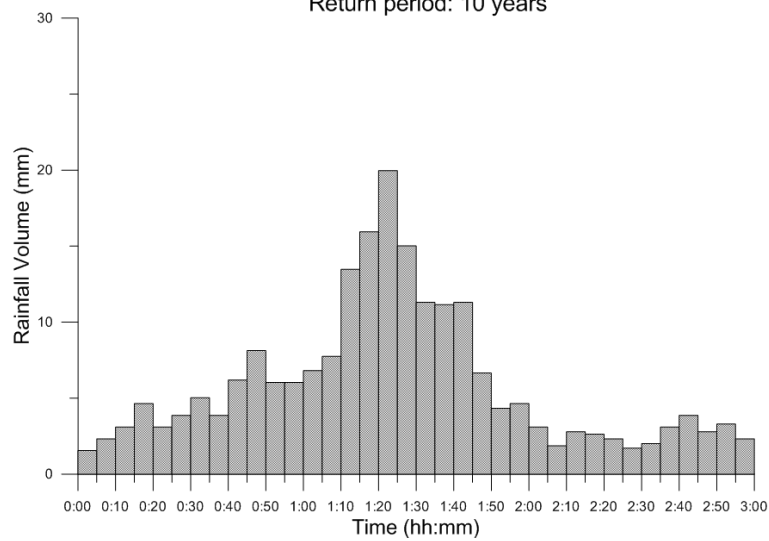
180-minutes design hyetograph,  
Return period: 2 years

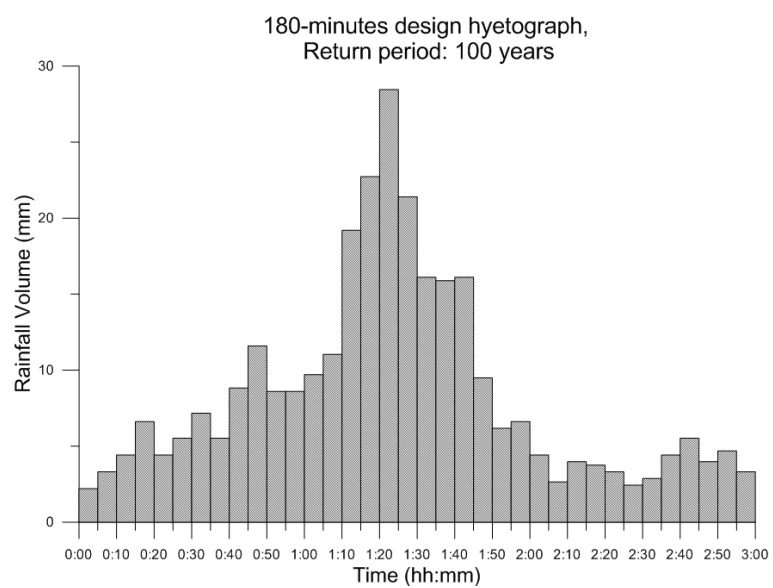
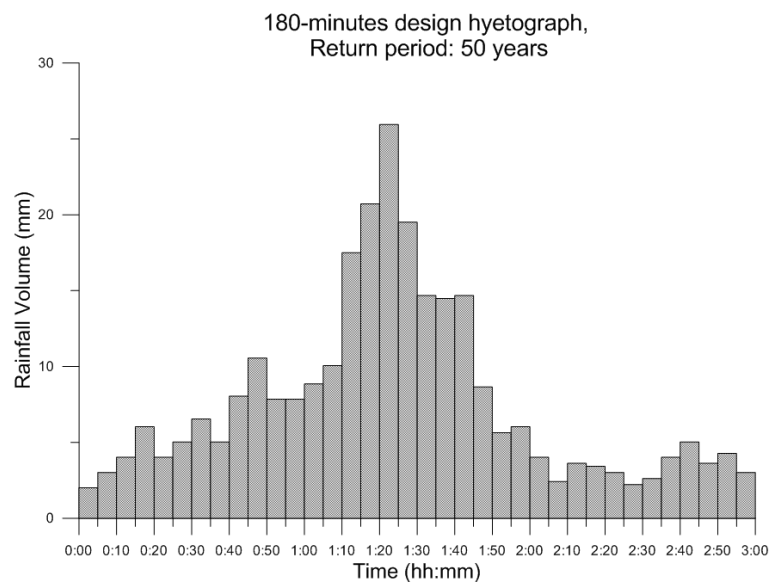
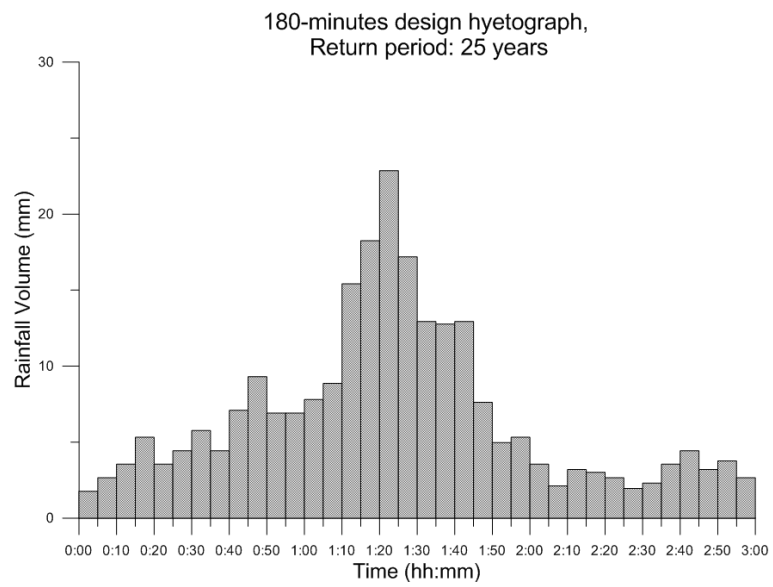


180-minutes design hyetograph,  
Return period: 5 years



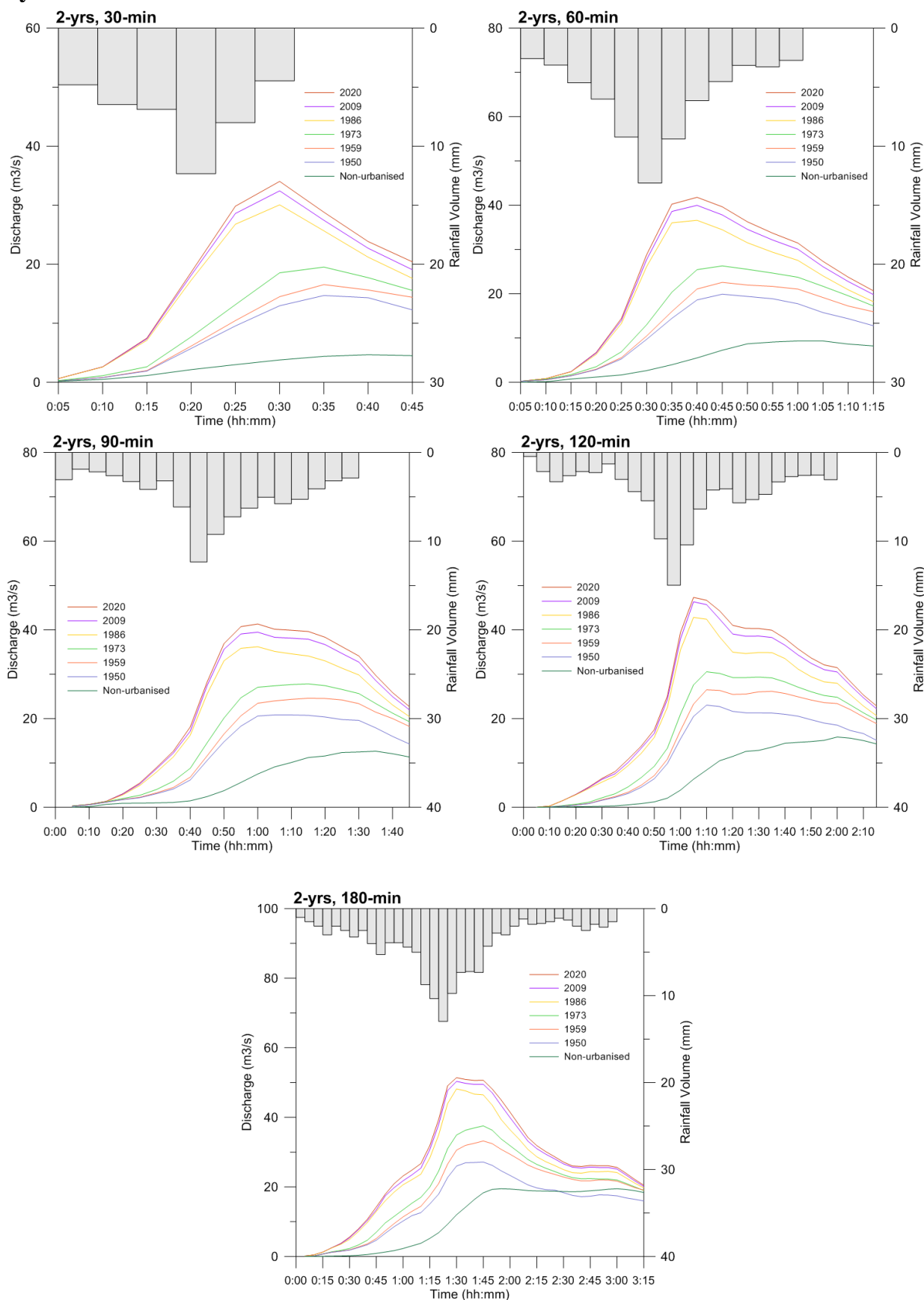
180-minutes design hyetograph,  
Return period: 10 years



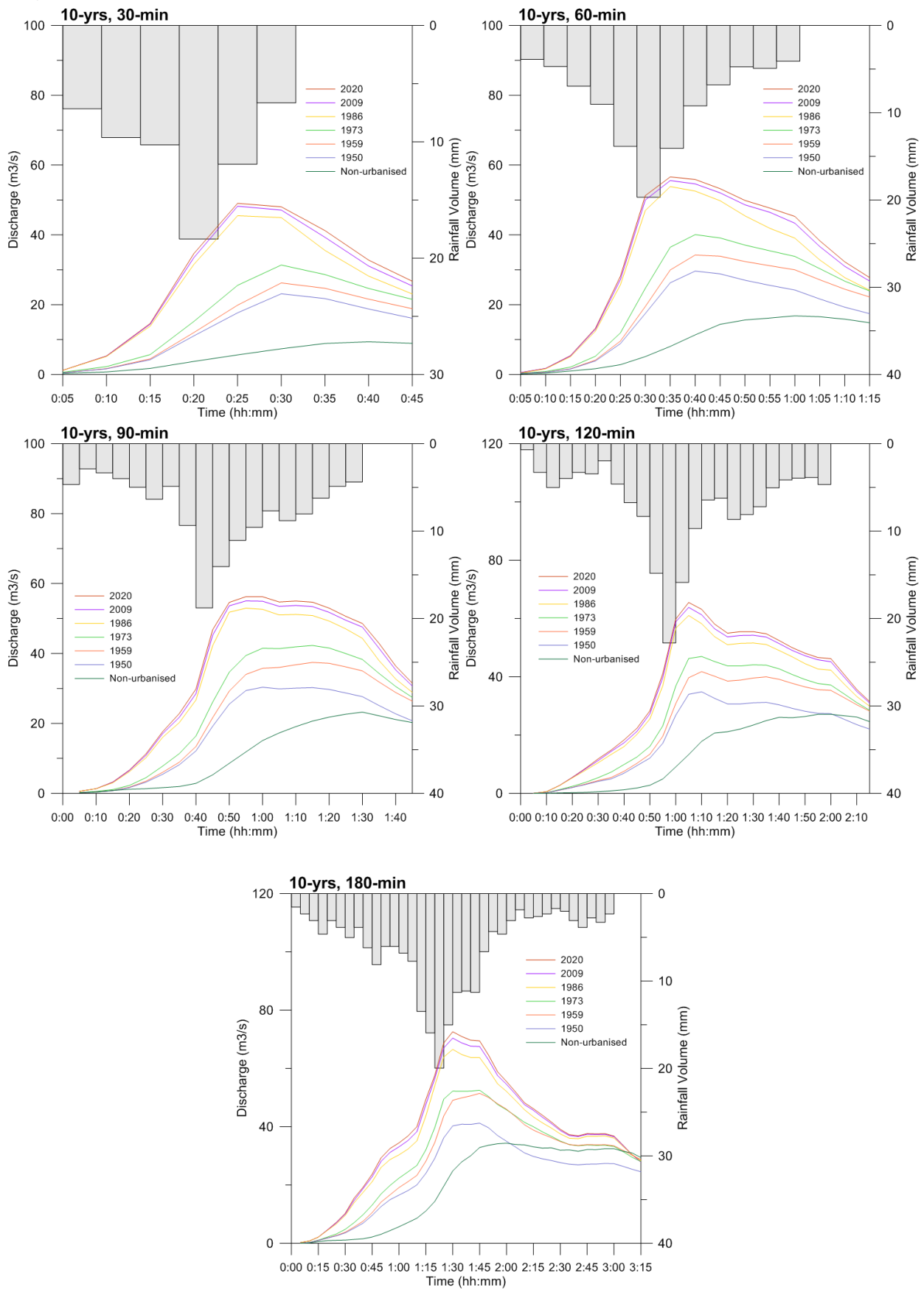


## Appendix 13. Design hydrograms for the return periods of 2, 10, 25, 50 and 100 years.

2-yrs

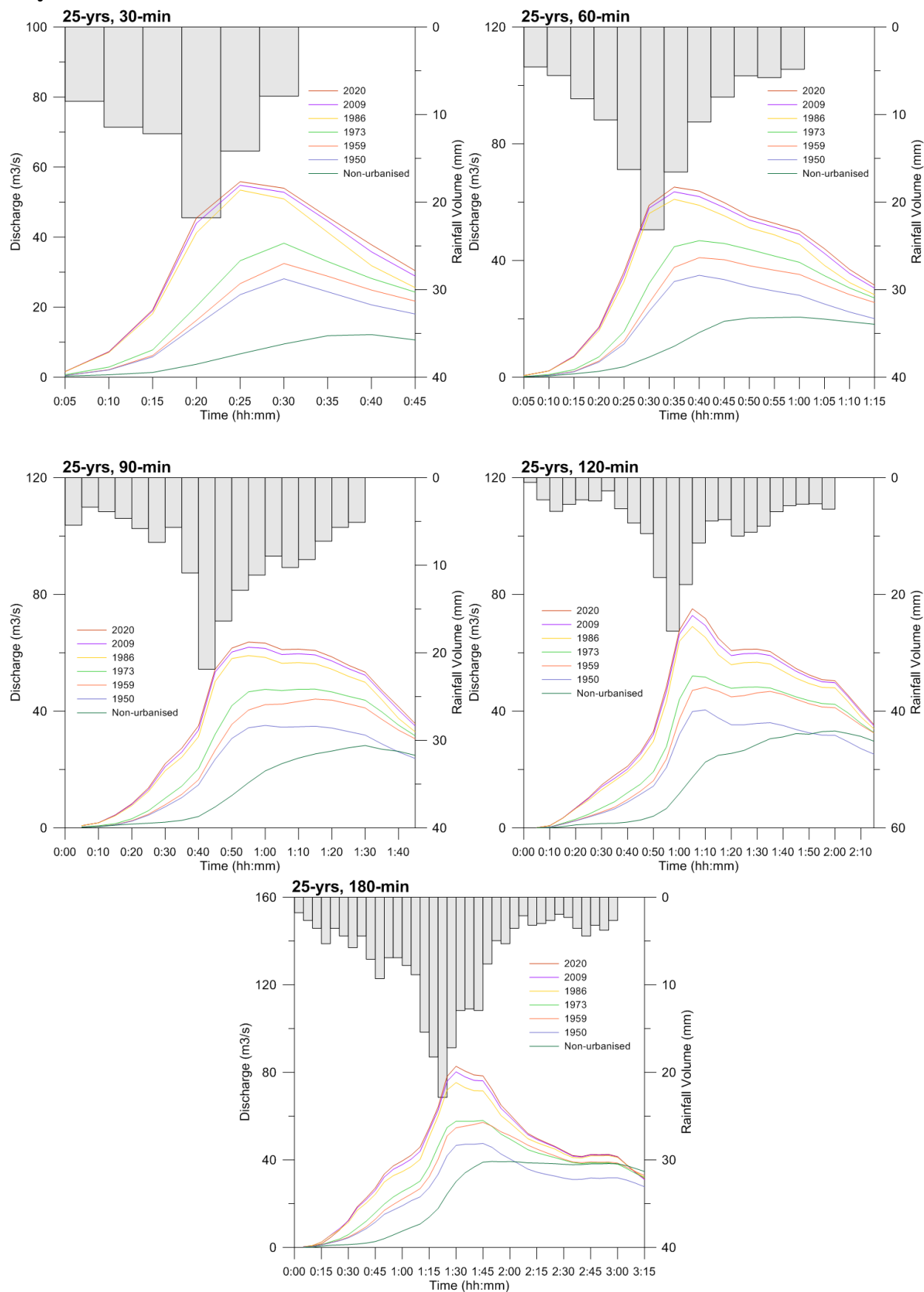


# 10-ylrs

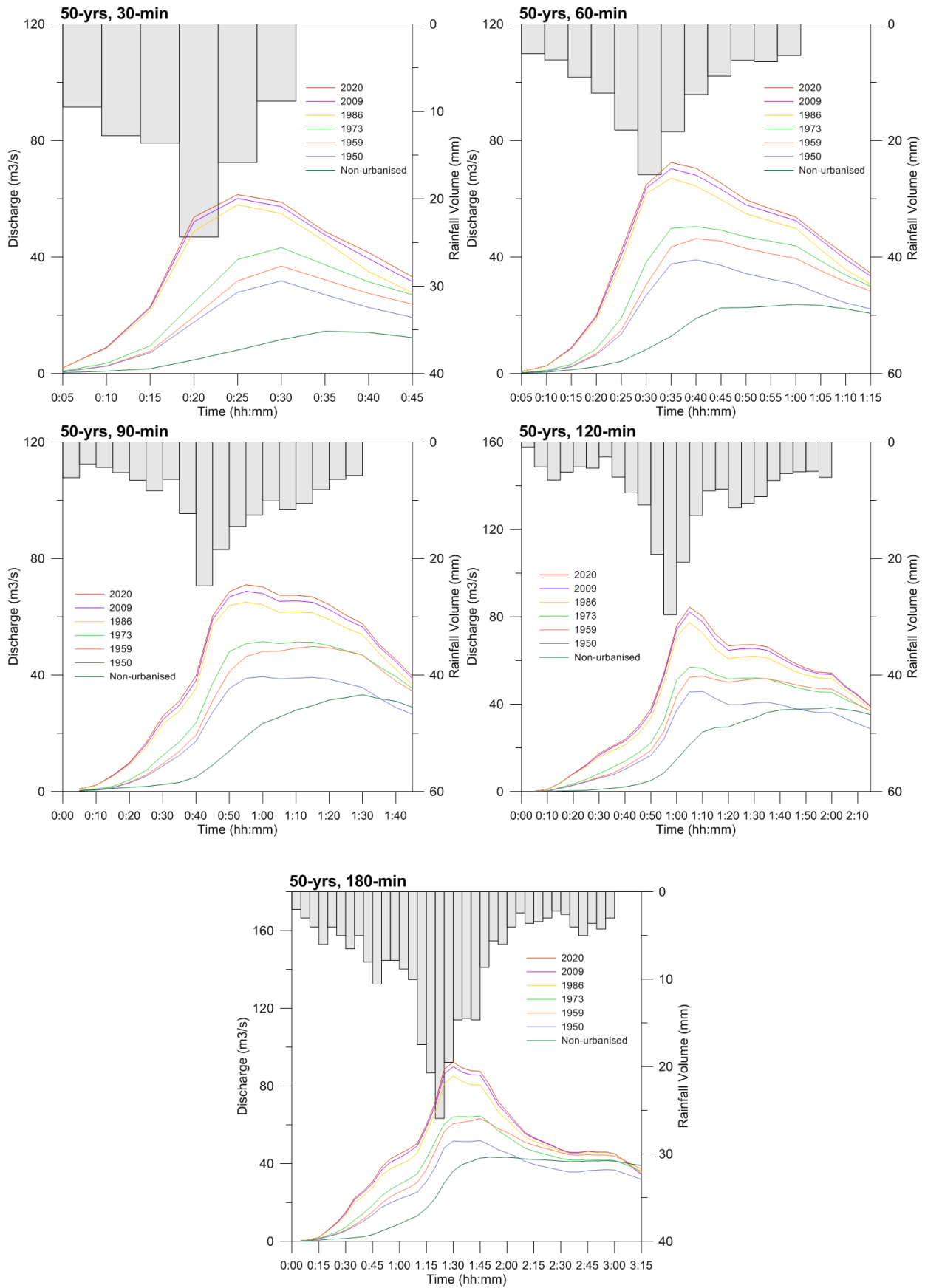




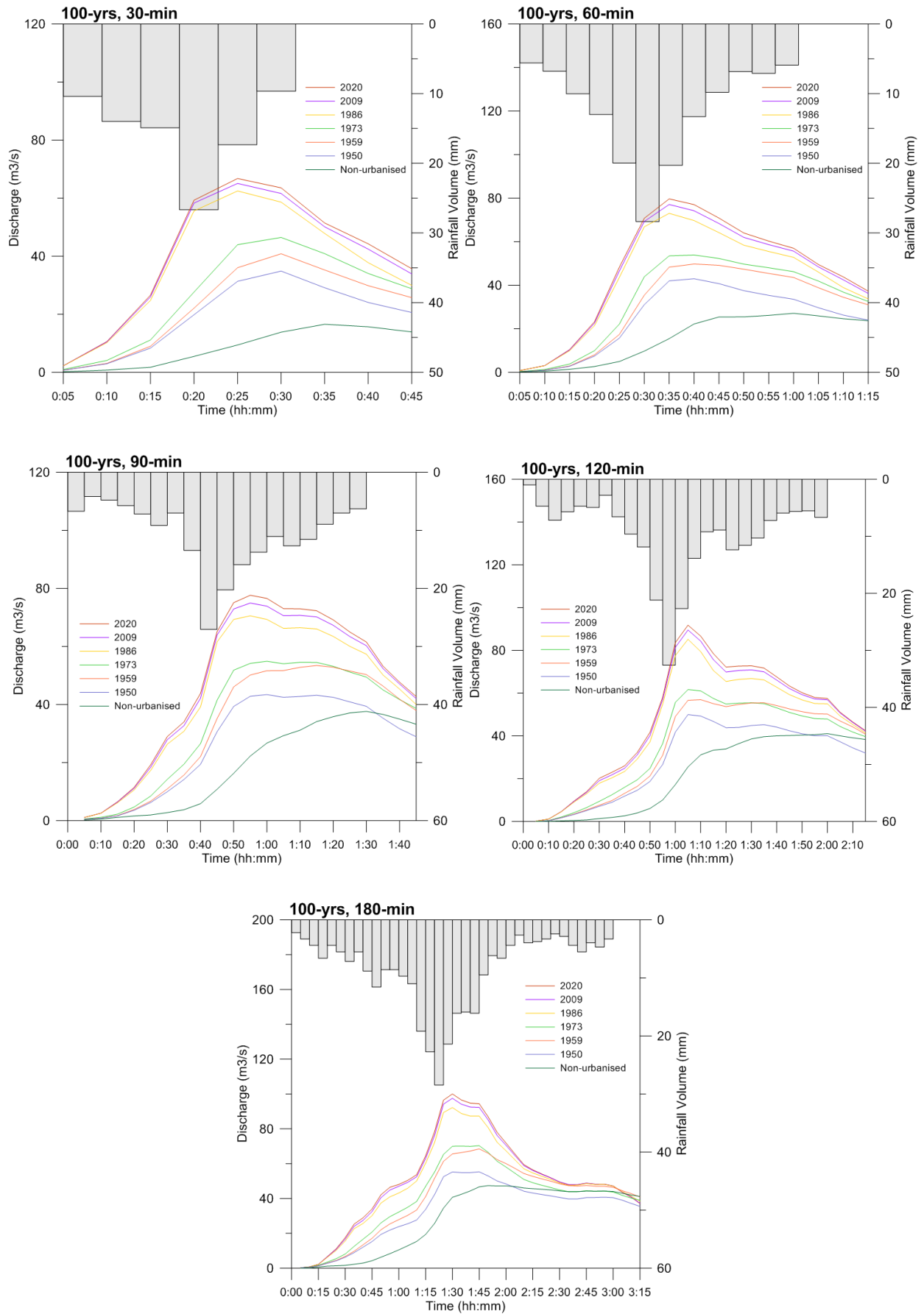
## 25-yrs



## 50-ysrs



# 100-yrs



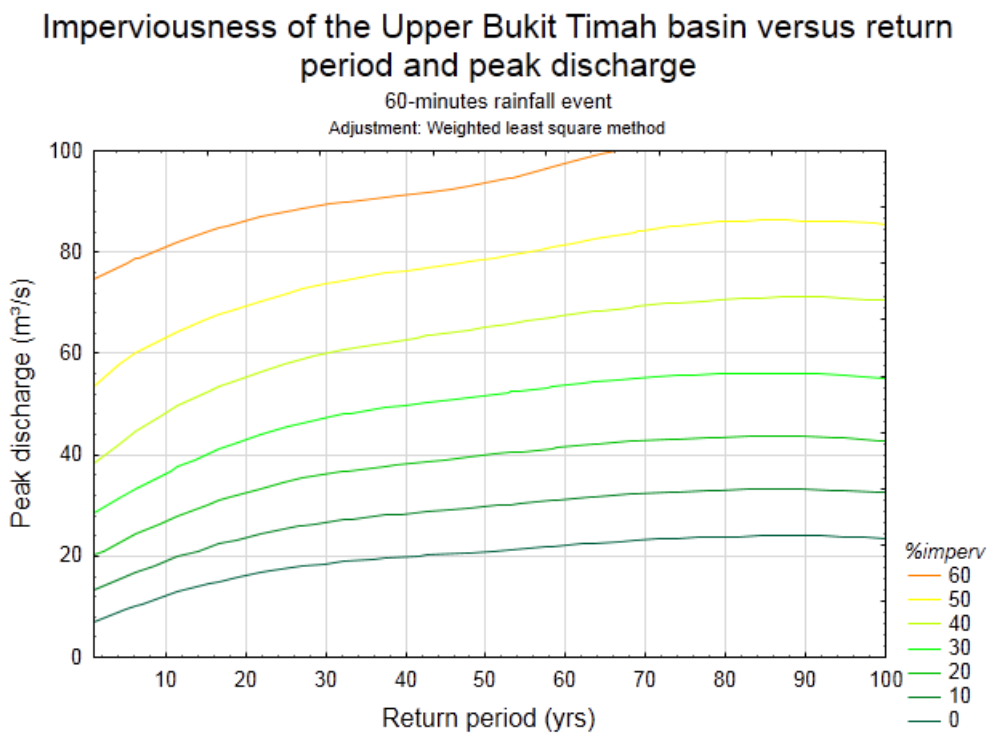
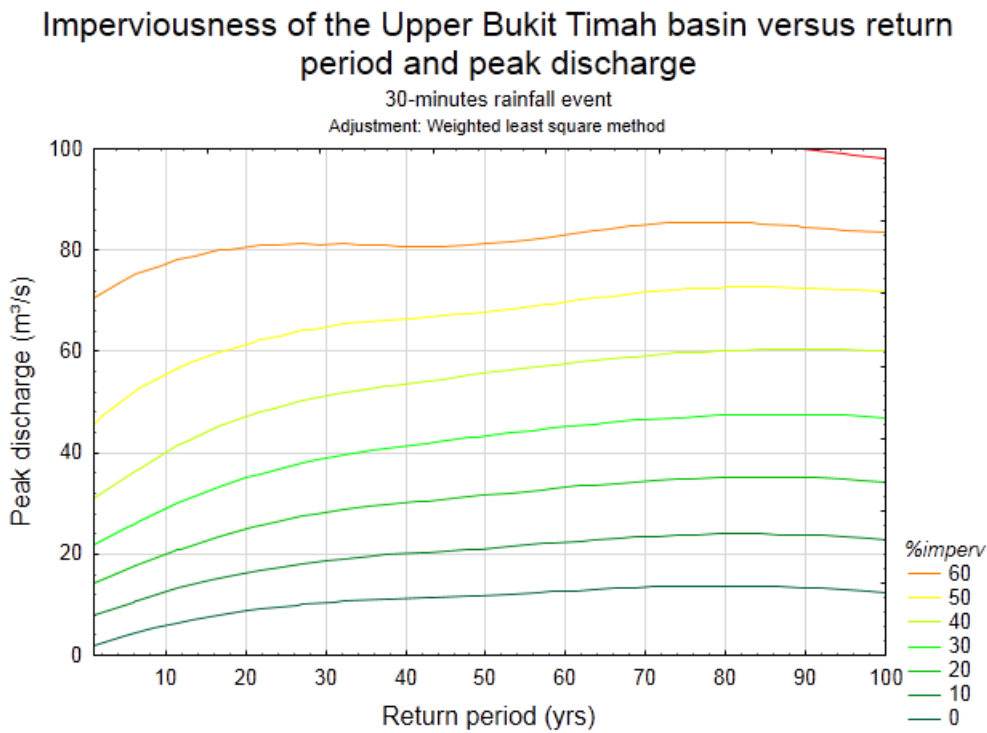
## Appendix 14. Modelled peak discharge for each design rainfall event

	T2					T5					T10				
	30	60	90	120	180	30	60	90	120	180	30	60	90	120	180
<b>Non-urb.</b>	4.66	9.33	12.65	15.84	19.48	7.65	13.64	19.5	22.75	28.12	9.38	16.81	23.24	27.13	34.34
<b>1950</b>	14.7	19.89	20.82	23.04	27.15	19.5	25.64	26.33	30	35.23	23.13	29.63	30.36	34.85	41.22
<b>1959</b>	16.54	22.56	24.59	26.49	33.2	21.99	29.5	32.25	35.61	44.8	26.24	34.23	37.44	41.78	51.45
<b>1973</b>	19.51	26.28	27.82	30.55	37.54	26.67	34.23	36.37	41.38	47.73	31.37	40.07	42.28	46.97	52.52
<b>1986</b>	30.06	36.58	36.2	42.81	48.17	39.1	48.73	47.95	54.7	58.85	45.5	53.84	52.96	61.04	66.54
<b>2009</b>	32.43	39.96	39.48	46.33	50.33	42.68	50.28	49.86	56.69	61.76	48.22	55.56	55.03	63.82	70.42
<b>2020</b>	34.03	41.78	41.32	47.32	51.4	44.08	51.11	50.98	57.88	63.39	49.03	56.61	56.25	65.51	72.59

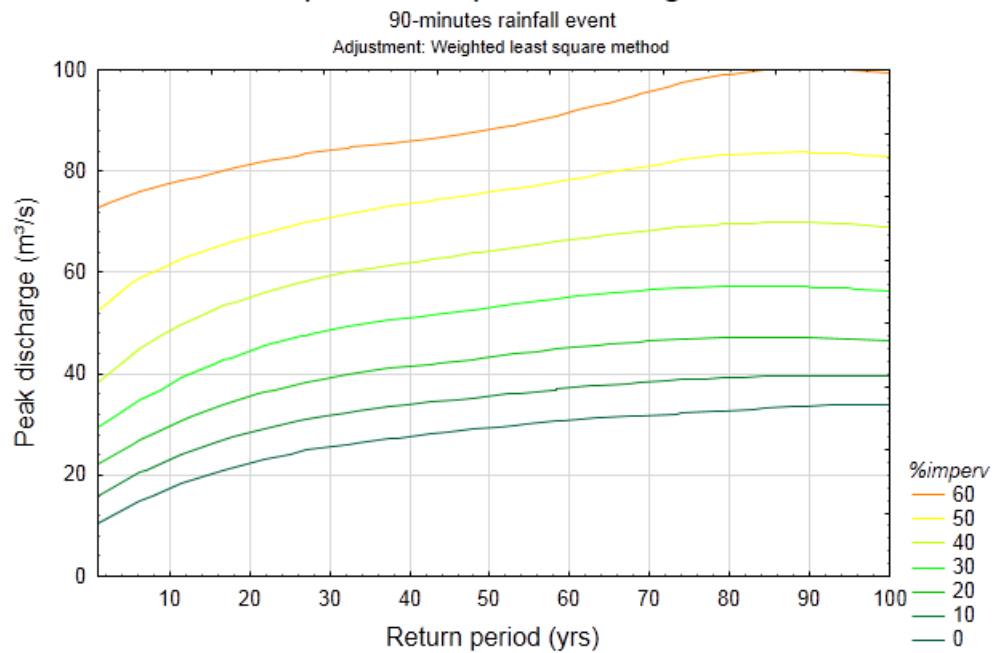
  

	T25					T50					T100				
	30	60	90	120	180	30	60	90	120	180	30	60	90	120	180
<b>Non-urb.</b>	12.17	20.59	28.21	33.17	39.28	14.54	23.76	33.24	38.48	43.34	16.55	27.12	37.61	41.08	47.42
<b>1950</b>	28.11	34.9	35.09	40.43	47.51	31.82	39	39.45	45.89	51.85	34.87	42.98	43.41	49.96	55.32
<b>1959</b>	32.47	40.96	44.11	48.18	57.16	36.91	46.36	49.81	52.85	63.2	40.83	49.74	53.43	56.94	68.48
<b>1973</b>	38.27	46.78	47.53	52.05	58	43.24	50.47	51.46	56.99	64.53	46.46	53.88	54.88	61.64	70.34
<b>1986</b>	53.43	60.96	59.02	69.01	75.32	57.98	67.02	65.05	77.4	85.16	62.47	73.02	70.55	85.16	92.2
<b>2009</b>	54.8	63.53	61.89	72.79	80.22	60.12	70.33	68.74	82.21	89.92	65.06	77.08	74.95	89.51	97.54
<b>2020</b>	55.83	65.15	63.65	75.07	82.76	61.44	72.44	70.99	84.38	92.17	66.76	79.65	77.63	91.76	100.03

Appendix 15. Graphs of imperviousness versus return period and peak discharge



## Imperviousness of the Upper Bukit Timah basin versus return period and peak discharge



## Imperviousness of the Upper Bukit Timah basin versus return period and peak discharge

